UNIVERSITÀ DELLA CALABRIA

UNIVERSITA' DELLA CALABRIA

Dipartimento di Chimica e Tecnologie Chimiche

Scuola di Dottorato

Scuola Dottorale Scienza e Tecnica "Bernardino Telesio"

Indirizzo

Metodologie Chimiche Inorganiche (ICM)

CICLO

XXVII

Sintesi e caratterizzazione di materiali bioattivi e/o cromonici a base di complessi di metalli di transizione

Settore Scientifico Disciplinare CHIM/03 Chimica Generale e Inorganica

Direttore: Ch.mo Prof. Roberto Bartolino

Firma _____

Supervisore: Ch.mo Prof. Alessandra Crispini

Firma _____

Dottorando: Dott./ssa Bárbara Sanz Mendiguchía

Firma _____

UNIVERSITÀ DELLA CALABRIA

UNIVERSITY OF CALABRIA

Departament of Chemistry and Chemical Technologies

Doctorate School

Bernardino Telesio – Doctorate School of Science and Technique

Inorganic Chemistry Methods (ICM)

CYCLE

XXVII

Synthesis and characterization of bioactive and/or chromonic materials based on transition metal complexes

CHIM/03 General and Inorganic Chemistry

School Director: Ch.mo Prof. Roberto Bartolino

Supervisor: Ch.mo Prof. Alessandra Crispini

PhD Candidate: Dott./ssa Bárbara Sanz Mendiguchía

To Prof. Daniela Pucci

Table of Contents

Abstract

Negli ultimi anni la sintesi di complessi metallo organici è diventata una importante area di ricerca nel campo della teragnostica, sfruttando le propietà di alcune molecole di agire contemporaneamente sia nell'ambito della diagnosi che della terapia. Il presente lavoro di tesi ha riguardato la sintesi di nuovi complessi di metalli di transizione e la loro completa caratterizzazione con possibili proprietà antitumorali mediante meccanismo di intercalazione.

Per ottenere tale scopo sono stati utilizzati gli ioni Zn(II) e Cu(II) come metalli centrali coordinati a due diverse tipologie di leganti chelanti con natura aromatica, allo scopo di ottenere sistemi eterolettici, ionici e neutri con proprietà intercalanti.

Il frammento metallo organico principale, sulla base del quale costruire per modificazioni successive i differenti complessi sintetizzati, è costituito dallo ione metallico centrale coordinato per chelazione ad una bipiridina ed ad un legante O,O chelante. Le varie funzionalizzazioni sul legante bipiridinico ed i differenti leganti O,O chelanti sono di seguito riportati nel Schema 1.

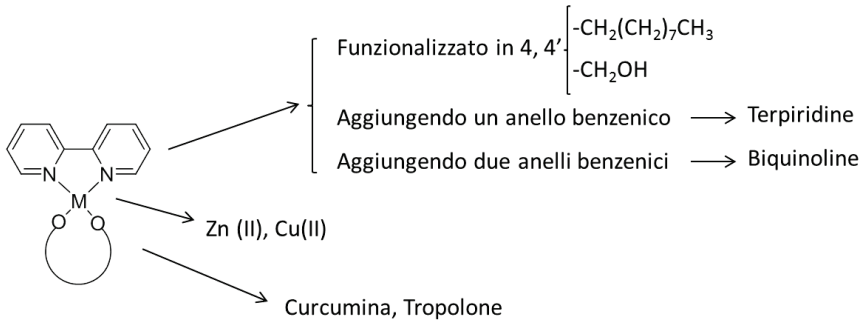

Schema 1.

Il complesso **1,** sintetizzato precedentemente dal gruppo di ricerca con il quale è stato svolto il presente lavoro di tesi, presenta ottima attività citotossica e meccanismo di azione di tipo intercalativo, come dimostrato dagli studi condotti tra il complesso stesso ed frammenti di DNA liquido cristallini. Sulla base di questi risultati, e cercando di superare il limite relativo alla scarsa solubilità in solventi acquosi del complesso **1**, modifiche strutturali, quali introduzione di ionicità e cambiamento dello ione metallico centrale sono state effettuate mediante le opportune strategie sintetiche. I complessi ionici **2** e **3** sono stati ottenuti con successo e ampiamente

caratterizzati, così come l'analogo complesso di Cu(II) **4**.

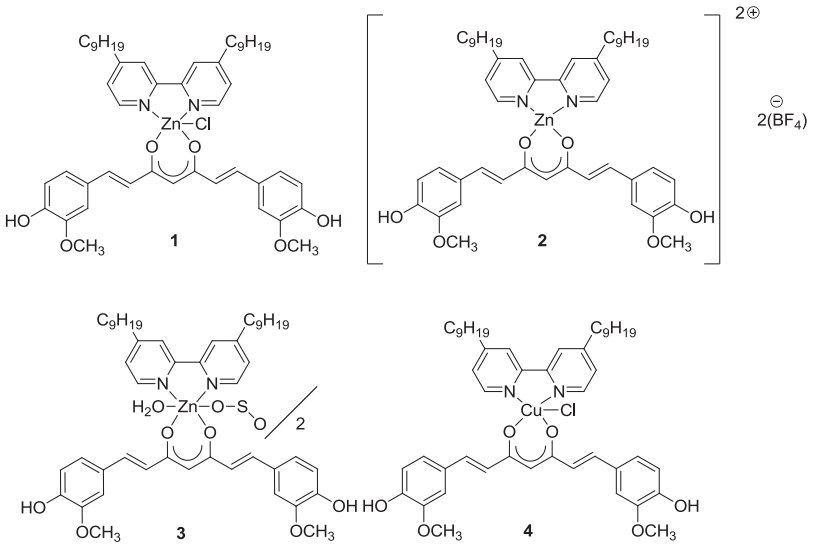

Figura 1. Struttura molecolare dei complessi **1**, **2**, **3** e **4**.

L'effetto citotossico dei complessi **2** e **3** è stato valutato per investigare l'azione a diverse concentrazioni in cellule SHSY-5Y di neuroblastoma umano, in coltura su membrane di PCL. Si osserva inoltre che il composto **2** ha attività citotossica maggiore a concentrazione più bassa, rispetto a il complesso modelo **1** e il complesso **3**. Il complesso **2** anche presenta una parziale solubilità in acqua. Per aumentare la solubilità in acqua dei complessi curcuminici si è deciso di sintetizare un complesso simile al complesso modelo **1** cambiando lo zinco (II) per un rame (II), ottenendo il complesso **4**. Purtroppo, il cambio di metalo non ha aumentato la solubilità in acqua.

Sulla base di questi complessi ed al fine di continuare a migliorare le caratteristiche chimico fisiche, quali solubilità e quindi biodisponibilità in acqua, si è deciso di sintetizare complessi simili

contenenti il legante N,N-chelante funzionalizzato nella posizione 4, 4' con un gruppo $–CH_2OH$, il quale potrebbe aumentare la solubilità e l'attività con i sistemi biologici tramite legami a ponte d' idrogeno. Il complesso **1A,** sintetizzato precedentemente dal gruppo di ricerca con il quale è stato svolto il presente lavoro di tesi, presenta ottima attività citotossica nonostante anche questo complesso abbia scarsa solubilità. Pertanto si è decisso di cambiare la curcumina con un diverso legante O,O-chelante come il tropolone (Fig. 2). Mantendo i gruppi sustituenti si è deciso di estender la parte aromatica (bichinolina e terpiridina) per facilitare le interazioni responsabili.

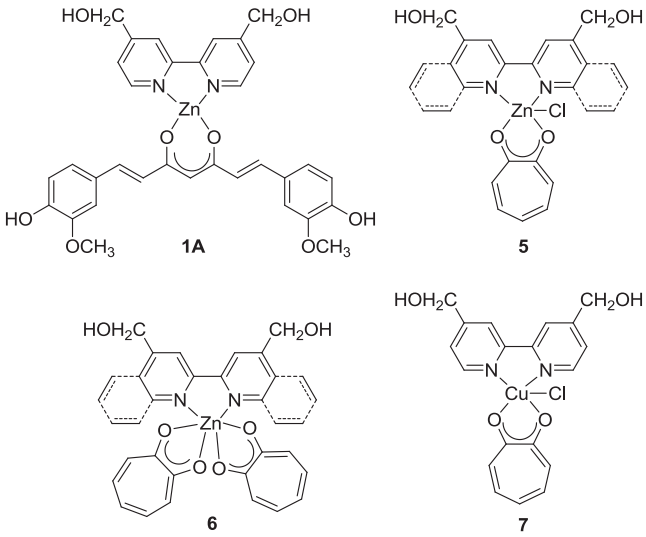

Figura 2. Struttura molecolare dei complessi **1A**, **5**, **6** e **7**.

Il complesso **7** presenta solubilità in acqua mentre che i complessi **5** e **6** sono insolubili, per questo si è decisso di usare la técnica della co-cristallizzazione per aumentare la solubilità di questi complessi e renderli più disponibili e meno tossici allo stesso tempo. Questa tecnica

si basa sulla formazione di un composto attraverso interazioni non covalenti tra una molecola biologicamente attiva ed una molecola biocompatibile. I complessi sono stati fatti reagire con saccarina in modo da permettere la co-cristallizzazione. I prodotti ottenuti sono stati cristallizzati in acqua e mediante analisi su cristallo singolo i composti mostrati in Figura 3 sono stati ottenuti:

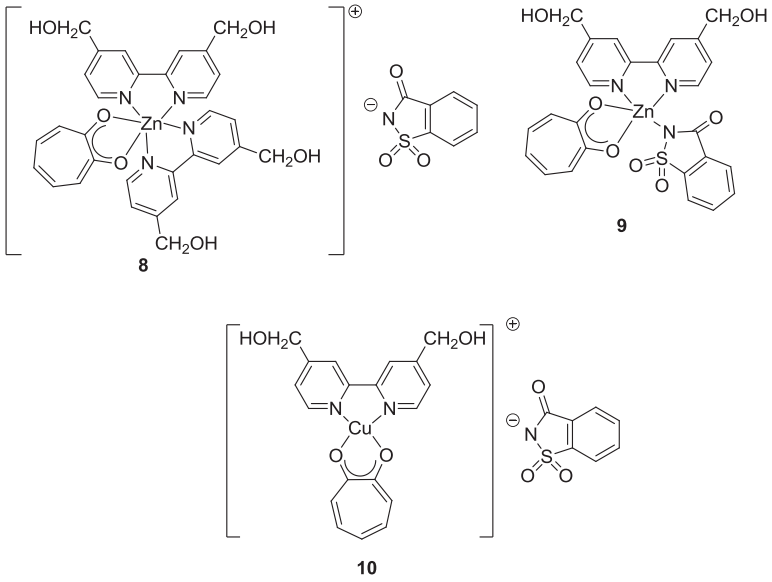

Figura 3. Struttura molecolare dei complessi **8**, **9** e **10**.

Per testare la capacità dei nuovi complessi sintetizzati come potenziali agenti intercalanti, si è deciso di sintetizare complessi che abbiano propietà liquido cristalline cromoniche, in quanto é noto che il DNA forma strutture colonnari cromoniche mediante legami idrogeno. Questo, da un lato, ci permette di usarli come modelli simili al DNA (Figura 4) al fine di testare la capacità di intercalazione nei confronti di

altri complessi, e dall'altro ci consente di usarli come intercalatori aumentando l´affinità nei confronti del DNA.

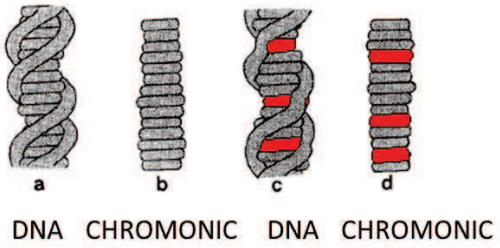

Figura 4. Intercalazione nel DNA e nei cristalli liquidi chromonici.

I cristalli liquidi chromonici si organizano in strutture a colonna, hanno gruppi aromatici planari, gruppi ionici o idrofilici nella periferia ed infine interazioni devono presentare interazioni face to face. Sono stati sintetizzati i composti mostrati in Figura 5 con proprietà liquido-cristalline:

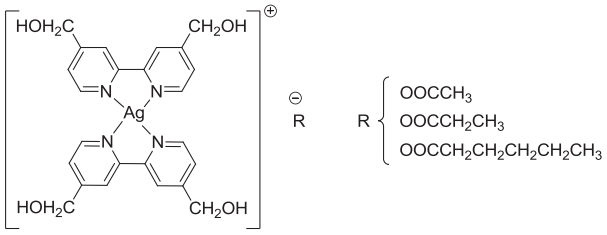

Figura 5. Struttura molecolare dei complessi chromonici.

Nel corso del triennio di dottorato ho svolto un periodo di 9 mesi al "Institute of Medical Sciences" dell'universitá di Aberdeen, dove ho sintetizzato nuove molecole interagenti con recettori CB1. Utilizzando come modello la molecola di Rimonabant (Figura 6) e una seconda

molecola (Figura 6) con migliore affinità, si è deciso di sintetizare delle nuove molecole che abbiano una struttura tale da avere maggiore affinità nei confronti dei recettori CB1 e che allo stesso tempo mostrino mimori effetti collaterali quali i rischi neurologici e psichiatrici mostrati dal Rimonabant. Le molecole sintetizzate dovranno essere dapprima testate, per studiare le interazioni con i recettori CB1 ed in seguito, marcandoli con ^{18}F, verrá studiato il loro funzionamento attraverso la Tomografia ad Emissione di Positroni (PET).

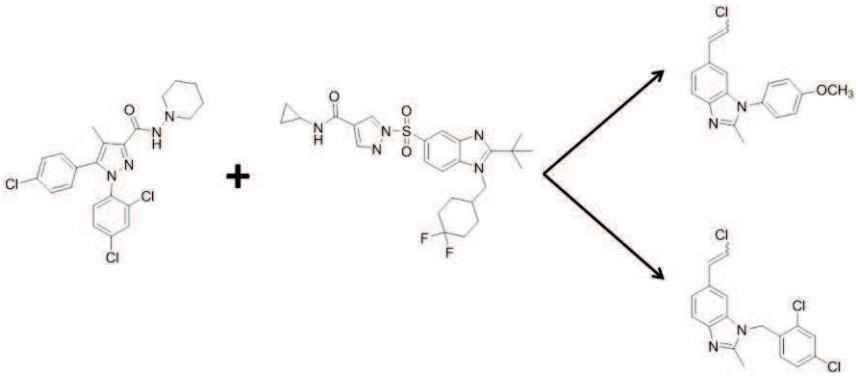

Figura 6. Sintesis di nuovi ricettori CB1.

Abstract

The goal of this thesis is the synthesis of a new generation of metal complexes containing planar, aromatic π-delocalised ligands and acting as possible metal-based antitumor drugs through intercalation and/or DNA G-quadruplex binding. To engineer these new complexes with antitumor activity, three metals have been used, respectively Zn(II), Cu(II) and Ag(I). These metals can be considered a good alternative to platinum because they exhibit an extensive coordination chemistry, they are low costs, widely used in medical chemistry and less toxic than Pt(II). Furthermore, several ligands have been used to fulfil the coordination sphere of these metal centres. In particular, N,N-chelating ligands with different aromatic regions and substituent groups, and O,O-chelating ligands. The latters were chosen as a function of their well known biological and antitumor activity.

Due to the physiological roles of Zinc(II) species in cells and organs,[1] a large interest is growing in the use of Zn(II) coordination complexes in medical therapeutic applications and biosensors. Zn(II) is also involved in the regulation of mitochondrial apoptosis of many mammalian cells.

[1] (a) **Vahrenkamp, H.** 2007, Dalton Trans., pp. 4751-4759; (b) **Anzellotti, A.I. Farrell, N. P**. 2008, Chem. Soc. Rev., Vol. 37, pp. 1629-1651.

In this context, recently a low cost Zn(II) complex has been synthetized and characterized, showing promising cytotoxic activity against different human cancer cells (Fig. 1).[2]

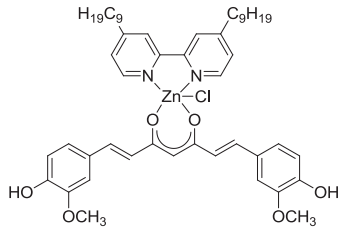

Figure 1. Structures of the complex: [(bpy-9)Zn(curc)Cl].

Therefore, in order to continue this research work and aiming to increase the cytotoxic activity and the solubility of this starting derivative, new Zn(II) complexes have been synthesized and characterized. In these complexes, structure variations have been performed around the coordination sphere of the Zn(II) centre, in order to modulate both the geometry and the electrostatic nature of the resulting Zn(II) derivatives.

Subsequently, the metal centre has been changed to Cu(II). Copper is a transition element and in solution has two common oxidation states, +1 (preferred tetrahedral four-coordinated geometry) and +2 (typically square-planar or trigonal planar geometry). Cu(II) is an essential metal for the body, less toxic than Pt(II) and implicated in

[2] **Pucci, D. Bellini, T. Crispini, A. D'Agnano, I. Liguori, P. F. García Orduña, P. Pirillo, S. Valentini A. Zanchetta, G.** 2012, Med. Chem. Commun., Vol. 3, pp. 462-468.

cerebral activities, nervous and cardiovascular systems. A large number of Cu(II) complexes have been screened for antitumor activity.[3,4]

The structure variations around the metal centre (in both Zn(II) and Cu(II) complexes) was realized by changing the substituents at the periphery of the N,N chelating ligands and/or the type of the N,N- and respectively the O,O-chelating ligands. Initially, the substituent groups ($-C_9H_{19}$) on the N,N-chelating ligand present in the reference Zn(II) complex (Fig. 1), have been replaced with hydrophilic ($-CH_2OH$) groups, giving rise to the 4,4'-dihydroxymethyl-2,2'-bipyridine ligand capable to interact *via* hydrogen bonds interactions to increase the solubility and the bioactivity (Fig. 2).

Nevertheless, the Zn(II) containing the the 4,4'-dihydroxymethyl-2,2'-bipyridine ligand presented low water solubility. To increase the solubility of these complexes co-crystallization with saccharin by liquid assistant grinding has been accomplished, yielding water soluble compounds.

Furthermore, an increase of the aromatic part of the N,N-chelating ligand was accomplished by changing the bipyridine ligands with biquinolines and terpyridine, in order to facilitate the possible intercalation and the G-quadruplex stabilization modes (Fig. 2b,c).

[3] **Chen, Q-Y. Fu, H-J. Zhu, W-H. Qi, Y. Ma Z-P. Gao, J.** 2011, Dalton Trans., Vol. 40, pp. 4414.
[4] **Zhou, C. Y. Zhao, J. Wu, Y. B. Yin C. X. Yang, P.** 2007, J. Inorg. Biochem., Vol. 101, pp. 10-18.

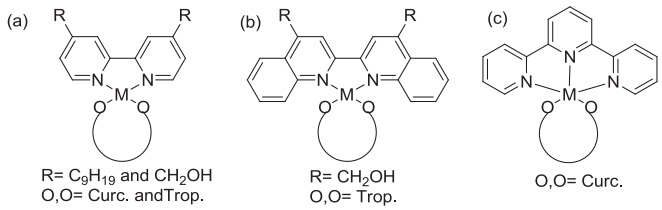

Figure 2. Model complexes for intercalation and/or G-quadruplex binding.

As O,O-chelating ligands, curcumin was used in continuation with the model Zn(II) complex.

Following the possible structural modifications, the O,O-chelating ligand was subsequently substituted with tropolone. These two ligands are well known for their good biological activities. Their chemical structure is reported in Figure 3.

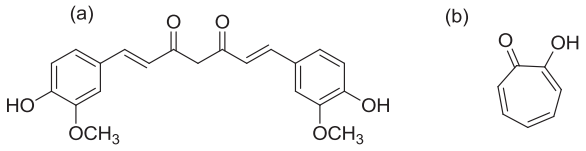

Figure 3. (a) Curcumin and (b) Tropolone.

Curcumin is a yellow spice derived from the rhizome of Curcuma longa Linn. It is used in traditional medicine in China, India and Iran since a long time, in the treatment of many diseases like diabetes, liver disease, rheumatoid disease, atherosclerosis, infectious disease and cancers.[5] Nevertheless, curcumin has a poor solubility in water and photosensitivity.

[5] **Ashkani-Esfahani, A. Noorafshan, S.** 2013, Curr. Pharm.l Des., Vol. 19, pp. 2032-2046.

Tropolone is a natural compound with a seven-member aromatic ring. This ligand presents powerful biological activity such as antibacterial, anticancer, antioxidant, antiviral, anti-inflammatory, insecticidal and antidiabetic.[6] Its antitumor action is attributable to the presence of the diketone structure, which facilitates the formation of metal chelates in the presence of various metal ions.[7,8]

In order to design metal containing chromonic liquid crystals, able to be used as intercalators (due to the miscibility of the chromonic phases) and/or DNA model to test intercalation agents, new ionic N,N-coordinated Ag(I) complexes having two 4,4'-dihydroxymethyl-2,2'-bipiyridine chelated ligands and carboxylate counterions, in which the length of the counterion has been varied, were synthesized and characterized (Fig. 4). These are indeed the first Ag(I) complexes that resulted to organize into chromonic mesophases.

The chemistry of Ag(I) complexes is in general extremely versatile in building supramolecular 'soft' ionic systems by coordination with oligopyridines and varying the counterions. Moreover, the choice of the hydroxyl substituents on the bipyridine ligand is related to their potential ability to help in the formation of solvate species and then to form networks of intermolecular interactions via hydrogen bonds.

---

[6] **Bentley, R.** 2008, Nat. Prod. Rep., Vol. 25, pp. 118.
[7] **Zhao, J.** 2007, Curr. Med. Chem., pp. 2597-2621.
[8] **Ononye, S. N. VanHeyst, M. D. Oblak, E. Z Zhou, W. Ammar, M. Anderson, A. C. Wright, D. L.** 2013, ACS Med. Chem. Lett., Vol. 4, pp. 757-761.

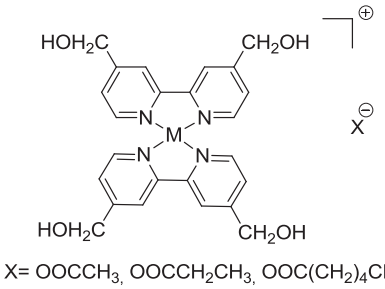

Figure 4. First chromonic Ag (I) liquid crystals.

Chapter 1

Metal complexes in medical chemistry

Medical inorganic chemistry played an important role in the history as proved by several examples recover up to now. In Egypt, the water was sterilised by copper (3000 BC) and the zinc was used to healing wounds (1500 BC), gold was used in Arabia and China in a number of medicines 3500 years ago, during the Renaissance, mercurous chloride was used as diuretic and in the early twentieth century a treatment for Syphilis, based on arsenical, was development by Paul Ehrlich.[9,10] Many metallic elements have a wide range of medical applications (Scheme 1.1), because of the attraction between the electron deficient metal ions and the electron rich molecules such as proteins and DNA.

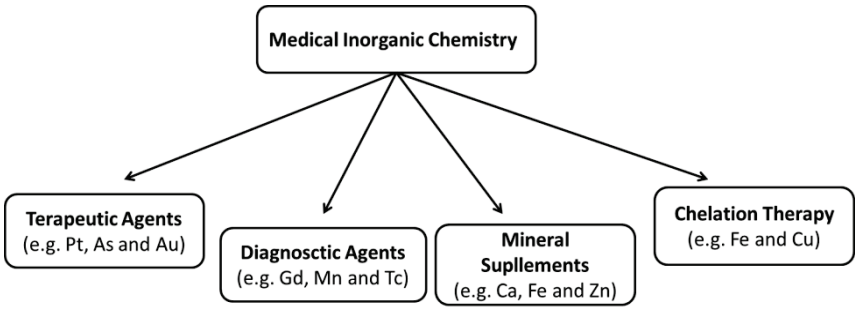

Scheme 1.1. Areas of Medical Inorganic Chemistry.

[9] **Abrams, C. Orving and M. J.** 1999, Chem. Rev., Vol. 99, pp. 2201-2204.
[10] **Griffith, D. Gaynor and D. M.** 2012, Dalton Trans., Vol. 41, pp. 13239-13257.

Although the metals have been used throughout our history, medical inorganic chemistry as a discipline started with the discovery of cisplatin, *cis*[$Pt(NH_3)_2Cl_2$], in 1965 by Barnet Rosenberg.[11,12] Pt-based combination chemotherapy is still the most used treatment for specific type of cancer such as testicular and ovarian.

Nowadays, antitumor agents can be divided in two groups based on their mechanism of action. The first group is the classical antitumor metal agents, where the interaction with DNA is done through covalent bonds. The second group is defined as non-classical antitumor metal agents, in which the compounds interact with DNA by non-covalent interactions, such as $\pi-\pi$ stacking or hydrogen bonds.

1.1 Classical antitumor metal agents

Since the serendipitous discovery of cisplatin medical properties over 40 years ago, today this metal drug is still considered one of the best-selling anticancer drug over the worldwide for the treatment of testicular and ovarian cancer.[13]

Cancer represents the major cause of death and disease worldwide. Although 50 years have passed since the discovery of cisplatin anticancer activity, its mechanism is still not completely clear.

[11] **Rosenberg, B. Vancamp, L. Trosko, J. E. Mansour, V. H.** 1969, Nature, Vol. 222, pp. 385-386.
[12] **Rosenberg, R. Renshaw, E. Vancamp, L. Hartwick, J. Drobnick, J.** 1967, J. Bacteriol., pp. 716-721.
[13] **Kelland, L.** 2007, Nature Reviews, pp. 573-584.

Briefly, the history of cisplatin as cancer therapy drug is summarised in Figure 1.1.

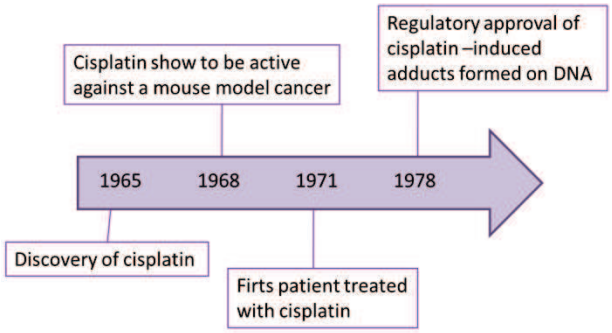

Figure 1.1. Milestones in the development of cisplatin for cancer therapy.

In particular, in 1965 Rosenberg and co-workers were interested to investigate whether cell division might be influenced by electric or magnetic dipole. They were using platinum electrodes (consider to be inert) in the growth chamber of *Escherichia coli*, when something unexpected happened. The bacteria become very long filaments, and did not replicate. Chemical analysis identified two active complexes, the *cis* and *trans* isomers of the diamminedichloroplatinum(II) complex reported in Figure 1.2. Extensive chemical analysis led them to the conclusion that *cis*$[Pt(NH_3)_2Cl_2]$, formed by electrolysis from the platinum electrodes, was responsible to inhibit the bacterial replicative cycle.[11] On the contrary, the *trans* isomer was much less active. The possibility to inhibit cell division generated great interest in the possible use of this metal complex in cancer therapy. Three years later, cisplatin was used for the treatment of a murine transplantable tumour in mice causing marked tumour regression. After *in vivo* tests, in 1971 the first patients were treated by cisplatin.[11,12]

Cisplatin Transplatin

Figure 1.2. Diamminedichloroplatinum(II) isomers.

Several studies have shown that the mechanism of action of cisplatin, based on aquation and ligand exchange, is activated within the cell.[14] Cisplatin is administered intravenously in a saline solution to prevent aquation. Furthermore, in the blood the concentration of chloride ions (*ca*. 100 mM) is sufficiently high to prevent hydrolysis. Cisplatin might enter cells using passive diffusion or transporters (copper transporter CTR1).[15] Inside the cell (intracellular chloride concentrations *ca*. 4-23 mM) the drug will transform by substitution of one or two chlorides (leaving group) with water molecules, to generate various reactive platinum species (Fig. 1.3).[14] These new adducts make covalent bonds with two adjacent guanines of the same strand of DNA or rarely with two guanines in opposite DNA strands. It is not surprising that cisplatin makes covalent bonds with the guanine nitrogen atoms (N_7) since these sites are the most electron-dense and accessible sites in DNA (Fig. 1.3). These new ionic Pt(II) species will change the secondary structure of DNA inhibiting transcription and replication preventing cancer cells growth.[16]

[14] **Siddik, Z. H**. 2003, Oncogene, Vol. 22, pp. 7265-7279.
[15] **Sadler, A. M. Pizarro and P. J.** 2009, Biochimie, Vol. 91, pp. 1198-1211.
[16] **Gibson, D.** 2009, Dalton Trans., pp. 10681-10689.

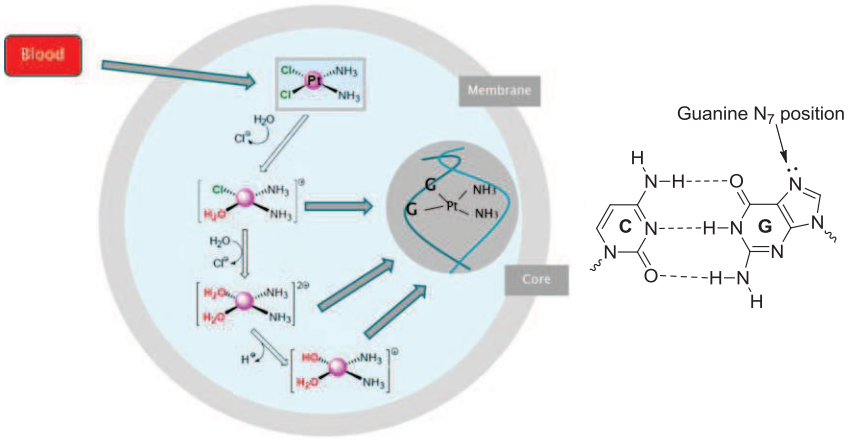

Figure 1.3. Cisplatin mechanism inside cells and the guanine position for the covalent bond with cisplatin.

Cisplatin remains the most used metal complex in the treatment of various cancerous malignancies, being very effective, particularly for patients with testicular, ovarian, cervical, bladder and head/neck tumours. Nevertheless, cisplatin administration is often limited because of its particularly toxicity (e.g. vomiting, nausea, ear damage, loss of sensation in hands and kidney toxicity). Another drawback is the intrinsic and acquired resistance possessed by various tumours, causing the lack of response to subsequent cycles of cisplatin treatment. Hence, the medical inorganic chemists have been working to discover less-toxic analogues retaining cisplatin anticancer activity. A large number of complexes have been developed and tested, as 'second-generation' and 'third-generation' platinum drugs for clinical practice to provide benefits to cancer patients.

1.1.1 Covalent binding mode: cisplatin analogues

A large number of platinum(II) based compounds structurally similar to cisplatin have been developed and tested. The platinum drug family tree is presented in Scheme 1.2.[13]

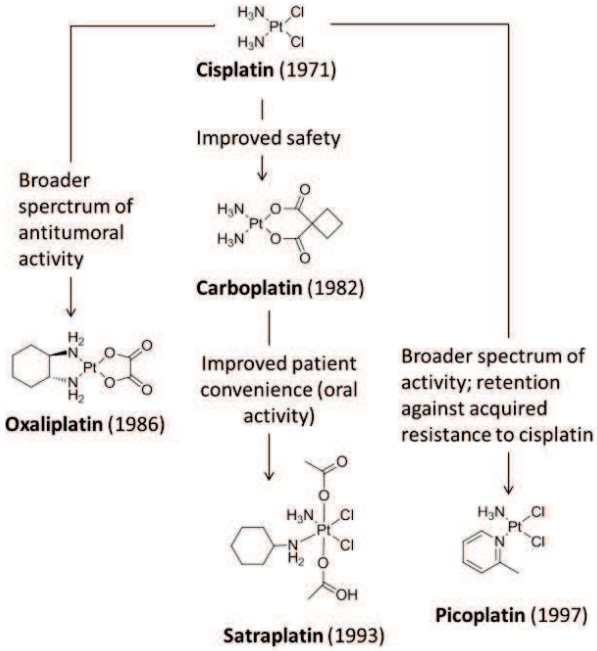

Scheme 1.2. Platin drug 'family tree'.

These Pt(II) complexes, following the classical structure/properties relationship elaborated from cisplatin activity, should have two leaving ligands (which can become just one bidentate labile leaving ligand) and

ammine ligands coordinated to the Pt(II) ion, neutral nature and *cis* configuration.[14,17]

In order to reduce toxicity and improve activity, the type of ligands around the Pt(II) ion has been varied. One of these variation resulted in carboplatin, the first cisplatin analogue used in patients.[18] The structure is slightly different than cisplatin, where two chloride ligands have been substituted with a bidentate dicarboxylate. Carboplatin exhibits lower reactivity and slower DNA binding kinetics, although it forms the same reaction adducts. However, carboplatin has proved to be a chemotherapeutic drug used for ovarian, lung, head and neck tumours. Many years later, oxaliplatin (a cyclohexane-1,2-diamine Pt(II) complex) emerged in continuation with cisplatin. This metal complex has shown better efficacy against tumours than cisplatin and carboplatin, but also causes neurotoxicity at a severity level, limiting its use.[19] More than 10 years later the first patient has been treated with carboplatin, satraplatin was synthesized to be an orally active version of carboplatin. Satraplatin is an octahedral Pt(IV) compound, that is reduced inside cells loosing the two axial acetate ligands and giving rise to more active Pt(II) analogues. This antitumor agent presents a good activity in human cancer cells with acquired cisplatin resistance.[20]

---

[17] **Harper, B. W. Krause-Heuer, A. M. Grnat, M. P. Manohar, M. Garbutcheon-Sigh, K. B. Aldrich-Wright, J. R.** 2010, Chem. Eur. J., Vol. 16, pp. 7064-7077.

[18] **Harrap, K. R.** 1985, Cancer Treat. Rev., Vol. 12, pp. 21-33.

[19] **Küng, A. Strickmann, D. B. Galanski, M. Keppler, B.K.** 2001, J. Inorg. Chem., Vol. 86, pp. 691-698.

[20] **Kelland, L. R. et al.** 1993, Cancer Res., Vol. 53, pp. 2581-2586.

Picoplatin was designed to provide steric bulky ligands around the Pt(II) centre, changing an ammine ligand with methyl-pyridine ligand. This structure was shown to lead to a relative reduction in inactivation by thiol containing species in comparison to cisplatin. Picoplatin retains activity against a wide range of cisplatin-resistant and oxaliplatin-resistant cells *in vitro*, which was independent of whether resistance was due to reduced transport, increased cytoplasmic detoxification or increased DNA repair. Moreover, picoplatin possesses antitumor activity in *vivo* by both the intravenous and oral routes, binding in a very similar manner to cisplatin. Clinical studies have revealed dose-limiting toxicities similar to carboplatin.[21]

It is well known that transplatin shows less anticancer activity than cisplatin. Since many other complexes in the *trans* configuration also were found to be ineffective, it was assumed that a *cis* configuration of the labile groups is required for the antitumor activity of such compounds. However, in the last 20 years, a good number of *trans* Pt(II) complexes have shown an interesting antitumor activity in *vitro* and in *vivo*. One of the last example is represented by the complex $[Pt(CQ)_2(Cl)_2]$(CQ= choloroquine base) reported in Figure 1.4, where the CQ ligand bound to the Pt(II) metal centre through the tertiary amine.[22] This Pt(II) complex interacts with DNA by covalent binding mode and has shown, in six human tumour cell lines, better activity than cisplatin.

[21] **Holford, J. Sharp, S. Y. Abrams, M. Kelland, L. R**. 1998, Br. J. Cancer, Vol. 77, 3, pp. 366-373.
[22] **Navarro, M. Castro, W. Higera Padilla, A. R. Sierraalta, A. Abad, M. J. Taylor, P. Sánchez Delgado, R.** 2011, J. of Inorg. Chem., Vol. 105, pp. 1684-1691.

It is interesting to note that the its cytotoxic activity is correlated with the strong interaction observed between this complex and DNA, similar to that shown by cisplatin.

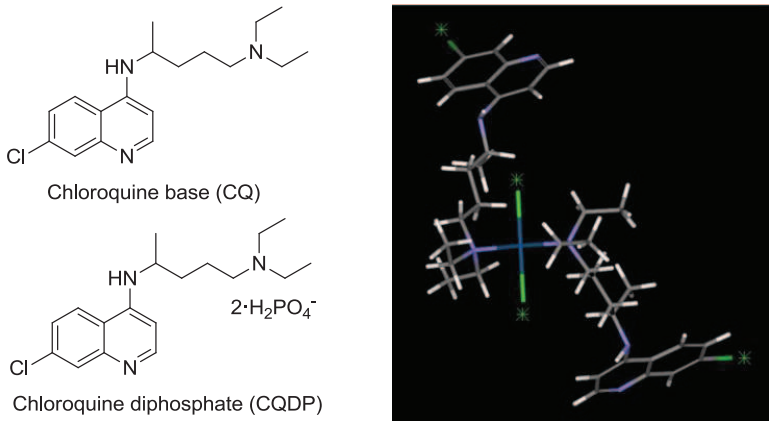

Figure 1.4. Molecular structure of CQ, CQDP and optimized structure of $[Pt(CQ)_2(Cl)_2]$.

An analogue complex, $[Pt(CQDO)_2Cl_2]$ (Fig. 1.4) has been studied. This Pt(II) complex bound DNA through electrostatic interactions and hydrogen bonds, showing less anticancer activity than complex $[Pt(CQ)_2(Cl)_2]$.[22]

The different structural changes around the metal ion, to obtain platinum complexes with better properties than cisplatin, have induced in researchers the curiosity to find strategies for the development of new anticancer metal-based drugs. One strategy is the synthesis of new metal complexes with the same cisplatin binding mode, but containing different metal ions and different molecular geometries.

1.1.2 Covalent binding mode: non-platinum complexes

The limitation of platinum complexes (high toxicity and incidence of drug resistance) has provided the motivation to research alternative chemotherapeutic strategies for the isolation of effective antitumor compounds based on other metal centres.

The interest for discovery of more efficient metal-based drugs, has given rise to the synthesis of new Pd(II) complexes analogues to cisplatin. Pd(II) has a very similar chemistry to Pt(II), forming squared planar complexes. Two cisplatin analogues were synthesized, *cis*-$[Pd(NH_3)_2Cl_2]$ and *cis*-$[Pd(DACH)Cl_2]$(DACH = (1R,2R)-(-)-1,2-diaminecyclohexane) (Fig. 1.5a).[23] In contrast to cisplatin, these two Pd(II) complexes do not show antitumor activity. They hydrolysed very fast interacting with several molecules contained in biological fluids, preventing Pd(II) complexes to reach DNA. To develop antitumor palladium drugs, the Pd(II) complexes must be stabilized by strongly coordinated nitrogen ligands and suitable leaving groups. An example is the new Pd(II) complex $[(bipy)Pd(SeO_3)]$ (bipy= 2,2'-bipyridine) reported in Figure 1.5b, bearing two chelating (N,N) and (O,O) ligands. This Pd(II) complex presents better cytotoxicity than cisplatin making it as a good candidate for anticancer therapy.[24] Numerous palladium complexes with promising activity against some specific tumour cell

[23] **Butour, S. Wimmer, F. Wimmer, F. Castan, P.** 1997, Chemico-Biological Interactions, Vol. 104, pp. 165-178.
[24] **Mansuri-Torshizi, H. Mital, R. Srivastava, T. S. Parekh H. Chitnis, M. P.** 1991, J. Inorg. Biochem., Vol. 44, pp. 239-247.

lines have been synthesized, applying structural changes around the metal ion such as the change of both leaving ligands and the amine groups or the isomerism. In general, research results indicated that most of the *trans*-palladium complexes showed a better activity than *cis*-platinum and superior activity than that of *cis*-palladium isomers. For example the complex reported in Figure 1.5c, $[(MP)_3Pd(Br)]Br$ (MP= 2-mercaptopyridine), has shown better cytotoxicity than cisplatin and than its Pt(II) analogues.[25]

Ruthenium complexes have been also studied as alternative to platinum compounds. One example is the Ru(II) complex $[(PDTA)RuCl_2]$ (PDTA= 1,2-propylenediamine-N,N,N',N'-tetraacetic acid) reported in Figure 1.5d. This Ru(II) complex has been tested in five different tumour cell lines, showing good activity. The complex is exceptionally well tolerated and shows an absolute lack of toxicity at all given doses.[26]

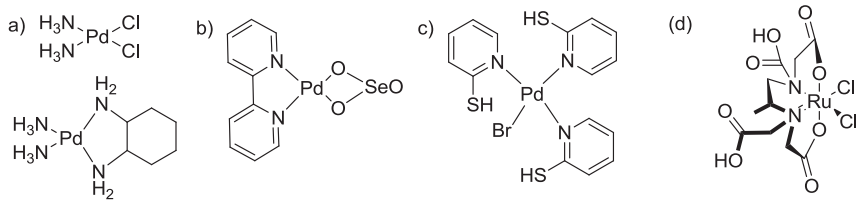

Figure 1.5. Metal complexes with antitumor activity. (a) *cis*-$[Pd(NH_3)_2Cl_2]$ and *cis*-$[Pd(DACH)Cl_2]$, (b) $[(bipy)Pd(SeO_3)]$, (c) $[(MP)_3Pd(Br)]Br$ (d) $[Ru(PDTA)Cl_2]$.

[25] **Camarra, M. Berti, T. D'Ancona, S. Cherchi, V. Sindellari, L.** 1996, Anticancer Res, Vol. 17, pp. 975-980.
[26] **Vilaplana, R. Romero, M. A. Quiros, M. Salas, J. M. Gonzalez-Vilchez, F.** 1995, Met. Based Drugs, Vol. 2, pp. 211-219.

Another strategy for the design of new anticancer metal-based drugs is the synthesis of new metal complexes (defined as non-classical antitumor metal agents) with an alternative DNA binding mode based on non-covalent interactions, such as electrostatic, $\pi-\pi$ interactions or hydrogen bonds.

1.2 Non-classical antitumor metal agents

In the search of new metal complexes showing antitumor activity, a good option was the synthesis of antitumor agents able to interact with DNA by non-covalent interactions.

DNA offers many potential non-covalent binding sites due to its size and complexity. Metal complexes as well as pure organic molecules are able to bind DNA *via* three reversible interaction modes: groove binding (electrostatic interactions), intercalation ($\pi-\pi$ stacking, hydrogen bonding and electrostatic interactions) and insertion ($\pi-\pi$ stacking interactions) (Fig. 1.6).[27] Certain small molecules bind DNA by groove binding, producing a small distortion in DNA. In a detailed analysis of DNA structure, there are two types of grooves that can be seen. The major groove has the nitrogen and oxygen atoms of the base pairs pointing inward toward the helical axis, whereas in the minor groove, the nitrogen and oxygen atoms point outwards. The grooves twist around the molecule on opposite sides. In the case of

[27] **Strekowski, L. Wilson, B.** 2007, Mutat. Res., Vol. 623, pp. 3-13.

groove binding, reversible intermolecular association such as electrostatic binding occurs due to the interaction between cations and the negatively charged phosphate backbone at the exterior surface of DNA (Fig. 1.6a).[28] On the contrary, intercalators are compounds interacting *via* π-π stacking interactions through their aromatic planar surface and two base pairs. For an optimal intercalation, the planar part of the molecule should have a minimum surface[29] of about 28 $Å^2$ (reached by three to four condensed five or six membered rings) (Fig. 1.6b).[28] The intercalation produces a distortion in the DNA chain, inhibiting cellular replication processes. The majority of non-covalent DNA binding compounds are groove binders or intercalating agents, but there are a small number of compounds interacting with DNA as insertors. Insertion is similar to intercalation, but the insertion agents eject the DNA bases with their planar ligands, acting as a π-stacking replacement in the DNA base stack. The insertion agents present bigger aromatic portion than the intercalating agents, and one example of metal ionic complex is $[\Delta\text{-Rh(bpy)2(chrysy)}]^{3+}$ acting as insertion agent have the coordinated ligand is chrysi (chrysi = 5,6-chrysene quinine diimine) (Fig. 1.6c).[29]

[28] **Zeglis, B. M. Pierre, V. C. Barton, J. K.** 2007, Chem. Commun., pp. 4565-4579.
[29] **Pierre, V. C. Kaiser, J. T. Barton, J. K.** 2007, PNAS, Vol. 104, 2, pp. 429-434.

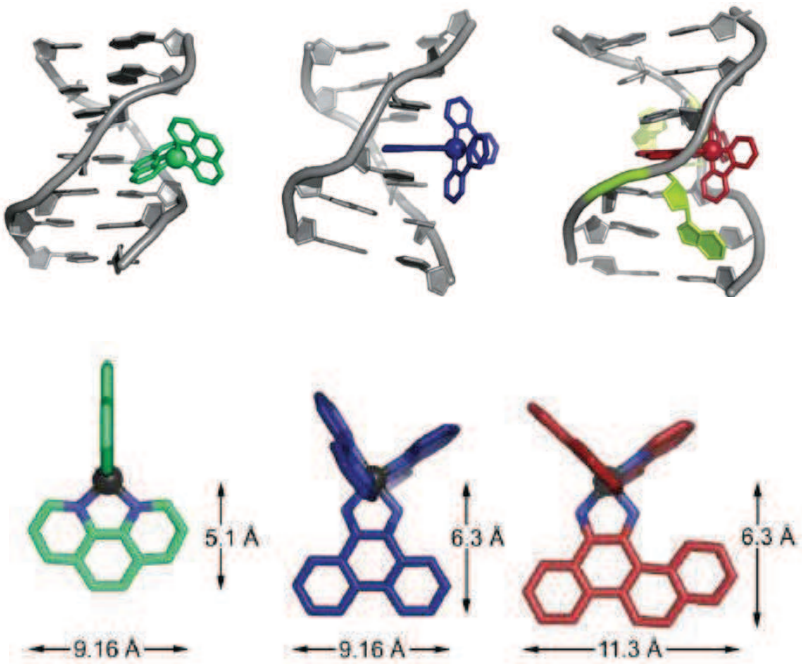

(a) Grove binding (b) Intercalation (c) Insertion

Figure 1.6. The binding modes of metal complexes with DNA and the candidates to bind DNA.

Continuing the research of new metal-based drug with different cisplatin mechanism of action, intercalation has been shown to be a good strategy for anticancer treatment.

1.2.1 Intercalation

Intercalation was first proposed by Lerman[30] to explain the strong affinity for DNA of certain heterocyclic aromatic dyes such as acridines. In particular, Lerman observed a markedly enhanced viscosity and diminution of the sedimentation coefficient of solutions formed by DNA with small amounts of aromatic dyes, contrary to those expected on the basis of aggregation or simple electrostatic effects. These peculiar changes suggested considerable modification of the usual helical structure of DNA, being explained by an intercalation of the compounds between adjacent nucleotide-pair layers by extension and unwinding of the deoxyribose-phosphate backbone. The hydrodynamic changes were therefore the consequences of the diminished bending between layers, the lengthening of the molecule, and the diminished length-specific mass.

Furthermore, the intercalation of coloured fluorescent compounds into DNA has proved to be a rewarding method to detect and understand the intercalation process in itself. For example, ethidium bromide is an aromatic compound that, when exposed to ultraviolet light, shows fluorescence with an orange colour, intensifying almost 20-fold after binding to DNA.[31] The reason for ethidium bromide's intense fluorescence after binding with DNA is the hydrophobic environment found between the base pairs. By moving

[30] **Lerman, L. S.** 1961, J. Mol. Biol., Vol. 3, pp. 18-30.

[31] **Vardevanyan, P.O. Antonyan, A.P. Manukyan G.A. Karapetyan, A.T.** 2001, Exp. and Mol. Medicine, Vol. 33, 4, pp. 205–208.

into this environment and away from the solvent, the ethidium bromide cation is forced to shed any water associated molecules. As water is a highly efficient fluorescent quencher, the removal of water molecules allows the ethidium bromide to fluorescence. Major advances in research have been made with fluorescently labelled DNA.[32]

The structural modifications inducted by intercalating agents can lead to functional changes, often to inhibition of transcription and replication and DNA repair processes, which make intercalators potent mutagens. The intercalating molecule binds DNA by reversible interactions, causing structural modifications with consequent inhibition of the cell replication processes. Nowadays there is a noticeable interest in the use of intercalating agents to inhibit the cellular reproduction for cancer treatment.

Metal complexes showing DNA intercalative mechanism are built up by at least one intercalating ligand coordinated to the metal centre. These ligands have to be oriented parallel to the base pairs and protruding away from the metal centre (Fig. 1.7).[33]

[32] **Bauer, W. Vinogrand, J.** 1970, J. Mol. Biol., Vol. 54, pp. 281-289.
[33] **Barton, B. P. Hudson and J. K.** 1998, J. Am. Chem. Soc., Vol. 120, pp. 6877.

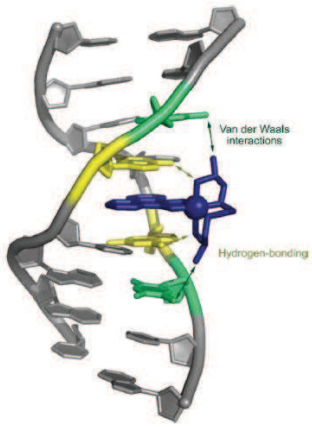

Figure 1.7. Crystal structure of a metallo-intercalator demonstrating the intercalation *via* major grove.

Several Pt(II) complexes with square-planar geometry can bind DNA by intercalation. For example in the complex $[Pt(terpy)(HET)]^+$ (terpy= terpyridine, HET= 2-hydroxyethanethiolato), whose chemical structure is presented in Figure 1.8a, the presence of terpyridine aromatic rings provides a substantial degree of overlap with base pairs. Figure 1.8a shows also the Pt(II) complex intercalated between the two base pairs in the double helical fragment.[34]

Metal intercalation has been also extended to octahedral complexes using Ru(II) derivatives containing multi-heterocyclic aromatic ligands, such as phenantroline (phen) or 9,10-phenanthrenequinone diimine (phi) (Fig. 1.8b,c). The most studied example is the ionic system $[Ru(phen)_2(dppz)]Cl_2$ (Fig. 1.8b). The

[34] **Wang, A. H. Nathans, J. van der Marel, G. van Boom, J. H. X Rich, J. H.** 1978, Nature, Vol. 276, pp. 471-474.

complex excited states are highly deactivated by water, showing no luminescence in aqueous solution at room temperature. Nevertheless, intense photoluminescence appears when it intercalates into DNA, because of the local region of "non-water" provided by DNA around the metal complex.[35] The chiral complex $[Ru(phen)_3]Cl_2$ build up by three phenantroline ligands reported in Figure 1.8c, bind to DNA also by intercalation.[36] Hypochromicity representing a 17% decrease in intensity in the metal to ligand charge-transfer band and enhanced luminescence accompany binding to the duplex reflecting the decreased mobility of the complex when sandwiched into the helix.

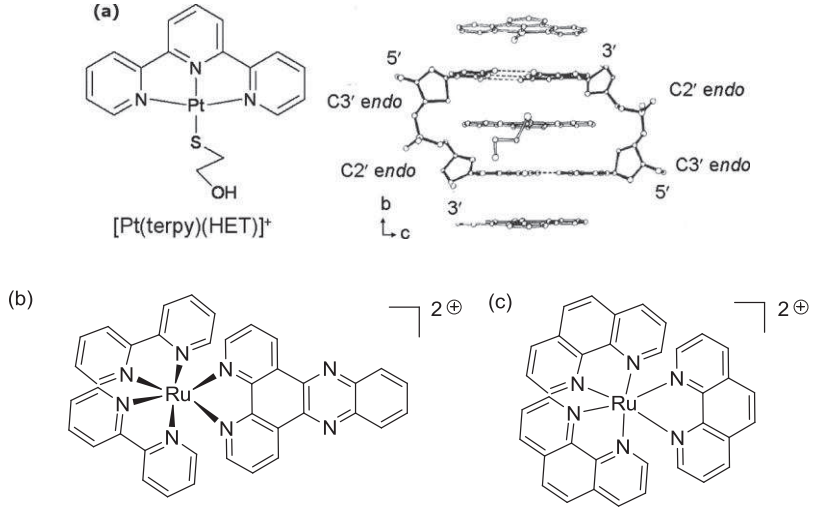

Figure 1.8. (a) Molecular and crystal structure of $[Pt(terpy)(HET)]^+$, (b) $[Rh(phen)_3]Cl_3$, (c)$[Rh(bpy)_2phi]Cl$ and (d) $[Ru(phen)_2(dppz)]^{2+}$.

[35] **Friedman, A. E. Chambron, J. C. Sauvage, J. P. Turro N. J. Barton, J. K.** 1990, J. Am. Chem. Soc., Vol. 112, pp. 4960-5962.
[36] **Barton, J. K. Danishefsky, A. T. Golberg, J. M.** 1984, J. Am. Chem. Soc., Vol. 106, pp. 2172-2176.

A new alternative intercalation mode is called intercalation by dual function (the intercalating complex can react with DNA by both covalent bond and aromatic intermolecular interactions). One example of a metal complex showing this type of DNA binding mode is $[(tpy)Ru(dtdeg)PtCl]Cl_3$ (tpy=2,2':6',2''-terpyridine, dtdeg= bis[4'-(2,2':6',2''-terpyridiyl)]-diethylenenglycol ether) (Fig. 1.9), containing a "Ru(tpy)" fragment with a flexible chain joined to a Pt(II) system at the end. This Pt(II)/Ru(II) complex, indeed, was designed to bind covalently with DNA, by mean of the Pt(II) moiety, and intercalating DNA through the molecular fragment "(Ru(tpy))"(Fig. 1.9).[37]

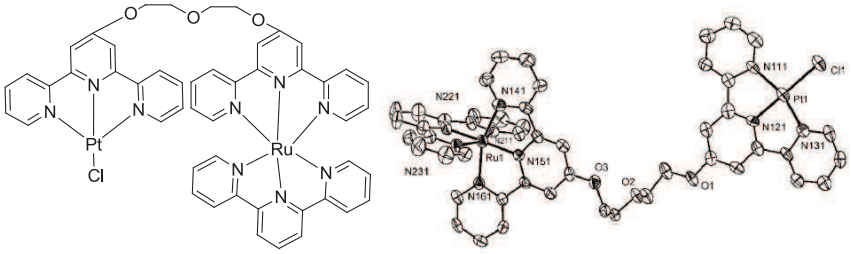

Figure 1.9. $[(tpy)Ru(dtdeg)PtCl]Cl_3$.

Currently, investigations continue in the search of new metal-complexes with an improved affinity for DNA. Three examples of Cu(II) and Zn(II) DNA intercalating complexes recently published are shown in Figure 1.10.[2,38,39]

[37] **van der Schilden, K. Garcia, F. Kooijman, H. Spek, A. L. Haasnoot J. G. Reedijk, J.** 2004, Angew. Chem. Int. Ed., Vol. 43, pp. 5668-5670.
[38] **Raman, N. Mahalakshmi, R. Mitu, L.** 2014, Spectrochimica Acta Part A, Vol. 131, pp. 355-364.

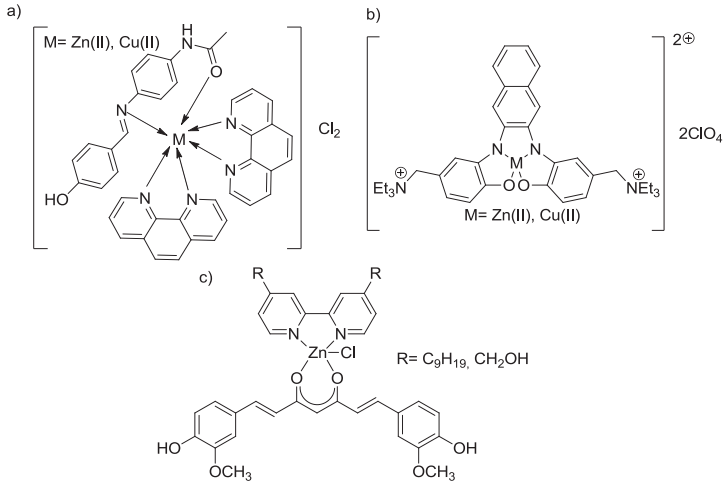

Figure 1.10. New copper(II) and zinc(II) metallo-intercalators.

Several metallo-intercalator systems are based on Zn(II) and Cu(II) metal complexes, as the ones presented in Figure 1.10. Indeed, Zn(II) and Cu(II) metal ions are essential metals for the growth and development of biological systems[40], are low cost metals, with extensive coordination chemistry and in the case of Zn(II) may yield luminescent complexes.

As seen in the above examples, most of the ligands used for the design of intercalating metal agents are based on the use of (N,N) aromatic chelating ligands, changing the substituent groups or the aromatic core.

---

[39] **Lauria, A. Bonsignore, R. Terenzi, A. Spinello, A. Giannici, F. Longo, A. Almerico, A. M. Barone, G.** 2014, Dalton Trans., Vol. 43, pp. 6108.
[40] (a) **Armaroli, N. Accorsi, G. Cardinali, F. Listorti, A**. 2007, Top. Curr. Chem., Vol. 280, pp. 69-115. (b) **Stefanidou, M. Maravelias, C. Dona, A. Spiliopoulou, C.** 2006, Arch. Toxicol., Vol. 80, pp. 1-9.

All the above described metal-based anticancer agents are known to have DNA as main target. However, several studies are now devoted to the development of new compounds able to stabilize the secondary structure of DNA, called G-quadruplex (GQ).

1.2.2 G-quadruplex binding

As was stated up to now, platinum compounds are mostly used in clinical trials. Nevertheless, their high toxicity and resistance mechanisms, endeavoured researchers to concentrate their efforts world-wide in the discovery and the development of new agents able to be active against cancer by choosing novel selective therapeutic targets, such as G-quadruplex.[41]

Genetic information is stored in specific sequences of nucleic acids forming the DNA structure. Watson and Crick in 1953 proposed an anti-parallel double helical structure for DNA (duplex DNA) in which the two strands are held together through canonical adenine/thymine and guanine/cytosine base pairing (Fig. 1.11a).[42] Several studies on the DNA structure showed that DNA can adopt a wide variety of topologies. In particular, guanine rich sequences of DNA can form a secondary structure called G-quadruplex (GQ). This DNA secondary structure is formed by four guanine bases assembled into a planar structure *via*

[41] **Neidle, S. Balasubramanian and S.** 2009, Curr. Opin. Chem.l Biol., Vol. 13, pp. 345-353.
[42] **Watson, J. D. Crick, F. H.** 1953, Nature, Vol. 171, pp. 737-738.

eight Hoogsteen hydrogen bonds. The guanines carbonyl groups create a strong negative electrostatic potential stabilized by the presence of alkali-metal cations (such as Na^+ or K^+) (Fig. 1.11b).[43]

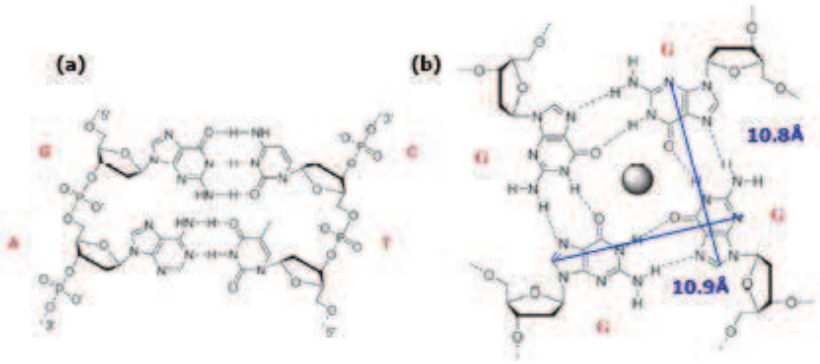

Figure 1.11. (a) The canonical A/T and G/C base pairing. (b) The GQ structure.

Recent studies have shown that there are more than 350000 guanine-rich sequences in human genome with strong tendency to form G-quadruplex structures, in particular at chromosomal extremities (telomeres).[44,45,46] Chromosome ends, or telomeres, are composed of the tandem repeat sequences TTAGGG. In somatic cells, during the cell replication, the telomeres are gradually shortened until the cell death. On the contrary, in tumour cells the activity of telomerase inhibits this action. Telomerase is an enzyme over-expressed in approximately 85% of cancer cells, and it seems to be the

[43] **Murrat, P. Singht V. Defranq, E.** 2011, Chem. Soc. Rev., Vol. 40, pp. 5293-5307.
[44] **Hupper, J. L.** 2008, Biochimie, Vol. 90, pp. 1140-1148.
[45] **Balasubramanian, J. L. Huppert and S.** 2007, Nucleid Acids Rev., Vol. 35, pp. 406-413.
[46] **Todd, A. K.** 2007, Methods, Vol. 43, pp. 246-251.

cause of tumour cell immortality. The development of compounds capable to stabilize this type of DNA secondary structures is considered a new anticancer strategy.[41,42,47,48,49]

Eventually, the GQ stabilization occurs via π–π stacking and electrostatic interactions.[50] Therefore, an effective agent for G-quadruplex stabilisation should have several structural features, such as a large planar surface (for binding by π-stacking to the guanine quartet), positive charge area at the centre of the molecule (to interact with grooves and loops of the G-quadruplex and the phosphates backbone), similar dimensions to GQ (Fig. 1.11) and selectivity for GQ over duplex DNA (intercalation agent).[51]

G-quadruplex stabilization agents can bind to the GQ structures by end-stacking and intercalation.[37] The dimension and shape of G-quadruplex stabilization agents are crucial for the binder mechanism (Fig. 1.12).

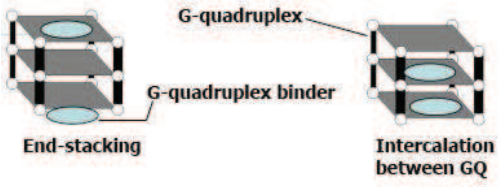

Figure 1.12. Different GQ binding modes.

[47] **Prommier, J. P. LEbeau, J. Ducray C. Sabatier, L.** 1995, Biochimie, Vol. 77, pp. 817-825.
[48] **Blasco, M. A.** 2003, Eur. J. Cell Biol., Vol. 82, pp. 441-446.
[49] **Cuesta, J. Read M. A. Neidle, S.** 2003, Mini-Rev. Med. Chem., Vol. 3, pp. 11-21.
[50] **Teulade-Fichou, D. Monchaud and M. P.** 2008, Org. Biomol. Chem., Vol. 6, pp. 627-636.
[51] **Wang, J. T. Zheng, X. H. Xia, Q. Mao, Z. W. Ji, L. N. Wang, K.** 2010, Dalton Trans., Vol. 39, pp. 7214-7216.

A wide variety of techniques have been employed to study interactions of the designed stabilization agents with G-quadruplex DNA, aiming also to obtain data for structure–activity relationship studies. The key challenge in GQ stabilization agents design is to make them selective for G-quadruplex structures in comparison to duplex DNA or other secondary structures. Because of the high degree of structural polymorphism in GQ, it is important to determine the binding sites of the GQ stabilization agents and their interaction modes (Fig. 1.12).

Some of these techniques are X-Ray diffraction (revealing the dimensions of the complex), circular dichronism (the titration of G-quadruplex with GQ binders induces changes in the CD spectrum), or biological studies such as G-4 FID (based on the ability of a given ligand to displace the fluorescent probe thiazole orange from a G-quadruplex architecture) and FRET-melting (fluorescence resonance energy transfer is based on the monitoring of the stability imparted by a ligand to a fluorescently labelled G-quadruplex structure).

Up to now, several metal complexes with different shape and dimensions, able to act as GQ binders have appeared in the literature. It has been seen that a simple Pt(II) ionic complex as $[Pt(phen)_2](PF_6)_2$ induces the stabilization of G-quadruplex (Fig. 1.13a). CD assays have shown that the CD spectrum of human telomeric DNA gave two bands at about 290 nm (positive band) and 250 nm (negative band). These two bands upon addition of the Pt(II) complex and in the presence of potassium cations, increase in intensity and reaching saturation. These data clearly suggest that the Pt(II) complex strongly stabilized G-

quadruplex conformation because CD offers a reliable means for following the structural conversion of the quadruplex to the unfolded conformation.[52] Structural analysis have been done to reveal the structural affinity between the Pt(II) complex and the G-quadruplex. The dimensions of the Pt(II) complex are very similar to the guanine quartet dimensions (the maximal length of the complex is 10.4 Å very close to the 10.8 Å of the G-quadruplex) (Fig. 1.13a and Fig. 1.11b). The dimension and the structure of this Pt(II) complex are important for G-quadruplex stabilization.[51]

Recently, Pt(II) and Pd(II) complexes with metallo-rectangle shapes (rectangle structure with 12.90 Å of width), reported in Figure 1.13b, were synthesized and where shown to have a high affinity and selectivity for G-quadruplex over duplex DNA.[53] Indeed, different studies have demonstrated their G-quadruplex affinity, such as ESI-MS (electrospray mass spectrometry) studies and biological assays such as G-4 FID and FRET studies. Upon addition of the Pt(II) and Pd(II) complexes to the corresponding DNA structure previously incubated with thiazole orange (TO), an increase in TO's fluoresce intensity was observed. For FRET studies, the Pt(II) and Pd(II) complexes were mixed with different sequences of DNA, showing an increase in melting

---

[52] (a) **Monchaud, D. Yang, P. LAcroix, L. Teulade-Fichou, M. P. Mergny, J. L.** 2008, Angew. Chem. Int. Ed., Vol. 47, pp. 4858. (b) **Rahman, K. M. Reszka, A. P. Gunaratnam, M. Haider, S. M. Howard, P. W. Fox, K. R. Neidle, S. Thurston, D. E.** 2009, Chem. Commun., pp. 4097. (c) **Tan, J. H. Ou, T. M. Hou, J. Q. Lu, Y. J. Huang, S. L. Luo, H. B. Wu, J. Y. Huang, Z. S. Wong, K. Y. Gu, L. Q.** 2009, J. Med. Chem., Vol. 52, pp. 2825.

[53] **Gosh, S. Mendoza, O. Cubo, L. Rosu, F. Gabelica, V. White, A. J. P. Vilar, R.** 2014, Chem. Eur. J., Vol. 20, pp. 4772-4779.

temperature induced by the high degree of G-quadruplex stabilization. Finally, the experimental and computational studies have indicated that these dimetallic rectangles interact with G-quadruplex DNA structures by end-stacking. Their structure is retained in solution (particularly in the case of platinum) and this is likely to be the reason for their high selectivity for quadruplex versus duplex DNA (Fig. 1.13b).

The first example of a G-quadruplex DNA binder based on gold(III) is the complex $[Au(pzpy)_2Cl]$ (pzpy= 2-(3'-Pyrazolyl)pyridine) (Figure 1.13c). The size of this $[Au(pzpy)_2]^+$ ion is about 9.8 Å x 8.4 Å similar to G-quadruplex structure. Fluorescent intercalator displacement (FID), surface plasmon resonance (SPR) and circular dichroism (CD) studies clearly indicated that this Au(III) complex stabilizes the GQ DNA. Again, the geometry of the Au(III) complex and its size resulted to be fundamental to function as a good quadruplex DNA binder. [54]

[54] **Suntharalingam, K. Guota, D. Sanz Miguel, P. J. Lippert, B. Vilar, R.** 2010, Chem. Eur. J., Vol. 16, pp. 3613-3616.

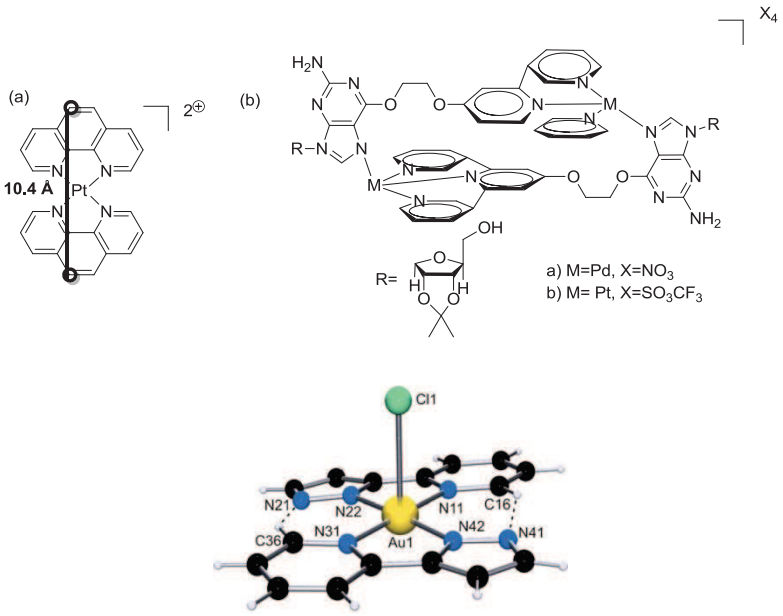

Figure 1.13. G-quadruplex binders: a) Pt(II) ionic complex, $[Pt(phen)_2](PF_6)_2$, b) metallo-rectangle shape Pd(II) and Pt(II) complexes, c) gold (III) complex, $[Au(pzpy)_2Cl]$.

1.3 Liquid Crystals for/as DNA intercalating agents

The ability of duplex DNA to form liquid crystalline phases was found in the late 1940s.[55,56] Since that time, DNA studies have revealed that linear DNA fragments in aqueous solutions have remarkable self-assembly capability forming multiple liquid crystalline phases (chiral

[55] **Luzzati, V. Nicolaieff, V.** 1959, J. Mol. Biol., Vol. 1, pp. 127.
[56] **Robinson, C.** 1961, Tetrahedron, Vol. 13, pp. 219.

nematic and columnar phases) whose nature depends on the DNA concentration.

Initially all these forms of ordering and self-assembly were observed in solutions of long DNA molecules with more than 100 base pairs and were explained on the basis of their elongated shape, their partial flexibility, their acidic nature, and their helical structure. Furthermore, these molecules respect the Onsager theory[57] postulating that in the case of cylindrical particles having length L and diameter d, an orientational ordering of the cylinders, favoured by a balance of orientational and translational entropy at volume fractions, above a critical value of $\sim$ 4d/L. According to this theory, no ordering is expected in sub-Onsager regime (L < 4d).

Subsequently, several research groups have presented evidences that solutions of very short duplex B-DNA, display the same type of liquid crystalline ordering, and specifically chiral nematic and columnar phases.[58] The explanation of the mesophase formation in this case cannot be the same, since for these short strands L < 3d, and thus there is not enough shape anisotropy to satisfy the Onsager criterion. Therefore it was shown that the liquid crystalline ordering is a manifestation of the stacking forces acting between the paired terminal bases of different oligomeric duplexes.[59] Indeed, paired nucleobases are planar polycyclic aromatic hydrocarbons (PAHs), thus

[57] **Onsager**, **L.** 1949, Ann. New York Acad. Sci., Vol. 51, pp. 627-659.
[58] **Zanchetta, G. Nakata, M. Buscaglia, M. Clark, N. A. Bellini, T.** 2008, J. Phys. Condens. Matter., Vol. 20, pp.494214.
[59] **Nakata, M. Zanchetta, G. Chapman, B. D. Jones, . C. D. Cross, J. O. Pindak, R. Bellini, T. Clark**, **N. A.** 2007, Science, Vol. 318, pp.1276.

forming hydrophobic stacking in aqueous solution for avoiding exposure to water, leading to attractive interactions that acts to hold them together, forming aggregates. This lead to the suggestion that the DNA duplex is a kind of chromonic liquid cristal.[60]

It is not surprising that many biological systems exhibit liquid crystalline behaviour due to their intrinsic combination of fluidity and order. These two features are the definition of liquid crystals.

1.3.1 Liquid Crystals: general definition

The liquid crystalline state is a phase of matter which lies between the crystalline solid (order) and the isotropic liquid state (mobility and fluidity). The origin of the anisotropic properties of liquid crystals (LCs) is mainly due to the anisotropy in shape of the constituent molecular unit. Liquid crystal-forming molecules, termed mesogens, are generally divided into calamitic and columnar mesogens. The formation of mesophases (liquid crystalline phases) is due though the use of both temperature (*thermotropic LCs*) and solvent (*lyotropic LCs*).[61,62]

[60] **Lydon, J.** 1998, in Handbook of liquid crystals, ed. D. Demus, J. Goodby, G. W. Gray, H. W. Spiess and V. Vill, Wiley-VCH, Weinheim, Vol. 2B, pp. 98.
[61] **Atwood, J. W. Steed, J. L.** 2009, Supramolecular Chemistry.
[62] **Laschat, K. V. Axenov and S.** 2014, Materials, Vol. 4, pp. 206-259.

1.3.1.1 Thermotropic Liquid Crystals

Thermotropic liquid crystals can be divided in two principal categories based on the building unit molecular shape in: *calamitic* (rod–like mesogens, molecules with a long and cylindrical core with aliphatic chains) and *discotic* (caused by disc-like molecules, containing a flat and circular core surrounded by aliphatic chains) (Fig. 1.14).

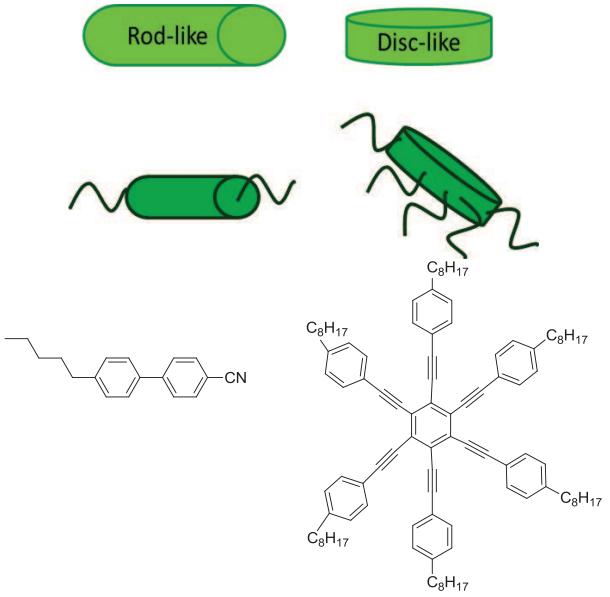

Figure 1.14. Rod-like and disc-like example molecules: 4'-*n*-pentyl-4-cyanobiphenyl as rod-like and hexakis((4-octylphenyl)ethylnyl)benzene as disc-like.

There are three main classes of calamitic mesophases: *nematic* (N), *smetic* (Sm) and *cholesteric*.[60] Nematic phase is characterized by a high degree of long-range orientational order of the molecules but no long-range translational order (Fig. 1.15a). In *smetic* phases, molecules

maintain the general order of the nematic phase but are aligned in layers. The two main smetic phases are smetic A (S_{mA}) and smetic C (S_{mC}). In the smectic A phase, molecules can rotate about their long axes within a given plane in which are orthogonally oriented, but they cannot readily slide past one another (Fig. 1.15b). Small differences between the space filling of the rigid cores and the pendant terminal chains can be compensated by tilting the aromatic cores with respect to the layer normal, giving rise to tilted smectic phases (*e. g.* S_{mC} phase reported in Figure 1.15c). A number of at least 12 different symmetries smetic phases have been characterized (labeled S_A-S_L).

In the cholesteric phase, molecules, instead of lining up in parallel way, are twisting in an ordered fashion. This phase shows very interesting optical properties (Fig. 1.15d).[61]

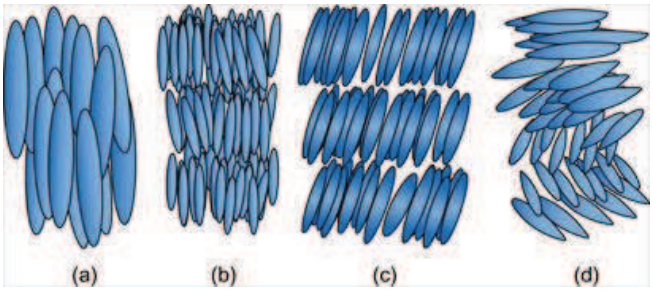

Figure 1.15. Calamitic phases: a) nematic phase, N, b) smectic A phase, SmA, c) smectic C phase, SmC and d) cholesteric nematic phase, N*.

Discotic molecules self-assemble into columns like a pile of coins.[62] Columnar LCs (or discotics) can be divided according to the reciprocal columnar organization in the 2D space. In particular, the symmetry of

the cell geometry arising from the organized columns can be distinct into different categories: columnar hexagonal (Col_h) and columnar rectangular (Col_r) (Fig. 1.16), but also other lower phase symmetries were reported like columnar oblique or tetragonal.

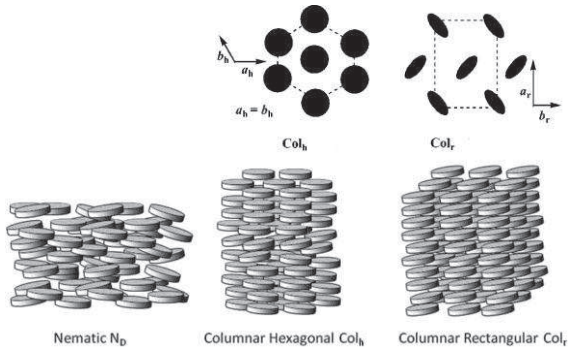

Figure 1.16. Discotic phases, columnar representation and schematic representation of the 2D lattices.

Molecular shape, reduced symmetry, microphase separation and self-organisation are important factors that drive the formation of various liquid crystalline phases. The delicate interplay of the molecular interactions coupled with these factors can induce remarkable phase structures and behaviours.

Both organic and inorganic molecules may form liquid crystalline phases. Metal-containing liquid crystals are called metallomesogens. The discipline of metallomesogens has been actively investigated.[63,64,65,66] Properties such as enhanced electronic

[63] **Donnio, B. Guillon, D. Deschenaux, R. Bruce, D. W**. 2003, Compr. Coord. Chem. II, Vol. 6, Metallomesogens. J. A. McCleverty and T. J. Meyer (Eds.), Elsevier: Oxford.

polarizability and hyperpolarizability, dichroism, paramagnetism and reactivity have been observed or are expected to result on inclusion of a metal centre in a liquid-crystal compound. Further, induced intermolecular interactions, e.g. metal-metal (metallophilic), ligand-ligand and metal-ligand, can have profound consequences on the properties and self-assembling abilities, and often lead to the emergence of new physical properties.

Moreover, metallomesogens allow easy access to non-conventional functional mesomorphic materials because of the huge diversity of organic structures that can be used in coordination complexes, as well as the different coordination geometries provided by the metals.[64] This, in turn may lead to new types of molecular organization and potentially to new mesophase symmetries. The interest comprises both molecular and supramolecular level. An important variety of new structures has been described in the last few years, inconceivable with purely organic compounds.

Another important aspect of the incorporation of metal ions resides in the induction, modification or enhancement of the mesomorphism of the free parent ligands. New rational design methodologies to produce organized molecular assemblies with

---

[64] **Donnio, B. Duncan W. B.** 1999, Liquid Crystals II, Structure and Bonding, Vol. 95, pp. 193-247.
[65] **Serrano, J. L.** 1996, Metallomesogens: Synthesis, Properties, and Applications, Ed. J. L. Serrano.
[66] **Giménez, R. Lydon, D. P. Serrano, J. L.** 2002, Curr. Opin. Solid State Mater. Sci, Vol. 6, Issue 6, pp. 527–535.

specific interactions (*e.g.* dipolar and metal-ligand interactions) are, therefore, not only important but also challenging.

Numerous metallomesogens were reported up to date, based on practically almost all available metals, like Ag(I)[67], Au(I)[68], Zn(II)[69], Pd(II)[70], Pt(II)[71], etc. Indeed, also high coordination number metal complexes can exhibit mesomorphism, although initially it was believed that their bulky geometries were incompatible with mesophases formation. Indeed, with properly designed ligands, liquid crystalline materials are now reported with octahedral Ir(III)[72], Ru(III)[73]

---

[67](a) **Pucci, D. Barberio, G. Bellusci, A. Crispini, A. La Deda, M. Ghedini, M. Szerb, E. I.** 2005, Eur. J. Inorg. Chem., Vol. 12, pp. 2457 – 2463. (b) **Pucci, D. Barberio, G. Bellusci, G. *et al.*** 2005, Mol. Cryst. Liq. Cryst., Vol. *441*, pp. 251 – 260. (c) **Pucci, D. Barberio, G. Bellusci, A. Crispini, A. Donnio, B. Giorgini, L. Ghedini, M. La Deda, M. Szerb, E. I.** 2006, Chem. Eur. J. Vol. 12, pp. 6738-3747. (d) **Bellusci, A. Chedini, M. Giorgini, L. Gozzo, F. Szerb, E. I. Crispini, A. Pucci, D.** 2009, Dalton Trans., pp. 7381-7389. (e) **Pucci, D. Crispini, A. Ghedini, M. Szerb, E. I. La Deda, M.** 2011, Dalton Trans., **Vol.** 40, pp. 4614 – 4622. 2013. (f) **Szerb, E. I. Pucci, D. Crispini, A. La Deda, M.** 2013, Mol. Cryst. Liq. Cryst., **Vol.** 573, pp. 34 – 45.

[68] **Fujisawa, K. Kawakami, N, Onishi, Y. Izumi, Y. Tamai, S. Sugimoto, N. Tsutsumi, O.** 2013, J. Mater.Chem. C, Vol. 1, pp. 5359-5366.

[69] **Pucci, D. Crispini, A. Ghedini, M. La Deda, M. Liguori, P. F. Pettinari, C. Szerb, E. I.** 2012, *RSC Adv.,* **Vol.** 2, pp. 9071 – 9078.

[70] **Ghedini, M. Pucci, D. Crispini, A. Aiello, I. Barigelletti, F. Gessi, A. Frnacescangeli O.** 1999, Appl. Organometal. Chem., Vol13, pp. 565–581.

[71] **Ghedini, M. Pucci, D. Crispini, A. Barberio, G.** 1999, Organometallics, Vol. 18, pp. 2116-2124.

[72] (a) **Szerb, E. I. Talarico, A. M. Aiello, I. Crispini, A. Godbert, N. Pucci, D. Pugliese, T. Ghedini, M.** 2010, Eur. J. Inorg. Chem., pp. 3270 – 3277. (b) **Santoro, A. Prokhorov, A. M. Kozhevnikov, V. N. Whitwood, A. C. Donnio, B. Williamsand, J. A. G. Bruce, D. W.** 2011, J. Am. Chem. Soc., Vol. 133, pp. 5248–5251.

metal ions, or even with the higher coordination number complexes of lanthanide metal ions[74].

As stated before, with properly designed ligands, a wide variety of mesophases and symmetries can be induced in metallomesogens. In Fig. 1.17 are presented examples of Ag(I) metallomesogens exhibiting columnar mesophases of different symmetries depending on the nature of the bipyridine ligand substituents and the counterions.

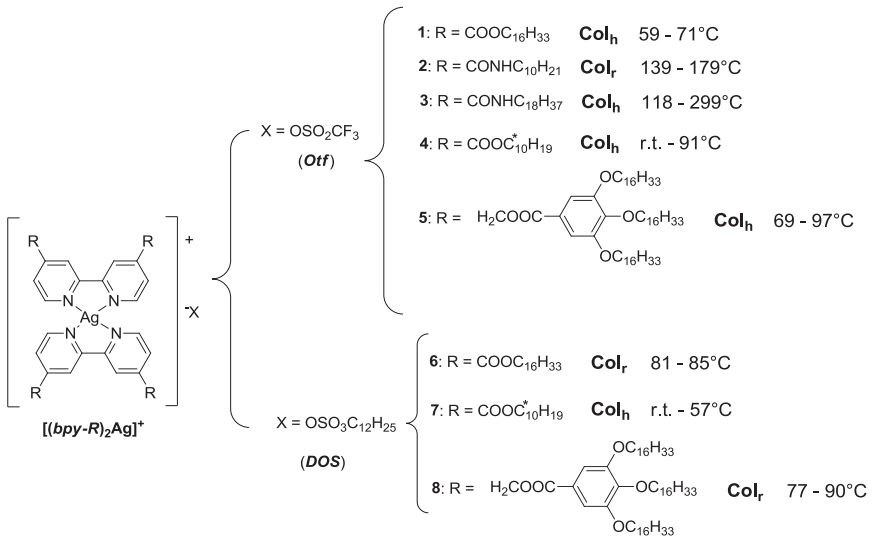

Figure 1.17. Chemical structure and mesomorphism for ionic Ag(I) complexes containing two bipyridine-based ligands.[67-75]

---

[73] **Pucci, D. Bellusci, A. Crispini, A. Ghedini, M. Godbert, N. Szerb, E. I. Talarico, A. M.** 2009, J. Mater.Chem., Vol 19, pp. 7643–7649.

[74] (a) **Szerb, E. I. Crispini, A. La Deda, M. Pucci, D. Liguori P. F. Petinari, C.** 2011, Mol. Cryst. Liq. Cryst., Vol. 549, pp. 86–99. (b) **Binemmans, K.** 2009, J. Mater. Chem., Vol. 19, pp. 448–453.

[75] **Pucci, D. Barberio, G. Bellusci, A. Crispini, A. Ghedini, M. Szerb, E. I.** 2005, Mol. Cryst. Liq. Cryst., Vol. 441, pp. 251.

1.3.1.2 Lyotropic Liquid Crystals

Lyotropic liquid crystals form mesophases by the combined action of solvent and temperature. Conventional lyotropic liquid crystal molecules contain flexible rod-shape aliphatic chains ending with ionic groups. One example is the potassium palmitate reported in figure 1.18.[76]

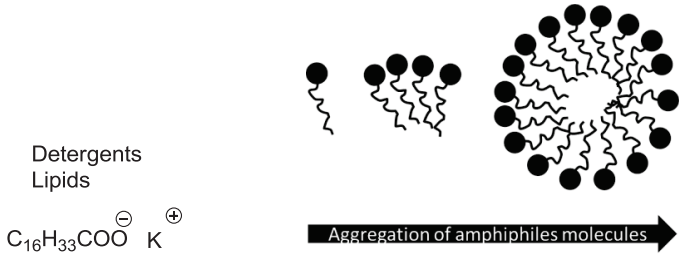

Figure 1.18. Amphiphilic molecules.

Generally, mesogenic molecules able to form lyotropic mesophases in solvents (mostly water) are usually amphiphilic in nature (dual hydrophilic/hydrophobic character).[59] The ambivalent nature of an amphiphile leads to a competition between the hydrophilic parts, attempting to increase their contact with water, and the hydrophobic ones trying to avoid it. Therefore, in high enough concentrations, beyond the so-called critical micelle concentration (*cmc*), the molecules arrange themselves into micellar aggregate,s with defined topologies, such as hollow spherical, rod-, and disc-like micelles, in which the segregation in space occurs, keeping unlike parts

[76] **Patel, P. J. Collins J. S.** *Handbook of liquid crystal research.* New York : Oxford University Press, 1997.

isolated from unlike solvent (Fig. 1.18). With a further increase of concentration, the micelles begin to interact and to self-assemble into ordered arrays of supramolecular aggregates or lyotropic mesophases. The occurrence of the mesophase is thus driven by the hydrophilic/hydrophobic balance, packing constraints (chain and surface areas) and solvent effects. The nature of the mesophase is strongly connected to the type of aggregation, and the curvature between the polar/apolar interface. For instance, disc-like micelles will form nematic (discotic, N_D), and lamellar L_α phases, cylindrical micelles will give rise to columnar organisations such as columnar nematic (N_{Col}), and columnar (hexagonal, H, and rectangular, R) phases, and spherical micelles will arrange themselves into micellar cubic phases.[77]

Chromonic liquid crystals are considered to be a special sub-class of lyotropic liquid crystals, in which molecules with structures completely different than the conventional amphiphilic mesogens arrange themselves in solvent generating mesophases.

1.3.2 Chromonic Liquid Crystals

Chromonic liquid crystals (CLC) have recently attracted the attention of researchers because of their unique properties consisting in the combination of liquid crystalline properties (self-ordering, ease of alignment, sensitivity to changing conditions and additives) coupled with their optical and electro-optical properties. These characteristics

[77] **Donnio, B.** 2002, Curr. Opin. Colloid Interface Sci, Vol. 7, pp. 371,394

make possible the development of a range of sophisticated devices, including polarizers, optical compensators, light-harvesting devices and micropatterned materials.[78,79,80,81,82,83,84,85] Furthermore, the fact that they are water-based makes them ideal candidates in biosensors for medical diagnosis.[81,86] The most extensively studied chromonic mesogen is the disodium cromoglycate (DSCG reported in Figure 1.19), an antiasthmatic drug studied initially by Woodard and co-workers in the 1970s and then investigated more extensively by Lydon and co-workers.[60,61] Studying the DSCG it was discovered that this compound, with V-shape, formed two novel liquid crystalline birefringent phases when dissolved in water. Several investigations have also shown that the structural units in both mesophases are columns of stacked molecules.

---

[78] **Tam-Chang, I. K. Iverson and S.** 1999, J. Am. Chem. Soc., Vol. 121, pp. 5801-5802.

[79] **Matsunaga, D. Tamaki, T. Akiyama H. Ichimura, K.** 2002, Adv. Mater., Vol. 14, pp. 1477.

[80] **Iverson, I. K. S. Casey, M. Seo, W. Tam-Chang, S.** 2002, Lagmuir, Vol. 18, pp. 3510-3516.

[81] **Nastishin, Y. A. Liu, H. Schenider, T. Narazemko, V. Vasyuta, R. Shiyanovskii, S. V. Lavrentovich, O. D.** 2005, Phys. Rev. E: Stat., Nonlinear, Soc. Matter. Phys., Vol. 72, p. 041711.

[82] **Lavrentovich, O. D. et al.** 7, 294, 370, 13 US Pat., November 2007.

[83] **Nazarenko, V. G. Boiko, O. P. Park, H. S. Brodyn, O. M. Melchenko, M. M. Tortora, L. Nastishin Y. A. Lavrentovich, O. D.** 2010, Phys. Rev. Lett., Vol. 105, pp. 017801.

[84] **Simon, K. A. Burton, E. A. Cheng, F. Varghese, N. Falcone, E. R. Wu L. Luk, Y.** 2010, Chem. Mater., Vol. 22, pp. 2434-2441.

[85] **Lydon, J.** 2010, Mater. Chem., Vol. 20, pp.10071-10099.

[86] **Helfinstine, S. L. Lavrentovich O. D. Woolverton, C. J.** 2006, Lett. Appl. Microbiol., Vol. 43, pp. 27-32.

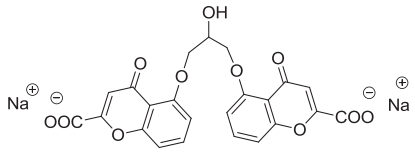

Figure 1.19. The molecular structure of disodium cromoglycate.

Chromonics were considered as a sub-class of lyotropic liquid crystals with well-defined new liquid crystalline structures and properties.[60,61] A breakthrough in the history of this class of compounds was the realization that chromonic phases are formed by a range of drugs, dyes and nucleic acids and similar water soluble, aromatic molecules, and have distinct and well defined structures and properties.

Although the behaviour of these dynamic 'soft' phases is not completely understood yet, Lydon, Attwood and co-workes showed the main differences between the chromonic molecules and the conventional amphiphilic lyotropic ones.[60,61] Chromonic molecules generally lack of amphiphilic nature. The presence of a planar and aromatic π-delocalised core (with a disc-like shape) and solubilizing groups (*e.g*. CO_2^-, SO_3^-) at the periphery of the molecules, are the main characteristics of this type of liquid crystals. In a polar solvent, molecules tend to aggregate into stacks due to electrostatic interactions, hydrophobic and $\pi-\pi$ stacking interactions between the aromatic cores.[83]

At all concentrations, there is some degree of aggregation and as the concentration increases, the distribution of the aggregates size

shifts to higher and higher numbers of molecules. Therefore, instead of exhibiting a critical micellar concentration like the conventional lyotropic amphiphiles (*cmc*), these systems show isodesmic aggregation.[87] If the concentration is high enough to form large and interacting rod-like aggregates, liquid crystalline phases are formed.

There are two principal chromonic mesophases, which have become known as the N (nematic) and M (hexagonal) phases. In the N phase columns lie in a nematic array, with no positional order (similar to thermotropic nematic N_{col} phases) (Fig. 1.20a). On the other hand, the M phase is obtained by columns arranged in a hexagonal lattice (Fig. 1.20b).

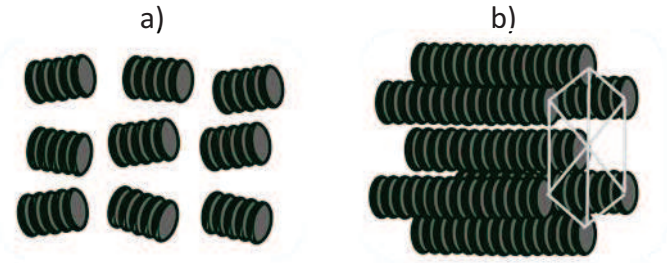

Figure 1.20. The structure of the chromonic N (a) and M (b) phases.

In many aspects, chromonic systems are closer to columnar thermotropic LCs than to conventional amphiphiles. There is a noticeable correspondence between the chromonic M and the thermotropic Col_h phases, with columns lying in a hexagonal lattice in both cases. The principal difference consists in the fact that in the

[87] (a) **Maiti, P. K. Lansac, Y. Glaser, M. A. Clark, N. A.** 2002, *Liq. Cryst*., Vol. 29, pp. 619-626 (b) **Tomasik M. R. Collins, P. J.** 2008, *J. Phys. Chem. B*, Vol. **112**, pp.9883-9889 (c) **Collings, P. J. Dickinson A. J. Smith, E. C.** 2010, *Liq. Cryst*. Vol. **37**, pp. 701-710.

thermotropic columnar phase the columns lie in a sea of alkyl chains, whereas the chromonic columns lie in a sea of water. Furthermore, there may be a chromonic analogue of the Col_r with columns arranged in a rectangular lattice (chromonic O phase) and perhaps chromonic phases analogous to the tilted columnar phases (H and J aggregates).[78] However this comparison should not be carried too far, because no chromonic analogue of the thermotropic N_D phase has been encountered and there is usually a distinction in terms of the molecular shape, with columnar molecules being approximately circular discs and chromonic molecules being distinctly bladelike.

The formation of conventional amphiphilic mesophases is based on the aggregation of molecules in solution (micelle previously reported in Figure 1.21). In contrast, for chromonic systems, the fraction of the total molecular surface exposed to the solvent decreases as the columns lengthen, but there is no optimum aggregate size directly comparable to a micelle (Fig. 1.21).[85]

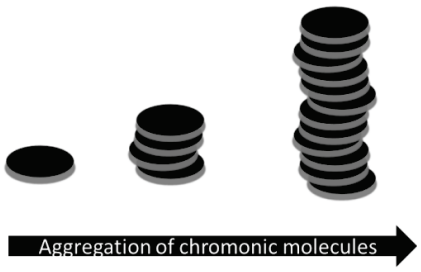

Figure 1.21. Chromonic aggregation of molecules.

The stability of these phases depends on both temperature and concentration. The majority of chromonic liquid crystals (CLCs) reported to date are based on organic system featuring the properties highlighted above (Figure 1.22a,b). Nevertheless, lately also some metal complexes have been shown to form CLC phases. Metal complexes have broad range of oxidation states and coordination geometries offering new opportunities for the design of original CLC mesophases, rendering them advantageous over their organic counterparts. Indeed, metal complexes may offer different functionalities, modulated by the type of coordinated ligands, as well as intriguing spectroscopic, catalytic and redox properties.[77]

The first molecules reported to exhibit chromonic mesophases in acqueous ammonia solution were copper(II) and cobalt(II) complexes of sodium tetracarboxylatophthalocyanine (Figure 1.22c).[88] These molecules have a structure compatible with the main principles of designing chromonic molecules, respectively they have charged large aromatic groups able to stack into columns by π–π interactions and solubilising groups at the periphery. Several other similar systems were further synthesised and investigated, mainly phthalocyanines and porphyrins metal complexes. They arranged in water solution only in columnar mesophases. It was shown that the stability of the mesophases strongly depends on the nature, number and position of the solubilising groups decorating the periphery of the macrocyles and to a lesser extent on the type of metal and aromatic core. The role of

[88] **Gaspard, S. Hochapfel, A. Viovy, R.** 1979, C. R. Acad Sci Paris C, Vol. 289, pp. 378-390.

the metal was considered not to be essential in the formation of the columnar mesophases in that the disc-like free-bases have themselves a natural tendency to stack into columns. However, depending on the valence and oxidation state of the metal centre, its introduction may preclude the stacking of the macrocyles into columns, and thus the mesophase formation.

Recent studies have also revealed that d^8 metal complexes such as that of platinum(II) with planar coordination geometry can form nanostructures driven by intermolecular metal-metal and/or ligand–ligand interactions.[89,90] In particular, phosphorescent cationic organoplatinum (II) complexes (Figure 1.22d) were reported to exhibit chromonic phases with high viscosities in aqueous solution. The principal features of these complexes were: the absence of long aliphatic chains, attractive metallophilic $d^8 \cdots d^8$ together with ligand-ligand interactions and hydrophilic counterions.

[89] **Lu, W. Chen, Y. Roy, V. A. L. Sin-Yin S. Che. C-M.** 2009, Angew. Chem. Int. Ed., Vol. 48, pp. 7621-7625.
[90] **Xiao, X-S. Lu W. Che, C-M.** 2014, Chem. Sci. , Vol. 5, pp. 2482-2488.

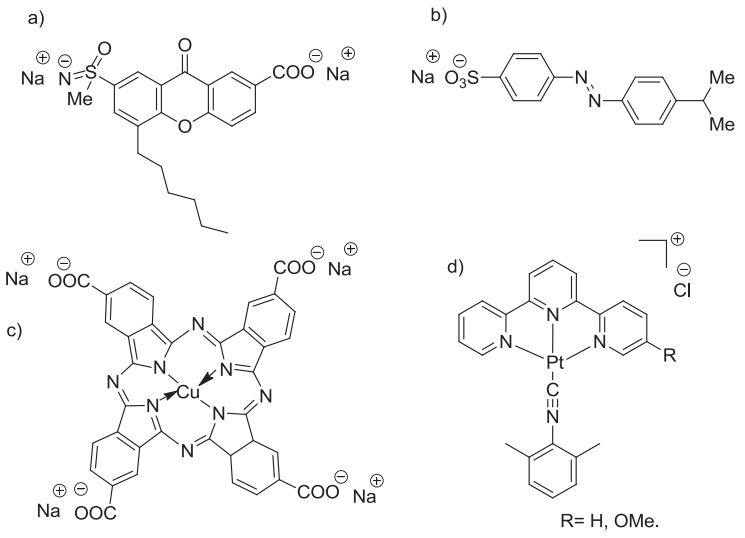

Figure 1.22. Chromonic molecules, (a) RU 31156, (b) Methyl orange and (c) Copper tretacarboxyphthocyanine, and (d) Pt(II) complex.

Polarized optical microscopy (POM) is one of the techniques commonly used to characterized generally liquid crystals, and in particular chromonic mesophases. N and M phases of DSCG are reported in Figure 1.23.[91] Unoriented samples of the N chromonic phase show the typical schelieren texture of a low-viscosity nematic liquid crystalline phase. The M phase is more viscous than N phase and has a grainier texture with herringbone zones, indicating a higher degree of ordering. In fact, the letters N and M used to designate the two principal types of chromonic phases, originated from these optical textures, the letter N from the similarity of the texture shown by this to that formed by thermotropic nematic systems, and respectively the

[91] **Lydon, J.** 2011, Liquid Crystals, Vol. 38, pp. 1663-1681.

letter M because similar herringbone textures were previously identified in the 'middle' phases of conventional amphiphile systems.[60]

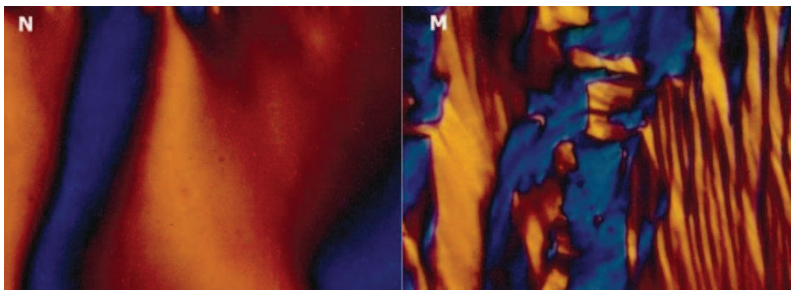

Figure 1.23. Optical textures of the chromonic N and M phases of DSCG.

In addition to POM characterization, X-Ray diffraction is an important technique for differentiating chromonic phases. The diffraction patterns of nematic and hexagonal phases show a high–angle reflection corresponding to the face-to-face aromatic stacking repeat distance of about 3.4 Å within columns. The position of this peak does not change with temperature or concentration or for one compound to another. The N phase gives a diffuse inner axial reflection corresponding of the column-to-column distances. In the M phase pattern, this is replaced by several moderately sharp reflections in the ratio $1:1/\sqrt{3}:1/\sqrt{4}$ characteristic of a hexagonal phase (Fig. 1.24).

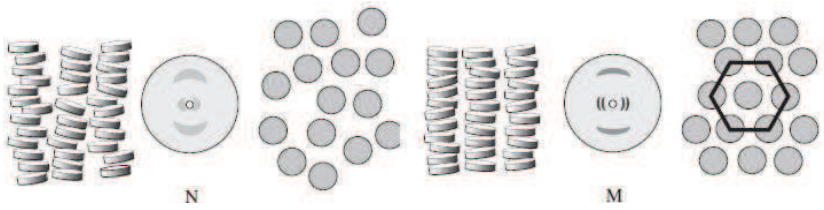

Figure 1.24. X-ray diffraction patterns of the chromonic N and M phases.

Miscibility is another important feature of liquid crystalline systems. Miscibility is the property of substances to mix in all portions, forming an homogeneous solution. Complete miscibility between chromonic liquid crystals and various molecules has been found in only few cases, but the intercalation of water soluble aromatic species in chromonic system appears to be widespread. The intercalation of coloured dyes into chromonic systems has proved to be a rewarding study. One example very well studied is the dissolution of ethidium bromide in the DSCG mesophases.[92] When the stain is intercalated shows a strong fluorescence, meaning that is dissolved inside the columns and not in the presence of water molecules which quenches its emission. Generally the changes of fluorescence in coloured dyes are an indicator of their intercalation.

Concluding, it was shown that in conventional chromonic systems (Fig. 1.25a), molecules with an aromatic planar core and solubilizing groups at the periphery organize themselves in columns through electrostatic and $\pi-\pi$ interactions. Several studies of DNA have shown similar lyotropic liquid crystalline behaviour, with a validated chromonic nature for short length chains, the mechanism of self-assembly being assured by the presence of the bases with planar aromatic core and the phosphate chain at the periphery, therefore by hydrophobic, electrostatic and $\pi-\pi$ interactions (Figure 1.25b). The discovery of liquid crystalline phases of DNA solutions and the

[92] **Mundry, K. Sleep, J. C. Lydon, J. E.** 1995, Liquid Crystals, Vol. 19, 1, pp. 107-112.

possibility that the same dyes intercalate in DNA and chromonic systems, allows the use of chromonic systems as possible DNA model to test intercalation agents (Fig. 1.25c,d). Moreover, the miscibility property gives the possibility to use chromonic liquid crystals as a potential intercalator.[60]

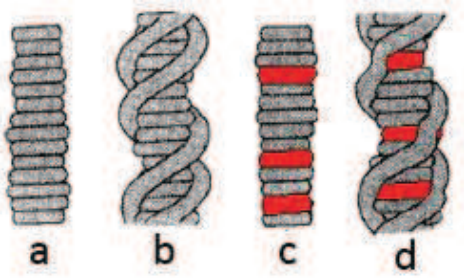

Figure 1.25. a)Chromoni aggregation, b) DNA chain, c) Intercalation of a gest molecule in a chromonic system and d) Intercalation of a guest molecule in DNA.

1.4 Metal-based drug co-crystals

Since the development of numerous oral anticancer agents (and therefore drugs in their solid state) the methods to achieve metal based drugs with improved solubility and bioavailability has significantly increased.

An important aspect of drug development is determining which specific solid form of an active pharmaceutical ingredient (API) should be selected. This process is a nontrivial exercise, since API can be polymorphic, due to the presence of the exterior groups. Polymorphs are defined as crystalline forms with distinct crystal structures of the

same chemical compound. A critical part of the drug development is the investigation of the polymorphic behaviour of an API, because polymorphism can greatly influence pharmaceutical properties, such as stability, solubility, bioavailability, etc. [93]

Frequently, the crystalline forms of an API exhibit low solubility, and it might be appropriate to use a more soluble multicomponent form such as salts in the case of ionisable APIs and co-crystals form for neutral APIs.

Salts formation is one of the primary solid-state approach used to modify the physical properties of an API. Salt formation is an acid-base reaction between the API and the acidic or basic substance (Fig. 1.26).[94] Salt formation is a two component system, having an acid (A), a base (B) and one or more solvents. A salt is formed by transfer of a proton (H^+) from an acid (A) to a base (B):

$$A - H + B \rightarrow (A^-)(B^+ - H)$$

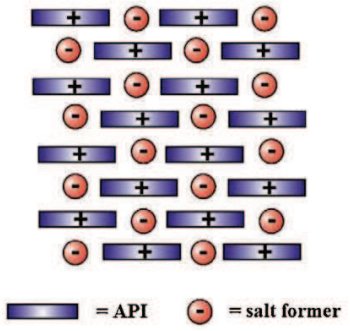

Figure 1.26. Schematic representation of API salts.

[93] **Aitupamula, S. Chow, P. S. Tan, R. B. H.** 2014, Cryst. Eng. Comm., Vol. 16, pp. 3451.
[94] **Thakuria, R. Delori, A. Jones, W. Lipert, M. P. Roy, L. Rodríguez Hornedo, N**. 2013, Int. J. of Pharm., Vol. 453, pp. 101-125.

However, a major limitation within this approach is that the API must possess a suitable ionisable site. Co-crystals are an alternative to salts when the API does not have the appropriate structural properties in order to be ionized.

Various definitions of co-crystals have appeared in the literature, but a simple working definition can be taken as "a stoichiometric multi-component system connected by non-covalent interactions where all the components present are solid under ambient conditions". [95]

In recent years, the study of co-crystals has generated considerable interest in their potential use in the pharmaceutical field. A pharmaceutical co-crystal is considered to be composed of an active pharmaceutical ingredient (API) and an appropriate coformer (molecules compatible with a particular API, usually organic molecules) held together by weak interactions (Fig. 1.27).[93] The co-crystallization improves the physicochemical properties of the API and its bioactivity.

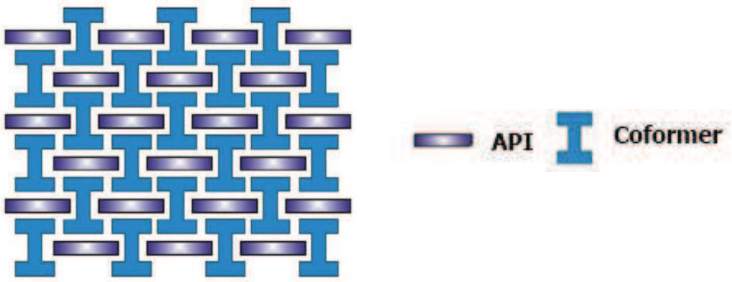

Figure 1.27. Schematic representation of API co-crystals.

[95] (a) **Aakeroy, C. B. Salmon, D. J.** 2005, CrystEngComm., Vol. 7, pp. 439-448.(b) **Bholanga, B. R. Nangia, A.** 2008, New. J. Chem., Vol. 32, pp. 800-807. (c) **Jones, W. Motherwell, W. D. S. Trask, A. V.** 2006, MRS Bulls, Vol. 31, pp. 875-879.

Co-crystals contain two or more components with complementary geometries (such as host/guest) which are held together by the presence of supramolecular synthons. The API structures need to contain exterior functional groups interacting with specific coformer to obtain co-crystals. Supramolecular interactions typically involving non covalent interactions are hydrogen bonds, halogen bonds and π–interactions. One example of hydrogen bonds supramolecular synthon typical of some co-crystals is the carboxylic acid/amide and carboxylic acid/aromatic nitrogen (Fig. 1.28).

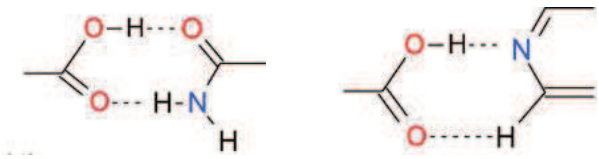

Figure 1.28. Hydrogen bonds in supramolecular heterosintons.

Synthesis of co-crystals as well as salts can be accomplished by several methods, primarily by solid state synthesis.

In the last years, the research related to the synthesis of molecular materials through mechanochemical methods has been recognized as an alternative to solvent-based methods. Mechanochemical synthesis is used for two reasons: firstly, because is effective and advantageous in ever-widening types of synthesis and secondly, because is defined as a solvent-free synthesis, important for avoiding the implications for environmental contamination.

Mechanochemistry is concerned with chemical transformations induced by mechanical means, such as compression, shear, or friction.

Mechanochemistry has been applied to the synthesis of supramolecular systems such as co-crystals.[96]

Solid state synthesis can be as simple as grinding two reactants by manual methods (in a pestle and mortar) or non-manual methods (such as ball milling) (Fig. 1.29). There are two techniques for the synthesis *via* grinding: neat (dry) grinding consists of mixing co-crystal components together, and respectively liquid assisted grinding, where a small amount of liquid is added to the grinding mixture.

Figure 1.29. Grinding manual or mechanical.

In contrast to neat grinding, in liquid assisted grinding there is a small amount of a liquid phase (not expected to diminish during the reaction), acting as a lubricant for the reaction and providing a medium to facilitate mixture.

In the last years, also a new technique to obtain co-crystals was used. The rapid evaporation of a specific solvent solution of compounds *via* rotary evaporator (rotavap) is useful to obtain a

[96] **James, S. L. Adams, C. J. Bolm, C. Braga, D. Collier, P. Friscic, T. Grepioni, F. Harrism K. D. M. Hyett, G. Jones, W. Jrebs, A. Mack, J. Maini, L. Orpen, A. G. Parkin, I. P. Shearouse, C. Steed, J. W. Waddell, D. C.** 2012, Chem. Soc. Rev., Vol. 41, pp. 413-447.

number of possible co-crystal forms simultaneously. The method is easy to operate, and in particular, consists in the preparation of a stoichiometric solution of the corresponding API and coformers in a selected solvent. Subsequently, the solvent has to be dried rapidly under pressure by using the rotavap and when the solvent evaporation is completed, the obtained dry powders have to be collected and characterized. This technique provides an alternative route to the solid state mechanochemical methods due to the increase of products yields.[97]

There are many examples of co-crystals of organic molecules. In contrast, metal-based drugs co-crystals are very unusual due to the difficulty to find a complementarity in shape between the metal-based API and the suitable coformer.[98]

1.4.1 Organic co-crystals

Several organic co-crystals have been published, where the crystal engineering facilitates the discovery of pharmaceutical co-crystals with better properties than the original API. Some examples will be reported below.

Carbamazepine (CBZ) is an anti-epileptic drug with low water solubility. The poor solubility has led to the synthesis of several CBZ co-crystals by using as coformers benzoquinone, nicotidamide or formic

[97] **Bag, P. P. Patni, M. Reddy, C. M.** 2011, Cryst. Eng. Comm., Vol. 13, pp. 5650.
[98] **Sasmal, S. Hazra, S. Sarkar, S. Mohanta, S.** 2010, J. Coord. Chem., Vol. 63, 10, pp. 1666-1677.

acid. The most studied CBZ co-crystal has been obtained by using saccharin as coformer. The interactions between CBZ and saccharin in the derived co-crystal, have been observed by using single crystal X ray analysis, as reported in Figure 1.30. The co-crystal is held by C=O···H-N hydrogen bonds and C-H···O interactions between CBZ and saccharin. This new co-crystal shows significantly improved stability and favourable pharmacokinetics when compared to the API.[99]

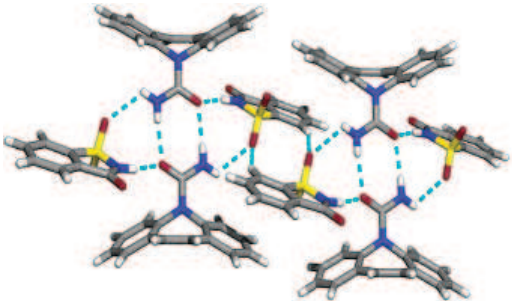

Figure 1.30. Organic co-crystals: Sac= Saccharin, CBZ= Carbamazepine, CBZ-Sac= Co-crystal Carbamazepine-Saccharine.

Tadalafil (TDF), for example, is used for the erectile dysfunction treatment and is also is being investigated as a treatment for pulmonary arterial hypertension. This compound presents a longer half-life but a slower onset of action, probably caused by the low aqueous solubility. To improve its solubility, several pharmaceutical acceptable alcohols, methylparaben (MPB), propylparaben (PPB) and hydrocinnamic (HBA) have been selected as coformers for the TDF co-crystallization. The structures were determined by single crystal X-Ray

[99] **Fleischman, S. G. Kuduva, S.S. McMahon, J.A. Moulton, B. Bailey Walsh, R.D. Rodríguez Hornedo N. Zaworotko, M. J. Crys.** 2003, Growth Des., Vol. 3, 6, pp. 909-919.

analysis, and TDF molecules are observed to be linked by N-H···O hydrogen bonds with coformers forming the supramolecular structures (Fig. 1.31).[100]

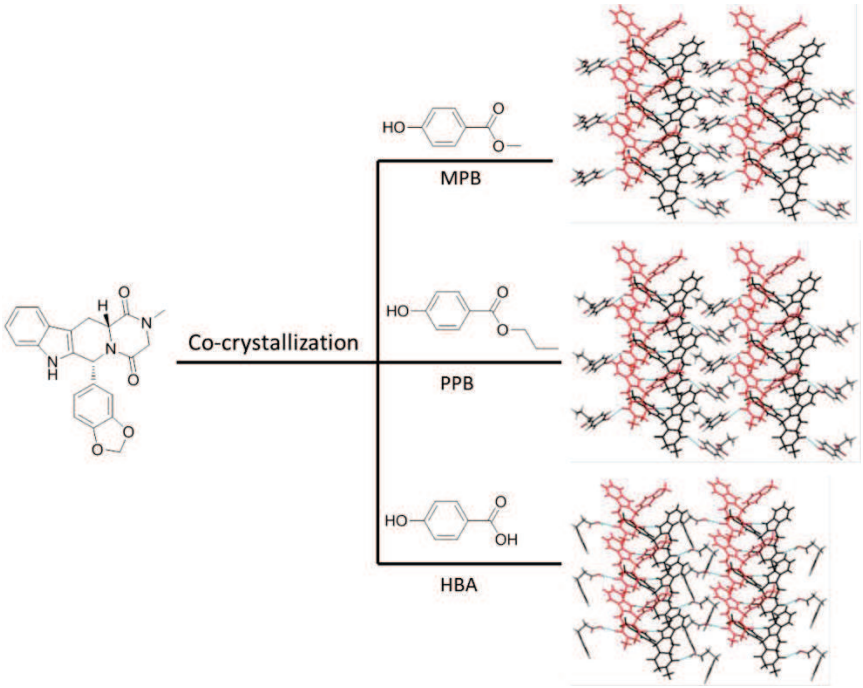

Figure 1.31. Crystal packing of Tadalafil and pharmaceutical acceptable alcohols.[100]

Curcumin is a spice derived from the rhizome of the herb *Curcuma Longa*. Curcumin possesses different pharmacological activities, but the effectiveness of this compound is limited by low solubility and poor bioavailability in aqueous medium. The molecules exist as keto-enol tautomes. The instability of curcumin may be ascribed to the β-diketone linker in the seven carbon atom chain. Co-cristallization of

[100] **Weyna, D. R. Cheney, M. L. Shan, N. Hanna, M. Wojtas Q. Zaworotko, M. J.** 2012, Cryst. Eng. Comm., Vol. 14, pp. 2377-2380.

curcumin with resorcinol increases the solubility and improves stability compared to free curcumin (Fig. 1.32).[101]

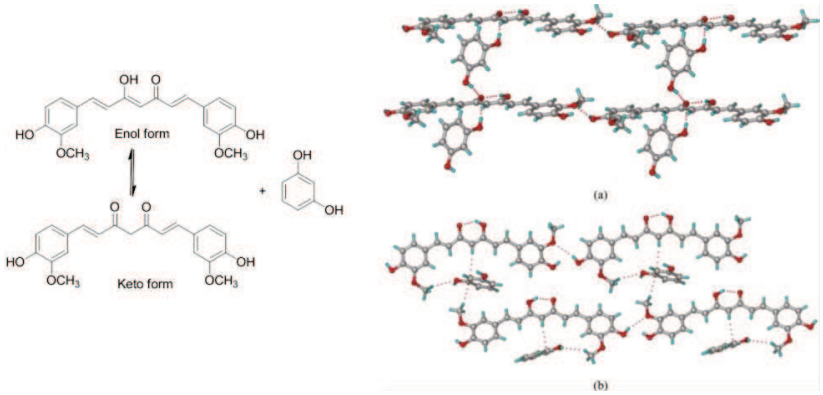

Figure 1.32. (a) A O-H···H hydrogen bonds between curcumin and resorcinol molecules. (b) O-H···O, C-H···O and C-H···π intercations between curcumin and resorcinol molecules.

1.4.2 Inorganic Co-crystals

The majority of transition metal complexes incorporate ligands that are directly linked to the metal centre, and constitute the first-sphere of coordination. However, further ligands can bind to the first-sphere of the metal complex as a result of non-covalent interactions, affording second-sphere coordination. In the last years the second-sphere coordination has been studied for co-crystallization.

The literature shows that there is only a limited number of reports for the preparation of metal complexes co-crystals.

[101] **Sanphui, P. Goud, N. R.. Khandavilli U.B. R Nagia, A**. 2011, Cryst. Growth Des., Vol. 11, pp. 4135-4145.

For example, the study of the co-crystallization processes between the complex [Ni(valphen)] (the chemical structure of the ligand valphen is reported in Figure 1.33) and ammonium salts led to different supramolecular arrangements in the crystals depending on the host/guest ration used in the reactions.[102] In particular, the co-crystallization between [Ni(valphen)] and ammonium perchlorate in a 2:1 molar ratio, afforded co-crystals with the composition $2[Ni(valphen)]\cdot NH_4ClO_4$. The supramolecular dimer is established *via* $\pi-\pi$ interactions with the neighbouring dimers *via* the aromatic rings. The ammonium ion is sandwiched between two [(Ni(valphen)] (Fig. 1.34). On the other hand the co-crystallization between [Ni(valphen)] and ammonium perchlorate in a 4:3 ratio, affords co-crystals with the composition $4[Ni(valphen)]\cdot 3NH_4ClO_4$. Three ammonium cations are sandwiched between four [(Ni(valphen)]entities resulting a complex with a quadruplex deck architecture (Fig. 1.35).

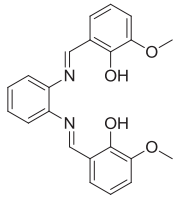

valphen

Figure 1.33. Valphen molecule

[102] **Cucos, A. Ursu, A. Madalan, A. M. Duhayon, C. Sutter, J. P. Andruh, M.** 2011, Cryst. Eng. Comm., Vol. 13, pp. 3756-3766.

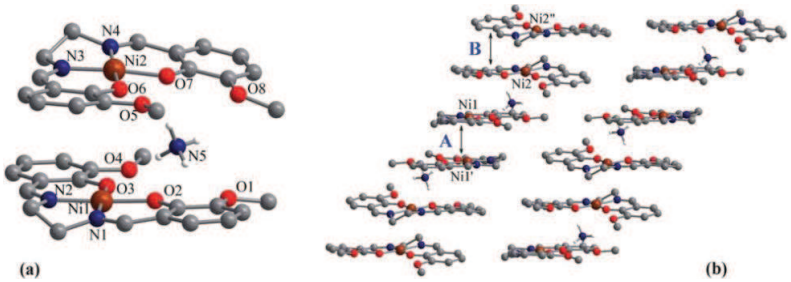

Figure 1.34. (a) 2[Ni(valphen)]·NH_4^+ structure and (b) packing diagram showing the π–π intercations.

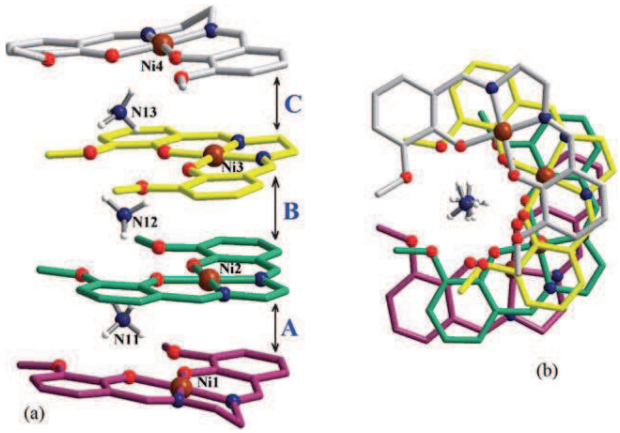

Figure 1.35. (a) side and (b) top view of co-crystal [Ni(valphen)]·$3NH_4^+$.

Co-crystallization sometimes happens by serendipity. The synthesis of the metal complex $[(bpy\text{-}OH)_3Zn](PF_6)_2$ (bpy-OH= 4,4'-bis(dimethoxy)-2,2'-bipyridine) reported in Figure 1.36a showed an unexpected product, the co-crystal $\{[(bpy\text{-}OH)_3Zn](PF_6)_2\}\cdot(bpy\text{-}OH)\cdot 2H_2O$ reported in Figure 1.36b.[103] The crystalline structure of this Zn (II) complex proved the inclusion into the crystalline framework of a free un-coordinated ligand molecule. The un-coordinated ligand,

[103] **Yadav, Y. J. Mastropietro, T. F. Szerb, E. I. Talarico, A. M. Pirillo, S. Pucci, D. Crispini A. Ghedini, M.** 2013, New J. Chem.,Vol. 37, pp. 1486.

adopting the *N,N trans* conformation typically observed for the pure ligand, is sandwiched between two crystallographically equivalent [(bpy-OH)$_3$Zn] cations, generating a sort of supramolecular tetracationic adduct. π–π stacking interactions and hydrogen bonds established between coordinated and co-crystallized ligands are responsible for the formation of the new tetracationic complex.

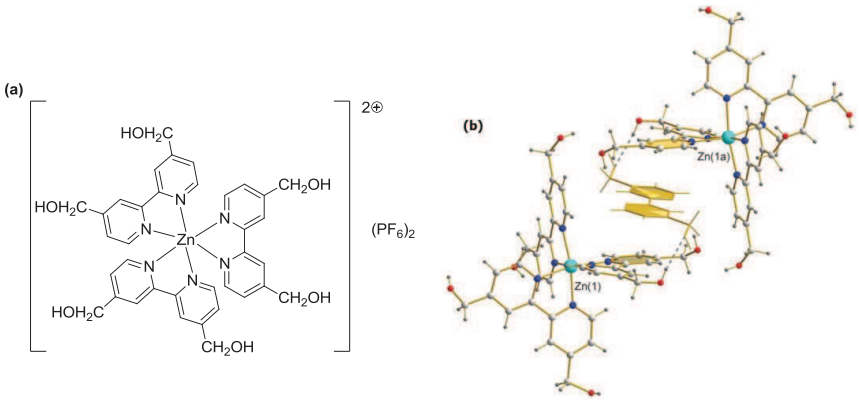

Figure 1.36. View of the suramolecular tetra-cationic complex supported by π–π stacking and weak hydrogen bonding intercations.

The importance of hydrogen bonds in obtaining this structure was further confirmed by the attempt to obtain the same supramolecular tetracationic adducts using analogues bipyridine ligand, but which lack of hydroxyl groups. Indeed, substantial differences in terms of stoichiometry, supramolecular organization and photophysical properties of the final products have been observed when using a (4,4'-bis(methoxy)-2,2'-bipyridine). In this case, regardless of the type of synthesis or reaction conditions, always a simple octahedral tricoordinated ionic complex was obtained.

Chapter 2

Synthesis and characterization of M(II) complexes (M(II)= Zn, Cu) containing aromatic nitrogen ligands

All the Zn(II) and Cu(II) derivatives therein reported have been synthesized by adapting new synthetic strategies according to the type of the complex desired. The new complexes have been characterized in the solid state by using IR spectroscopy, thermal analysis (TGA, thermogravimetric analysis) and, when possible, single crystal X-Ray diffraction.

Moreover, the characterization in solution has been performed by ^{1}H NMR spectroscopy (in the case of Zn(II) complexes), conductivity measurements (in order to define the eventual ionic nature of the new derivatives) and UV-vis spectroscopy (in order to evaluate their stability both in water and in physiological conditions as well as their eventual emissive properties).

2.1 4,4'-dinonyl-2,2'-bipyridine (bpy-9) Zn(II) and Cu(II) complexes

Recently, new fluorescent complexes with antitumoral activity showing an alternative mechanism of action than cisplatin have been synthesized. One example is the neutral complex [(bpy-9)Zn(curc)Cl], **A**, reported in Figure 2.1.[2] The molecular structure of complex **A** showed the Zn(II) ion in a five-coordinated distorted square pyramidal geometry. In particular, the basal plane is formed by the two chelating ligands, namely 4,4'-dinonyl-2,2'-bipyridine (bpy-9) and curcumin (curc) respectively, while a chloride ion is located on the apex of the pyramid (Fig. 2.1).

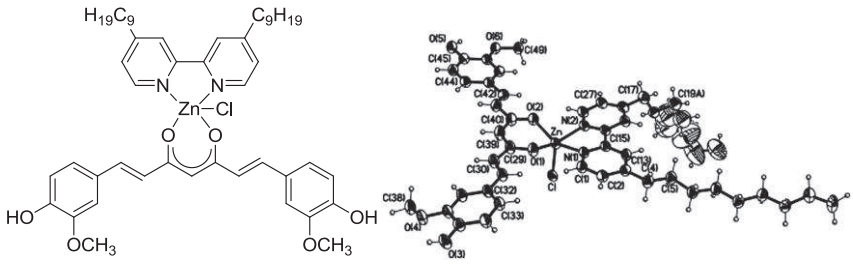

Figure 2.1. Molecular structure of [(bpy-9)Zn(curc)Cl].

This heteroleptic Zn(II) complex has been synthesized through the reaction of the precursor complex [(bpy-9)$ZnCl_2$] with curcumin (curc) and triethylamine in dichloromethane. The precursor complex was previously obtained by the reaction of $ZnCl_2$ with the bpy-9 ligand. Complex **A** has been spectroscopically and structurally characterized, and tested *in vitro* towards different human cancer cell lines.

Moreover, complex **A** photophysical behaviour has been investigated by UV-vis spectroscopy in DMSO solution and it was observed that this Zn(II) complex exhibits a strong absorption band in the UV-vis region in the range 408-450 nm. As regards the fluorescence, complex **A** in DMSO solution has been shown to be emissive, with the maxima centred at 543 nm and an emission quantum yield of 0.14. The presence of intrinsic fluorescence in complex **A** allows in a single molecule the combination of emissive properties with the anticancer properties yielding an excellent tool for investigating their mechanism of action through optical methods, without the need of external agents.

Complex **A** has been tested *in vitro* towards a panel of human cell prostate cancer cells (DU145) and colorimetric assays have been used for calculating the IC_{50} (meaning the drug concentration causing 50% inhibition of the desired activity). This Zn(II) complex induced 50% of cytotoxicity at doses of about 12.5 μM, being even more effective than cisplatin (33 μM). Furthermore, the mechanism of action of complex **A** was suggested to be through a partial inter-base intercalation.[2] Indeed, the presence of intrinsic fluorescence in the model complex **A**, allows the investigation of its mechanism of action through optical methods, without additional external agents. The method used was based on the spontaneous liquid crystalline ordering in concentrated solutions of synthetic oligonucleotides, which easily allows strand sequences to be designed in order to check for sequence-specific binding modes or to verify fine structural dependencies. Fluorescence polarized microscopy demonstrated an anisotropic interaction of complex **A** with the DNA

helical structure. Indeed, it was found that the fluorescent groups preferentially align perpendicular to the helices, indicating some form of intercalation, in contrast with previous reports where curc was found to act as groove-binder.[104] The larger angular spread found for curc and complex **A** with respect to ethidium bromide (EB), a well-known fluorescent intercalator used as reference molecule to tag DNA strands with high affinity[105], suggests a more complex geometry of binding than pure intercalation, which tilts the molecules away from the helical axes, possibly combining intercalation with some interaction with the grooves.

These encouraging results showed that Zn(II) complexes may be successful candidates as anticancer agents with alternative mechanism of action than cisplatin. Nevertheless, a major drawback of complex **A** was its low water solubility (although it is soluble in dichloromethane, chloroform, ethanol, methanol, acetone and DMSO).

Therefore, structural changes have been done starting from this model complex **A**, in order to follow the influence of the variation around the metal ion on the solubility and biological activity of the resulting complexes and to investigate the structure-properties relationship in this class of derivatives.

Consequently, new metal(II)-curcumin based heteroleptic complexes have been synthesized and fully characterized in this research work. Starting from the neutrality of complex **A**, due to the

[104] **Zsila, F. Bikadi, Z. Simonyi,** 2004, M. Org. Biomol. Chem., Vol. 2, pp. 2902–2910.
[105] **LePecq, B. Paoletti, C. A. J.** 1967, Mol. Biol., Vol. 27, pp. 87–106.

coordination to the metal centre of the chloride ion, the first structural change performed, concerned the generation of corresponding ionic derivatives containing counterions with different, if none, coordination ability. In particular, depending on the nature of the counterion, the modulation of both the geometry and the electrostatic nature of the resulting Zn(II) complexes can be induced.

This change was made by using two different ionic Zinc(II) starting salts (namely zinc tetrafluoroborate ($Zn(BF_4)_2$) and zinc sulfate ($ZnSO_4$)) in the reaction with bpy-9. In particular, keeping the same N, N chelating ligand, bpy-9, and ancillary ligand, curc, two completely different Zn(II) species have been obtained by changing the chloride ligand with tetrafluoroborate and sulphate. In the first case, a ionic derivative [(bpy-9)Zn(curc)](BF_4), **1**, has been obtained, while with the use of the sulphate ion acting as a bridging group through two Zn(II) centre, a dimeric neutral derivative [$(Bpy\text{-}9)_2Zn_2(curc)_2(SO_4)(H_2O)_2$], **2**, has been isolated.

The new Zn(II) complexes (**1** and **2**) described subsequently, were structurally characterized, their photophysical properties were investigated and their antitumor activity was tested in vitro against the human neuroblastoma cell line SH-SY5Y in a biohybrid membrane.

Subsequently, in order to follow the change of the metal ion on the cytotoxic activity and solubility of the model complex **A**, the analogues Cu(II) complex was synthesized and characterized. In addition to the excellent biological activity, Cu(II) complexes are known to be in most cases water soluble. The new Cu(II) complex (**3**) is pentacoordinated, having 4,4'-dinonyl 2,2'-bipyridine (bpy-9) as the

main ligand, and respectively curcumin and chlorine (Cl) as ancillary ligands. The complex was fully characterized structurally and the photophysical properties were investigated.

2.1.1 Synthesis and characterization of [(bpy-9)Zn(curc)](BF$_4$), 1

As described before, the first structural change performed around the general framework of complex **A**, concerned the variation of the Cl ligand, with a non coordinating anion, that is tetrafluroborate, in order to obtain e ionin derivative. In particular, following the synthetic method used for model complex **A**, $Zn(BF_4)_2$ was used instead of $ZnCl_2$.

The synthetic methodology involves, as first step, the synthesis of the precursor complex **I** (Scheme 2.1). A slight excess of $Zn(BF_4)_2$ reacts with bpy-9 ligand at room temperature, giving rise, in good yield, to the precursor **I**.

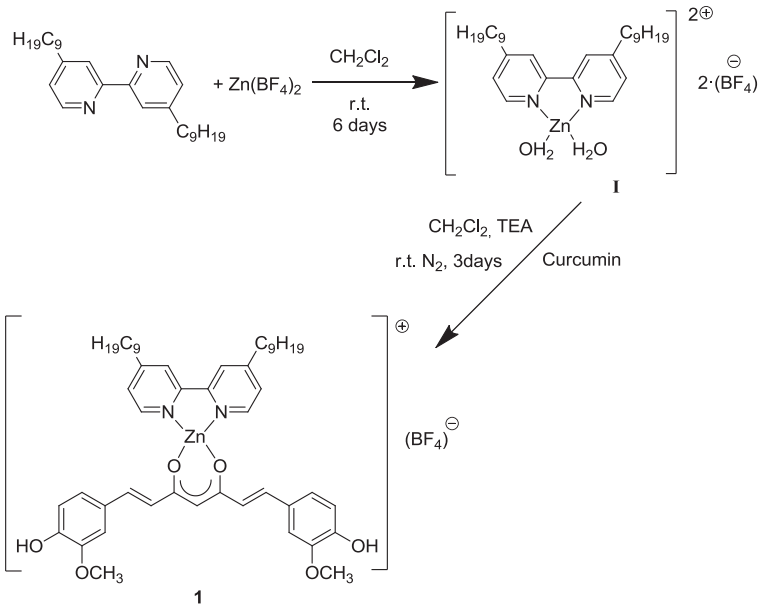

Scheme 2.1. Chemical synthesis of complex **1**.

Regarding the precursor complex **I**, the experimental elemental analysis data is in agreement with the calculated percentage of the molecular formula which points towards a Zn(II) complex having one bpy-9 ligand, two molecules of water and two BF_4 ions.

The strong band centred at 1058 cm^{-1} observed in the IR spectrum of **I** is compatible with a structure in which the BF_4 acts as counterion.[106] The IR spectra results are the first data confirming the successful coordination of bpy-9 to the Zn(II) metal centre, by the shift of the carbon-carbon band in the free ligand from 1596 cm^{-1} to 1613

[106] **Cuerva, C. Ovejero, P. Campo, J. A. Cano, M.** 2014, New J. Chem., Vol. 38, pp. 511.

cm^{-1} and the carbon-nitrogen band from 1551 cm^{-1} to 1559 cm^{-1}. [107] Furthermore, in the 3000 – 2840 cm^{-1} region, the C-H stretching vibrations of the methyl and/or methylene groups can be detected.[108]

As a further characterization, the ^1H NMR spectra was recorded in $CDCl_3$ solution. In the aromatic region of the ^1H NMR spectra all 6 aromatic protons belonging to the two pyridine rings of the bpy-9 ligand were correctly identified and assigned in the range between 8.1 to 7.4 ppm. A further confirmation of the successful coordination of the bipyridine ligand to the Zn(II) metal centre is given by the shielding of the aromatic proton signal in ortho with respect to the pyridine N atom, and the deshielding of the other two aromatic protons signals, when compared with the free ligand spectrum. [107] The ^1H NMR spectra of precursor complex **I** shows in the aliphatic region two multiplets centred at 2.77 ppm and 1.28 ppm and respectively two triplets centred at 1.67 and 0.86 ppm, with the integrals showing the correct number of protons of the aliphatic chains according to the molecular structure presented.

Finally, the conductivity measurements confirmed the ionic nature of the precursor complex **I**, the molar conductivity being in the acceptable Λ_M range for univalent electrolytes in dichloromethane solution.[109]

---

[107] **Liguori, P. F. Valentini, A. Palma, M. Bellusci, A. Bernarduni, S. Ghedini, M. Panno, M. L. Pettinari, C. Marchetti, F. Crispini, A. Pucci, D.** 2010, Dalton Trans. Vol. 39, pp. 4205-4212.

[108] **Silverstein, R. M. Webster, F. X**. Spectrometric Identification of Organic Compounds, State University of New York. Ed. John Wiley & Sons, Inc.

[109] **Geary, W. J**. 1971, Coord. Chem. Rev., Vol. 7, pp. 81-122.

The photophysical behaviour of complex **I** has been investigated by UV-Vis spectroscopy in ethanol solution at room temperature. The absorption spectra show relatively strong absorption bands centred at 283 nm and 304 and a strong band centred at 283 nm. Furthermore, the luminescence spectra recorded for complex **I** shows an emission band centred at 304 nm. The emission band supports the complexation of the bipyridine ligand, being the ligand in itself non emissive.

The final Zn(II) complex **1** was obtained in good yield thought the reaction of **I** with one equivalent of purified curcumin in the presence of triethylamine, in dichloromethane, at room temperature (Scheme 1). The curcumin ligand purchased from Aldrich, was used after purification since the commercial product is a mix of different similar components as reported by D. Pucci *et al.*[110]

The proposed stoichiometry of complex **1** was confirmed by elemental analysis, with one bpy-9, one curcumin and a BF_4 anion *per* metal centre. The complex **1** IR spectrum confirms the coordination of the curc ligand to the Zn(II) ion, by the shift of the carbon-oxygen band typical of the free curcumin from 1625 cm^{-1} to 1606 cm^{-1}, and the absence of the broad band due to the H-bonded enol proton in the region of 2600-3800 cm^{-1}.[111] On the other hand, a strong band centred at 1058 cm^{-1} is compatible with the presence of the BF_4^- acting as counterion.

---

[110] **Pucci, D. Bloise, R. Bellusci, A. Bernardini, S. Ghedini, M. Pirillo, S. Valentini, A. Crispini, A.** 2007, J. Inorg.Chem., Vol. 101, pp. 1013-1022.

[111] **Benassi, R. Ferrari, E. Lazzari, S. Spagnolo, F. Saladini, M.** 2008, J. Mol. Struc., Vol. 892, pp. 168-176.

The ^{1}H NMR spectrum of complex **1**, recorded in $CDCl_3$, contains, in the aromatic region, the signals of the protons belonging to the bpy-9 and curc ligands, correctly identified and assigned in the range of 8.1 to 5.8 ppm. Moreover, in the aliphatic region, the signals of the 38 protons belonging to the aliphatic chains of the bipyridine ligand are found in the range of 2.8 to 0.9 ppm.

As in the case of complex **A**, the lack of the curcumin intramolecular hydrogen bonded enolic proton, validates the chelation between the Zn(II) ion and the curcumin ligand. Moreover, the intensities of the signals are in agreement with a 1:1:1 metal-to-N,N ligand-to-curcumin stoichiometry.

Finally, conductivity measurements assessed the 1:1 electrolyte nature of complex **1**, being the molar conductivity obtained in dichloromethane solution in the Λ_M range for monovalent electrolytes in the this solvent.[108]

The photophysical behaviour of **1** has been investigated by UV-Vis spectroscopy in ethanol solution at room temperature. Complex **1** exhibits absorption bands at 293 nm and 305 nm and a strong absorption band at 429 nm (Fig. 2.2a). In order to test complex **1** stability in solution, absorption measurements have also been conducted over time and in physiological pH conditions.[112] In contrast with the consistent degradation observed for the free curcumin

[112] **Ricciardi, L. Pucci, D. Pirillo, S. La Deda, M.** 2014, J. Lumin., Vol. 151, pp. 138-142.

ligand[113], complex **1** shows a good stability because both the shape and the absorption maximum positions remain unchanged after 24, 48 and 72 h (Fig. 2.2b).

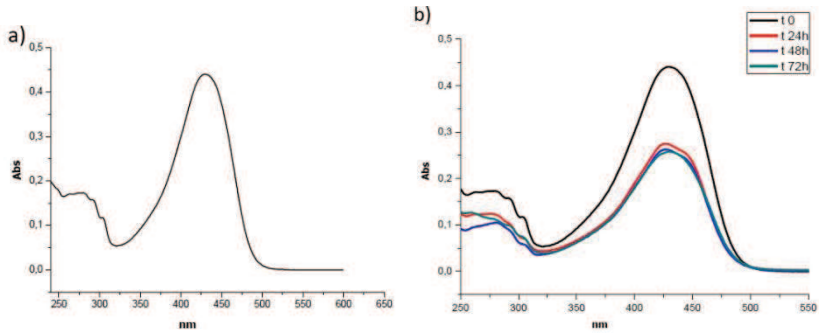

Figure 2.2. Absortion spectrum of complex **1** at room temperature in ethanol solution (a) and absorption spectra under physiological conditions (pH 7.2 after 0, 24, 48 and 72h) (b).

Moreover, complex **1** preserves the luminescence characteristic of the curc molecule (Fig. 2.3a), being emissive in ethanol solution (549 nm) with a photoluminescence quantum yield (ϕ= 0.076) higher than that of free curcumin (ϕ= 0.033) (Fig. 2.ab).

[113] **Burgos Norón, E. Calderón Montaño, J. M. Salvador, J. Robles, A. López Lázaro, M.** 2010, Int. J. Cancer, Vol. 126, pp. 1771-1775.

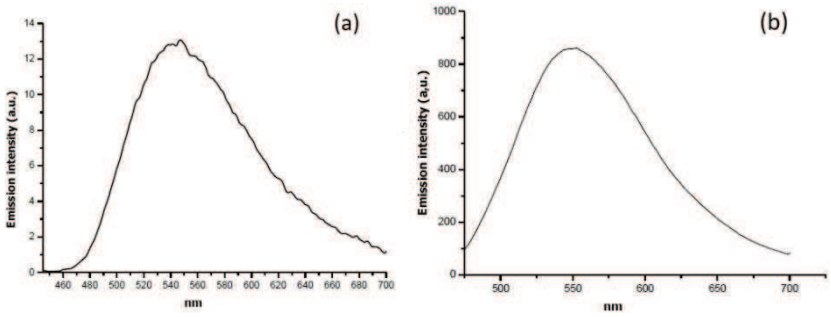

Figure 2.3. Emission spectra at room temperature of curcumin (a) and complex **1** (b) for excitation at 429 nm and 435 nm, respectively.

The structural change performed in order to transform complex **A** in the corresponding complex **1** ionic in nature, has only partially improved the solubility properties shown by complex **A**. In fact, complex **1** shows better solubility than complex **A** (soluble only in DMSO as solvent) being found partial soluble in water and alcohol solvents, and only very soluble in chlorurated solvents, and DMSO.

2.1.2 Synthesis and characterization of [(bpy-9)$_2$Zn$_2$(curc)$_2$(SO$_4$)(H$_2$O)$_2$], 2

Following the structural modification proposed in order to obtain analogous ionic derivatives, another counterion, SO_4^{2-}, with coordination ability intermediate between chloride and tetrafluoroborate ions, was chosen. The same synthetic methodology as in the case of complexes **A** and **1** was followed.

In particular, precursor complex **II** has been obtained by adding 1.5 equivalents of $ZnSO_4$ in water to a methanol solution containing the required quantity of bpy-9 (Scheme 2.2).

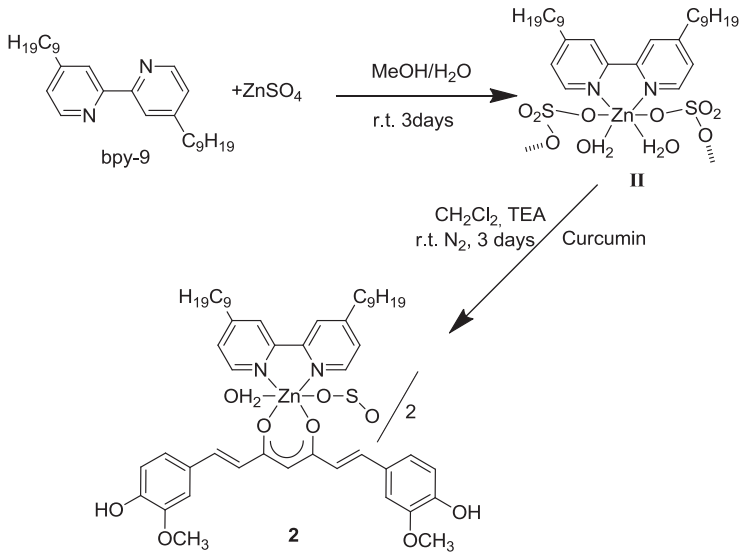

Scheme 2.2. Chemical synthesis of complex **2**.

The elemental analysis of complex **II** supported a molecular structure formed by the Zn(II) centre, a bpy-9 ligand, two water molecules, and a SO_4 group.

As previously presented for the precursor complex **I**, in the IR spectra of complex **II**, the C=C band of the free bpy-9 is shifted from 1596 cm^{-1} to 1618 cm^{-1} and the C=N band is shifted from 1551 cm^{-1} to 1561 cm^{-1} confirming that the coordination of bpy-9 to the Zn (II) metal centre was successful. On the other hand, the strong band centred at 1117 cm^{-1} is indicative of a structure in which the sulphate group acts as μ-bridging ligand, connecting two Zn(II) ions to form a dimer, as

already observed in the case of a 2,2'-bipyridine analogous previously reported.[114]

The ^{1}H NMR spectrum of the precursor complex **II** further confirmed the Zn(II) coordination to the bpy-9 ligand. In particular, a deshealding of the aromatic proton signal in ortho with respect to the pyridinic N atom is observed when compared with the free ligand spectrum. This is contrary to what observed for the ionic precursor complex **I**, which has the same ligand coordinated to the same Zn(II) metal centre, where an upfield shift of the same proton was detected, supporting the different molecular structure of the precursor complex **II** with respect to the precursor complex **I**.

The photophysical behaviour of the precursor complex **II** has been investigated by UV-Vis spectroscopy in methanol solution at room temperature. The absorption spectra contain strong absorption bands centred at 249 nm, 293 nm and 303 nm. Moreover, the recorded emission spectrum of the precursor complex **II** presents an emission band centred at 370 nm. As for precursor complex **I**, the emission band confirms the successful coordination of the non-luminescent ligand.

Complex **II** was further used in the synthesis of complex **2**, by reacting it with on equivalent of curc in presence of NEt_3 in dichloromethane solution, at room temperature. The resulting Zn(II) complex has been obtained in good yield (84%) (Scheme 2.2).

The elemental analysis is in agreement with a molecular structure formed by one Zn(II) metal centre, one bpy-9 and one curc ligands, one

[114] **Manohar, A. Ramalingam, K. Bocelli, G. Cantoni, A. J. Serb, J.** 2010, Chem. Soc., Vol. 75, 8, pp. 1085.

water molecule and only half ion of SO_4^-, suggesting again a bridging behaviour of the anion.

As in the case of complexes **A** and **1**, in the IR spectrum of complex **2**, the C=O band, typically at 1625 cm^{-1} of the free curcumin, is shifted to 1589 cm^{-1}, and the broad band due to the hydrogen bond enol proton in the region of 2600-3800 cm^{-1} is completely absent, confirming that the coordination of curc to the Zn(II) ion took place. Moreover, the characteristic bands of the sulphate anion at 1284, 1121 and 1032 cm^{-1} in the IR spectrum suggest that the sulphate is coordinated in a bridging fashion between two Zn(II) ions, as in the case of its precursor complex **II**.

As in the case of complex **1**, the ^1H NMR spectrum of complex **2** recorded in $CDCl_3$ solution, contains in the aromatic part the signals of the protons belonging to the bpy-9 and curc ligands, correctly identified and assigned and in the aliphatic region, the signals of the 38 protons belonging to the aliphatic chains of the bipyridine ligand. Moreover, the lack of intramolecular hydrogen bonded enolic proton of the curcumin, validates the Zn(II) coordination to the curcumin ligand and the intensities of the signals are agreement with a 1:1:1 metal-to-N,N ligand-to-curcumin stoichiometry.

Finally, the neutral character found in dichloromethane solution for **2,** together with the IR, ^1H NMR results and elemental analysis data, suggest that the sulphate is coordinated in a bridging fashion between two Zn(II) ions, as represented in Scheme 2.2.

The photophysical behaviour of **2** has been investigated by UV-Vis spectroscopy in ethanol solution at room temperature. The absorption

spectrum consists of absorption bands centred at 293 nm, 304 nm and a strong band at 304 nm. In order to test the stability in solution of complex **2** absorption measurements have also been conducted over time and in physiological pH conditions (Fig. 2.4).

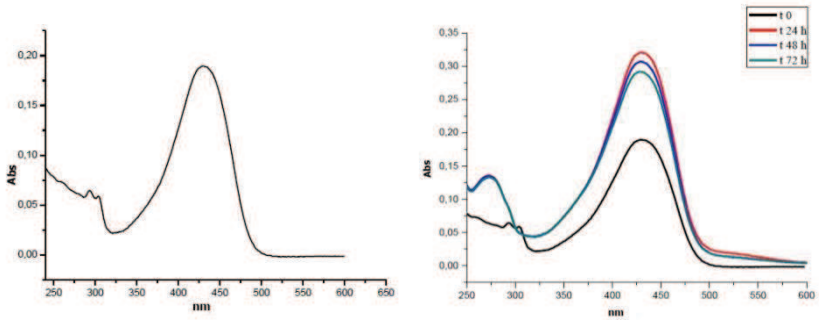

Figure 2.4. Absortion spectra at room temperature under physiological conditions (pH 7.2 after 0, 24, 48, 72h) of complex **2**.

As seen above, in contrast with the consistent degradation observed for the free curcumin ligand,[111] the Zn(II) complex **2** shows a good stability because both the shape and the absorption maximum positions remain unchanged after 24, 48 and 72 h. Moreover, complex **2** presents an emission band centred at 553 nm (Figure 2.5). The photoluminescence quantum yield is higher (ϕ= 0.075%) than that of free curcumin (ϕ= 0.033).

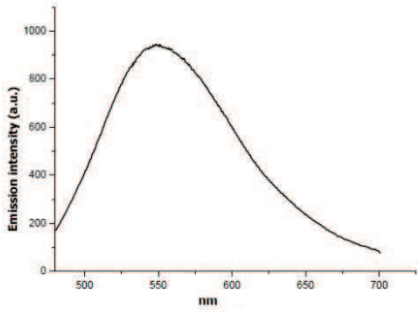

Figure 2.5. Emission spectrum in EtOH of complex **2**.

The use of the sulphate anion has impeded the formation of an ionic analogous of complex **A**, and probably due to the neutral nature of the formed complex **2**, its solubility has remained unchanged with respect to the reference derivative **A**, being found unsoluble in water.

2.1.3 Biological evaluation of complexes 1 and 2

The biological activity of these new Zn(II) metal complexes has been evaluated by tests on human neuroblastoma cell line SH-SY5Y, incubated with various concentrations of the compounds. On the basis of the confocal images of cells treated with the Zn(II) curcumin based complexes, which are fluorescent, the complexes were uptaken by cells and principally localized into the nucleus of cells at nucleoli level.

Both Zn(II) complexes show a dose-dependent effect on the viability of cells incubated for 24 and 48 hours, as reported in Figure

2.6. The percentage of metabolically active cells decreases with the increase of administered Zn(II) complex concentration.

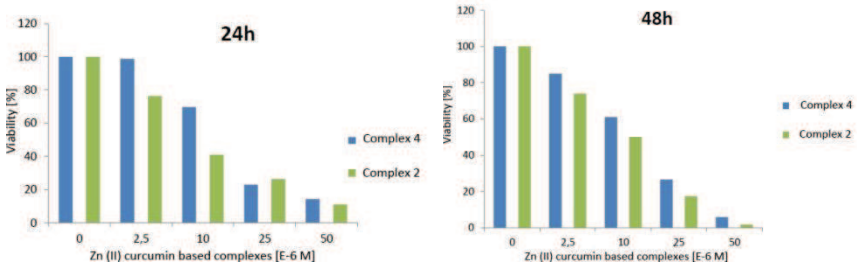

Figure 2.6. Changes in the cell viability of SHSY5Y cells after 24 h and 48 h of treatment with various concentrations of Zn (II) complexes **2** and **4**.

However, a significant decrease of cell viability has been detected already at low concentrations, especially in the presence of complex **1**. This Zn(II) complex shows a relevant cytotoxicity with an IC50 (the drug concentration causing 50% inhibition of the desired activity) of 7.9 μM after 24 h, respectively while complexes **A** and **2** exhibit 50% of toxicity at higher concentrations, but always in the range of concentrations 10-30 μM (Table 1).

Compound	IC50 (μM) SHSY-5Y
$[(bpy\text{-}9)_2Zn_2(curc)_2(SO_4)(H_2O)_2]$	14.6
$[(bpy\text{-}9)Zn(curc)](BF_4)$	7.9
[(bpy-9)Zn(curc)Cl]	16.1
Curcumin	13.6
Bpy-9	>100

Table 1. IC50 values of different compounds calculate on average values of % inhibition at various molecule concentrations.

On the basis of these results, complex **1** seems to be the most interesting candidate for anti-proliferative treatment. For this purpose the cells progressing according to their Anneix V and propidium iodide (PI) staining pattern was investigated, in order to evaluate whether the cell response is due to apoptotic or necrotic mechanism. Early apoptotic cells bind Annexin V but are not sensitive to intracellular staining with propidium iodide. This process is followed by changes in cell morphology and ultimate cell death.

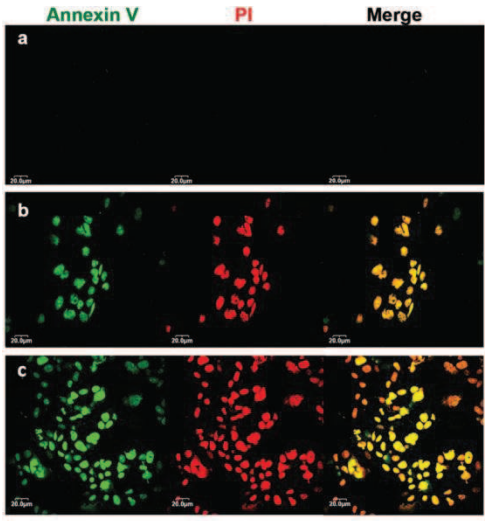

Figure 2.7. LSCM imagines of SHSY-5Y cells stained with Annexin V-FIT and PI after 24 h of culturing under: normal conditions (a) treatment with Zn (II) complex **1** at 8 μM (b) and 25 μM (c).

As cells progress through apoptosis, the integrity of the plasma membrane is lost, allowing PI to penetrate and label the cells with a strong yellow-red fluorescence (Fig. 2.7b,c). The induced apoptosis effect of Zn(II) complex **1**, at two different concentrations, on human neuroblastoma cells were evaluated in order to determine if cells are viable, apoptotic or necrotic through differences in plasma membrane integrity and permeability. Cells treated with complex **2** expressed both PI and bind Annexin V, as the Figure 2.7 shows above. The percentage of Annexin V and PI-positive cells markedly increased when cells were treated with high concentrations of Zn (II) complex (Fig. 2.7c). A peak of fluorescence intensity of Annexin V and PI was detected after

treatment with complex **1** at concentration of 25 μM as result of the apoptosis induction (Fig. 2.7c).

Concluding, the synthesis and characterization of two new heteroleptic Zn(II) curcumin based complexes has been achieved. Structural changes have been made starting from the reference complex [(bpy-9)Zn(curc)Cl], **A**, in order to introduce new functionalities, such as electrostatic interactions and/or covalent interactions. In particular, by using $Zn(BF_4)_2$ as precursor salt, a ionic derivative, $[(bpy\text{-}9)Zn(curc)]BF_4$, **1**, has been obtained, while with the use of the sulphate ion acting as a bridging group through two Zn(II) centre, a dimeric neutral derivative $[(Bpy\text{-}9)_2Zn_2(curc)_2(SO_4)(H_2O)_2]$, **2**, has been isolated. The new Zn(II) derivatives have been fully characterized both in the solid and solution state, showing great stability in aqueous medium even in physiological conditions and in the case of the ionic complex **1** better solubility in hydrophilic solvents with respect to the reference complex **A**. Moreover, in order to investigate the possible effects obtained by the structural changes performed around the Zn(II)-curcumin fragment, the biological activity of the new synthesized complexes have been evaluated by investigating the viability of human neuroblastoma cell line SH-SY5Y cultured in a biohybrid membrane system, able to support cell adhesion, proliferation and differentiation, incubated with various concentrations of the Zn(II) compound. It resulted that complex **1** exhibit significant cytotoxic activity, showing IC50 values of micromolar order, superior with respect to the reference compound [(bpy-9)Zn-(curc)Cl], **A**, already reported. This higher cytotoxicity probably is

caused by the ionic character inducing better solubility properties, which is the requisite for a drug to act as a good intercalator. On the basis of these results, in order to evaluate whether the cell response is due to apoptotic or necrotic mechanisms, in the case of comples **1**, the cells progressing according to their Annexin V and propidium iodide staining pattern have been investigated. Since a peak of fluorescence intensity for Annexin V and propidium iodide was detected after treatment with complexes **1** at concentrations of 25 μM, we can conclude that this is an evidence of the apoptosis induction. Additionally, the investigation of apoptotic markers indicates that complexes **1** induce cell apoptosis through a molecular mechanism involving the activation of JNK, caspase-3 and changes in MMP.

Therefore, the substitution of single building blocks around the Zn(II) curcumin fragment results in a concrete strategy in order to obtain more performing and even more promising emissive species to be used as highly active theragnostic agents.

The synthesis, characterization and the *in vitro* studies for antitumor activity of complex **1** and **2** has been published in the article number 1: D. Pucci, A. Crispini, B. Sanz Mendiguchía, S. Pirillo, M. Ghedini, S. Morelli and L. De Bartolo, Dalton Trans., 2013, 42, 9679, included in the Thesis Supplementary Information.

2.1.4 Synthesis and characterization of [(bpy-9)Cu(curc)Cl], 3

Furthermore, the change of the Zn(II) metal centre by the use of a similar metal ion, was investigated. In this aim, and willing to obtain a further increase of the cytotoxic activity and solubility of the model complex **A**, the analogues Cu(II) complex was synthesized and characterized. The literature shows that the majority of the Cu(II) complexes reported have relatively good water solubilities. The new Cu(II) complex synthesized has a similar pentacoordinated structure as the model complex **A**, having 4,4'-dinonyl 2,2'-bipyridine (bpy-9) as the main ligand, and respectively curcumin (curc) and chloride (Cl) as ancillary ligands.

Precursor complex **III** has been synthesized using the same synthetic strategy as for Zn(II) complex **A**, but changing the zinc salt with $CuCl_2$ (Scheme 2.3).

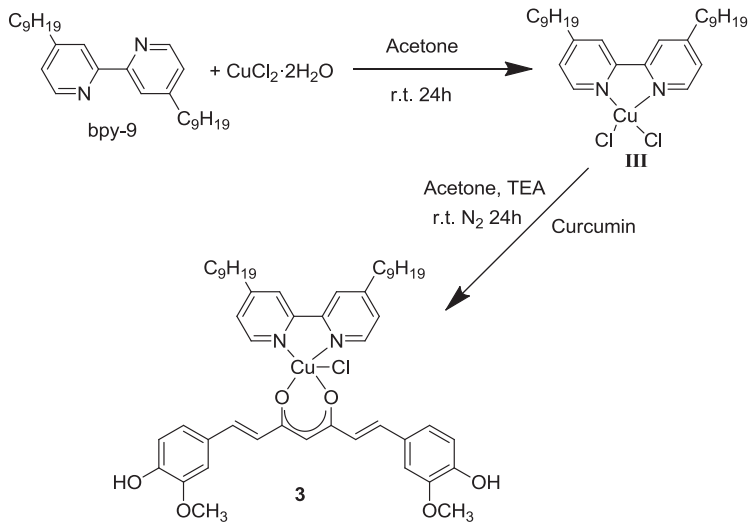

Scheme 2.3. Chemical synthesis of complex **3**.

The proposed stoichiometry for precursor **III** was confirmed by elemental analysis.

Furthermore, the IR spectrum of precursor complex **III** showed the typical shift of the C=C and C=N bands with respect to the free ligand bands, as in the case of the previous described two precursor Zn(II) complexes.

Nonetheless the neutral character proposed for this complex, conductivity measurements performed in methanol solution yielded values that are almost in the range of 1:1 electrolytes. Indeed, the value 78.58 $\Omega^{-1} \cdot cm^2 \cdot mol^{-1}$ found for precursor complex **III** is approaching the lower limit of the 80-115 $\Omega^{-1} \cdot cm^2 \cdot mol^{-1}$ values range reported for similar univalent derivatives. This may suggest a highly labile character of the chloride ligand, and therefore once dissolved in

methanol, the complex loses the chloride ligand and converts into an ionic specie.

The photophysical behaviour of precursor complex **III** has been investigated by UV-Vis spectroscopy in methanol solution at room temperature. Cu(II) complex exhibits absorption bands at 251 nm, 297 nm and 308 nm instead of the two bands at 247 nm and 282 nm exhibited by the free bpy-9 ligand. Moreover, complex **III** is not luminescent.

The reaction of precursor **III** with one equivalent of purified curc in the presence of triethylamine in acetone at room temperature (Scheme 2.3), produced complex **3**.

The elemental analysis of complex **3** is in agreement with the proposed structure. Furthermore, the IR spectrum shows the same bands as the one observed in the case of the analogues Zn(II) model complex **A**, supporting the same structure. In particular, in the IR spectrum of complex **3** the carbon–oxygen band typical of the free curc is shifted from 1625 cm^{-1} to 1623 cm^{-1} and the broad band due to the H-bonded enol proton in the region of 2600–3800 cm^{-1} is completely absent, confirming that the coordination of curc to the Cu(II) ion took place.

The neutral character of the final complex **3** was confirmed by conductivity measurements performed in methanol solution. Therefore, we can assume that the coordination sphere for complex **3** is saturated by one N, N-ligand, one O, O-chelating unit and a chloride ion, as in the model complex **A**.

The photophysical behaviour of **3** has been investigated by UV-Vis spectroscopy in methanol solution at room temperature. The absorption spectrum consist of absorption bands at 253 nm 263 nm, 307 nm, 347 nm, 427 nm and 451 nm very different than the absorption spectrum of precursor **III**. Moreover, complex **3** preserves the luminescence characteristics of the curcumin molecule (Fig. 2.8), being emissive in methanol solution at 560 nm confirming the formation of a new complex (ϕ= 0.01).

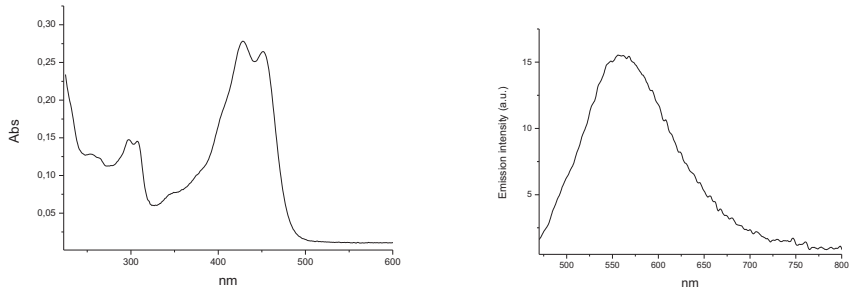

Figure 2.8. Absortion and emission spectra of complex **3**.

The various characterizations have shown the formation of a new Cu(II) complex, [(bpy-9)Cu(curc)Cl]. Contrary to what expected, the solubility in water of complex **3** was not significantly increased, having similar solubility to complex **A**.

2.2 Synthesis and characterization of curcumin-based complexes increasing the aromatic portion in the N,N chelating ligand

New Zn(II)–curcumin complexes were synthesized with the intent to increase the intercalating properties of complex **A**. Within this aim, the increase of the aromatic region of the N,N chelating ligand was achieved, by using an alternative N,N chelating ligand such as terpyridine (terp). The second structural change concerned the variation of the chloride ligand filling the coordination sphere of the Zn(II) centre in complex **A**. This change was made by using a different ionic Zinc(II) starting compound, in order to modulate the electrostatic nature and geometry of the new Zn(II) derivative.

The rigidity of the structure and the big aromatic section have made the terpyridine a good candidate for intercalating agent and/or G-quadruplex binder. The terpyridine also shows luminescence[115] , an excellent tool for investigating their mechanism of action through optical methods. Different terpyridine complexes of Zn(II) have been synthesized acting both as intercalating agents and/or G-quadruplex binders.[34,37]

[115] **Fink, D. W. Ohnesroge, W. E**. 1970, J. Phys. Chem., Vol. 74, pp. 72-77

2.2.1 Synthesis and characterization of [(terp)Zn(curc)Cl], 4

Following the synthetic strategy used for the synthesis of the model complex **A**, the analogues complex containing the terpyridine as main ligand presented in Scheme 2.4, was obtained.

Precursor complex **IV** has been synthesized adding a slight excess of Zinc(II) chloride in acetonitrile to a solution of terpyridine ligand in dichloromethane at room temperature for 48 hours (Scheme 2.4).

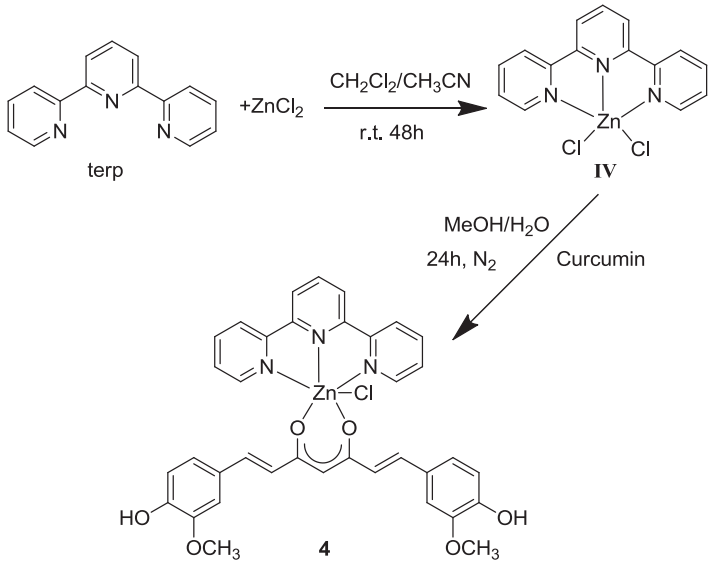

Scheme 2.4. Chemical synthesis of complex **4**.

The elemental analysis confirms the molecular formula of precursor complex **IV**. Furthermore, in the IR spectrum the C=C band of the free terp ligand is shifted from 1580 cm^{-1} to 1595 cm^{-1} and the

C=N band is shifted from 1561 cm^{-1} to 1581 cm^{-1} confirming that the coordination of terp to the Zn(II) is took place.

A further confirmation of the successful coordination of the terpyridine ligand to the Zn(II) metal centre was given by the ^{1}H NMR spectrum, with the downfield shift of the aromatic proton signals. The neutral character was confirmed by conductivity measurements performed in DMSO solution. Indeed, the found value of 9.67 $\Omega^{-1} \cdot cm^{2} \cdot mol^{-1}$, is too low to suggest an ionic specie, since the range reported for 1:1 electrolytes, in the same solvent, is 50-70 $\Omega^{-1} \cdot cm^{2} \cdot mol^{-1}$.

The photophysical behaviour of **IV** has been investigated by UV-Vis spectroscopy in water solution at room temperature. The absorption spectrum of complex **IV** contains a strong absorption band centred at 230 nm, while the free terpyridinic ligand shows a band centred at 290 nm. This blue shift of the absorption maxima supports the successful coordination of the ligand to the Zn(II) metal centre. Moreover, complex **IV** is found luminescent, having an emission band centred at 360 nm with a relatively good phosphorescence quantum yield (ϕ= 0.058). The maximum of the luminescence is red shifted with respect to the free ligand, which emits at 350 nm.

The Zn(II) complex **4** has been obtained in good yield (71%) through reaction of precursor **IV** with one equivalent of purified curcumin in the presence of thriethylamine, in methanol, at room temperature (Scheme 2.4). Unfortunately, this Zn (II) complex resulted to be only slightly soluble in DMSO, differently than its precursor.

The elemental analysis confirms the molecular structure of complex **4** proposed in scheme 2.4. Furthermore, in the IR spectra the

C=O band typically of the free curcumin is shifted from 1625 cm^{-1} to 1620 cm^{-1}. Moreover, the broad band due to the hydrogen bond enol proton in the region of 2600-3800 cm^{-1} is completely absent and the C=C band of the complex **IV** is shifted from 1580 cm^{-1} to 1582 cm^{-1} confirming that the coordination of curcumin to the Zn(II) ion took place.

Due to the its low solubility in DMSO, it was not possible to record an uunequivocal ^{1}H NMR spectra. Indeed, the broadness of the proton signals does not permitted to correctly identify all the aromatic protons, although some key signals coming from the two ligands can be distinguished.

The photophysical behaviour of **4** has been investigated by UV-Vis spectroscopy in DMSO solution at room temperature. The absorption spectrum consists of absorption bands centred at 278 nm, 316 nm, 332 nm and a strong band at 335 nm (Fig. 2.9). Moreover, complex **4** shows an emission band in methanol solution at 543 nm with a low photoluminescence quantum yield (ϕ= 0.006) (Fig. 2.9).

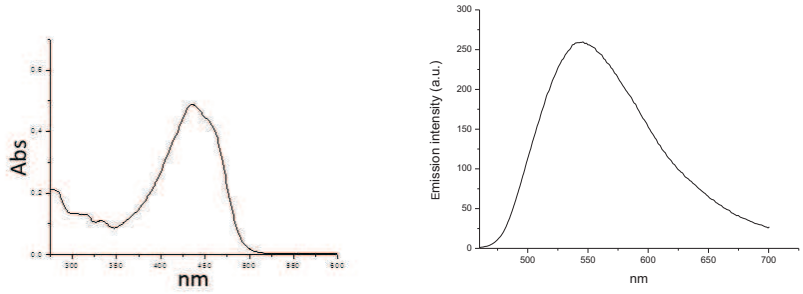

Figure 2.9. Absorption and emission spectra of complex **4** at room temperature.

The structural change performed in order to increase the aromatic portion of complex **A**, did not improved the solubility properties of the analogues complex **4** containing terp ligand instead of bpy. Nevertheless, because precursor **IV** showed water solubility, the insolubility of complex **4** may be due to the curc ancillary ligand. Therefore, a further structural change was pursued that is the introduction of a non-coordinative counterion, to obtain an ionic complex, as in the case of complex **1**.

2.2.2 Synthesis and characterization of $[(terp)_2Zn](BF_4)_2$, 5

As stated before, in the attempt to modulate the electrostatic nature of the resulting Zn(II) complex, $Zn(BF_4)_2$ salt was used as precursor in the reaction with terp ligand. The same synthetic procedure discussed before, was followed, and in particular, precursor complex **V** has been synthesized adding a slight excess of $Zn(BF_4)_2$ to a solution of terp ligand in dichloromethane at room temperature for 6 days (Scheme 2.5).

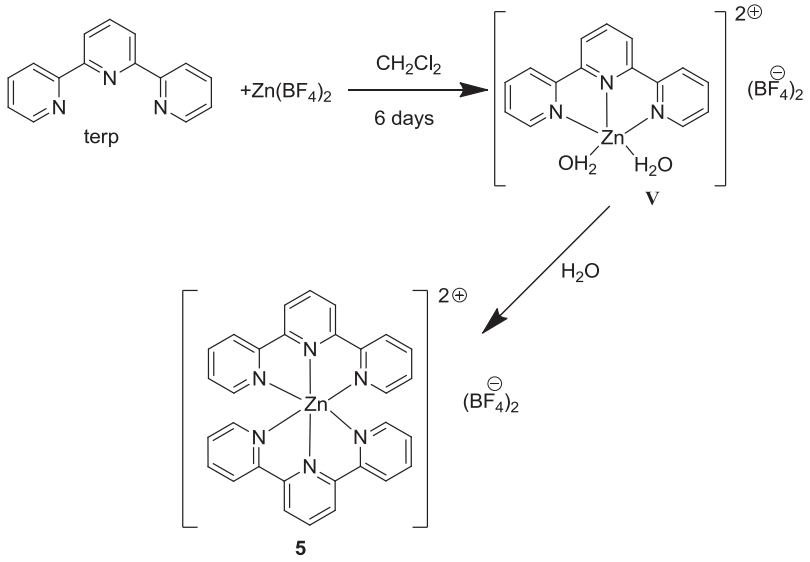

Scheme 2.5. Chemical synthesis of complex **5**.

The elemental analysis confirms the molecular formula of precursor complex **V**, proposed in Scheme2.5. In the IR spectra, the C=C band of the free terp is shifted from 1580 cm^{-1} to 1595 cm^{-1} and the C=N band is shifted from 1561 cm^{-1} to 1580 cm^{-1} confirming that the coordination of terp to the Zn(II) took place. On the other hand, the strong band centred at 1084 cm^{-1} confirms the presence of the tetrafluoroborate ion.[106]

A further confirmation of the successful coordination of the terpyridine ligand to the Zn(II) metal centre is given in the ^{1}H NMR spectra by the downfield shift of the aromatic proton signals.

The ionic character was confirmed by conductivity measurements performed in methanol solution. Indeed, the value found 202.36 Ω^{-}

$^{1}\cdot cm^{2}\cdot mol^{-1}$, assessed its 2:1 electrolyte nature, being in the acceptable Λ_M range for bivalent electrolytes in the respective solvent.

The photophysical behaviour of precursor complex **V** has been investigated by UV-Vis spectroscopy in methanol solution at room temperature. The absorption spectrum consists of absorption bands centred at 233 nm, 264 nm, 275 nm, 282 nm, 319 nm and 330 nm, confirming the formation of the complex because the teryridinic ligand shows a band centred at 290nm. Moreover, complex **V** presents an emission band centred at 355 nm with a good photoluminescence quantum yield ((ϕ= 0.046), also in this case the presence of luminescence confirm the formation of a new complex because terp ligand shows an emission band centred at 350 nm.

In the attempt to perform the reaction between complex precursor **V** and the curc ligand in a mixture of methanol and water solution, a notable change of colour has been observed when **V** was dissolved in water (from transparent to pink). Complex **5** has been obtained in the form of pink crystals then by slow evaporation of its water solution. Single crystal X-Ray diffraction has revealed the formation of a ionic Zn(II) complex in an octahedral environment, having two terpyridine ligands coordinated (Figure 2.10).

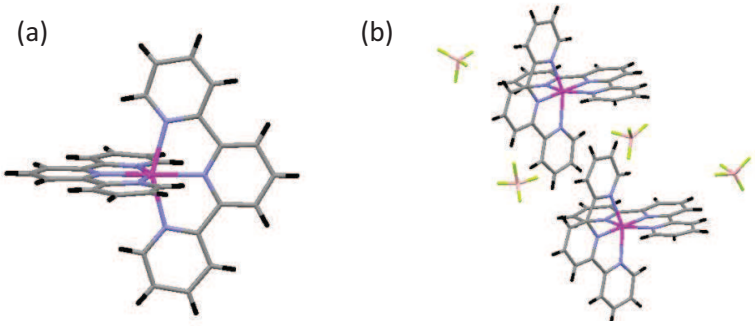

Figure 2.10. Molecular structure of cation complex (a) and two molecules of complex **5** for asymmetric unit (b).

Finally, since precursor complex **V** in water solution undergoes instantaneously rearrangement yielding complex **5**, the reaction with curcumin was not further carried on.

2.3 4,4'-bis(dimethoxy)-2,2'-bipyridine (bpy-OH) Zn(II) and Cu(II) complexes

Another structural change that may be relatively easy to achieve is the change of the substituent groups on the N,N chelating ligand, by introducing specific functionalities to induce desired properties on the final material. Therefore, subsequently hydrophilic molecular substituents were introduced in order to increase the solubility and the bioactivity of the resulting Zn(II) and Cu(II) complexes. Indeed, the introduction of hydrophilic OH groups, may, not only increase the solubility properties of the resulting complexes, but also renders the obtained molecules suitable to form hydrogen bonds and hence,

supramolecular assemblies, whose properties may differ substantially from the single molecular properties.

Therefore, complex **B**, analogues to complex **A** but having hydroxymethyl groups instead of the simple alkyl chains on the N,N chelating ligand, was synthesized and characterized.[2]

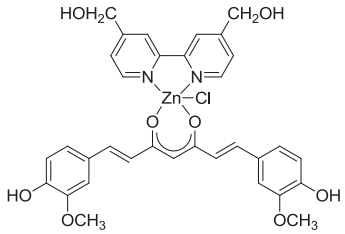

Figure 2.11. Molecular structure of **B**, [(bpy-OH)Zn(curc)Cl].

This heteroleptic Zn(II) complex, containing 4,4'-bis(hydroxymethyl)-2,2'-bipyridine (bpy-OH) as the main ligand and curc and chloride as ancillary ligands, has been synthesized following the synthetic strategy used for the previously described complexes **A** and **1**. As precursor ligand was used 4,4'-bis(hydroxymethyl)-2,2'-bipyridine, synthesized as described in the literature.[116] Complex **B** has been further spectroscopically and structurally characterized, and tested *in vitro* towards different human cancer cell lines.

The photophysical behaviour of complex **B** has been investigated by UV-vis spectroscopy in DMSO solution, and it was observed that this Zn(II) complex exhibits a strong absorption at 429 nm. As regards the fluorescence, complex **B** in DMSO solution has been shown to be

[116] **Will, G. Boschloo, G. Nagara Rao, S. Fitzmaurice, D.** 1999, J. Phys. Chem. B, Vol. 103, pp. 462.

emissive, with the maxima centred at 521 nm and an emission quantum yield of 0.11. The presence of intrinsic fluorescence in complex **B** allows in a single molecule combination of anticancer properties with an excellent tool for investigating their mechanism of action through optical methods, without the need of external agents.

Complex **B** has been tested *in vitro*, towards a panel of human cell prostate cancer cells (DU145) and colorimetric assays have been used for calculating the IC_{50}. This Zn(II) complex induced 50% of cytotoxicity at doses about 34 μM, its activity being similar with cisplatin (33 μM). This encouraging results showed that Zn(II) complexes containing bpy-OH as the main ligand may be successful candidates as anticancer agents. Nevertheless, similarly to complex **A**, the major drawback of complex **B** seems to be its low solubility (resulted to be only soluble in DMSO). Therefore, several structural changes have been done on the model complex **B**, in order to improve the solubility and bioactivity of the resulting complexes.

The low water solubility shown by complex **B** has proved ultimately that, in order to improve this physical property in these type of bipyridine metal complexes, as well as bioavailability, the next structural change to be done should concern the variation of the O,O chelating ligand. Therefore, the curc ligand has been replaced with tropolone (Trop) ligand, obtaining complexes with 1:1 and 1:2 stoichiometry ratio metal-to-ligand. Subsequently, the variation of the metal centre was pursued, and therefore, the analogues complexes containing Cu(II) metal centre and Trop were synthesized and characterized.

2.3.1 Synthesis and characterization of [(bpy-OH)Zn(Trop)Cl], 6

Following the structural modification already proposed, another O, O chelating ligand with the same coordination ability as curcumin was chosen. The new Zn(II) complex **6** synthesized has a similar pentacoordinated structure as the model complex **B**, having 4,4'-bis(hydroxymethyl)-2,2'-bipyridine as the main ligand, and respectively tropolonate and chloride (Cl) as ancillary ligands.

The same synthetic strategy used for the synthesis of the model complex **B** was followed, and in particular, the dichloro precursor **VI** was prepared by the reaction of a small excess of zinc chloride with a solution of bpy-OH in acetone at room temperature for 24 hours (Scheme 2.6).

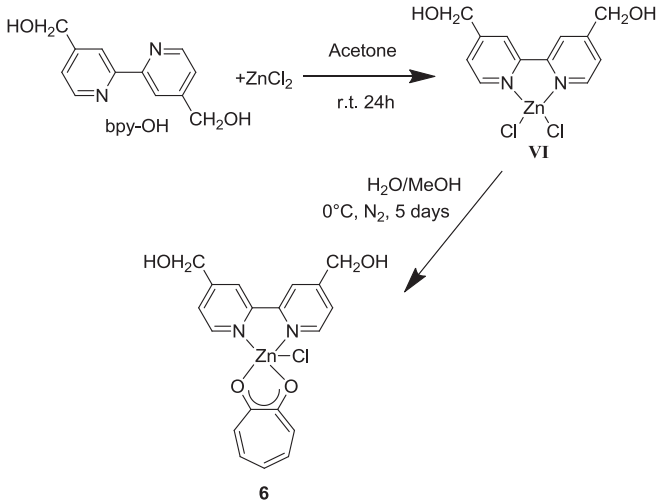

Scheme 2.6. Synthesis of complex **6.**

The elemental analysis performed, confirmed the proposed stoichiometry of the precursor complex **VI** reported in Scheme 2.6. Furthermore, in the IR spectra, the OH band of the free bpy-OH is shifted from 3367 cm^{-1} to 3481 cm^{-1} and the carbon-carbon band is shifted by about 17 cm^{-1} with respect to the bpy-OH free ligand, confirming that the coordination to the Zn(II) took place.

A further confirmation of the successful coordination of the bpy-OH ligand to the Zn(II) metal centre is given in the ^{1}H NMR spectra by the deshield shift of aromatic proton signals with respect to bpy-OH free ligand. This is consistent with the presence of a chelate system around the Zn(II) ion.

Conductivity measurements have been performed in DMSO solution, confirming the neutral character of the precursor complex **VI**. Indeed, the value found 10 $\Omega^{-1} \cdot cm^{2} \cdot mol^{-1}$, is too low to suggest an ionic specie, since the range reported for 1:1 electrolytes is 50-70 $\Omega^{-1} \cdot cm^{2} \cdot mol^{-1}$.[109]

The photophysical behaviour of precursor **VI** has been investigated by UV-Vis spectroscopy in DMSO solution at room temperature. The absorption spectrum exhibits absorption bands at 246 nm, 258 nm, 283 nm and 304 nm and a strong absorption band at 294 nm Moreover, complex precursor **VI** presents an emission band centred at 325 nm, the presence of luminescence confirming the formation of a new complex because the bpy-OH ligand does not show luminescence (ϕ= 0.043).

The final Zn(II) complex **6** was then obtained through the reaction of **VI** with one equivalent of trop. In particular, to a solution of **VI** in

water, an equimolecular amount of potassium trop salt in methanol was added drop wise very slowly, at 0°C. After the addition of the salt, the reaction mixture was allowed to reach room temperature, and further stirred for 5 days. In these conditions, complex **6** is formed.

Complex **6** shows different solubility properties than complex **A**, being soluble in methanol, ethanol and DMSO.

The elemental analysis confirms a structure formed by the two chelating ligands, bpy-OH and trop, one Zn(II) ion and one chloride ion.

In the IR spectrum, the carbon–oxygen band of the trop ligand is shifted with respect to the free ligand, confirming that the coordination to the Zn(II) took place.

In the aromatic region of the ^{1}H NMR spectrum of **6**, all 11 protons of the bpy and trop ligands were correctly identified and assigned, in the range of 8.7 and 6.7 ppm. A downfield shift of the aromatic proton signals is observed, confirming the successful coordination to the Zn(II) metal centre. Finally the signals attributed to the -CH_2OH group of bpy-CH_2OH ligand were identified as singlets at 5.68 ppm for the OH and 4.71 ppm for the CH_2 deshielded with respect to the free bpy-OH (5.53 ppm and 4.62 ppm respectively). Importantly, the integrated ratio between aromatic protons of the two ligands in complex **6**, showed the presence of one bpy and one Trop moieties per Zn(II) centre.

Finally, the neutral character and therefore the chloride coordination to the Zn(II) centre, was confirmed by conductivity measurements performed in ethanol solution.

In order to test the stability in solution, the behaviour of complex **6** has been investigate by UV-Vis spectroscopy in methanol at room

temperature. The absorption spectrum of the complex contains absorption bands at 302 nm, 351 nm and 368 nm. These bands are different than the absorption bands of complex **VI** confirming the presence of a new complex. Measurements conducted over time have proved the good stability of this system, since both the shape and absorption maximum positions remained unchanged after 24 and 72h (Fig. 2.12).

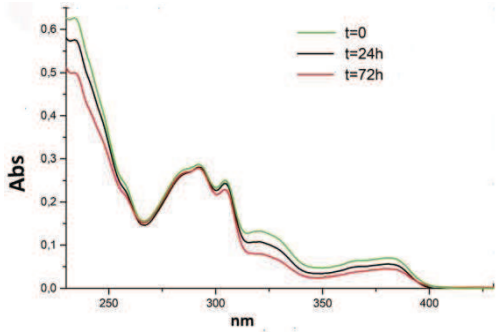

Figure 2.12. Absorption spectra at room temperature (after 0, 24, 72h) of complex **6.**

Moreover, complex **6** resulted to be emissive, exhibiting an emission band centred at 421 nm, the presence of luminescence confirming once more the formation of a new complex, precursor **VI** showing an emission band centred at 325 nm (Fig. 2.13).

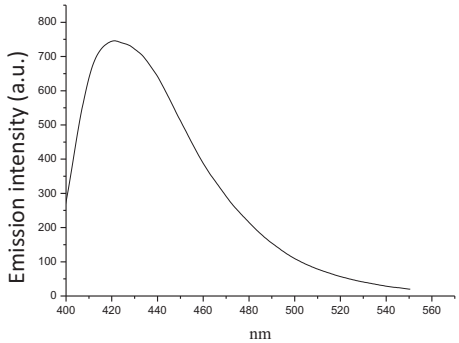

Figure 2.13. Emission spectra of complex **6**.

From slow evaporation in ethanol solution, yellow crystals have been obtained. Single crystal X-Ray diffraction analysis showed that the Zn(II) ion is in a five-coordinated distorted square-pyramidal geometry. The basal plane is formed by the two chelating ligands, bpy-OH and tropolone respectively, while the chloride ion is located on the apex of the pyramid (Fig. 2.14).

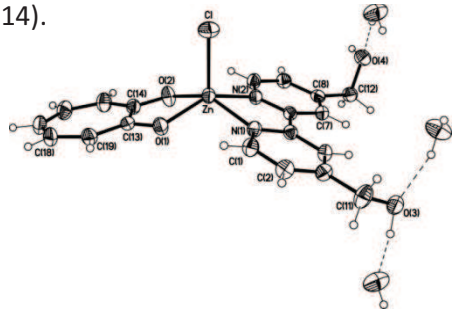

Figure 2.14. Molecular structure of complex **6**.

Both distances and angles around the Zn(II) ion are in agreement with those found in the molecular structure of the reference Zn(II) complex **A**.[1] The two "bite" angles relative to the two chelated ligands are O(1)-Zn- O(2) 78.61(5)° and N(1)Zn-N(2) 77.44(5)°, while the average angle formed by the apical chloride ligand with the coordinated N and O atoms is 105.16(4)°. The two chelated rings within the basal plane of the coordination sphere are not coplanar, showing a dihedral angle between the two mean planes of 33.9°. Complex **6** crystallizes with two water molecules in the asymmetric unit, although it is found not soluble in water.

2.3.2 Synthesis and characterization of [(bpy-OH)Zn(Trop)$_2$], 7

The versatility of the Zn(II) ion coordination allows the synthesis also of a bis-tropolonate complex, as reported previously for similar complexes.[107] Therefore, complex **7** was synthesized in an attempt to investigate the impact of the presence of one or two tropolonates ligands around the metal ion on the potential antiproliferative activity of the resulting complexes.

Complex **7** was obtained modifying the reaction conditions for complex **6** and the stoichiometry of the precursors (Scheme 2.7). In particular, to the precursor complex **VI** water solution containing, a solution of two equivalent of potassium salt was added, and the reaction mixture was stirred at r.t. for 19 hours. In these conditions, complex **7** is formed.

This Zn(II) complex is soluble in the same solvents as complex **6**, therefore in methanol, ethanol and DMSO.

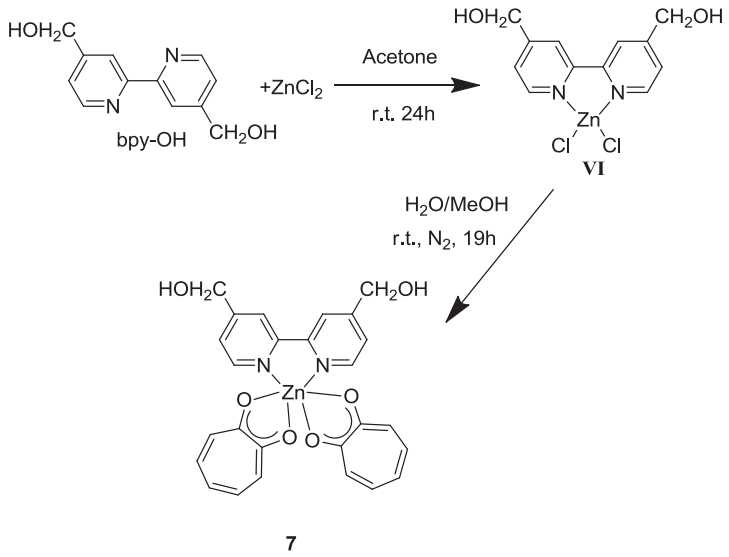

Scheme 2.7. Synthesis of complex **7.**

The elemental analysis data performed on complex **7** confirmed the proposed structure presented in Scheme 2.7, respectively the complex is formed by one bpy-OH ligand, two trop ligands and one Zn(II) ion.

Furthermore, in the IR spectra of complex **7**, the band centred at 1618 cm^{-1}, assigned to the carbon-oxygen stretching, confirms the chelation between trop ligand and the Zn(II) metal centre

The ^{1}H NMR spectrum of complex **7** contains in the range 8.7 ppm – 6.8 ppm, the signals corresponding to the aromatic protons of the two ligands, respectively bpy-OH and Trop. Furthermore, an upfield shift of these protons is observed, revealing a shielding of the respective protons, therefore, a different environment with respect to

complex **6**. Indeed, the integrals of the aromatic protons are in agreement with a 1:2 bpy to trop ratio.

The photophysical behaviour of complex **7** in DMSO solution has been investigated by UV-Vis spectroscopy at room temperature. The absorption spectrum is different than the spectrum of complex **6**, exhibiting bands centred at 283 nm, 295 nm, 329 nm, 337 nm, 374 nm and 393nm (Fig. 2.15). Moreover, complex **7** emits, with an emission band centred at 422 nm, similar to the emission of complex **6**.

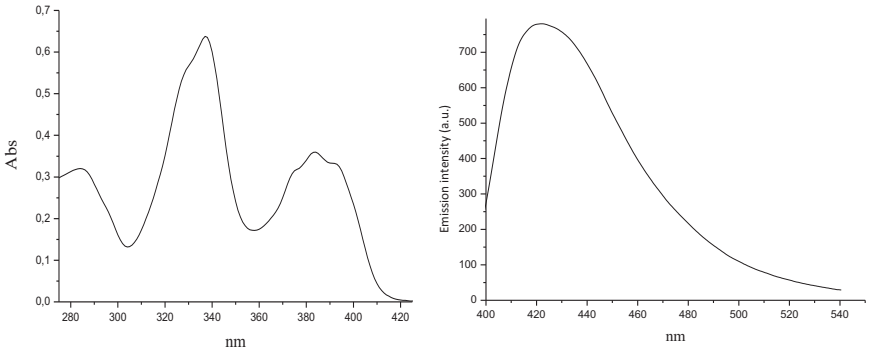

Figure 2.15. Absorption and emission spectra of complex **7**.

The molecular structure of complex **7** has been determined by single crystal X-Ray analysis. The crystals were obtained by slow evaporation of an ethanol solution. It has been found that the central metal ion is six coordinated by four oxygen atoms of two bidentate tropolonates and two nitrogen atoms of the bipyridine ligand. The "bite" angles as well as the Zn-O bond distances of the two chelated tropolonate ligands are comparable with those found recently in a similar bis-tropolonate Zn(II) derivative[107] (Fig. 2.16).

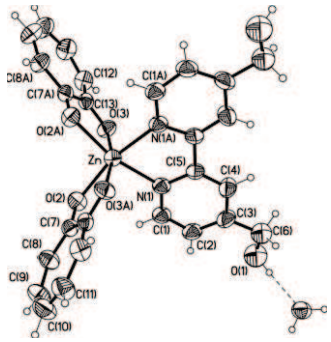

Figure 2.16. Molecular structure of complex **7**.

As already seen in the case of complex **6**, the presence of the OH groups on the bipyridine ligand caused the co-crystallization of the complex with water molecules in the asymmetric unit, interacting *via* hydrogen bonds. In any case, the same solubility properties have been observed in the case of complex **7**, being not water soluble.

2.3.3 Synthesis and characterization of [(bpy-OH)Cu(Trop)Cl], 8

Although the replacement of the curcumin ligand by the chelating O,O tropolone one has sensibly increased the solubility properties of the bipy-OH resulting Zn(II) complexes, the variation of the metal centre was pursued, and the Cu(II) complexes, analogues of the Zn(II) **6** derivative, were further synthesized and characterized. In particular, complex **8** has a similar pentacoordinated structure as the complex **6**,

having bpy-OH as the main ligand, and the tropolone (trop) chelated to the Cu(II) centre, and the chloride ligand coordinated as ancillary ligands.

A similar synthetic strategy used in the case of complex **6**, was followed, involving, in the first place, the synthesis of the precursor complex **VII**, as reported in Scheme 2.8.

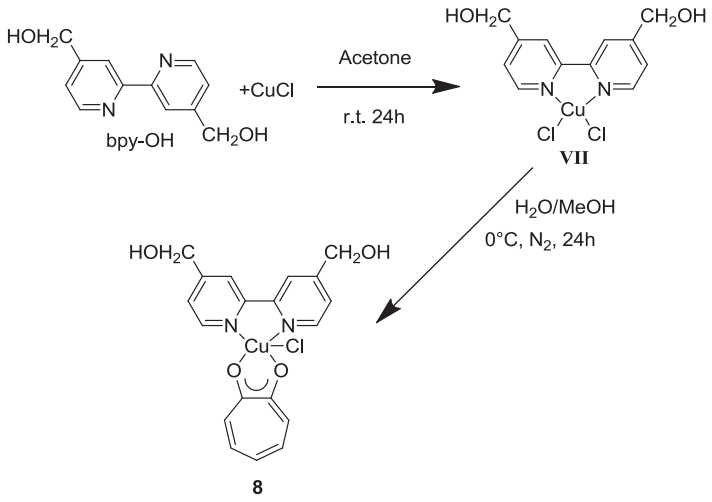

Scheme 2.8. Synthesis of complex **8.**

Regarding the precursor complex **VII**, the experimental elemental analysis data is in agreement with the calculated percentage of the molecular formula which points towards a Cu(II) complex having one bpy-OH and two chloride ligands *per* metal centre.

In the IR spectra of precursor, the C=C band of the free bpy-OH is shifted from 1602 cm^{-1} to 1592 cm^{-1} and the C=N band is shifted from 1559 cm^{-1} to 1514 cm^{-1} confirming that the coordination of bpy-OH to the Cu(II) took place.

Nonetheless the neutral character proposed for this complex, conductivity measurements performed in methanol solution yielded values that are in the range of 1:1 electrolytes. Indeed, the value 100 $\Omega^{-1} \cdot cm^2 \cdot mol^{-1}$ found for precursor complex **VII** is between the limit of the 80-115 $\Omega^{-1} \cdot cm^2 \cdot mol^{-1}$ range of values reported for similar univalent derivatives. This may suggest a labile character of the chloride ligand, and therefore once dissolved in methanol, complex **VII** looses the chloride ligand and converts into an ionic specie as seen above in the case of precursor **III**.

The photophysical behaviour of **VII** has been investigated by UV-Vis spectroscopy in water solution at room temperature, where the Cu(II) complex exhibits absorption bands at 253 nm, 297 nm and 308 nm. The absorption bands are different to the ones exhibited by the free ligand bpy-OH in the same solvent confirming the formation of precursor complex **VII** took place. Regarding the luminescence, precursor **VII**, like the free bipy-OH ligand, does not emit.

Through slow evaporation of a complex **VII** water solution, blue crystals have been obtained. Single crystal X-Ray diffraction analysis shows the Cu(II) ion in a four-coordinate squared planar configuration (Fig. 2.17). The central metal ion is coordinated by two nitrogen atoms of the bipyridine ligand and two chloride ligands. The symmetric unit is then completed by the presence of a water molecule, which is probably crystallized over the long crystallization process.

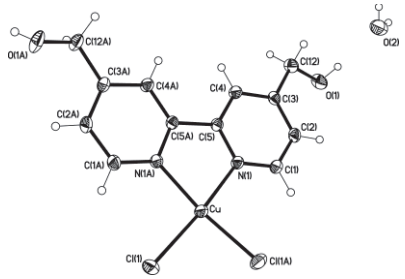

Figure 2.17. Molecular structure of **VII**.

The reaction of precursor **VII** with one equivalent of potassium tropolonate salt, at the conditions reported in Scheme 8, yields the formation of complex **8**. This complex is soluble in methanol, ethanol, DMSO and water. In particular, its solubility in water has been deeply investigated by spectrometric measurements, yielding the *S* 10^3 (mol/dm^3) value of 5.36(2), as reported and discussed in Table 3.1, Chapter 3.

Elemental analysis has been performed, confirming the proposed stoichiometry reported in Scheme 2.8. Furthermore, in complex **8** IR spectrum, the carbon-oxygen band of the trop ligand is shifted with respect to the free ligand, confirming its successful coordination to the Cu(II) metal centre.

Regarding the conductivity measurements, the value of 149.42 $\Omega^{-1} \cdot cm^2 \cdot mol^{-1}$ found for complex **8** is too high to suggest a neutral specie. This finding may be related, again, to the labile character of the chloride ligand. Therefore, once dissolved in methanol, the complex looses the chloride ligand converting into an ionic specie.

The photophysical behaviour of **8** has been investigated by UV-Vis spectroscopy in water solution at room temperature. Complex **8**

exhibits several absorption bands at 241 nm, 295 nm, 310 nm, 333 nm and 377 nm. In order to test its stability in solution, absorption measurements have also been conducted over time (Fig. 2.18).

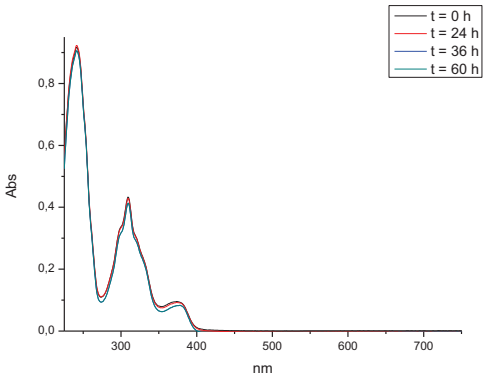

Figure 2.18. Complex **8** Absorption spectra at room temperature (after 0, 24, 36, 60h)**.**

Moreover, like its precursor complex **VII** and the bpy-OH ligands, complex **8** is not luminescent.

The molecular structure of complex **8** has been obtained by single crystal X-Ray analysis by a slow evaporation of its water solution. The single crystal X-Ray analysis (Fig. 2.19) revealed that Cu(II) ion is penta-coordinated, in a square-pyramidal geometry (τ = 0.04, similar value found for the Zn(II) derivative **6** of 0.03),[117] with the basal plane formed by the two chelating ligands, bpy-OH and trop respectively, while the chloride ion is located on the apex of the pyramid.

[117] **Addison, A. W. Rao, T. N.** 1984, J. Chem. Soc. Dalton Trans., pp. 1349-1356.

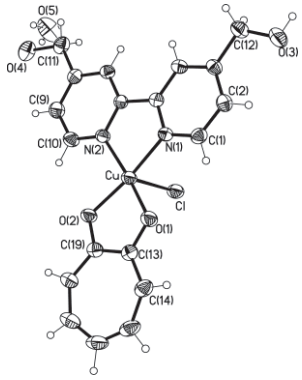

Figure 2.19. Molecular structure of complex **8**.

As expected, by changing the metal centre from Zn(II) (in complex **6**) to Cu(II), bond distances and angles within the coordination sphere are found very different (Table 2.1). The main observable change is related to total planarity within the basal plane between the two chelated rings, with a torsion angle between the two mean planes of 6.6°. The two "bite" angles relative to the two chelated ligands are O(1)-Cu- O(2) 83.3(1)° and N(1)Cu-N(2) 82.1(1)°, while the average angle formed by the apical chloride ligand with the coordinated N and O atoms is 94.6(1)°.

	Complex 6	Complex 8
M-O(1)	2.0260(12)	1.933(3)
M-O(2)	2.0493(13)	1.922(3)
M-N(1)	2.0961(14)	1.974(3)
M-N(2)	2.1033(13)	1.980(3)
M-Cl	2.2717(6)	2.7375(13)
O(1)-M-O(2)	78.61(5)	83.34(11)
N(1)-M-N(2)	77.44(5)	82.11(12)
O(1)-M-N(1)	93.97(5)	98.37(12)
O(1)-M-N(2)	148.40(5)	169.39(13)
O(2)-M-N(1)	146.93(6)	171.77(12)
O(2)-M-N(2)	92.07(5)	94.73(12)
Cl-M-O(1)	105.87(4)	98.75(9)
Cl-M-O(2)	107.49(4)	99.92(9)
Cl-M-N(1)	105.53(4)	87.81(9)
Cl-M-N(2)	105.73(4)	91.86(10)

Table 2.1. Bond distances (Å) and angles (°) of complexes **6** and **8**.

Complex **8** crystallizes with one water molecules in the asymmetric unit, and, differently than the analogous Zn(II) derivative **6**, it is found highly soluble in water.

Due to the success in the seriously improved water solubility of complex **8**, and considering its size, as measured from the crystal structure, of about 11.3 Å x 8.7 Å (Figure 2.20), similar to G-quadruplex structure, the binding properties of complex **8** with human telomeric DNA were investigated by isothermal titration calorimetry (ITC).

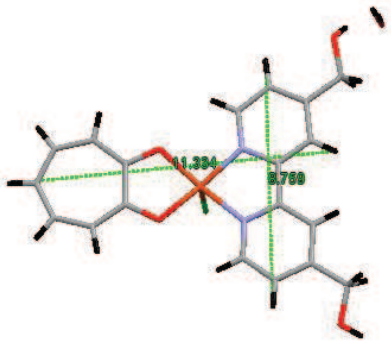

Figure 2.20. Molecular structure complex **8** showing its size.

The binding data obtained by TCI reveal a positive enthalpy variation. Generally, the formation of new interactions (in this case between complex **8** and human telomeric DNA) should be an exothermic process, therefore accompanied by a negative enthalpy variation. In this case, the found positive value is indicative of the existence of other processes not associated to the interactions between this two components. Therefore, complex **8**, at least from this preliminary results, does not behave as a G-quadruplex binder (Figure 2.21).

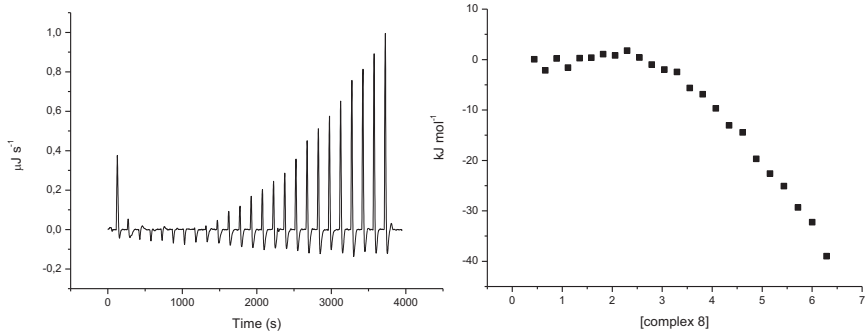

Figure 2.21. ITC profile for complex **8** and human telomeric DNA in a stoichiometry 6.5:1 ratio, respectively.

The structural characterization of complexes **6** and **7** has been published in the article number 2: Non-classical anticancer agents: on the way to water soluble zinc(II) heteroleptic complexes. B. Sanz Mendiguchía, D. Pucci, T. F. Mastropietro, M. Ghedini, A. Crispini, Dalton Trans., 2013, 42, 6768, included in the Thesis Supplementary Information. The structural data of complexes **VII** and **8** are reported as CIF files in the Thesis Supplementary Information.

2.4 Synthesis and characterization of tropolone-based complexes increasing the aromatic portion in N,N chelating ligand

New Zn(II) heteroleptic complexes containing N,N and O,O-chelating ligands, were synthesized by using an aromatic nitrogen ligand with an extended aromatic portion when compared to bipyridines, with the aim to improve, eventually, the intercalating properties found for the reference complex **B**. In this aim, a bisquinoline ligand bearing the same functionalities seen in the case of bipy-OH, that is 4,4'-bis(hydroxymethyl)-2,2'-biquinoline (bq-OH), was used. Therefore, two new Zn(II) complexes analogues to derivatives **6** and **7**, respectively, having one and two trop ligands as ancillary ligands and bq-OH as main ligand were further synthesized and characterized. The same synthetic strategies used for complexes **6** and **7** were followed for the synthesis of the new biquinoline containing Zn(II) complexes.

2.4.1 Synthesis and characterization of [(bq-OH)Zn(Trop)Cl], 9

Complex **9** was obtained following the synthetic methodology used for the synthesis of the analogues bipyridinic complex **6**. This involves previously the synthesis of the precursor complex **VIII** (Scheme 9), from bq-OH and $ZnCl_2$. The biquinolinic ligand was previously synthesized as described in the literature.[67c] The preparation of precursor **VIII** has been performed through the reaction between a slight excess of zinc(II) chloride with a solution of the bq-OH ligand in acetone at room temperature for 24 hours (Scheme 2.9).

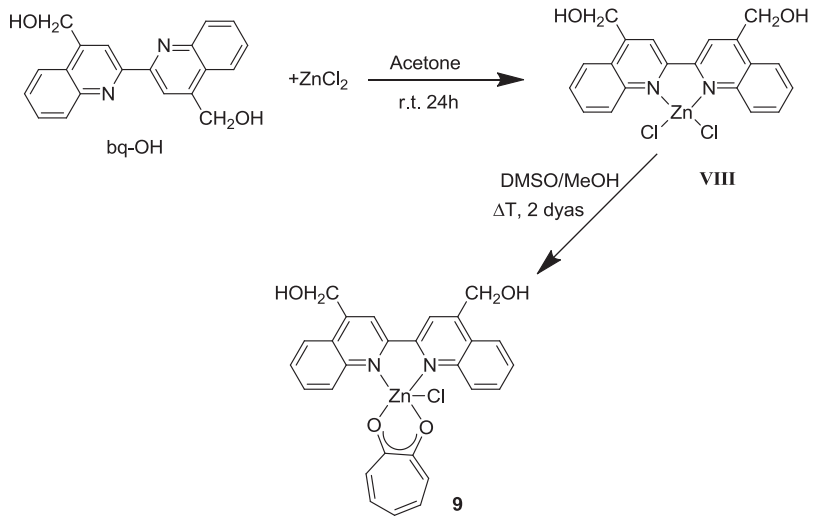

Scheme 2.9. Synthesis of complex **9.**

Elemental analysis has been performed on the precursor complex **VIII**, confirming the proposed stoichiometry presented in Scheme 9.

In the IR spectrum of precursor **VIII**, the C=C and C=N bands are shifted by about 5-7 cm^{-1} with respect to the corresponding N, N-free ligand, confirming that the coordination to the Zn(II) took place.

In the ^{1}H NMR spectrum of the precursor complex **VIII**, an upfields shift of the aromatic proton signals with respect to the free ligand is observed, confirming the successful coordination to the Zn(II) metal centre.

The neutral character was confirmed by conductivity measurements performed in DMSO solution. Indeed, the measured conductivity value of 0.73 $\Omega^{-1} \cdot cm^{2} \cdot mol^{-1}$ is too low to suggest an ionic specie, since the range reported for 1:1 electrolytes is 50-70 $\Omega^{-1} \cdot cm^{2} \cdot mol^{-1}$.

The photophysical behaviour of **VIII** has been investigated by UV-Vis spectroscopy in DMSO solution at room temperature. The absorption spectrum of precursor complex **VIII** contains similar bands as for the free ligand, respectively at 317 nm, 328 nm and 339 nm.

The precursor **VIII** has been further used in the synthesis of complex **9**. This Zn(II) complex has been obtained adding a solution of precursor **VIII** in DMSO to a solution of one equivalent of potassium tropolonate in methanol (Scheme 2.9). Elemental analysis has confirmed the proposed stoichiometry reported in Scheme 2.9.

Furthermore, in the IR spectra the presence of the tropolone C=O band is shifted from 1599 cm^{-1} to 1594 cm^{-1}, confirming that the chelation to the Zn(II) ion took place.

In the aromatic region of the ^{1}H NMR spectrum of **9**, all 21 protons of the bq-OH and trop ligands were correctly identified and assigned, in

the range of 8.9 and 6.8 ppm. An upfield shift of the bq-OH proton signals and the downfield shift of the trop proton signal are observed respect the bq-OH and trop free ligands, confirming the successful coordination to the Zn(II) metal centre. Finally the signals attributed to the hydroxymethyl groups of bq-CH_2OH ligand were identified as singlets at 5.74 ppm for the OH and 4.13 ppm for the methylene group. Importantly, the integrated ratio between aromatic protons of the two ligands in complex **9**, showed the presence of one bq-OH and one trop ligand *per* Zn(II) centre.

The photophysical behaviour of **9** has been investigated by UV-Vis spectroscopy in DMSO solution at room temperature. The absorption spectrum shows absorption bands centred at 306 nm, 318 nm, 328 nm, 341 nm and 367nm (Fig. 2.20). Moreover, complex **9** presents an emission band centred at 420 nm, confirming the formation of a new complex being precursor **VIII** not emissive (Fig. 2.22).

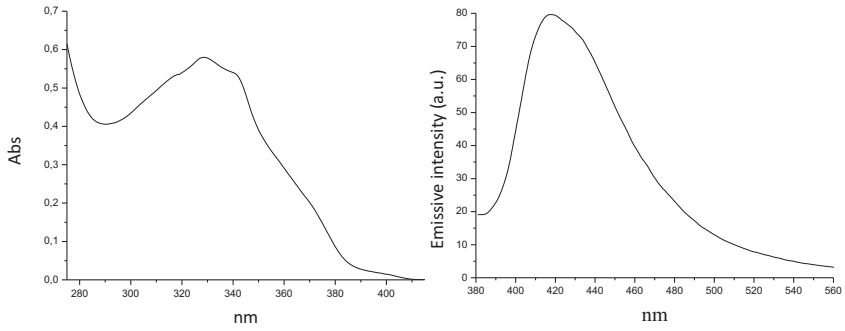

FIgure 2.22. Absorption and emission spectra of complex **9**.

2.4.2 Synthesis and characterization of [(bq-OH)Zn(Trop)2], 10

Complex **10** was prepared from the previous precursor **VIII** in the same way as complex **9**, but using 2 equivalents of potassium tropolonate and slightly modifying the reaction conditions (Scheme 2.10).

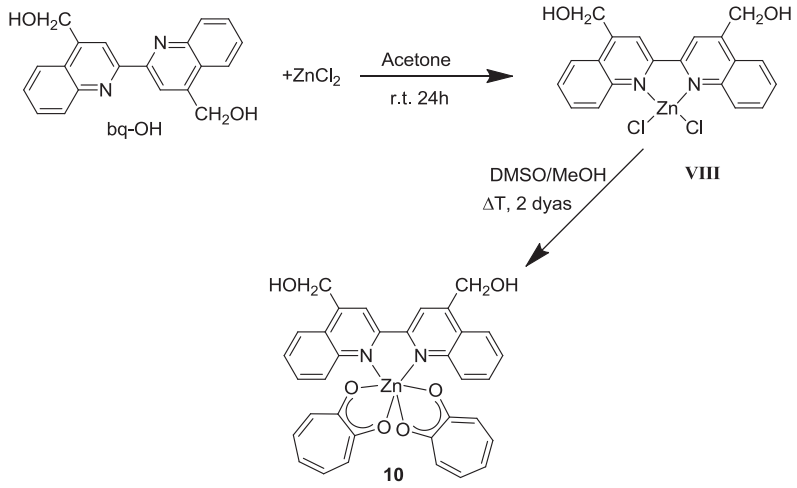

Scheme 2.10. Synthesis of complex **10.**

The elemental analysis data confirms the structure proposed in Scheme 2.10. The IR spectrum of complex **10** revealed the presence of a band, at 1592 cm^{-1} assigned to the carbon-oxygen stretching confirming the chelation between tropolone ligand and the Zn(II) ion.

The ^{1}H NMR spectrum of this complex has revealed the formation of complex **10**. In fact, the lack of the tropolone intramolecular

hydrogen bonded, validates the Zn(II) coordination to the tropolone ligand and the intensities of the signals are agreement with a 1:1:2 metal-to-N,N ligand-to-tropolone stoichiometry.

The behaviour of complex **10** in DMSO solution has been investigated by UV-Vis spectroscopy at room temperature in order to verify the formation of the complex. The absorption spectrum exhibited different bands at 333 nm, 373 nm, 383 nm and 394 nm (Fig. 2.21). Moreover, complex **10** presents an emission band centred at 422 nm. The presence of luminescence at 422 nm confirms the formation of a new complex (Fig. 2.23).

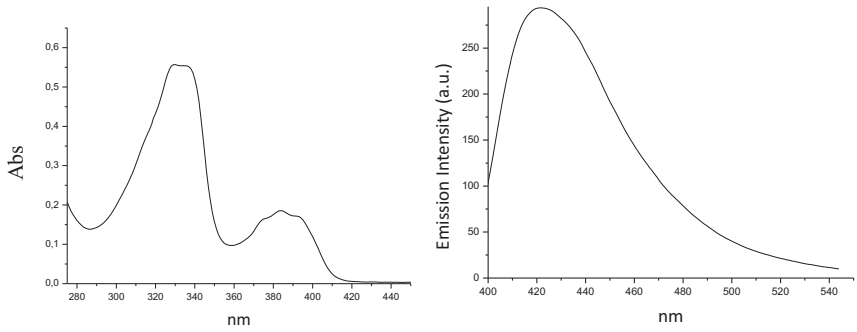

Figure 2.23. Absorption and emission spectra of complex **10**.

Chapter 3

Synthesis and characterization of tropolone-based metal containing co-crystals

The Zn(II) tropolone-based metal complexes **6** and **7**, presented in Chapter 2 suffer of scarce solubility in water. Due to the presence of molecular synthons such as the $–CH_2OH$ groups on the bipyridine ligand, able to interact with organic molecules to form, *via* hydrogen bonds, new supramolecular derivatives, these systems can be used as probes in the formation of inorganic co-crystals/salts. In this part of the thesis is reported the use of metal complexes **6** and **7** in reaction with an organic molecule (saccharin) in order to promote the formation of salts and co-crystals metal systems. Different methods, such as solution and liquid assisted grinding, have been used for the synthesis of this salts/co-crystals. Although in both cases the formation of co-crystals has not been reached neither by solid state reaction nor by solution methods, new Zn(II) derivatives have been isolated due to hydrogen exchange between saccharine and the tropolonate coordinated ligand (acid/base reaction), with different solubility properties.

In order to prove the validity of the reaction mechanism proposed, the same reactions have been conducted by using the Cu(II) analogous complex **8**. Reactions have been made with the same methods than

seen above, however including the rotavapor evaporation. The attempt to obtain metal-based co-crystals has led to the formation of new copper derivatives, based on an acid/base reaction. In this case, no rearrangement around the metal ion is observed, and only neutral species are formed.

3.1 Synthesis and characterization of [(bpy-OH)$_2$Zn(Trop)][Sac], 11

To increase the solubility of complex **6**, different methods for co-crystallization with saccharin have been performed, such as liquid assisted grinding and solution methods.

Liquid assisted grinding: A yellow powder was obtained by grinding the Zn(II) complex **6** with two equivalents of saccharin and small amount of water in a ball mill for 8 hours. From slow evaporation of water solution of the obtained powder, suitable crystals of complex **11** have been obtained. The reaction product has been characterized by X-ray diffraction powder (typical technique used to follow solid state reactions) and the corresponding patterns compared with those calculated on the basis of the single crystal structures.

The comparison between the powder diffraction pattern of the crystalline powder as obtained after the grinding and the one recorded from the crystals isolated from solution crystallization in water, reveals some important points (Figure 3.1).

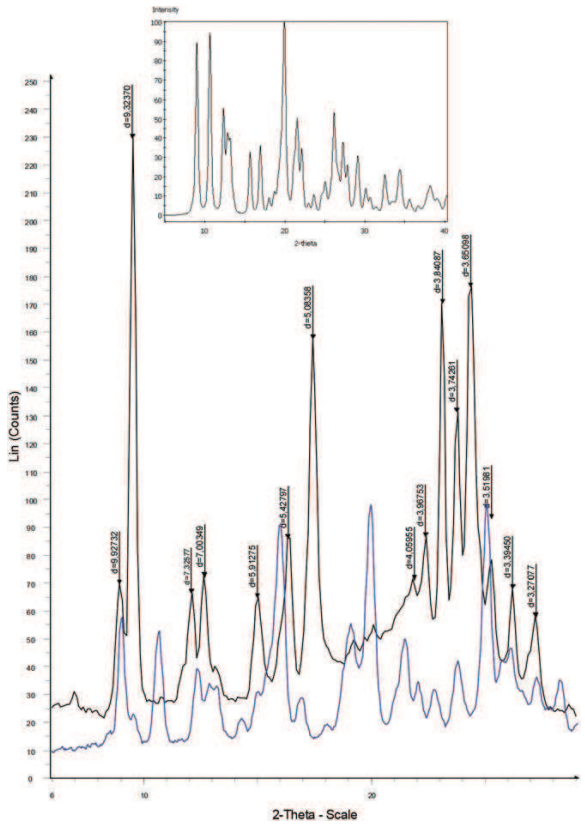

Figure 3.1. Comparison between (black) the X-ray powder diffractogram measured on single crystals of **11** and (blue) that measured on the crystalline powder obtained by grinding. In the inset the powder pattern of **6** calculated from single crystal analysis.

The final product isolated from solution as single crystals, shows a very different diffractogram when compared to that calculated on the basis of the single crystal structure of **11**.

However, the powder obtained mechanochemically contains only a small amount of the final product isolated from solution, while a

large portion of unreacted complex **6** is still present, as shown by the presence of commune diffraction peaks.

The single crystal analysis performed on the yellow crystals of **11** has revealed the formation of an ionic hydrate derivative of general formula $[(bpy\text{-}OH)_2Zn(Trop)]Sac^{\cdot}2H_2O$. The Zn(II) ion of the complex cation is in an octahedral geometry, coordinated to two bipyridine and one tropolonate chelated ligands (Figure 3.2).

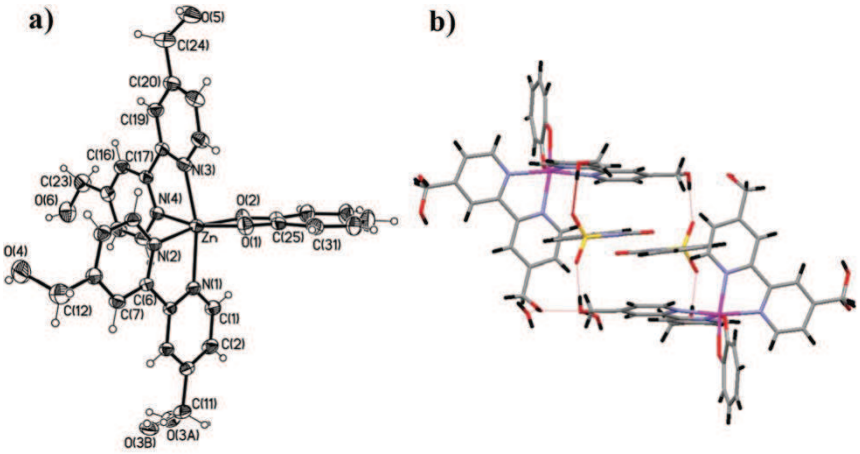

Figure 3.2. Molecular structure of complex **11** showing the complex cation with the atomic numbering scheme (a) its hydrogen bonding network with both the saccharinate anion and water molecules (b).

The saccharinate, transformed by using saccharin, behaves as the counter ion but also establishes strong S=O-H-O hydrogen bonds with the complex cation. The co-crystallized water molecules strongly interact with the hydroxyl groups of another bipyridine ligand.

The single crystal X-ray characterization of complex **11** has demonstrated that the expected formation of co-crystals has not been

reached, clearly proving how difficult and complicated by the somehow unexpected formation reactivity of the inorganic moiety is the achievement of metal-based co-crystals. The effective reaction, induced by an acid-base proton transfer between saccharin and one coordinated tropolonate, leads to the formation of complex **11**, *via* ligand exchanged. Although the reaction has been conducted in excess of saccharine, knowing the exact structure of the so formed complex **11**, the real stoichiometry ratio between complex **6** and saccharine should be indicated as 2:1 (Scheme 3.1).

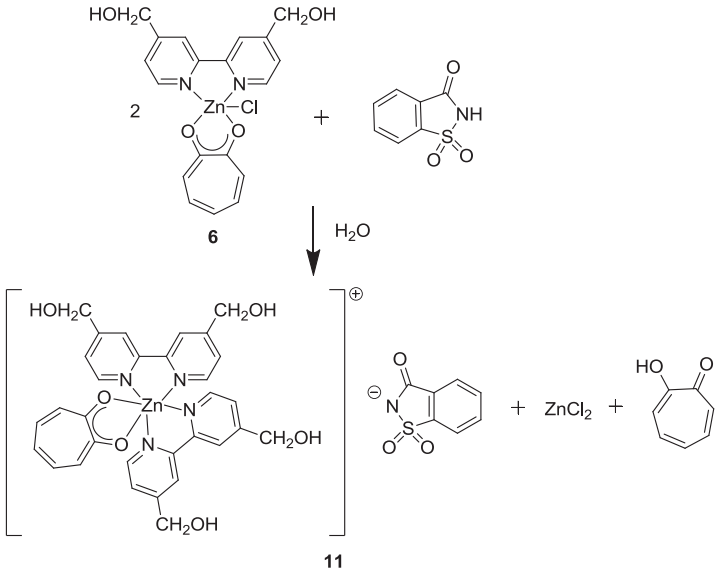

Scheme 3.1. Proposed effective reaction in the formation of **11** salt.

Complex **11** shows improved solubility, being water soluble, when compared to complex **6**.

Moreover, from water-solubility studies conducted by UV–Vis spectrophotometer on both **6** and **11** complexes, a distinct increased

water solubility of complex **11** was proved, being nearly three times higher (245 μM and 673 μM, respectively).

The photophysical behaviour of **11** has been investigated by UV-Vis spectroscopy in water solution where the complex **11** exhibits an absorption bands at 292 nm, 304 nm, 319 nm and 382 nm very different to the absorption spectrum of complex **6**. In order to test the stability in solution of complex **11** absorption measurements have also been conducted over time (Fig.3.3).

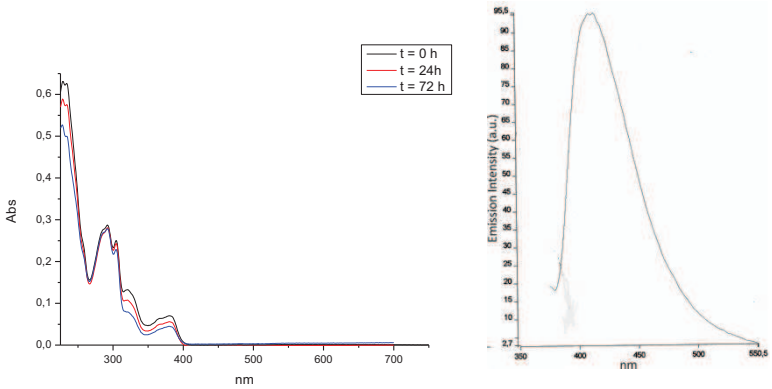

Figure 3.3. Absortion spectra at room temperature (after 0, 24, and 72h) and emission spectrum of complex **11**.

Moreover, complex **11** presents an emission band centred at 412 nm, different to the emission band of the free bpy-OH ligand, centred at 308 nm (Fig. 3.3).

In order to check the reproducibility of this synthesis, the reaction between **6** and saccharin was conducted also in water.

Solution method: Complex **11** has been obtained adding complex **6** to solution of 2 equivalent of saccharin in water solution (Scheme 3.1). For slow evaporation of this solution, yellow crystals were obtained.

The IR spectrum, powder diffraction pattern, ^{1}H NMR and UV-Vis are found perfectly superimposable with characterization of crystals of complex **11** obtained by liquid assisted grinding.

3.2 Synthesis and characterization of [(bpy-OH)Zn(Trop)(Sac)], 12

The proposed synthetic reaction proposed in the synthesis of complex **11**, has been confirmed by the reaction between complex **7** and saccharine. The reaction has been conducted by grinding the two powders with drops of methanol and the reaction product analyzed by X-ray diffraction (Figure 3.4).

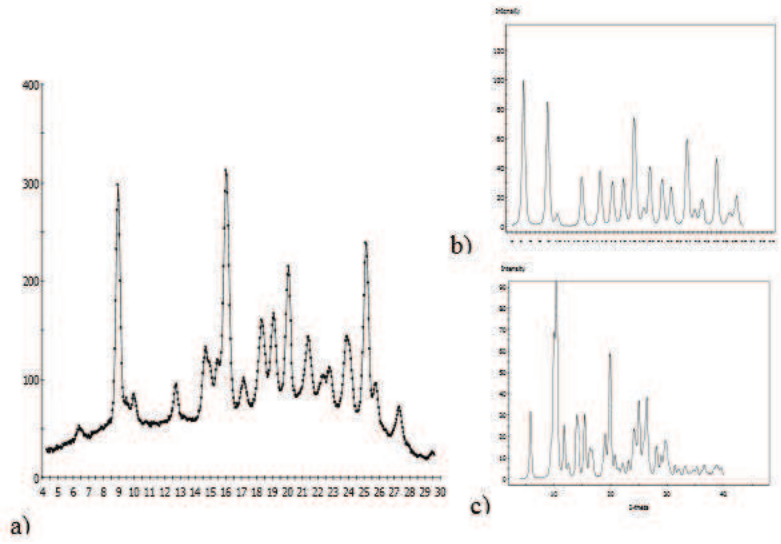

Figure 3.4. Powder patter of the crystalline powder obtained by grinding complex **7** and saccharine (a), compared with the diffractograms calculated from single crystal analysis of **7(**b) and **12**(c).

Although its diffractogram does not show any new reflections when compared to those of the raw reactants, single crystals of a new specie, complex **12**, has been isolated in small amount after slow evaporation of a methanol solution of the reaction product.

The single crystal analysis performed on the yellow crystals of **12** in ethanol has revealed the formation of the hydrate complex [(bpy-OH) Zn(Trop)Sacc]·H_2O reported in Figure 3.5, in which one chelated tropolonate has been replaced by the saccharin ion. The overall geometry around the Zn(II) ion is very similar to that of complex **6**, with the saccharinate ligand coordinated through the nitrogen atom on the apex of the pyramid.

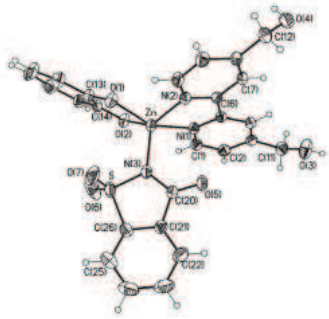

Figure 3.5. Molecular structure of complex **12**.

In this case, due to the hexa-coordination of the starting complex **7**, the proton transfer between saccharin and one coordinated tropolonate leaves the Zn(II) ion, now bis-chelated by one bipyridine and the remaining tropolonate, ready for the coordination to the so formed saccharinate ion. Eventually, this process is not particularly favourable, and very low yield of the new species **12** is not reached by a long crystallization process in methanol solutions of the crystalline reaction product. The proposed reaction mechanism, as reported in Scheme 3.2, implies the loss of one molecule of free tropolone ligand.

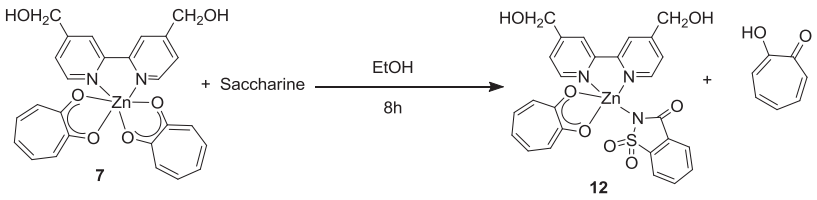

Scheme 3.2. Synthesis of complex **12.**

Differently than complexes **6** and **11,** this new derivative shows low solubility, being soluble only in ethanol.

The synthesis and characterization of complexes **6, 7, 11** and **12** has been published in the article number 2: Non-classical anticancer agents: on the way to water soluble zinc(II) heteroleptic complexes. B. Sanz Mendiguchía, D. Pucci, T. F. Mastropietro, M. Ghedini, A. Crispini, Dalton Trans., 2013, 42, 6768, included in the Thesis Supplementary Information.

3.3 Synthesis and characterization of [(bpy-OH)Cu(Trop)(Sac)], 13

The reaction to obtain the salt **11** is not a simple transformation of a possible API (complex **6**) into the corresponding salt. In order to prove the validity of the reaction mechanism proposed in the obtainment of the ionic derivative **11**, the same reactions have been conducted by using the Cu(II) analogous to the derivative **6**, that is complex **8**.

The reaction between complex **8** and saccharine has been conducted by using three different methods such as liquid assisted grinding, solution and rotary evaporator.

Liquid assisted grinding: by grinding the Cu(II) complex **8** with two equivalents of saccharin and small amount of water in a ball mill for 4 hours a blue powder was obtained.

From slow evaporation of the water solution of the obtained powder, suitable dark blue single crystals of complex **13** have been obtained in very high yield. The single crystal analysis performed on the blue crystals of **13** revealed the formation of a new derivative of the general formula [(bpy-OH)Cu(Trop)(Sac)] (Figure 3.6). The Cu(II) ion in the new complex, similarly to complex **8**, is penta-coordinated, in a slightly distorted square-pyramidal geometry (τ = 0.11, compared to 0.04 found in complex **8**),[119] with the basal plane formed by the two chelated ligands, bpy-OH and trop respectively, while the apex of the pyramid is occupied by the saccharinate ion coordinated through one of the $-SO_2$ group oxygen atom.

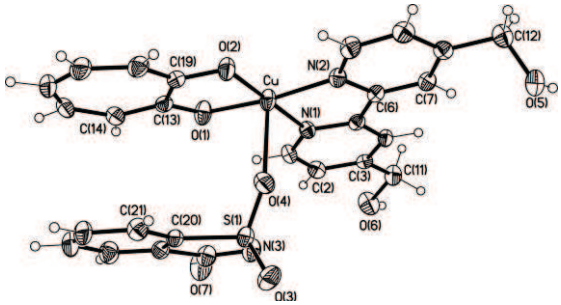

Figure 3.6. Molecular structure of complex **13**.

The distances and angles around the copper ion within the equatorial plane are typical for distorted square-pyramidal Cu(II)

complexes[118] and comparable with those values found for complex **8** (Table 3.1). The coordinated ligands are basically co-planar, with the dihedral angle between the two mean planes passing through the chelated rings of 6.5 °.

	Complex 8	**Complex 13**
Cu-O(1)	1.933(3)	1.941(2)
Cu-O(2)	1.922(3)	1.935(2)
Cu-N(1)	1.974(3)	1.977(2)
Cu-N(2)	1.980(3)	1.989(2)
Cu-O, Cl	2.7375(13)	2.529(2)
O(1)-Cu-O(2)	83.34(11)	84.06(8)
N(1)-Cu-N(2)	82.11(12)	82.13(10)
O(1)-Cu-N(1)	98.37(12)	96.52(9)
O(1)-Cu-N(2)	169.39(13)	175.95(9)
O(2)-Cu-N(1)	171.77(12)	171.95(9)
O(2)-Cu-N(2)	94.73(12)	97.41(9)
Cl-M-O(1)	98.75(9)	105.87(4)
Cl-M-O(2)	99.92(9)	107.49(4)
Cl-M-N(1)	87.81(9)	105.53(4)
Cl-M-N(2)	91.86(10)	105.73(4)

Table 3.1. Bond distances (Å) and angles (°) of complexes **8** and **13**.

Due to the Jahn-Teller effect the axial Cu-O contact is found to be much longer than the equatorial ones.

Summarizing, the reaction between complex **8** and saccharine, in the attempt to generate metal-based co-crystals, occurs via hydrogen

[118] (a) **Golenya, I. A. Gumienna-Kontecka, E. Haukka, M. Korsu, O. M. Kalugin, O. N. Fristky, I. O.** 2014, Cryst. Eng. Comm., Vol. 16, pp. 1904.(b) **Massoud, S. S. Junk, T. Mikuriya, M. Naka, Y. Mautner, F. A** 2014, Inorg. Chem. Commun., Vol. 50, pp. 48-50.

exchange between saccharine and the tropolonate coordinated ligand. Complex **13** is, therefore, obtained by an effective substitution of the apical chloride ligand in **8** with the in situ formed saccharinate ion, coordinated to the metal centre through one of the $–SO_2$ group oxygen (Scheme 3.3).

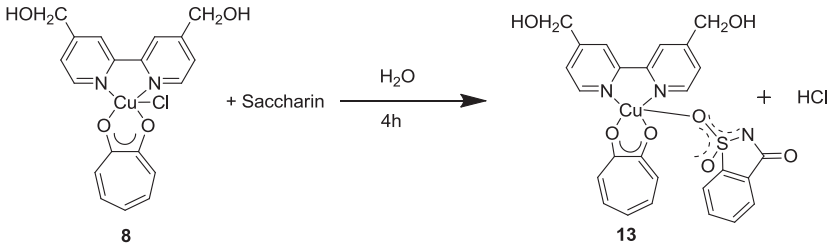

8 **13**

Scheme 3.3. Synthesis of complex **13.**

In order to prove the neutral nature of the new copper derivative **13** even in solution, conductivity measurements have been performed in water, yielding a value of 4.81 $cm^2 \cdot \Omega^{-1} \cdot mol^{-1}$, confirming the saccharinate coordination to the metal ion and, therefore, the neutrality of complex **13** even in solution.

Complex **13** is found to be soluble in methanol, ethanol, DMSO and water. In particular, its solubility in water has been deeply investigated by spectrometric measurements conducted by UV–Vis spectrophotometer, as already discussed for complex **8**, yielding a reduced solubility value when compared with **8** (Table 3.2).

Complexes	$S \cdot 10^3$, mol/dm^3
$C_{12}H_{17}Cl_2CuN_2O_3$ (**VII**),	2.58 ± 0.02
$C_{19}H_{19}ClCuN_2O_5$ (**8**)	5.36 ± 0.02
$C_{26}H_{21}CuN_3O_7S$ (**13**)	2.15 ± 0.02

Table 3.2. Solubility of complex **VII**, **8** and **13** in pure water at r.t.

From the obtained values, it is evident that complex **8** is found the most water soluble derivative and this result it is probably associated to its ionic nature in water solution (as proved by conductivity measurements) differently than what observed in the case of complex **13**. Both derivatives are neutral in the crystalline solid state with the chloride and saccharinate coordinated ligands, respectively, but, due to the labile nature of the chloride ligand, complex **8** becomes ionic in nature in the solution state.

The photophysical behaviour of **13** has been investigated by UV-Vis spectroscopy in water solution, where complex **13** exhibits absorption bands at 235 nm, 242 nm, 298 nm, 310 nm, 321 nm and 380 nm (Figure 3.7). Moreover, complex **13** does not shows an emission band.

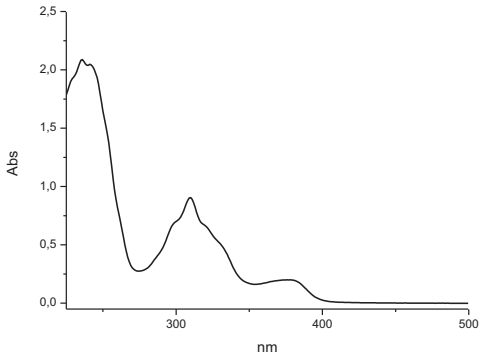

Figure 3.7. Absortion spectrum at room temperature of complex **13**.

Due to the evidence that conversion of complex **8** into the new derivative **13** is complete after the crystallization process in water and in order to check the reproducibility of this synthesis, the reaction between **8** and saccharin was conducted also *via* solution and rotary evaporator.

Solution method: Complex **13** has been obtained adding complex **8** to a solution of 1 equivalent of saccharin in water solution (Scheme 13). For slow evaporation of this solution, blue crystals were obtained.

The single crystal analysis performed on the blue crystals so obtained, revealed the formation of the same derivative **13** obtained by liquid assisted grinding reported in Figure 3.6.

Rotary evaporator: Complex **13a** has been obtained by adding complex **8** to a solution of 1 equivalent of saccharin in water solution. The resulting mixture was stirred for 1h. Then the solvent was evaporated *in vacuo*. For slow evaporation of the solid in water solution, green crystals were obtained.

Complex **13a** obtained by rotary evaporator was characterized by single crystal X-Ray diffraction and found to be the hydrate polymorph of complex **13** since one co-crystallised water molecule if found in the asymmetric (Fig. 3.8).

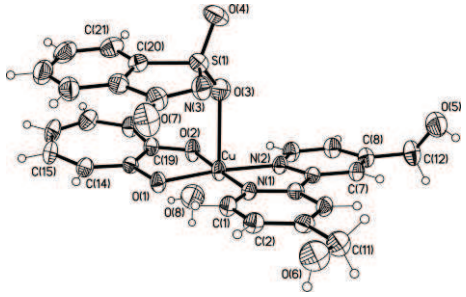

Figure 3.8. Molecular structure of complex **13a**.

The geometry around the Cu(II) ion is the same than complex **13**, being penta-coordinated, in a square-pyramidal geometry (τ = 0.07). The saccharinate ion is coordinated to Cu(II) ion through one of the –SO_2 group oxygen occupying the apical position of the pyramid.

Bond distances and angles around the metal centre are similar to those found in the anhydrous form **13**. Due to the Jahn-Teller effect the axial Cu-O contact is found to be much longer than the equatorial ones, being 2.534(5) Å.

In order to explain the different colour of the obtained crystals, photophysical investigations have been carried out on the crystalline solids **13** and **13a**. In both cases, the emission spectra have revealed a valuable luminescence in a range between the red region of the visible spectrum and the near infrared (730-820nm) (Fig. 3.9), highlighting that the blue/green colour of the samples is not due to their

photophysical properties but probably to different scattering phenomena.

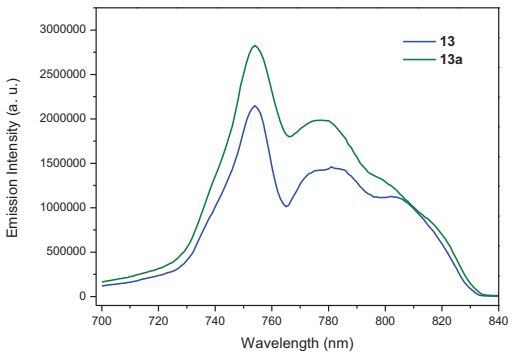

Figure 3.9. Emission spectra of crystalline solids **13** and **13a**.

The structural data of complexes **13** and **13a** are reported as CIF files in the Thesis Supplementary Information.

Chapter 4

Synthesis and characterization of chromonic liquid crystals

In the introduction Chapter of the present thesis, the chromonic liquid crystalline behavior of DNA solutions in water was described. In order to design possible liquid crystalline intercalators (due to the well known miscibility of the chromonic phases) and/or DNA model to test intercalation agents, new metal containing chromonic liquid crystals have been synthesized.

Ag(I) is a very versatile metal centre for designing liquid crystalline systems. Indeed, a large number of liquid crystals based on Ag(I) as metal centre with oligopyridines have been synthesized.[67-75] The type of ligands, substituents and/or counterions have a great influence on the type and symmetry of the mesophase exhibited by these Ag(I) complexes. In particular, as highlighted in Chapter 1, the tuning of the mesomorphic properties of a series of Ag(I) ionic complexes containing differently substituted bipyridines is related to the use of different counterions. These complexes exhibited columnar mesophases with different symmetries, as a function of the number of the alkyl chains on the bipyridine ligands, the type of the counterions or the coordination around the metal centre.

Willing to obtain Ag(I) complexes self-assembling into chromonic mesophases in water, new ionic N,N-coordinated Ag(I) complexes having two 4,4'-dihydroxymethyl-2,2'-bipiyridine (bipy-OH) as chelated ligands have been synthesized and characterized. Being these complexes ionic in nature, carboxylates with different alkyl chain length were used ss counterions. The Ag(I) silver salts containing the desired counterions were synthesized as reported in literature.[119,120] Furthermore, the choice of the hydroxyl substituents on the bipyridine ligand is related not only to the attempt to induce water solubility, but specially to their potential ability to interact *via* hydrogen bonds forming, eventually with water, supramolecular aggregates.

The ability of these silver(I) complexes to organize into columnar structures is highlighted in the solid crystalline state, by means of single crystal X-ray analysis performed on complex **14**.

One dissolved in water, complex **14**, as well as the other analogous, self-assemble giving rise to chromonic phases, characterized by their phase diagram completely resolved by polarized optical microscopy (POM) and X-ray powder diffraction techniques. Cryo-TEM experiments have also been carried out in order to directly reveal the chromonic nature at a suitable water concentration.[121]

---

[119] **Will, G. Boschloo, G. Nagaraja Rao, S. Fitzmaurice, D.** 1999, J. Phys. Chem. B, Vol. 103, pp. 8067-8079.

[120] **Yadav, J. J. Heinrich, B. De Luca, G. Talarico, A. M. Mastropietro, T. F. Ghedini, M. Donnio, B. Zerb, E. I.** 2013, Adv. Optical Mater., Vol. 1, pp. 844-854.

[121] **Gao, M. Kim, Y. K. Zhang, C. Borshch, V. Zhou, S. Park, H. S. Jakli, A. Lavrentovich, O. D. Tamba, M. G. Kohlmeier, A. Mehl, G. H. Weissflog, W.**

Furthermore, the chromonic phases have been aligned between two polymer covered glasses, following a method already reported in the literature[122] and showing transient twisted periodical stripe structures, a sign of elastic anisotropy.

Furthermore, to investigate the role of the counterion in the formation of these type of chromonic liquid crystals, several different counterions have been tested. In particular, the silver salts containing hexafluorophosphate, trifluorosulphonate and trifluoroacetate were used for the synthesis of the corresponding complexes, **17**, **18** and **19**. These complexes resulted insoluble in water, demonstrating the importance of the counterion in tuning the properties of the resulting complexes.

4.1 Synthesis and characterization of $[(bpy\text{-}OH)_2Ag][CH_3COO]$, 14

The same synthetic protocol used for the synthesis of similar complexes reported in literature with small modifications was followed.[67] In particular, the ligand bpy-OH was reacted with half equivalent of Ag(I) acetate in EtOH, under nitrogen atmosphere , in a

---

Studer, D. Zuber, B. Gnagi, H. Lin, F. 2014, Microsc. Res. Tech., Vol. 77, pp. 754-772.

[122] **Tone, C. M. De Santo, M. P. Buonomenna, M. G. Golemme, G. Ciuchi, F**. 2012, Soft Matter., Vol. 8, pp. 8478-8482.

vessel protected from light, for 4 hours (Scheme 4.1). Complex **14** was thus obtained, in relatively high yields (72%).

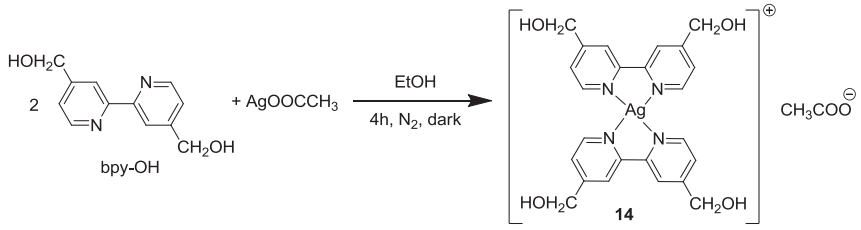

Scheme 4.1. Synthesis of complex **14.**

The elemental analysis data performed on complex **14** confirmed the proposed structure presented in Scheme 4.1.

The IR spectrum of complex **14** shows the corresponding asymmetric and symmetric stretching vibration frequencies for the carboxylate counterion at 1560 cm^{-1} (ν_{asym} (COO^-)) and at 1389 cm^{-1} (ν_{sym}(COO^-)), respectively.[123] Furthermore, the IR spectrum shows a large band at 3369 cm^{-1}, regardless of several attempts to dry the powders, and therefore reasonably attributable to the 2,2'-bipyridine and $–CH_2OH$ substituents.

The ^1H NMR spectrum of complex **14**, shows, as expected, the signals corresponding to the 12 aromatic protons of the bpy-OH ligands in the aromatic region, while in the aliphatic region a singlet corresponding to the methylene group of the bipy-OH substituent at 4.91 ppm and a singlet corresponding to the alkyl protons of the

[123] **Alcock, N. W. Tracy, V. M.** 1976, J. Chem. Soc. Dalton Trans., pp. 2243-2246.

carboxylate counterion at 1.89 ppm. Furthermore, the intensity of the signals indicates a 2:1 ratio between the ligand and the counterion. The successful coordination of the bpy-OH ligand to the Ag(I) metal centre is proved by the shift of the aromatic protons when compared to the free ligand spectrum. Indeed, the protons in *meta* and *para* positions with respect to the pyridine N atoms are both downfield shifted with approximately 0.15 ppm.

The ionic character was confirmed by conductivity measurements performed in methanol solution. Indeed, the value found 82.72 Ω^{-1} $\cdot cm^2 \cdot mol^{-1}$, is in the range of values reported for 1:1 electrolytes (80-115 $\Omega^{-1} \cdot cm^2 \cdot mol^{-1}$).

The photophysical behaviour of **14** has been investigated by UV-Vis spectroscopy in water solution. The absorption spectrum showing absorption bands centred at 235 nm and 281 nm (Fig. 4.1), instead of the only one band showed by the bpy-OH free ligand. Moreover, complex **14** does not presents emission properties in contrast to the emission properties of the N, N chelating ligand.

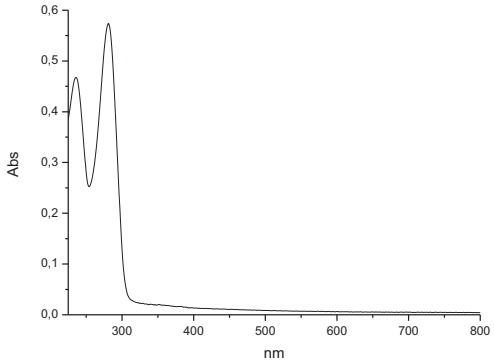

Figure 4.1. Absortion spectrum at room temperature of complex **14**.

The presence of solvent was revealed by TGA analysis. The thermogram shows loss of weight corresponding to one water molecule (Fig. 4.2) *per* complex.

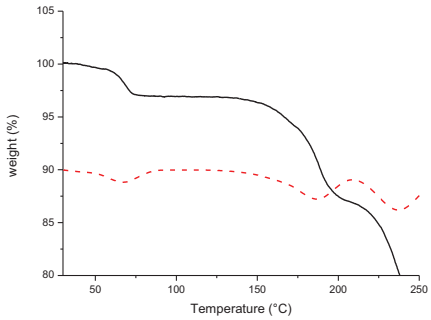

4.2. TGA trace of powder complex **14** with its derivative in dotted red (experimental mass loss 3.01% corresponds to one water molecule calcd. 2.92%).

From very slow evaporation of a methanol solution, yellow crystals of **14** have been obtained. Single crystal X-Ray diffraction analysis of complex **14** (Fig. 4.3), shows that the Ag(I) ion is in a tetra-coordination geometry bis-chelated by two bypiridine ligands. The asymmetric unit is then completed by the presence of the acetate anion and two water molecules, one of which is probably crystallized over the long crystallization process. Bond distances and angles around the silver ion are in good agreement with those already reported for similar complexes.[124]

[124] **Bellusci, A. Crispini, A. Pucci, D. Szerb, E. I. Ghedini, M.** 2008, Cryst. Growth Des., Vol. 8, pp. 3114-3122

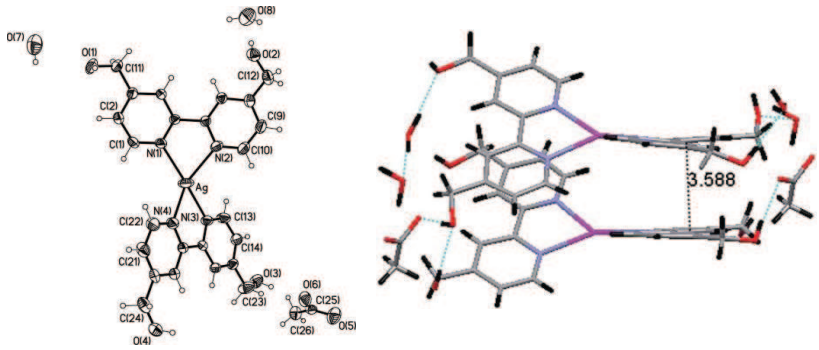

Figure 4.3. Perspective view of ionic complex **14** and view of the repeat unit of metal containing cations of complex **14.**

Both coordinated bipyridine ligands deviate from planarity, showing the internal torsion angles N–C–C–N of 9.4(5) and 4.4(5)°, respectively. Generally, symmetric bis-chelate pseudo tetrahedral complexes themselves are not chiral. Nevertheless complex **14** crystallizes in the chiral orthorhombic P2(1)2(1)2(1) space group. The symmetry within each bipyridine is broken by means of the different mutual orientations of the $–CH_2OH$ substituents (torsion angles around the $C_{arom}–C$ bond of: C(2)–C(3)–C(11)–O(1) 35.0(6)°, C(9)–C(8)–C(12)–O(2) 163.0(4)°, C(14)–C(15)–C(23)–O(3) 16.6(7)°, C(21)–C(20)–C(24)–O(4) 175.5(4)°), generating chirality around the metal centre. The relative orientation of the two ligands creates a helicity around the metal ion, and the absolute configuration has been properly resolved. Labelling the aromatic ring bearing the $–CH_2OH$ group with the same orientation in the two bipyridine ligands allows identification of the single crystallographic independent complex cation in Λ

configuration.[125]

The analysis of the intermolecular interactions existing within the asymmetric unit and in the 3D crystal packing of complex **14** is of particular interest for understanding the relationships between the structure and chromonic liquid crystal properties of this class of complexes. The presence of water molecules both in the powder and in the crystalline solid state of **14** has confirmed the usefulness of the properly functionalized 2,20-bipyridine with hydroxyl groups as well as the use of acetate anions in the formation of water aggregates species. The presence of water molecules and the acetate anion interacting via hydrogen bonds with the hydroxyl groups at the periphery of the metal containing cation generates the formation of cation dimeric repeating units despite the potential electrostatic repulsion (Fig. 4.3).

Within the dimeric unit, cations interact through aromatic π–π stacking interactions with a distance of about 3.6 °A (defined as the distance between the centroid of one aromatic ring and the mean plane passing through the above aromatic coplanar ring) and the silver ions of the closest cations are forced at a distance of 3.951 °A. The dimeric unit, regularly repeating along the *a* axis, gives rise to metal containing columns. A tight hydrogen bonding network is formed in the 3D space and the columns of metal cations are segregated between layers of acetate ions and water molecules by means of the O/H hydrogen bond type (Fig. 4.4).

[125] **Knof, U. von Zelewsky, A.** 1999, Angew. Chem., Int. Ed., Vol. 38, pp. 302–322.

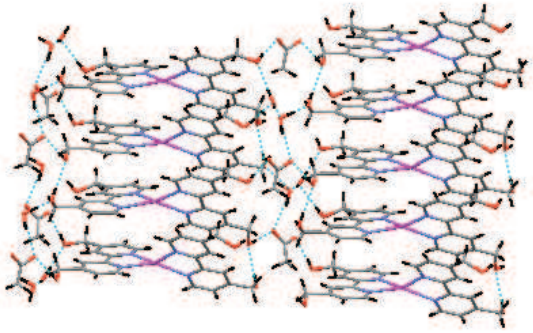

Figure 4.4. Solid state organization of complex **14** showing the formation of metal containing cation columns held together by means of hydrogen bonds formed with acetate anions and water molecules.

X-Ray powder diffraction measurements (PXRD) were carried out at room temperature, on 20 wt% and on 60wt% CLC non-aligned phases. In this case the nematic diffuse peak in the PXRD pattern is centred at $2\theta = 2.5°$, corresponding to a *d* value of 35.3 Å (Fig. 4.5a). A moderately sharp reflection in the high-angle region of the PXRD pattern is centred at 3.48 Å corresponding to the average stacking repeat distance within columns. The intensity of this high-angle reflection, sharper than the usually broad stacking repeat peak encountered in the discotic nematic phase, points towards the existence of a truly N chromonic phase. By changing concentration, moving to 60wt%, the low angle reflection moves to $2\theta = 4.88°$, which corresponds to a much lower *d* value of 18.1 Å (Fig. 4.5b). This observed *d* value reduction with the complex concentration in the water solution is consistent with a decrease of the average columns distance due to the diminished amount of "see water" in between chromonic molecules and concomitant increase of columnar

organization order. The presence in the small angle region of two other reflections, together with the first one in the ratio $1:\sqrt{3}:\sqrt{4}$, are characteristic of a 2D lattice of a hexagonal columnar phase, corresponding to the indexation (*hk*) = (10), (11) and (20), with a cell parameter *a* = 20.8 Å. This value is similar to the intermolecular distance found in the close-packed hexagonal structure of the crystal phase (of about 17 Å) indicating that the hexagonal arrangement in the mesophase is obtained from the crystalline solid state through decorrelation between columns with maintenance of the intra columns interactions. Indeed, the major feature in PXRD pattern of **14** of the presence of a chromonic M phase is a sharp high-angle reflection corresponding to the stacking repeat distance of 3.51 Å. This value is found to be slightly larger than the stacking repeat distance of 3.40 Å, usually reported for organic chromonic molecules. This increase is fundamentally due to the stacking within columns of non-planar molecules, aggregated through aromatic interactions between facing bipyridine fragments and consistent with the aromatic π–π stacking distance of about 3.6 Å found in the crystalline solid state.

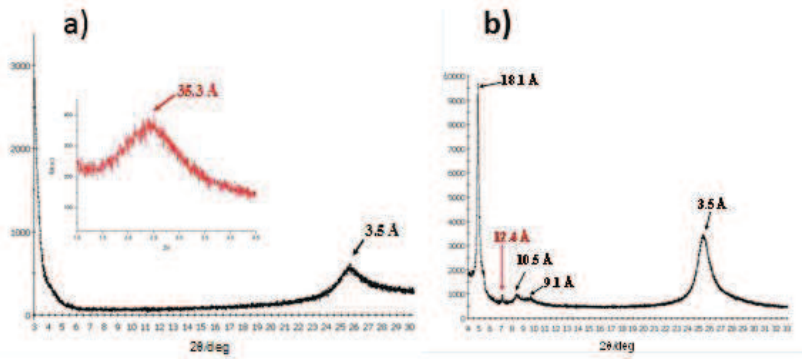

Figure 4.5. Complex **14** X-Ray diffraction pattern (low angle region in the inset) in the nematic phase at 20%wt concentration (a) and in the hexagonal phase at 60%wt concentration at room temperature (b).

The phase diagram of complex **14** was completely determined by POM and the relative type of mesophase confirmed by X-Ray diffraction analysis. Water solutions of complex **14** exhibit LC phases from 15% to 60% of concentration. In Figure 4.6, the phase diagram of complex **14** is reported with some POM pictures of the textures observed inside the cell.

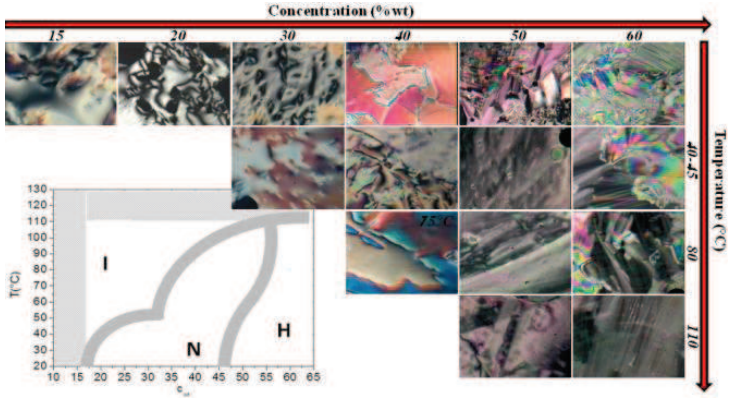

Figure 4.6. Phase diagram and POM pictures of the texture observed at different temperatures and concentrations, confirming the presence of LC phases.

At room temperature, from 15% to nearly 50% of concentration, complex **14** presents nematic (N) regions as proved by typical textures observed on POM. This phase directly melts into the isotropic phase by increasing temperature. At higher concentration complex **14** organizes into a hexagonal phase at room temperature. While at 50% the hexagonal phase transforms into the N phase by increasing temperature before isotropization, at 60% the nematic phase is suppressed, and the hexagonal phase is stable until isotropization at 120°C.

Cryo-TEM analysis carried out on complex **14** solution in its nematic phase (20%wt), directly demonstrate the assembly of the molecules into columnar aggregates and the nematic arrangement of the aggregates. Figs. 4.7a and 4.7b show typical side-view (corresponding to a planar orientation of the columns with the electron beam perpendicular to the LC film) and top-view (a homeotropic orientation) of the aggregates, respectively. The aggregates are represented by the dark stripes (Fig. 4.7a) and dots (Fig. 4.7b). The length of the aggregates mostly varies between 10 nm and 60 nm, measured from the side-views by assuming a planar orientation. Fig. 4.7a also reveals that the elongated aggregates are oriented along basically the same direction which is also the long axis of the aggregates.

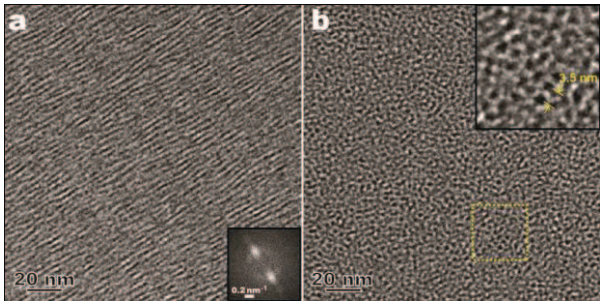

Figure 4.7. Cryo-TEM images of complex **14** aggregates in its nematic phase at 20%wt: side view (a) and top view (b). The inset of Fig. 4.7a is the corresponding FFT pattern. The inset of Fig. 4.7b is a magnified image of the marked area (30 nm × 30 nm) with a dashed square.

The top-views of the aggregates enable the direct observation of the distribution pattern of the aggregates in the plane perpendicular to the aggregate axis. The aggregates can arrange themselves into approximate hexagons and roughly straight lines (Fig. 4.7b and its inset) in local regions. However, it is quite clear that the overall distribution is random and no long-range order is formed.

The distances measured between the adjacent aggregates from the top views normally falls within the range of 3-4 nm with an average of 3.4 nm, which is in excellent agreement with the XRD result (35.3 Å). The ones measured from the side views are slightly smaller due the projection effect and have an average of ~3 nm. The fast Fourier transform (FFT) pattern in Fig. 4.7a shows two major diffused bright spots which are also elongated perpendicular to the aggregate axis. This indicates a rather largely varying distance between the aggregates and a slightly changing aggregate orientation. The above results clearly confirm that the 20%wt complex **1** solution has a nematic structure.

The presence of nematic and hexagonal phases at different weight

concentrations together with the non amphiphilic nature of this new Ag(I)complex and its ability to dissolve in water forming ordered aggregates, confirm the true chromonic nature of these mesophases. Therefore complex 14 represents one of the first chromonic metallomesogen although the liquid crystallinity is generated by molecules with non-conventional shapes.

For chromonic liquid crystals, miscibility, one of the most important liquid crystalline properties, is mainly attributed to a mechanism of intercalation between chromonic species and soluble aromatic derivatives, regarded as showing potential chromonic character. Due to the columnar overall structure in the guanine rich sequences of DNA forming the secondary structure called G-quadruplex (GQ) and the essential π delocalization within each column (in which four guanine bases are assembled into a planar structure *via* hydrogen bonds), G-quadruplex structures can be regarded as potential chromonic in character. Therefore, mixing chromonic liquid crystals and telemoric DNA (rich in guanine sequences and then able to form GQ structures) should be associated with an intercalation mechanism between the two systems. If intercalation occurs, the chromonic liquid crystal system can be considered as a GQ stabilizing agent interacting via π–π stacking and electrostatic interactions.

In order to prove that the new chromonic silver complex **14** can behave as a G-quadruplex binder *via* intercalation, its interaction with human telomeric DNA (TTAGGG)TT was investigated by isothermal titration calorimetry (ITC).

Several measurements have been done using different DNA/complex stoichiometries (1:6, 1:7.5 and 1.9) and the results cannot be interpreted unequivocally, because for each measurement different binding profiles were obtained.

Furthermore, in the attempt to get more information on the possible interactions between the complex and DNA, circular dichronism studies have been done using two different DNA/complex stochiometries 1:5 and 1:8, respectively. The results are presented in Fig. 4.10. The DNA profile does not show any significant conformational variation after the addition of complex **14** and no modification of melting temperatures. In conclusion, complex **14** does not seem to interact with human telomeric DNA, and therefore does not stabilise the GQ structure.

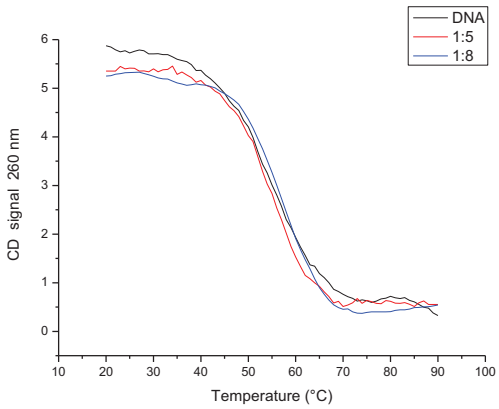

Figure 4.10. CD spectrum for the human telomeric DNA complex **14** and in a stoichiometry 1:5 and 1:8 respectively at λ= 260 nm.

4.2 Synthesis and characterization of [(bpy-OH)$_2$Ag][CH$_3$CH$_2$COO], 15

Furthermore, new chromonic Ag(I) complexes were obtained by increasing the length of the counterion. In the first place, Ag(I) propanoate salt was used following the same synthetic protocol used for the synthesis of complex **14** (Scheme 4.2).

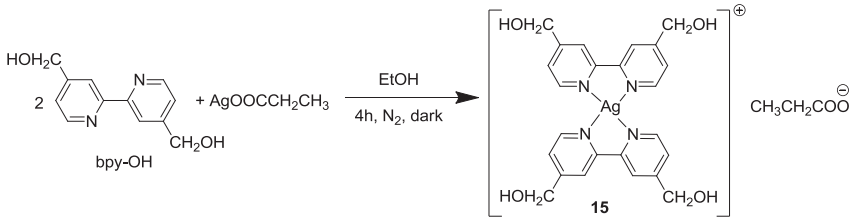

Scheme 4.2. Synthesis of complex **15.**

The proposed stoichiometry for complex **15** was confirmed by elemental analysis.

The IR spectrum of complex **15** shows the corresponding asymmetric and symmetric stretching vibration frequencies for the propanoate counterion at 1559 cm^{-1} (ν_{asym} (COO$^-$)) and at 1389 cm^{-1} (ν_{sym}(COO$^-$)), respectively.[123] Furthermore, the IR spectrum shows a large band at 3368 cm^{-1}, regardless of several attempts to dry the powders, and therefore reasonably attributable to the 2,2'-bipyridine –CH$_2$OH substituents.

The ionic character was confirmed by conductivity measurements performed in methanol solution. Indeed, the value found 87.83 Ω^{-1}

$\cdot cm^2 \cdot mol^{-1}$, is in the range of values reported for 1:1 electrolytes (80-115 $\Omega^{-1} \cdot cm^2 \cdot mol^{-1}$).

The ^1H NMR spectrum of complex **15** shows, as expected, the signals corresponding to the 12 aromatic protons of the bpy-OH ligands in the aromatic region. Moreover, in the aliphatic region, a singlet corresponding to the methylene group of the bipy-OH substituent at 4.82 ppm and the corresponding signals relative to the alkyl protons of the carboxylate counterion are observed at 2.15 ppm and 1.08 ppm. Furthermore, the intensity of the signals indicates a 2:1 ratio between the ligand and the counterion. After coordination of the ligand the same chemical shifts as in the case of complex **14** are observed, respectively a downfield shift of the *meta* and *para* protons with respect to the pyridinic N atom.

The photophysical behaviour of **15** has been investigated by UV-Vis spectroscopy in water solution. The absorption spectrum consists of absorption bands centred at 234 nm and 282 nm(Fig. 4.11). The presence of different bands than bpy-OH free ligand and the lack of emission properties confirm the formation of a new complex.

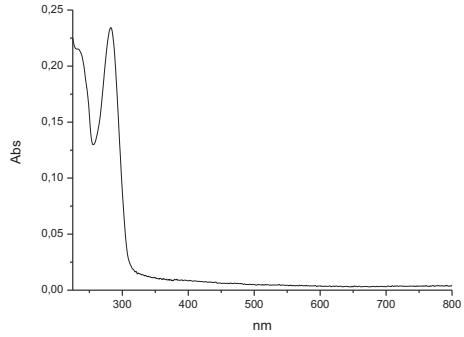

Figure 4.11. Absortion spectrum at room temperature of complex **15**.

The presence of solvent was revealed by TGA analysis. The thermogram shows loss of weight corresponding to one water molecule (Fig. 4.12).

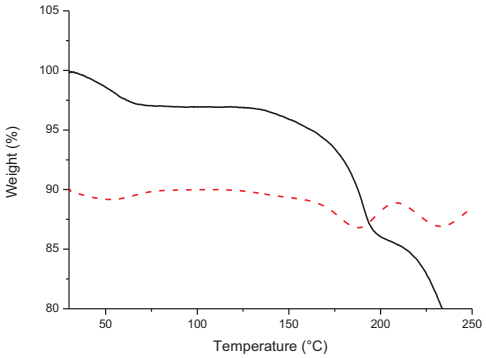

Figure 4.12. TGA trace of powder complex **15** with its derivative in dotted red (experimental mass loss 2.74% corresponds to one water molecule calcd. 2.85%).

X-Ray powder diffraction measurements (PXRD) were carried out at room temperature, on 20 wt% CLC non-aligned phase. At room temperature, the PXRD pattern of this complex at 20% wt in water, shows at low angle a nematic peak at 2θ = 2.3°, corresponding to a *d* value of 38.4 Å (Fig. 4.13). This increase of the nematic *d*-spacing when compared with the one of complex **14** recorded in the same conditions should be related to the increase of the molecular length, i.e. the increase of the carboxylate counterion chain length.

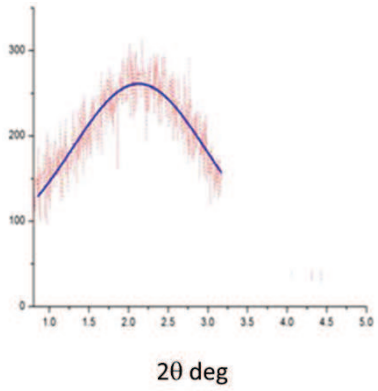

Figure 4.13. Complex **15** X-Ray diffraction pattern (low angle region in the inset) in the nematic phase at 20%wt concentration.

In the case of complex **15** the phase diagram shows the existence of only the nematic phase at all tested concentrations (Figure 4.14). Over 60%wt complex **15** does not completely dissolve in water solution.

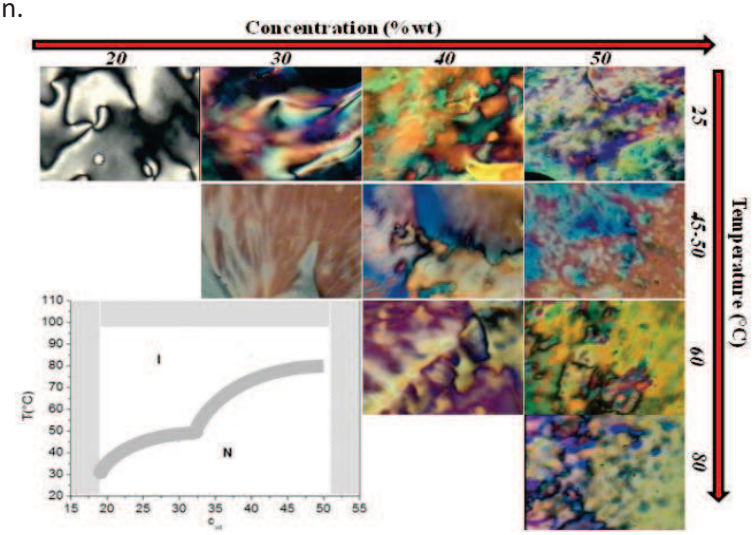

Figure 4.14. Phase diagram of complex **15** and POM pictures of the texture observed at different temperature and concentration, confirming the presence of LC phases.

The suppression of the hexagonal phase in complex **15**, and also the appearance of the nematic organization at higher concentration with respect to complex **14** are clearly related to the counterion. With the increase of the counterion chain length, its facility to be involved in hydrogen bonding with water molecules should be inhibited, probably blocking the formation of the cation dimeric repeating units and favouring their electrostatic repulsions.

4.3 Synthesis and characterization of [(bpy-OH)$_2$Ag][CH$_3$(CH$_2$)$_4$COO], 16

As seen in complex **15** the increase of the chain length in the counterion gives rise to changes on the liquid crystalline properties of the derived complexes.

Complex **16** was synthesized following the same procedure than seen above for complexes **14** and **15**, but using hexanoate silver salt as starting reactant (Scheme 4.3).

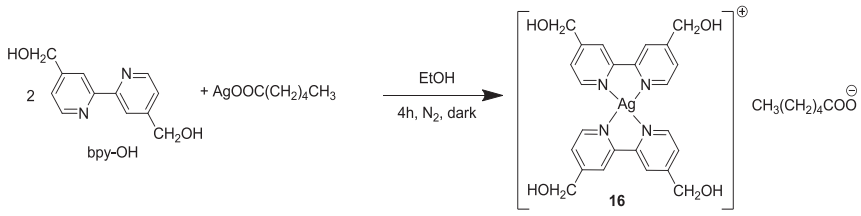

Scheme 4.3. Synthesis of complex **16.**

The elemental analysis performed, confirmed the proposed stoichiometry of the complex **16** reported in Scheme 4.3.

Furthermore, in the IR spectrum, the bands of the corresponding asymmetric and symmetric stretching vibration frequencies for the carboxilate counterion at 1564 cm^{-1} (ν_{asym} (COO^-)) and at 1408 cm^{-1} (ν_{sym}(COO^-)), respectively, confirm the presence of the carboxilate group.[123] Furthermore, the IR spectrum shows a large band at 3369 cm^{-1}, regardless of several attempts to dry the powders, and therefore reasonably attributable to the 2,2'-bipyridine $-CH_2OH$ substituents.

Conductivity measurements have been performed in methanol solution, confirming the ionic character of the complex **16**. Indeed, the value found 59.49 $\Omega^{-1} \cdot cm^2 \cdot mol^{-1}$, is in the range reported for 1:1 electrolytes.

The ^1H NMR spectrum of complex **16**, show as expected the signals corresponding to the 12 aromatic protons of bpy-OH in the aromatic region in the range 8.6 – 7.5 ppm. Moreover, in the aliphatic region a singlet corresponding to the methylene group of the bipy-OH substituent at 4.82 ppm and several signals corresponding to the alkyl protons of the carboxylate counterion between 2.13 ppm and 0.88 ppm are observed. The intensity of the signals indicates a 2:1 ratio between the ligand and the counterion. Furthermore, the same deshealding of the aromatic protons of the bpy-OH as observed in the case of complexes **14** and **15**, confirm the successful coordination of the ligand to the Ag(I) metal centre.

The photophysical behaviour of **16** has been investigated by UV-Vis spectroscopy in water solution. The absorption spectrum consists of

absorption bands centred at 235 nm and 282 nm (Fig. 4.16). The presence of different bands than bpy-OH free ligand and the lack of emission properties confirm the formation of a new complex.

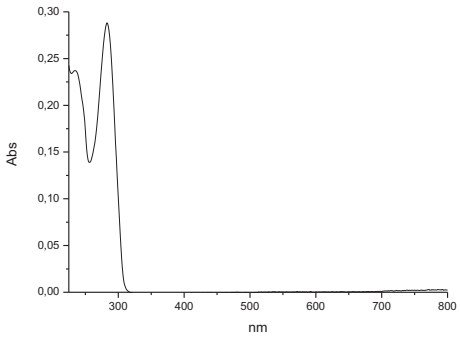

Figure 4.16. Absortion spectrum at room temperature of complex **16**.

The presence of solvent was revealed by TGA analysis. The thermogram shows loss of weight corresponding to one water molecule (Fig. 4.17).

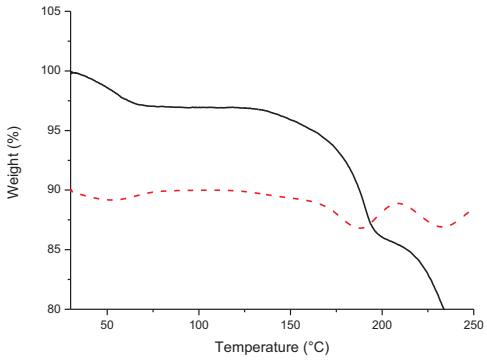

Figure 4.17. TGA trace of powder complex **16** with its derivative in dotted red (experimental mass loss 2.86% corresponds to one water molecule calcd. 2.68%).

The phase diagram and the X-Ray powder diffraction analysis of complex **16** was not investigated since the nematic phase appears at a concentration above 50 wt%. The decrease of the complex hydrophilicity is related to the increase of the carboxylate counterion chain lengths. As suggested for complex **15**, the suppression of the hexagonal phase in complex **16** and also the appearance of the nematic organization at higher concentration with respect to complex **14** and **15**, are clearly related to the counterion. With the increase of the counterion chain length, its facility to be involved in hydrogen bonding with water molecules should be inhibited, probably blocking the formation of the cation dimeric repeating units and favoring their electrostatic repulsions. Obviously, this trend is more evident in complex **16** then in complex **15**.

The synthesis and characterization of complex **14, 15** and **16** has been published in the article number 3: Unconventionally shaped chromonic liquid crystals formed by novel silver(I) complexes. D. Pucci, B. Sanz Mendiguchía, C. M. Tone, E. I. Szerb, F. Ciuchi, M. Gao, M. Ghedini, A. Crispini, J. Mater. Chem. C, 2014, 2, 8780, included in the Thesis Supplementary Information.

4.4 Synthesis and characterization of [(bpy-OH)$_3$Ag$_2$][(PF$_6$)$_2$], 17

To investigate the role of the counterion in the appearance of chromonic liquid crystalline properties in this class of complexes, several different counterions have been tested.

Complex **17** has been synthesized adding $AgPF_6$ to a solution of two equivalents of bpy-OH in ethanol. The reaction was stirred for 4 hours, under nitrogen in a vessel protected from light and then the pale yellow precipitate was filtered.

The elemental analysis does not confirm the molecular structure in which the 1:2 molar ratio between the silver ion and the bipy-OH ligand has been found in the analogous derivatives already discussed. Indeed, the most probable molar ratio of 2:3, calculated from the elemental analysis resulted, accounting for the formation of a dinuclear Ag(I) complex where two anion counterbalance the positive charges.

Conductivity measurements performed in methanol solution, differently than all the other Ag(I) bipy-OH derivatives reported up to now, evidenced a higher electrolyte type (the range reported for 1:1 electrolytes of 80-115 $\Omega^{-1} \cdot cm^2 \cdot mol^{-1}$) with a val of 128 $\Omega^{-1} \cdot cm^2 \cdot mol^{-1}$.

Various Ag(I) derivatives reported up to now revealed the importance of the counterions in imposing the final stoichiometry and the overall supramolecular organization, dictating the ligand/metal

ratio in the fulfilling of the Ag(I) coordination sphere.[67d,126] Indeed, in several cases, during the synthesis of new Ag(I) metal complexes with 4,4'-disubstituted-2,2'-bipyridines in a molar ratio of 2:1 with different Ag(I) salts, the formation of complexes with a ligand-to-metal ratio of 3:2 has been observed.

In particular, from the reaction between two equivalents of bpy-CH_3 (bpy-CH_3= 4,4'-dimethyl-2,2'-bipyridine) and one equivalent of $AgClO_4$ in acetonitrile/water solution, a mixture of 3:2 and 2:1 derivatives have been isolated. The separation of the complexes has been possible due to their different solubility properties. In the 3:2 specie, the two Ag(I) ions are chelated by a bipyridine ligand and held together through a third bridging ligand acting as a pincer and pulling the silver ions into such a proximity to form significant metal–metal interactions, as shown by single crystal X-ray diffraction studies (Figure 4.19a). The characterization of this 3:2 Ag(I) complex shows the presence of new aromatic signals in the ^1H NMR spectrum, corresponding to the bridging bipyridine ligand, and high conductivity value evidencing a higher electrolyte type.

In the case of the $[(bpy\text{-}CH_3)_3Ag_2](OTf)_2$ the synthesis of the 3:2 ligand-to-metal ratio is obtained also if 1:1 ratio between the ligand and the silver salt has been used. The crystal structure reported in Figure 4.19 is comparable with the Ag(I) structure described above, and consisting of two Ag(I) ions chelated by a bipyridine ligand and held together through a third brinding ligand acting as a pincer. The

[126] **Bellusci, A. Crispini, A. Pucci, D. Szerb, E. I. Ghedini, M**. 2009, Cryst. Growth Des., Vol. 8, 8, pp. 3114

conductivity measurements evidenced a higher electrolyte type than 1:1, but the ^{1}H NMR did not shown new aromatic signals.

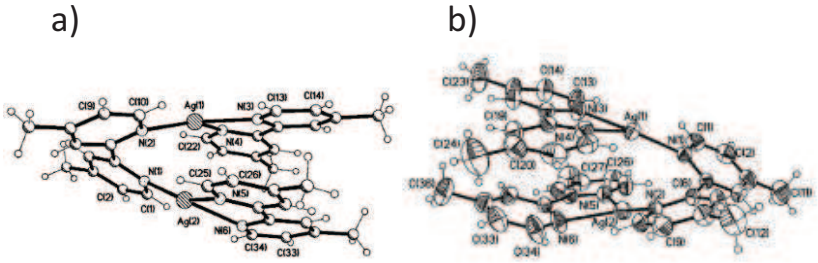

Figure 4.19. A perspective view and numbering scheme of the cations of complexes a) $[bpy\text{-}CH_3)_3Ag_2](ClO_4)_2$ and b) $[(bpy\text{-}CH_3)Ag_2](OTf)_2$.

The examples reported above, and the analytical data and the conductivity measurements performed on complex **17**, confirm the 3:2 metal-to-ligand stoichiometry with the $[(bpy\text{-}OH)_3Ag_2](PF_6)_2$ molecular formula for the complex **17**.

Furthermore, in the IR spectrum the presence of the PF_6 band at 845 cm^{-1} and the upfield shifted carbon-carbon band of the bpy-OH ligand confirm the formation of a complex **17**.

The ^{1}H NMR spectrum of Ag(I) complex **17** contains in the aromatic part the protons of the bpy-OH, downfield shifted with respect to the free ligand, and respectively in the aliphatic region the proton relative to the methylene group of the substituent at 4.82 ppm.

The photophysical behaviour of **17** has been investigated by UV-Vis spectroscopy in methanol solution. The absorption spectrum consists of one absorption band centred at 299 nm (Fig. 4.20).

Moreover, complex does not show emission. The absorption band and the lack of luminescence character are evidences of the new complex formation.

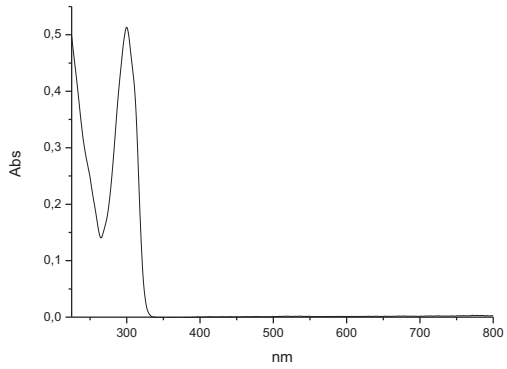

Figure 4.20. Absorption spectrum at room temperature of complex **17**.

Complex **17** does not show water solubility and hence no chromonic properties in water are observed.

4.5 Synthesis and characterization of [(bpy-OH)$_2$Ag][OTf], 18

Complex **18** was obtained adding the AgOTf salt to a solution of bpy-OH in ethanol. The reaction was stirred for 4 hours under nitrogen in a vessel protected from light and then the yellow precipitate was filtered (Scheme 4.5).

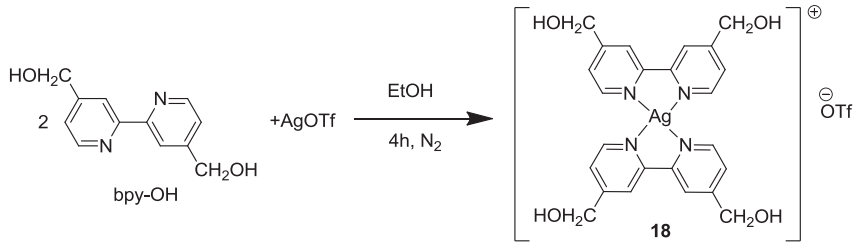

Scheme 4.5. Synthesis of complex **18.**

The elemental analysis confirms the molecular formula of complex **18**, formed by two bpy-OH ligand, one Ag(I) ion and one triflate counterion.

The IR spectrum of complex **18** revealed the presence of a band, at 1254 cm^{-1} assigned to the triflate ion in a non coordinated form.[67d] The carbon-carbon shifted band of the bpy-OH, confirm the chelation with the Ag(I) metal centre.

Furthermore, the value 73.34 $\Omega^{-1} \cdot cm^2 \cdot mol^{-1}$ found for complex **18** is in the limit of the values range reported for similar univalent derivatives. This may suggest ionic character of complex **18**.

The ^1H NMR spectrum of Ag(I) complex **18** contains in the aromatic part the 12 protons of the bpy-OH, downfield shifted with respect to the free ligand, and respectively in the aliphatic region the proton relative to the methylene group of the substituent at 4.82 ppm.

The behaviour of complex **18** in ethanol solution has been investigated by UV-Vis spectroscopy in order to further verify the formation of the complex. The absorption spectrum exhibited different bands at 248 nm, 286 nm and 313 nm (Fig. 4.21), differently from the free ligand absorption spectra. Moreover, complex **18** does not

presents an emission band, meanwhile bpy-OH emit at 308 nm. Regarding the luminescence, complex **18**, like the free bipy-OH ligand, does not emit. The differences observed between the photophysical behaviour of complex **18** with respect to the photopysical behaviour of bpy-OH, corroborate the successful coordination of the ligand to the Ag(I) metal centre.

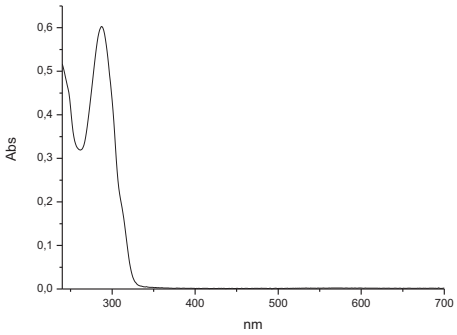

Figure 4.21. Absortion spectrum at room temperature of complex **18**.

This complex resulted insoluble in water, proving once again the importance of the counterion in tuning the properties of the resulting complexes. In particular, the lack of water solubility is due to the more hydrophobic character of the triflate counterion, with respect to the carboxylates.[127]

[127] **Bahadur, I. Letcher, T. M. Singh, S. Redhi, G. G. Venkatesu, P. Ramjugernath, D.** 2015, J. Chem. Termodinamics, Vol. 82, pp. 34-36.

4.6 Synthesis and characterization of [(bpy-OH)$_2$Ag][CF$_3$COO], 19

This Ag(I) complex was obtained adding $AgOOCCF_3$ to a solution of bpy-OH in ethanol. The reaction was stirred for 6 hours under nitrogen in a vessel protected from light and then the yellow precipitate was filtered (Scheme 4.6).

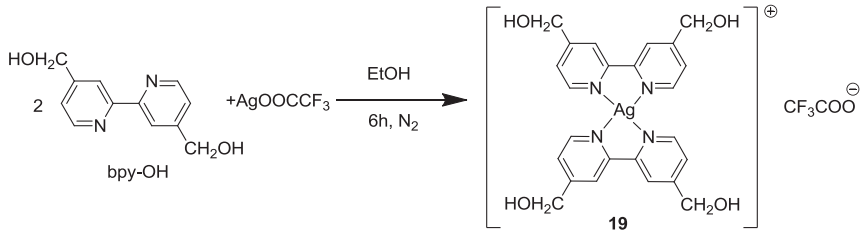

Scheme 4.6. Synthesis of complex **19.**

The elemental analysis confirms the molecular formula of complex **19**, proposed in Scheme 4.6.

In the IR spectrum, the CF_3 band at 818 cm^{-1} and the band at 1679 cm^{-1} ($\nu_{asy}C=O$) confirms the presence of the trifluoroacetate ion.[128]

A further confirmation of the successful formation of the complex **19** is given in the ^1H NMR spectra, where the downfield shift of the *meta* and *para* protons with respect to the pyridinic N atom is observed.

[128] **De Vos, D. Wolters, J.** 1980, Bull. Soc. Chim. Bel., Vol. 89, nº 10.

The ionic character was confirmed by conductivity measurements performed in methanol solution. Indeed, the value found 77.23 $\Omega^{-1}\cdot cm^2\cdot mol^{-1}$, assessed its 1:1 electrolyte nature, being in the acceptable Λ_M range for bivalent electrolytes in the respective solvent.

The photophysical behaviour of complex **19** has been investigated by UV-Vis spectroscopy in ethanol solution. The absorption spectrum consists of absorption bands centred at 283 nm and 239 nm, confirming the formation of the complex because the bpy-OH ligand shows only one band centred at 285nm (Fig. 4.22). Moreover, complex **19** does not presents an emission band. Also in this case the no presence of luminescence confirms the formation of a new complex because bpy-OH ligand shows an emission band centred at 308 nm.

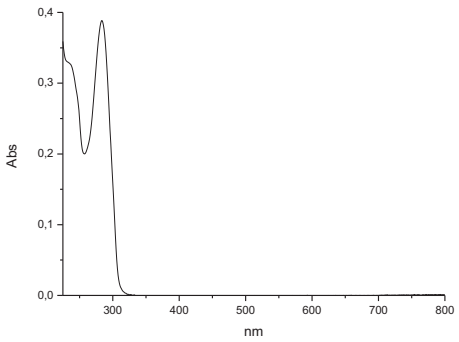

Figure 4.22. Absorption spectrum at room temperature of complex **19**.

The presence of the acetate group seems to be essential for the induction of chromonic liquid crystalline properties in these type of complexes. The variation of the counterions, and in particular the

trifluoroacetate, has led to the obtaining of the complexes **19** without chormonic liquid crystalline properties.

Chapter 5

General equipment and procedures

All commercially available chemicals were purchase from Aldrich Chemical Co. and were used without further purification. IR spectra (KBr pellets) were recorded on a Perkin-Elmer Spectrum One FT-IR spectrometer. 1H-NMR spectra were recorded on a Bruker WH-300 spectrometer in deuterated solvents with TMS as an internal standard. 1H-NMR and 13C-NMR spectra were recorded on a Varina VNMRS-400 spectrometer and calibrated using residual undeuterated solvent as internal reference. Analyses (MS) were performed using Agilent 1200 HPLC system coupled to Agilent G6120 single quadrupole detector equipped with an electrospray ionization (ESI) source in direct infusion modality. ESI MS spectra were recorded in positive mode, unless otherwise noted. Elemental analyses were performed with a Perkin-Elmer 2400 analyzer CHNS/O. Conductivity measurements were performed in solutions with an InoLab Cond Level 1-720 conductometer equipped with LR 325-001 immersion cell. The thermal stability was measured on a Perkin-Elmer Thermogravimetric Analyser Pirys 6 TGA. Melting points and mesophase textures were examined with a Leica DMLP polarizing microscope equipped a Leica DFC280 camera and CalCTec (Italy) heating stage. Spectrofluorimetric grade acetone (Acros Organics) was used for the photophysical investigations

in solution. Steadystate emission spectra were recorded on a Horiba Jobin Yvon Fluorolog 3 spectrofluorimeter, equipped with a Hamamatsu R-928 photomultiplier tube. Emission quantum yields of the sample in solution were determined using the optically dilute method on deuterated solutions whose absorbance at excitation wavelengths was <0.1; $Ru(bpy)_3Cl_2$ (bpy = 2,2′-bipyridine) in H_2O was used as a standard (Φ = 0.028). The experimental uncertainty on the emission quantum yields is 10%.

X-Ray single crystal analysis

X-ray data were collected at room temperature on a Bruker-Nonius X8 Apex CCD area detector equipped with a graphite monochromator and Mo Kα radiation (λ = 0.71073 Å). Data were processed through the SAINT[129] reduction and SADABS[130] absorption software. The structures were solved by standard Patterson methods through the SHELXTL NT[131] structure determination package and refined by full-matrix least squares based on F^2. In general, all non-hydrogen atoms were refined anisotropically and hydrogen atoms were included as idealized atoms riding on the respective carbon

[129] SAINT, *Version* 6.45 Copyright©, Bruker Analytical X-Ray Systems Inc., 2003.
[130] Sheldrich, G. M. SADABS. *Version* 2.10, Bruker AXS Inc., Madison, USA, 2003.
[131] SHELXTL-NT, *Version* 5.1 Copyright©, Bruker Analytical X-Ray Systems Inc., 199.

atoms with C–H bond lengths appropriate to the carbon atom hybridization. Hydrogen atoms of the co-crystallized water molecules have been included in calculated positions and restrained bond distances and angles have been used

X-Ray powder diffraction analysis

The powder X-ray diffraction patterns of complexes **6**, **11**, **7** and **12** were obtained using a Bruker AXS General Area Detector Diffraction System (D8 Discover with GADDS) with Cu-Kα radiation (λ = 1.54056 Å). Measurements were performed by placing samples in Lindemann capillary tubes with an inner diameter of 0.05 mm. The highly sensitive area detector was placed at a distance of 20 cm from the sample (2θ detector placed at 14°).

The powder X-ray diffraction patterns of complex **14** in its hexagonal phase and nematic phase in the wide angle region as well as in the solid state were obtained at room temperature by using a Bruker D2 PHASER Diffraction System equipped with a 1D high speed solid state LinxEye detector and Cu-Ka radiation (λ = 1.54056 Å). Measurements were performed by placing samples on a zero background sample holder with protection for solvent evaporation along the measurements. The X-ray patterns of complexes **14** and **15** in their nematic phase at low angle were obtained at room temperature using a D8 Discover, Bruker-AXS with Cu-Kα radiation (λ = 1.5418 Å). The LC solutions were hosted in a glass capillary (Mark tubes,

Hilgenberg, 80 mm length, outside diameter 0.8 mm or 1 mm and wall thickness 0.1 mm) placed in a home-made sample holder.

Solubility analysis

The spectrophotometric measurements to determine the solubility of the complexes had been conducted with a Varian Cary 50 Scan UV–Visible Spectrophotometer. The temperature of the cell–holder was kept at 298.15 K by a Grant circulating water bath. Matched quartz cells of thickness 1 cm were employed. The absorbance, A_λ, were recorded to ± 0.0001 units. The formulations of the parameters and the acquisition of the data have been managed with the aid of a computer connected to the tool.

The solubility (S, mol/dm^3) of the complexes was evaluated, at 298.15 K, in pure water by spectrophotometric measurements in the UV-Vis region. Saturated complexes solutions were prepared with a leaching apparatus suitable to prevent solid particles from coming into contact with the magnetic stirrer. As a matter of fact, preliminary measurements showed an increase of solubility over periods of weeks when the solid was in mechanical contact with the stirrer, because the solid was transformed into a dispersed phase. To avoid grinding by the stirrer, solid complexes were wrapped up in a highly retentive filter paper (Whatman 42) bag. This in turn was kept in a glass cylinder

containing pure water while continuously stirring with a magnetic bar. The experimental apparatus is reported in Figure 5.1.

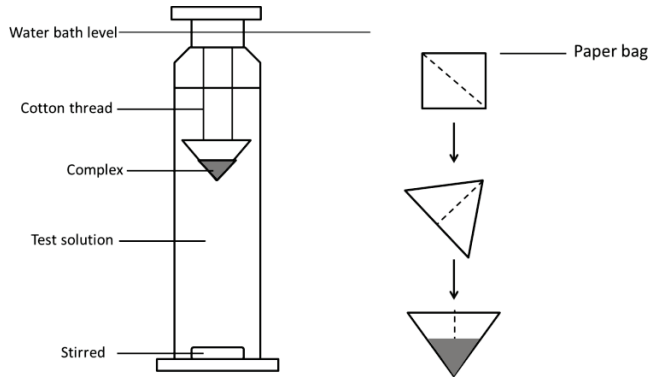

Figure 5.1. The apparatus for preparation of saturated complexes solutions.

The cylinder was then placed in a thermostatic water bath at 298.15 K and the complexes concentrations were monitored over the time, until it reached a constant value, which usually occurred in about 4 days. Finally, the absorption spectra in the UV-Vis region were recorded on a series of complexes solutions.

Taking as a blank the pure water, the absorbance, A_λ, may be expressed as equation:

$$A_\lambda = l\, \varepsilon\, [\text{cpx}]$$

where [cpx] is the equilibrium concentration of the complexes, l is the optical path and ε is the molar absorbivity. A_λ were measured between 190 and 780 nm to find suitable conditions for determining the solubility, S, of the complexes. Three replicates were run for each point.

Phase diagram analysis

Bright field, polarized optical microscopy (POM) images and conoscopy images for complexes **14** and **15** were collected using a microscope (Zeiss) with a 5X, 20X objective or a 100X objective, respectively. The calibration of the microscope hot stage was performed by checking the transition temperatures of the E7 liquid crystal. The samples were rotated on a circular stage located between a polarizer and an analyzer. Most images were taken with a colour CCD camera under polychromatic illumination.

Cryo-TEM measurements

The cryo-TEM observation was carried out using a FEI Tecnai F20 microscope (200 KV) equipped with an anti-contaminator, a low-dose operation mode, and a Gatan UltraScan 4000 CCD camera. To prepare cryo-TEM specimens, we employ a FEI Vitrobot (environmental chamber set to 22 °C) to plunge-freeze liquid crystal thin films supported by holey carbon coated grids. Liquid ethane was used as the cryogen in the rapid cooling process to ensure the preservation of the native structure. The vitrified LC specimens were then mounted on a Gatan 626-DH cryo-holder and transferred into the TEM. During the whole specimen transfer and TEM observation process, the TEM specimen was kept at temperatures below -170 °C. The TEM images

shown here were all taken from the electron-transparent areas suspended in the holes of the supporting carbon films.

Synthesis procedures

5.1 4,4'-dinonyl-2,2'-bipyridine (bpy-9) Zn(II) and Cu(II) complexes

5.1.1 Synthesis and characterization of complex I, [(Bpy-9)Zn(H_2O)$_2$][(BF_4)$_2$]

To a solution of 4,4'-dinonyl-2,2'-bipyridine (500mg, 1.22mmol) in dichloromethane

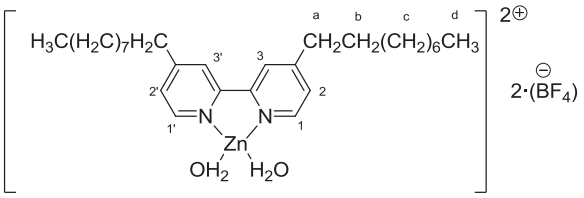

(20mL) was added a small excess of $Zn(BF_4)_2$ (435mg, 1.83mmol). The reaction mixture was stirred for 6 days at r.t. Subsequently, it was filtered on Celite and the solvent evaporated under reduce pressure. The solid was recrystallized by chloroform/diethyl ether (82% yield).

- Molecular weight: 683.68 g/mol
- Formula: $C_{28}H_{48}O_2N_2ZnB_2F_8$

- Melting Point: 140°C
- Elemental Analysis (%):

  Calculated: C= 49.19; H= 7.08; N= 4.10

  Found: C= 49.03; H= 6.99; N= 4.25

- IR (KBr) ν_{max}/cm^{-1}: 3435 (OH), 2925, 2853 (C-H), 1613 (C=C), 1559 (C=N), 1058 (B-F).
- ^{1}H NMR: (300MHz, $CDCl_3$): δ_H 8.05 (2H, s, $H_{3,3'}$), 7.90 (2H, d, *J*(H-H)= 5.35 Hz, $H_{1,1'}$), 7.47 (2H, t, *J*(H-H)= 5.36 Hz, $H_{2,2'}$), 2.77 (4H, m, $H_{a,a'}$), 1.67 (4H, t, *J*(H-H)= 6.86 Hz, $H_{b,b'}$), 1.28 (24H, m, $H_{c,c'}$), 0.86 (6H, t, *J*(H-H)= 6.6 Hz, $H_{d,d'}$).
- UV-vis (EtOH): λ_{abs} (ε, $mol^{-1}\cdot dm^3\cdot cm^{-1}$): 283 nm; 293 nm; 304 nm. λ_{emi}: 325 nm.
- $\Lambda_{diclhoromethane}$= 40.98 $cm^2\cdot\Omega^{-1}\cdot mol^{-1}$.

5.1.2 Synthesis and characterization of complex 1, [(Bpy-9)Zn(Curc)][$(BF_4)_2$]

To a solution of curcumin (200mg, 0.54mmol) in dichloromethane

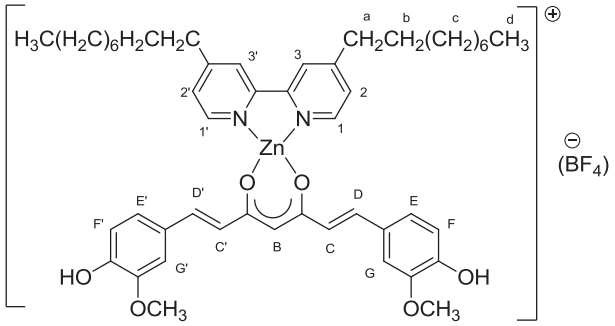

(10mL) was added triethylamine (56.64mg, 0.54mmol) under nitrogen obtaining a red solution. A solution of $[(Bpy\text{-}C9)Zn(H_2O)_2][(BF_4)_2]$ (332mg, 0.54mmol) in dichloromethane (10mL) was added to the red solution. The resulting orange solution was stirred under nitrogen for 3 days at room temperature. The solvent was evaporated *in vacuo* and then the product was recrystallized from petroleum ether to give a red solid (91% yield).

- Molecular weight: 1126.05 g/mol
- Formula: $C_{49}H_{63}O_6N_2ZnBF_4$
- Melting Point: 103°C
- Elemental Analysis (%):

  Calculated: C= 63.40; H= 6.82; N= 3.01

  Found: C= 62.95; H= 7.02; N=2.98

- IR (KBr) ν_{max}/cm^{-1}: 3426 (OH curc), 2925-2853 (C-H), 1626 (C=C), 1606 (C=O), 1587 (C=N), 1514 (C-C-$C_{chelated\ ring}$), 1058 (B-F).
- ^1H NMR: (300MHz, $CDCl_3$): δ_H 8.05 (2H, s, $H_{3,3'}$), 7.89 (2H, d, *J*(H-H)= 5.3 Hz, $H_{1,1'}$), 7.59 (2H, d, *J*(H-H)= 15.6 Hz, $H_{C,C'}$), 7.47 (2H, d, *J*(H-H)= 4.6 Hz, $H_{2,2'}$), 7.11(2H, d, *J*(H-H)= 6.58 Hz, $H_{E,E'}$), 7.05 (2H, d, $H_{G,G'}$), 6.92 (2H, d, *J*(H-H)= 8.23 Hz, $H_{F,F'}$), 6.47 (2H, d, *J*(H-H)= 7.7 Hz, $H_{D,D'}$), 5.80(2H, s, $H_{B,B'}$), 3.92 (6H, s, OCH_3), 2.78 (4H, t, *J*(H-H)= 8 Hz, $H_{a,a'}$), 1.67 (4H, m, $H_{b,b'}$), 1.33 (24H, m, $H_{c,c'}$), 0.86 (6H, t, J(H-H)= 6.6 Hz, $H_{d,d'}$).

- UV-vis (EtOH): λ_{abs} (ε, $mol^{-1}\cdot dm^3\cdot cm^{-1}$): 293 nm (17600); 304 nm (13042); 429 nm (49576). λ_{emi}: 549 nm.
- $\Lambda_{diclhoromethane}$= 22.34 $cm^2\cdot\Omega^{-1}\cdot mol^{-1}$.

5.1.3 Synthesis and characterization of complex II, [(Bpy-9)Zn(H_2O)$_2$][(SO_4)]

To a solution of 4, 4'-dinonyl-2,2'-bipyridine (500mg, 1.22mmol) in MeOH (20mL) was

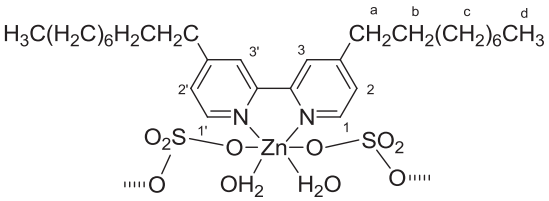

added a solution of $ZnSO_4\cdot 7H_2O$ (544mg, 1.83mmol) in water (5mL). After stirring for 3h, the white solid formed was filtered and washed in Et_2O to give the pure product (77% yield).

- Molecular weight: 606.12 g/mol
- Formula: $C_{28}H_{48}O_6N_2ZnS$
- Melting Point: 158°C
- Elemental Analysis (%):

  Calculated: C= 55.48; H= 7.98; N= 4.62

  Found: C= 55.57; H= 8.01; N= 4.55

- IR (KBr) ν_{max}/cm^{-1}: 3346 (OH), 2926, 2853 (C-H), 1618 (C=C), 1561 (C=N), 1144-1090 (SO_4).
- ^1H NMR: (300MHz, $CDCl_3$): δ_H 8.88 (2H, d, *J*(H-H)=5.3 Hz, $H_{3,3'}$), 8.45 (2H, s, $H_{1,1'}$), 7.60 (2H, d, *J*(H-H)= 5.3 Hz, $H_{2,2'}$), 4.92 (4H, m, $H_{a,a'}$), 1.77(4H, m, $H_{b,b'}$), 1.38 (24H, m, $H_{c,c'}$), 0.88 (6H, t, *J*(H-H)=6.6 Hz, $H_{d,d'}$).
- UV-vis (EtOH): λ_{abs} (ε, $mol^{-1}\cdot dm^3\cdot cm^{-1}$): 249 nm (138333); 293 nm (212393); 303 nm (211878). $\lambda_{\varepsilon mi:}$ 370 nm.
- $\Lambda_{diclhoromethane}$= 1.50 $cm^2\cdot\Omega^{-1}\cdot mol^{-1}$.

5.1.4 Synthesis and characterization of complex 2, [(Bpy-9)$_2$Zn$_2$(Curc)$_2$(SO$_4$)(H$_2$O)$_2$]

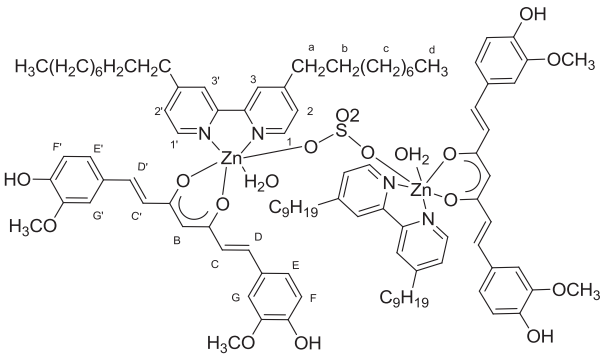

To an orange solution of curcumin (200mg, 0.54mmol) in dichloromethane (10mL) was added triethylamine (54.64mg, 0.54mmol), under nitrogen atmosphere. Once the solution changed to red color a dichloromethane solution (10mL) of precursor **II** (332mg, 0.54mmol) was added and the reaction mixture was stirred under

nitrogen for 5 days, at room temperature. The solvent was evaporated in *vacuo* and the product crystallized from petroleum ether to give a deep orange waxy solid (84% yield).

- Molecular weight: 1782.92 g/mol
- Formula: $C_{98}H_{130}O_{12}N_4Zn_2(SO_4)$
- Melting Point: 108°C
- Elemental Analysis (%):

  Calculated: C= 66.02; H= 7.35; N= 3.14

  Found: C= 65.69; H= 7.08; N= 3.14

- IR (KBr) ν_{max}/cm^{-1}: 3391 (OH curc), 2924, 2852 (C-H), 1622 (C=C), 1589 (C=O), 1561 (C=N), 1511 (C-C-C $_{chelate\ ring}$) 1280, 1121, 1032 (SO_4).
- ^{1}H NMR: (300MHz, $CDCl_3$): δ_H 9.37 (4H, s, $H_{1,1'}$), 7.84 (4H, s, $H_{3,3'}$), 7.56 (4H, d, *J*(H-H)= 15.8 Hz, $H_{D,D'}$), 6.92 (8H, m, $H_{E,E',G,G'}$), 7.90 (8H, m, $H_{2,2',F,F'}$), 6.44 (4H, d, $H_{C,C'}$), 5.78 (2H, s, H_B), 3.91 (12H, s, H_{OCH3}), 2.68 (8H, t, *J*(H-H)= 7.69 Hz, $H_{a,a'}$), 1.64 (8H, m, $H_{b,b'}$), 1.26 (48H, m, $H_{c,c'}$), 0.86 (12H, t, *J*(H-H)= 13.17 Hz, $H_{d,d'}$).
- UV-vis (EtOH): λ_{abs} (ε, $mol^{-1}\cdot dm^3\cdot cm^{-1}$): 293 nm; 304 nm; 430 nm. $\lambda_{\varepsilon mi:}$ 553 nm.
- $\Lambda_{diclhoromethane}$= 2.18 $cm^2\cdot\Omega^{-1}\cdot mol^{-1}$.

5.1.5 Synthesis and characterization of complex III, [(Bpy-C9)CuCl$_2$]

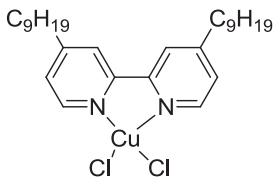

To a solution of 4,4′-dinonyl-2,2′-bipyridine (200mg, 0.49mmol) in acetone (30mL) was added $CuCl_2 \cdot 2H_2O$ (124.95mg, 0.735mmol). The reaction was stirred at r.t. for 24 hours. Then the solution was concentered in *vacuo* and the green product was precipitate by diethyl ether (80% yield).

- Molecular weight: 543.11 g/mol
- Formula: $C_{28}H_{44}O_2N_2CuCl_2$
- Melting Point: 169-173°C
- Elemental Analysis (%):

  Calculated: C= 61.90; H= 8.16; N= 5.16

  Found: C= 61.79; H= 8.17; N= 5.11

- IR (KBr) ν_{max}/cm^{-1}: 3043 (C-H), 2923, 2851 (C-H), 1615 (C=C), 1555 (C=N).
- UV-vis (MeOH): λ_{abs} (ε, $mol^{-1} \cdot dm^3 \cdot cm^{-1}$): 251 nm (11971); 297 nm (14106); 308 nm (13988).
- Λ_{MeOH}= 78.58 $cm^2 \cdot \Omega^{-1} \cdot mol^{-1}$.

5.1.6 Synthesis and characterization of complex 3, [(Bpy-C9)Cu(Curc)Cl]

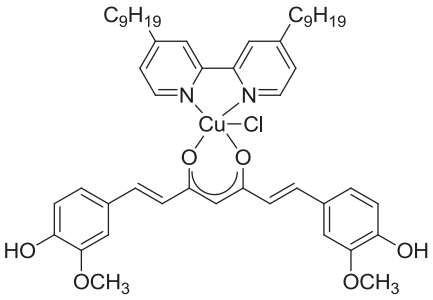

To an orange solution of curcumin (67mg, 0.184mmol) in acetone (10mL) was added triethylamine (0.025mL, 0.184mmol) under nitrogen atmosphere. After the colour of the reaction mixture change to red, a solution of [(Bpy-C9)$CuCl_2$] (100mg, 0.184mmol) in acetone (10mL) was added. The reaction was further stirred for 24h, at r.t. Subsequently, the yellow-green precipitate was filtered and washed with acetone (86% yield).To the red solution was added a solution of [(Bpy-C9)$CuCl_2$] (100mg, 0.184mmol) in acetone (10mL). The reaction was stirred for 24h, the yellow-green precipitate was filtered and washed in acetone (86% yield).

- Molecular weight: 875.03 g/mol
- Formula: $C_{49}H_{63}O_6N_2CuCl$
- Melting Point: 183-185°C
- Elemental Analysis (%):

  Calculated: C= 67.26; H= 7.26; N= 3.20

Found: C= 67.14; H= 7.51; N= 3.17

- IR (KBr) ν_{max}/cm^{-1}: 2925, 2852 (C-H), 1623 (C=O), 1606 (C=C), 1588 (C=N).
- UV-vis (MeOH): λ_{abs} (ε, $mol^{-1}\cdot dm^3\cdot cm^{-1}$): 253 nm (11261); 263 nm (10835); 307 nm (12935); 347 nm (12756); 427 nm (6660); 451 nm (23202). λ_{emi}: 560 nm. Yield: 1%.
- Λ_{MeOH}= 37.4 $cm^2\cdot\Omega^{-1}\cdot mol^{-1}$.

5.2 Synthesis and characterization of curcumin-based complexes increasing the aromatic portion in the N,N chelating ligand

5.2.1 Synthesis and characterization of complex IV,[(Terp)$ZnCl_2$]

To a solution of 2,2',6',2''-terpyridine (200mg, 0.85mmol) in CH_2Cl_2 (10mL) was added a solution of $ZnCl_2$ (231.67mg, 1.7mmol) in CH_3CN. The reaction was stirred r.t. and subsequently for 2days. Then the yellow precipitate was filtered and washed with petrol ether (94% yield).

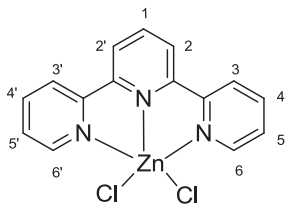

- Molecular weight: 369.56 g/mol
- Formula: $C_{15}H_{11}N_3ZnCl_2$
- Melting Point: >300°C
- Elemental Analysis (%):

  Calculated: C= 48.75; H= 3.00; N= 11.37

  Found: C= 48.02; H= 3.20; N= 11.24

- IR (KBr) ν_{max}/cm^{-1}: 3055 (C-H), 1595 (C=C), 1581 (C=N).
- ^1H NMR: (300MHz, $CDCl_3$): δ_H 8.79 (4H, d, $H_{3,3',6,6'}$), 8.70 (2H, d, $H_{2,2'}$), 8.56 (1H, t, J(H-H)= 7.82 Hz, H_1), 8.31 (2H, t, J(H-H)= 8.1 Hz, $H_{4,4'}$), 7.85 (2H, t, $H_{5,5'}$).
- UV-vis (H_2O): λ_{abs} (ε, $mol^{-1}\cdot dm^3\cdot cm^{-1}$): 230 nm (16233); 280 nm (11683); 320 nm (13870); 330 nm (13927). $\lambda_{\varepsilon mi:}$ 360 nm. Yield: 5.3%.
- Λ_{DMSO}= 9.67 $cm^2\cdot\Omega^{-1}\cdot mol^{-1}$.

5.2.3 Synthesis and characterization of complex 4, [(Terp)Zn(Curc)Cl]

To an orange solution of curcumin (99.46mg, 0.27mmol) in hot MeOH (30mL) was added

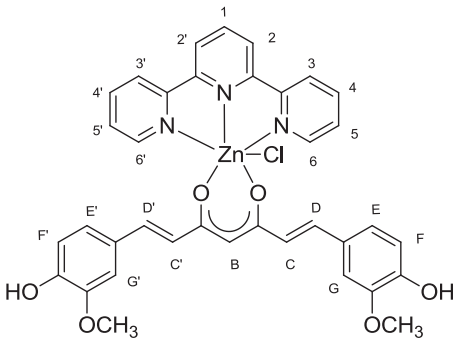

triethylamine (0.037mL, 0.27mmol) under nitrogen atmosphere. After 10 minutes a solution of [(Terp)$ZnCl_2$] (100mg, 0.27mmol) in water was added. The reaction was stirred for 3 days. The red precipitate formed was filtered and washed with MeOH and water (71% yield).

- Molecular weight: 719.4 g/mol
- Formula: $C_{36}H_{32}N_3O_7ZnCl$
- Melting Point: 214°C(dec)
- Elemental Analysis (%):

  Calculated: C= 60.10; H= 4.48; N= 5.87

  Found: C= 59.61; H= 4.59; N= 5.42

- IR (KBr) ν_{max}/cm^{-1}: 1620 (C=O), 1582 (C=N).
- UV-vis (DMSO): λ_{abs} (ε, $mol^{-1}\cdot dm^{3}\cdot cm^{-1}$): 278 nm (14933); 316 nm (9177); 332 nm (7826); 435 nm (34395). $\lambda_{emi:}$ 543 nm. Yield: 6%.
- Λ_{DMSO}= 7.89 $cm^2\cdot\Omega^{-1}\cdot mol^{-1}$.

5.2.4 Synthesis and characterization of complex V, [(Terp)Zn(H_2O)$_2$][(BF_4)$_2$]

A solution of $Zn(BF_4)_2$ (153mg, 0.65mmol) in CH_2Cl_2 (10mL) was added to a solution of 2,2',6',2''

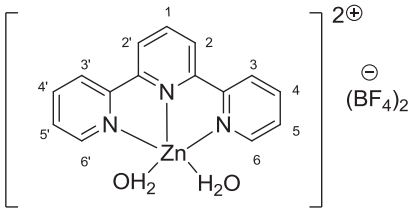

terpyridine (100mg, 0.42mmol) in 20mL of CH_2Cl_2. The reaction mixture was stirred for 6 days at r.t. Then the yellow precipitate formed was filtered (85% yield).

- Molecular weight: 508.29 g/mol
- Formula: $C_{15}H_{15}N_3O_2Zn(BF_4)_2$
- Melting Point: 270°C
- Elemental Analysis (%):

  Calculated: C= 35.44; H= 2.97; N= 8.27

  Found: C= 36.72; H= 2.67; N= 8.57

- IR (KBr) ν_{max}/cm^{-1}: 3425 (OH), 1595 (C=C), 1475 (C=N), 1084 (BF).
- ^{1}H NMR: (300MHz, DMSO): δ_H 8.83 (4H, m, $H_{3,3',6,6'}$), 8.56 (2H, d, *J*(H-H)= 7.89 Hz, $H_{2,2'}$), 8.21 (1H, t, *J*(H-H)= 7.82 Hz, H_1), 7.89 (2H, t, *J*(H-H)= 6.31 Hz, $H_{4,4'}$), 7.80 (1H, s,H_5), 7.45 (1H, t, *J*(H-H)= 7.24 Hz, $H_{5'}$).
- UV-vis (MeOH): λ_{abs} (ε, $mol^{-1}\cdot dm^3\cdot cm^{-1}$): 233 nm (57249); 264 nm (26339); 275 nm (33311); 282 nm (40398); 319 nm (45501); 330 nm (45780). $\lambda_{\varepsilon mi:}$ 355 nm. Yield: 4.6%.
- Λ_{MeOH}= 202.36 $cm^2\cdot\Omega^{-1}\cdot mol^{-1}$.

5.2.4 Synthesis and characterization of complex 5, [(Terp)$_2$Zn][(BF$_4$)$_2$]

For slow evaporation of [(Terp)Zn(H_2O)$_2$][(BF_4)$_2$] (10mg, 0.019mmol) in 1 mL of water, pink crystals of complex **5** were obtained.

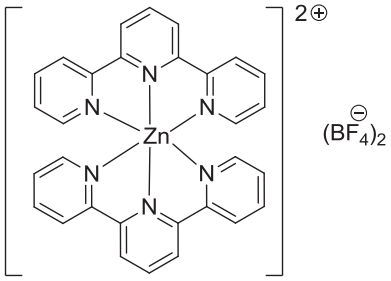

5.3 4,4'-bis(dimethoxy)-2,2'-bipyridine (bpy-OH) Zn(II) and Cu(II) complexes

5.3.1 Synthesis and characterization of complex VI, [(Bpy-OH)ZnCl$_2$]

To a solution of [(Bpy-OH)] (0.3g, 1.38mmol) in hot acetone (50mL) was added $ZnCl_2$ (0.28g, 2.07mmol). The solution was allowed to reach r.t. and was subsequently stirred for 1 day. The solid formed was filtered out and washed with hot acetone (95%yield).

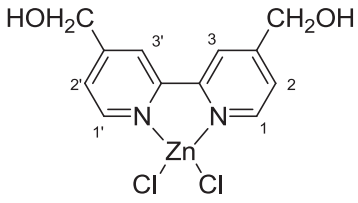

- Molecular weight: 352.52 g/mol
- Formula: $C_{12}H_{12}O_2N_2ZnCl_2$
- Melting Point: >350°C
- Elemental Analysis (%):

  Calculated: C= 40.88; H= 3.43; N= 7.95

  Found: C= 40.67; H= 3.36; N= 7.88

- IR(KBr) ν_{max}/cm^{-1}: 3481 (OH), 3078-3031 (C-H), 298-2889 (C-H), 1619 (C=C).
- ^1H NMR: (300MHz, DMSO): δ_H 9.36 (2H, s, $H_{1,1'}$), 9.28 (2H, s, $H_{3,3'}$), 8.37 (2H, s, $H_{2,2'}$), 6.51 (2H, s, OH), 5.51 (4H, d, *J* (H-H) = 5.42 Hz, CH_2).
- UV-vis (DMSO): λ_{abs} (ε, $mol^{-1}\cdot dm^3\cdot cm^{-1}$): 246 nm (3395), 258 (1830), 282 (4907), 293 (7962), 304 (7256). λ_{emi}: 325 nm.
- Λ_{DMSO} = 10 $cm^2\cdot\Omega^{-1}\cdot mol^{-1}$.

5.3.2 Synthesis and characterization of complex 6, [(Bpy-OH)Zn(Trop)Cl]

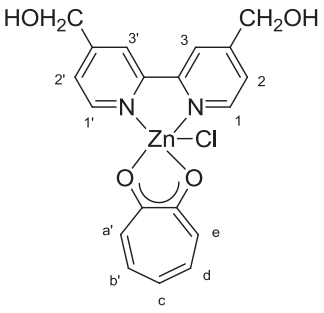

To a solution of [(Bpy-OH)$ZnCl_2$] (0.3g, 0.851mmol) in an ice bath (9mL) was added very slowly, dropwise, a solution of potassium tropolonate (0.136g,

0.851mmol) in MeOH (75mL). The resulting yellow solution was allowed then to reach r.t. and was further stirred under nitrogen for 5 days. Subsequently, the solvent was evaporated in *vacuo.* The product was recrystallized by EtOH to give a yellow solid (54% yield.)

- Molecular weight: 439.19 g/mol
- Formula: $C_{19}H_{17}ClN_2O_4Zn$
- Melting Point: 232°C
- Elemental Analysis (%):

  Calculated: C= 52.08; H= 3.91; N= 6.39

  Found: C= 51.87; H= 3.83; N= 6.20

- IR (KBr) ν_{max}/cm^{-1}: 3280 (OH), 3057 (C-H), 2927-2899 (C-H), 1614 (C=O), 1591 (C=C).
- ^1H NMR: (300MHz, CD_3Cl): δ_H 8.76 (2H, m, $H_{1,1'}$), 8.53 (2H, s, $H_{3,3'}$), 7.71 (2H, s, $H_{2,2'}$), 7.44 (4H, m, $H_{a,b,d,e}$), 6.98 (1H, t, H_c), 5.68 (2H, s, OH), 4.71 (4H, s, CH_2).
- UV-vis (MeOH): λ_{abs} (ε, $mol^{-1}\cdot dm^3\cdot cm^{-1}$): 302 nm (3467); 351 nm (4319); 368 nm (16818). λ_{emi} : 421 nm.
- $\Lambda_{Ethanol} = 15.4\ cm^2\cdot\Omega^{-1}\cdot mol^{-1}$.
- Water solubility= 245 μM.

5.3.3 Synthesis and characterization of complex 7, [(Bpy-OH)Zn(Trop)$_2$]

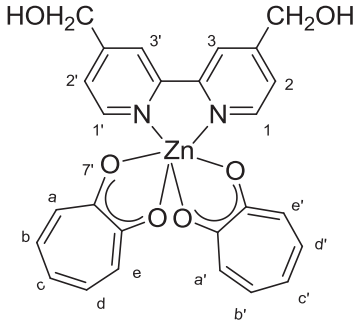

A solution of potassium tropolonate (0.227g, 1.42mmol) in hot MeOH (8mL) was added to a solution of [(Bpy-OH)$ZnCl_2$] (0.25g, 0.709mmol) in hot water (15mL). The resulting yellow solution was allowed to reach r.t. and was further stirred under nitrogen atmosphere for 19h. The yellow solid obtained was filtered and washed with water (92% yield).

- Molecular weight: 523.84 g/mol
- Formula: $C_{26}H_{22}O_6N_2Zn$
- Melting Point: 290°C
- Elemental Analysis (%):

  Calculated: C= 59.61; H= 4.23; N= 5.35

  Found: C= 59.48; H= 4.10; N= 5.10

- IR (KBr) ν_{max}/cm^{-1}: 3306 (OH), 2832 (C-H), 1618 (C=O), 1593 (C=C).
- ^1H NMR: (300MHz, MeOD): δ_H 8.61 (2H, s, $H_{1,1'}$), 8.46 (2H, s, $H_{3,3'}$), 7.56 (2H, d, *J*(H-H)= 5.35 Hz, $H_{2,2'}$), 7.38 (4H, m, $H_{a,a',e,e'}$), 6.98 (4H, d, *J*(H-H)= 11 Hz, $H_{b,b',d,d'}$), 6.89 (2H, d, *J*(H-H)= 9.35 Hz, H_c), 4.81(4H, s, CH_2).

- UV-vis (DMSO): λ_{abs} (ε, $mol^{-1}\cdot dm^3\cdot cm^{-1}$): 283 nm (16855); 295 nm (11757); 329 nm (29497); 337 nm (33551); 374 nm (16385); 393 nm (17325). λ_{emi}: 422 nm.

5.3.4 Synthesis and characterization of complex VII, [(Bpy-OH)CuCl$_2$]

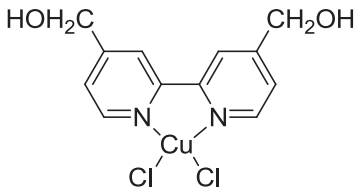

To a solution of [(Bpy-OH)] (0.1g, 0.46mmol) in hot acetone (50 mL) was added 1.5 eq. of $CuCl_2\cdot 2H_2O$ (0.12g, 0.69mmol). After stirring for 24 hours, the green-blue solid formed was filtered out and washed in acetone (90% yield).

- Molecular weight: 350.69 g/mol
- Formula: $C_{12}H_{12}O_2N_2CuCl_2$
- Melting Point: 267°C(dec)
- Elemental Analysis (%):

  Calculated: C= 41.10; H= 3.45; N= 7.99

  Found: C= 40.85; H= 3.49; N= 7.67

- IR (KBr) ν_{max}/cm^{-1}: 3340 (OH), 3022(C-H), 1621(C=O), 1592 (C=C), 1514 (C=N).

- UV-vis (water): λ_{abs} (ε, $mol^{-1}\cdot dm^3\cdot cm^{-1}$): 253 nm (14200); 297 nm (26980); 308 nm (27575).
- Λ_{MeOH} =100.14 $cm^2\cdot\Omega^{-1}\cdot mol^{-1}$.
- Water solubility= 2.58 μM

5.3.5 Synthesis and characterization of complex 8, [(Bpy-OH)Cu(Trop)Cl]

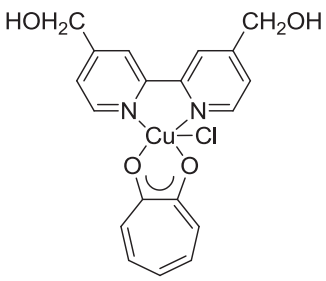

To a solution of [(Bpy-OH)$CuCl_2$] (0.05g, 0.136mmol) in an ice bath (5.5mL) was added very slowly, dropwise, a solution of potassium tropolonate (0.02g, 0.136mmol) in MeOH (3mL). The resulting green solution was allowed then to reach r.t. and was further stirred under nitrogen for 24 hours. Subsequently, the solvent was evaporated in *vacuo.* The product was recrystallized by MeOH/Ether ethylic to give a green solid (97% yield).

- Molecular weight: 436.35 g/mol
- Formula: $C_{19}H_{17}O_4N_2CuCl$
- Melting Point: 234°C(dec)
- Elemental Analysis (%):

Calculated: C= 52.30; H= 3.93; N= 6.42

Found: C= 51.97; H= 3.96; N= 6.20

- IR (KBr) ν_{max}/cm^{-1}: 3339 (OH), 3022 (C-H), 2901 (C-H), 1620 (C=O), 1592 (C=C), 1515(C=N).
- UV-vis (water): λ_{abs} (ε, $mol^{-1}\cdot dm^3\cdot cm^{-1}$): 241 nm (41661); 295 nm (13926); 310 nm (19643); 333 nm (9385); 377 nm (4243).
- Λ_{MeOH}= 149.42 $cm^2\cdot\Omega^{-1}\cdot mol^{-1}$.
- Water solubility= 5.36 μM

5.4 Synthesis and characterization of tropolone-based complexes increasing the aromatic portion in N,N chelating ligand

5.4.1 Synthesis and characterization of complex VIII, [(Bq-OH)$ZnCl_2$]

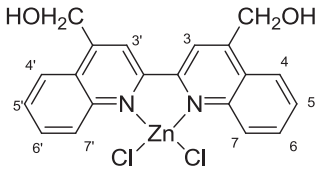

To a solution of [(Bq-OH)] (0.7g, 2.21mmol) in hot acetone (140mL) was added $ZnCl_2$ (0.43g, 3.15mmol). The reaction mixture was allowed to reach r.t. and then was stirred for 1 day. Subsequently, the obtained a yellow solid was filtered and washed with hot acetone (80% yield).

- Molecular weight: 452.64 g/mol
- Formula: $C_{20}H_{16}O_2N_2ZnCl_2$
- Melting Point: >300°C
- Elemental Analysis (%):

  Calculated: C= 53.07; H= 3.56; N= 6.19

  Found: C= 53.20; H= 3.30; N= 6.10

  - IR (KBr) ν_{max}/cm^{-1}: 3517 (OH), 3115-3072 (C-H), 1593 (C=C), 1547 (C=N).
  - ^{1}H NMR: (300MHz, DMSO): δ_H 8.91 (2H, s, $H_{3,3'}$), 8.19 (2H, d, *J*(H-H)= 7.74 Hz, $H_{7,7'}$), 8.09 (2H, d, *J*(H-H)= 8.1 Hz, $H_{4,4'}$), 7.82 (2H, t, *J*(H-H)= 7.39 Hz, $H_{6,6'}$), 7.65 (2H, t, *J*(H-H)= 7.48 Hz, $H_{5,5'}$), 5.78 (2H, t, *J*(H-H)= 5.49 Hz, OH), 5.14 (4H, d, *J*(H-H)= 5.34 Hz, CH_2).
  - UV-vis (DMSO): λ_{abs} (ε, $mol^{-1}\cdot dm^3\cdot cm^{-1}$): 317 nm (30175); 328 nm (32395); 339 nm (26619).
  - Λ_{DMSO}= 0.73 $cm^2\cdot\Omega^{-1}\cdot mol^{-1}$.

5.4.2 Synthesis and characterization of complex 9, [(Bq-OH)Zn(Trop)Cl]

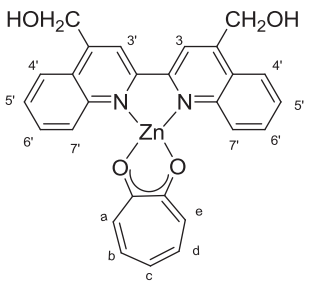

To a solution of [(BqOH)$ZnCl_2$] (200mg, 0.4mmol) in DMSO (5mL) was added a

solution of Ktrop (70.5mg, 0.4mmol) in MeOH (30mL). The reaction was stirred for 48h under reflux. The solid was filtered and the solvent was evaporated under vacuo. The solid was obtained by recrystallization in MeOH/ ether (30% yield).

- Molecular weight: 537.84 g/mol
- Formula: $C_{27}H_{21}O_4N_2ZnCl$
- Melting Point: 294°C
- Elemental Analysis (%):

  Calculated: C= 60.24; H= 3.93; N= 5.21

  Found: C= 51.47; H= 3.88; N= 5.71

- IR (KBr) ν_{max}/cm^{-1}: 3399 (OH), 1594 (C=O).
- ^{1}H NMR: (300MHz, DMSO): δ_H 8.90 (2H, s, $H_{3,3'}$), 8.20 (2H, d, *J*(H-H)= 14.82 Hz, $H_{7,7'}$), 8.09 (2H, d, *J*(H-H)= 8.24 Hz, $H_{4,4'}$), 7.83 (2H, t, *J*(H-H)= 14.82 Hz, $H_{6,6'}$), 7.66 (2H, t, *J*(H-H)= 14.27 Hz, $H_{5,5'}$), 7.40 (2H, t, *J*(H-H)= 19.76 Hz, $H_{b,d}$), 7.16 (2H, d, *J*(H-H)= 9.88 Hz, $H_{a,e}$),6.87 (1H, t, *J*(H-H)= 18.66 Hz, H_c), 5.74 (2H, t, *J*(H-H)= 5.49 Hz, OH), 5.13 (4H, d, *J*(H-H)= 5.49 Hz, CH_2).
- UV-vis (DMSO): λ_{abs} (ε, $mol^{-1}\cdot dm^3\cdot cm^{-1}$): 306 nm (26270); 318 nm (27701); 328 nm (32213); 342 nm (29616); 368 nm (12158). λ_{emi} = 420 nm.

5.4.3 Synthesis and characterization of complex 10,[(Bq-OH)Zn(Trop)$_2$]

To a solution of [(BqOH)ZnCl$_2$] (200mg, 0.4mmol) in DMSO (4mL) was added a solution of Ktrop (156mg, 0.9mmol) in EtOH (15mL). The reaction was stirred for 24 hours. The yellow precipitate was filtered and recrystallized with MeOH hot/cold (53% yield).

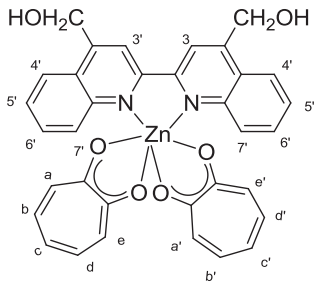

- Molecular weight: 623.96 g/mol
- Formula: $C_{34}H_{26}O_6N_2Zn$
- Melting Point: >300°C
- Elemental Analysis (%):

  Calculated: C= 65.45; H= 4.20; N= 4.49

  Found: C= 65.10; H= 4.74; N= 4.30

- IR (KBr) ν_{max}/cm^{-1}: 3204 (OH), 1592 (C=O), 1507 (C=C), 1426 (C=N).
- ^{1}H NMR: (300MHz, DMSO): δ_H 8.92 (2H, s, $H_{3,3'}$), 8.20 (2H, d, *J*(H-H)= 8.44 Hz, $H_{7,7'}$), 8.09 (2H, d, *J*(H-H)= 8.43 Hz, $H_{4,4'}$), 7.82 (2H, t, *J*(H-H)= 15.4 Hz, $H_{6,6'}$), 7.66 (2H, t, *J*(H-H)=15.04 Hz, $H_{5,5'}$), 7.41 (4H, t, *J*(H-H)=20.54 Hz, $H_{a,e,a',e'}$), 7.18 (2H, d, *J*(H-H)=11.01 Hz, $H_{b,d,b',d'}$), 6.87 (2H, t, *J*(H-H)=18.71 Hz, $H_{c,c'}$), 5.76 (2H, t, *J*(H-H)=11.01 Hz, OH), 5.15 (4H, d, *J*(H-H)=5.51 Hz, CH_2).

- UV-vis (DMSO): λ_{abs} (ε, $mol^{-1}\cdot dm^3\cdot cm^{-1}$): 333 nm (34623); 373 nm (9891); 383 nm (11583); 394 nm (10480). λ_{emi}: 422 nm.

5.5 Co-Crystals of 4,4'-bis(dimethoxy)-2,2'-bipyridine (bpy-OH) Zn (II) and Cu (II) complexes

6.5.1 Synthesis and characterization of complex 11, [(Bpy-OH)$_2$ZnTrop][Sac]

Solid state reaction [(Bpy-OH)Zn(Trop)Cl] (0.05g, 0.109mmol), saccharin (0.04g, 0.218mmol) and water (40μL) have been grinded in ball mill for 8h. From slow evaporation of water solution of the obtained powder, suitable crystals have been obtained.

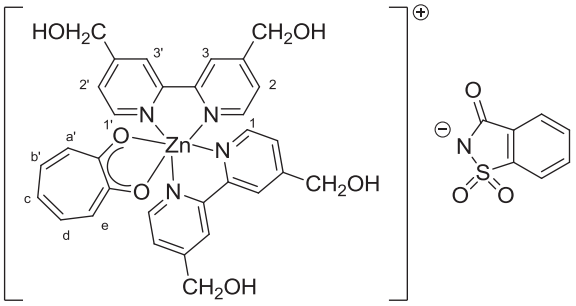

- Molecular weight: 803.15 g/mol
- Formula: $C_{38}H_{33}N_5O_9ZnS$
- Melting Point: 240°C
- IR (KBr) ν_{max}/cm^{-1}: 3365 (OH), 2924 (C-H), 1667 (C=O),

1509 (C=C).

- ^{1}H NMR: (300MHz, D_2O): δ_H 8.27 (4H, s, $H_{1,1'}$), 8.15 (4H, s, $H_{3,3'}$), 7.71-7.60 (4H, m, H_{sacc}), 7.41 (6H, m, $H_{2,2',a,e}$), 7.22 (2H, d, $H_{b,d}$), 6.98(1H, t, H_c).
- UV-vis (water): λ_{abs} (ε, $mol^{-1}\cdot dm^3\cdot cm^{-1}$): 292 nm (23379); 304 nm (20237); 319 nm (8912); 382 nm (4590). λ_{emi}: 412 nm.
- Water solubility = 673 μM

Solution reaction [(Bpy-OH)Zn(Trop)Cl] (0.07g, 0.153mmol) was added to a water solution of saccharin (0.06g, 0.307mmol). The resulting mixture was refluxed for 24 hours; then the temperature was decreased to room temperature and the yellow precipitate formed was filtered out.

- IR (KBr) ν_{max}/cm^{-1}: 3365 (OH), 2923 (C-H), 1667 (C=O).
- ^{1}H NMR: (300MHz, D_2O): δ_H 8.27 (4H, s, $H_{1,1'}$), 8.15 (4H, s, $H_{3,3'}$), 7.71-7.60 (4H, m, H_{sacc}), 7.41 (6H, m, $H_{2,2',a,e}$), 7.22 (2H, d, $H_{b,d}$), 6.98 (1H, t, H_c).
- UV-vis (water): λ_{abs} (ε, $mol^{-1}\cdot dm^3\cdot cm^{-1}$): 292 nm (35294); 304 nm (31249); 322 nm (16852); 382 nm (9272). λ_{emi}: 412 nm.

5.5.2 Synthesis and characterization of complex 12, [(Bpy-OH)Zn(Trop)(Sac)]

Solid state reaction:

$[(Bpy\text{-}OH)Zn(Trop)_2]$ (0.05g, 0.14mmol), saccharin (0.05g, 0.28mmol) and EtOH (20μL) have been grinded in the ball mill for 4 hours. From slow evaporation of an ethanolic solution of the obtained powder, suitable crystals have been obtained.

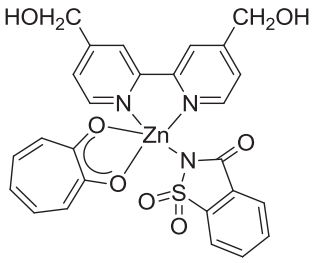

5.5.3 Synthesis and characterization of complex 13, [(Bpy-OH)Cu(Trop)Cl][Sacc]

Solid state reaction:

[(Bpy-OH)Cu(Trop)Cl] (0.03g, 0.06mmol), saccharin (0.03g, 0.131mmol) and water (50μL) have been grinded in ball mill for 2h. After

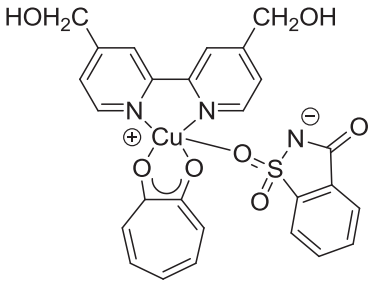

this 50μL of water was added and have been grinded in ball for other 2 hours. From slow evaporation of water solution of the obtained powder, suitable dark blue crystals have been obtained.

- Molecular weight: 583.07 g/mol
- Formula: $C_{26}H_{21}N_3CuO_7S$
- Melting Point: 220°C(dec)
- Elemental Analysis (%):

  Calculated: C= 53.56; H= 3.63; N= 7.21

  Found: C= 52.91; H= 3.88; N= 6.95

- IR (KBr) ν_{max}/cm^{-1}: 3508 (OH), 3182 (C-H), 2912 (C-H), 1630 (C=O), 1593 (C=C), 1513 (C=N).
- UV-vis (water): λ_{abs} (ε, $mol^{-1}\cdot dm^3\cdot cm^{-1}$): 235 nm; 242 nm; 298 nm; 310 nm; 321 nm; 380 nm.
- Λ_{water}= 4.81 $cm^2\cdot\Omega^{-1}\cdot mol^{-1}$.
- Water solubility= 2.15 μM

Solution reaction: [(Bpy-OH)Cu(Trop)Cl] (0.05g, 0.11mmol) was added to a water solution of saccharin (0.02g, 0.11mmol). The resulting mixture was stirred for 24 hours; then for slow evaporation, blue crystals have been obtained.

Rotary evaporatin reaction: [(Bpy-OH)Cu(Trop)Cl] (0.05g, 0.11mmol) was added to a water solution of saccharin (0.02g, 0.11mmol) and was stirring for 1 hour. Then, the solvent was evaporated in *vacuo*. Water was added to the solid and green crystals have been obtained.

5.6 Liquid crystals

5.6.1 Synthesis and characterization of complex 14, [(Bpy-OH)$_2$Ag][CH$_3$COO]·H$_2$O

To a solution of 2 eq. of Bpy-OH (100 mg, 0.46 mmol) in EtOH was added 1 eq. of $AgOOCCH_3$ (30 mg, 0.23 mmol). The solution was stirred 4 hours under nitrogen in a vessel protected from light. The solution was filtered, washed with EtOH, concentrate under reduced pressure and recrystallized from n-hexane (72% yield).

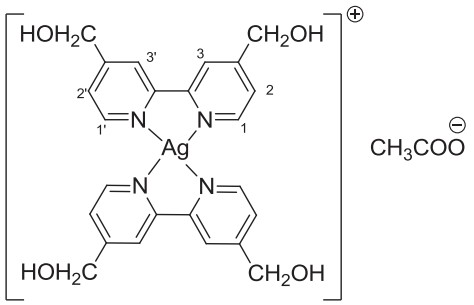

- Molecular weight: 619.42 g/mol
- Formula: $C_{26}H_{31}O_7AgN_4$

- Melting Point: 182°C
- Elemental Analysis (%):

  Calculated: C= 50.42; H= 5.04; N= 9.05

  Found: C= 50.41; H= 4.77; N= 9.14

- IR (KBr) ν_{max}/cm^{-1}: 3369 (OH), 2920-2818 (C-H), 1602 (C=C), 1560 (ν_{asy} C=O), 1407 (ν_{sym} C=O).
- ^{1}H NMR (300MHz, MeOD): δ_H 8.58 (4H, d, *J*(H-H)= 5.07 Hz, $H_{1,1'}$), 8.39 (4H, s, $H_{3,3'}$), 7.58 (4H, d, *J*(H-H)= 4.66 Hz, $H_{2,2'}$), 4.91 (8H, s, CH_2), 1.89(3H, s, CH_3).
- UV-vis (H_2O): λ_{max} (ε, $mol^{-1}\cdot dm^3\cdot cm^{-1}$): 235 nm (61699); 281 nm (72087).
- Λ_{MeOH}= 82.72 $cm^2\cdot\Omega^{-1}\cdot mol^{-1}$.
- TGA trace of powder: experimental mass loss 3.01% corresponds to one water molecule calcd. 2.92%.

5.6.2 Synthesis and characterization of complex 15, $[(Bpy\text{-}OH)_2Ag][CH_3CH_2COO]\cdot H_2O$

To a solution of 2 eq. of Bpy-OH (100 mg, 0.46 mmol) in EtOH was added 1 eq. of $AgOOCCH_2CH_3$ (41.6 mg, 0.23 mmol). The solution was stirred 4 hours under nitrogen and darkness. The solution was filtered, washed with EtOH, concentrate under reduced pressure and recrystallized from n-hexane. (63% yield).

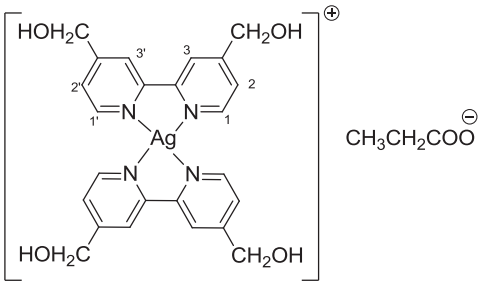

- Molecular weight: 613.41 g/mol
- Formula: $C_{27}H_{31}O_7AgN_4$
- Melting Point: 171°C (dec)
- Elemental Analysis (%):

  Calculated: C= 51.36; H= 4.95; N= 8.87

  Found: C= 51.26; H= 5.14; N= 8.86

- IR (KBr) ν_{max}/cm^{-1}: 3370 (OH), 2884-2833 (C-H), 1603 (C=C), 1562 (ν_{asy} C=O), 1407 (ν_{sym} C=O).
- ^1H NMR (300MHz, MeOD): δ_H 8.58 (4H, d, *J*(H-H)= 5.1 Hz, $H_{1,1'}$), 8.38 (4H, s, $H_{3,3'}$), 7.58 (4H, d, *J*(H-H)= 4.6 Hz, $H_{2,2'}$), 4.83 (8H, s, CH_2), 2.15 (2H, q, *J*(H-H)= 22.86, H_a), 1.08 (3H, s, CH_3).

- UV-vis (MeOH): λ_{max} (ε, $mol^{-1}\cdot dm^3\cdot cm^{-1}$): 234 nm (13608); 282 nm (14822).
- Λ_{MeOH}= 87.83 $cm^2\cdot\Omega^{-1}\cdot mol^{-1}$.
- TGA trace of powder complex: experimental mass loss 2.74% corresponds to one water molecule calcd. 2.85%.

5.6.3 Synthesis and characterization of complex 16, $[(Bpy\text{-}OH)_2Ag][CH_3CH_2CH_2CH_2CH_2COO]\cdot H_2O$

To a solution of 2 eq. of Bpy-OH (100 mg, 0.46 mmol) in EtOH was added 1 eq. of $AgOOCCH_2CH_2CH_2CH_2CH_3$ (51 mg, 0.23 mmol). The solution was stirred 6 hours under nitrogen and darkness. The solution was filtered, washed with EtOH, concentrate under reduced pressure and recrystallized from n-hexane (71% yield).

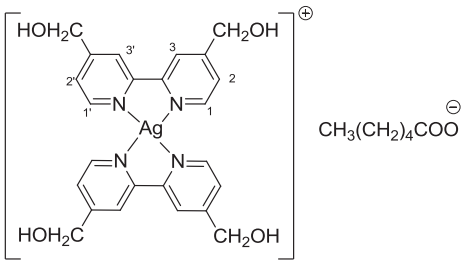

- Molecular weight: 673.51 g/mol
- Formula: $C_{30}H_{37}O_7AgN_4$
- Melting Point: 139°C (dec)
- Elemental Analysis (%):

Calculated: C= 53.50; H= 5.54; N= 8.32

Found: C= 53.38; H= 5.51; N= 8.45

- IR (KBr) ν_{max}/cm^{-1}: 3369 (OH), 1604 (C=C), 1564 (ν_{asy} C=O), 1408 (ν_{sym} C=O).
- ^1H NMR (300MHz, MeOD): δ_H 8.57 (4H, d, *J*(H-H)= 5.25 Hz, $H_{1,1'}$), 8.38 (4H, s, $H_{3,3'}$), 7.57 (4H, d, *J*(H-H)= 6.53 Hz, $H_{2,2'}$), 4.82 (8H, s, CH_2), 2.13 (2H, t, *J*(H-H)=7.8 Hz, H_a), 1.58 (2H, m, *J*(H-H)= 7.52 Hz, H_b), 1.31(4H, m, $H_{c,d}$), 0.88 (3H, t, *J*(H-H)= 6.91 Hz,CH_3).
- UV-vis (MeOH) λ_{max} (ε, $mol^{-1}\cdot dm^3\cdot cm^{-1}$): 235 nm (16008); 283 nm (19439).
- Λ_{MeOH}= 59.49 $cm^2\cdot\Omega^{-1}\cdot mol^{-1}$.
- TGA trace of powder complex: experimental mass loss 2.86% corresponds to one water molecule calcd. 2.68%.

5.6.4 Synthesis and characterization of complex 17, $[(Bpy\text{-}OH)_3Ag_2][PF_6]_2$

To a solution of Bpy-OH (0.15g, 0.69mmol) in EtOH under N_2 and dark was added $AgPF_6$ (0.174g, 0.69mmol). The reaction was stirring for 4 hours, then the grey

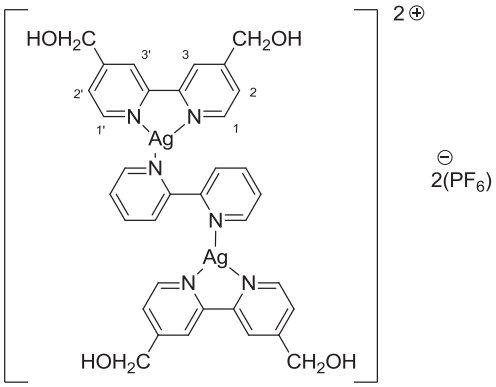

precipitate was filtered and caracterized (42% yield).

- Molecular weight: 1154.37 g/mol
- Formula: $C_{36}H_{36}O_6Ag_2N_6F_{12}P_2$
- Melting Point: 200°C (dec)
- Elemental Analysis (%):

  Calculated: C= 37.46; H= 3.14; N= 7.28

  Found: C= 37.93; H= 3.59; N= 7.42

- IR (KBr) ν_{max}/cm^{-1}: 3369 (OH), 2886-2831 (C-H), 1603 (C=C), 1459 (C=N), 845 (PF_6).
- ^1H NMR (300MHz, MeOD): δ_H 8.60 (4H, d, *J*(H-H)= 4.95 Hz, $H_{1,1'}$), 8.37 (4H, s, $H_{3,3'}$), 7.6 (4H, d, *J*(H-H)= 4.8 Hz, $H_{2,2'}$), 4.82 (8H, s, CH_2).
- UV-vis (MeOH): λ_{max} (ε, $mol^{-1}\cdot dm^3\cdot cm^{-1}$): 299 nm (30140).
- Λ_{MeOH}= 128 $cm^2\cdot\Omega^{-1}\cdot mol^{-1}$.

5.6.5 Synthesis and characterization of complex 18, [(Bpy-OH)$_2$Ag][OTf]

To a solution of Bpy-OH (0.10g, 0.46mmol) in EtOH under N_2 and dark was added AgOTf (0.06g, 0.23mmol). The reaction was

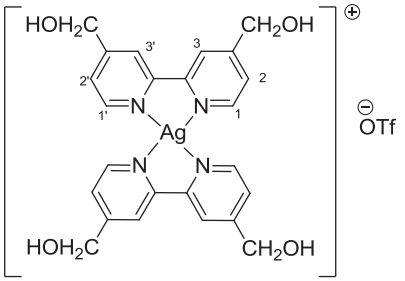

stirring for 4 hours, then the yellow precipitate was filtered and caracterized.(74% yield)

- Molecular weight: 689.41 g/mol
- Formula: $C_{25}H_{24}O_7AgN_4F_3S$
- Melting Point: 233-246°C (dec)
- Elemental Analysis (%):

  Calculated: C= 43.55; H= 3.51; N= 8.13

  Found: C= 43.09; H= 3.25; N= 8.18

- IR (KBr) ν_{max}/cm^{-1}: 3420 (OH), 2911-2834 (C-H), 1607 (C=C), 1460 (C=N), 1254 (OTf).
- ^1H NMR (300MHz, MeOD): δ_H 8.58 (4H, d, *J*(H-H)= 5.22 Hz, $H_{1,1'}$), 8.40 (4H, s, $H_{3,3'}$), 7.59 (4H, d, *J*(H-H)= 6.6 Hz, $H_{2,2'}$), 4.91 (8H, s, CH_2).
- UV-vis (EtOH) λ_{max} (ε, $mol^{-1}\cdot dm^3\cdot cm^{-1}$): 313 nm (12398); 286 nm (43043); 248 nm (31697).
- Λ_{MeOH}= 73.34 $cm^2\cdot\Omega^{-1}\cdot mol^{-1}$.

5.6.6 Synthesis and characterization of complex 19, [(Bpy-OH)$_2$Ag][OOCCF$_3$]

To a solution of Bpy-OH (0.10g, 0.46mmol) in EtOH under N_2 and dark was added CF_3COOAg (0.05g, 0.23mmol). The reaction was stirring for 6 hours, then the yellow precipitate was filtered and caracterized (50% yield).

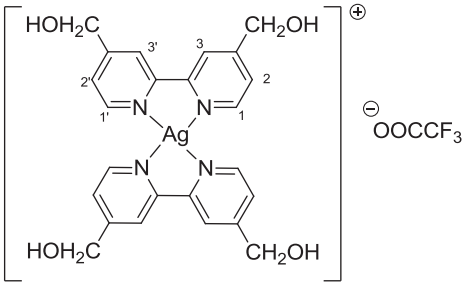

- Molecular weight: 671.37 g/mol
- Formula: $C_{26}H_{26}O_7AgN_4F_3$
- Melting Point: 217-226°C (dec)
- Elemental Analysis (%):

  Calculated: C= 46.51; H= 3.90; N= 8.35

  Found: C= 46.25; H= 4.14; N= 10.79

- IR (KBr) ν_{max}/cm^{-1}: 3376 (OH), 2891-2826 (C-H), 1679 (ν_{asy} C=O), 818 (CF_3).
- ^{1}H NMR (300MHz, MeOD): δ_H 8.58 (4H, d, *J*(H-H)= 5.21 Hz, $H_{1,1'}$), 8.40 (4H, s, $H_{3,3'}$), 7.59 (4H, d, *J*(H-H)= 5.08 Hz, $H_{2,2'}$), 4.91 (8H, s,CH_2).

- UV-vis (EtOH) λ_{max} (ε, $mol^{-1} \cdot dm^3 \cdot cm^{-1}$): 283 nm (25384); 239 nm (20833).
- Λ_{MeOH}= 77.23 $cm^2 \cdot \Omega^{-1} \cdot mol^{-1}$.

Chapter 6

Working experience at the Institute of Medical Sciences of Aberdeen, Scotland (UK)

During the PhD, an abroad stage was undertaken at the Institute of Medical Sciences of Aberdeen, in the group of Prof. Matteo Zanda. The principal task was the synthesis of two new selective CB1 receptors, very important for potential clinical developments. This period was also significant for the development of organic synthetical skills, that will help to develop new ligands able to chelate transition metal centres.

The endocannabinoid system comprises, to date, two cannabinoid receptors CB1 and CB2, five endogenous lipid-like ligands and the enzymes involved in their formation and breakdown. This system is implicated in a number of physiological functions in the central and peripheral nervous system and in peripheral organs.[132]

The CB1 cannabinoid receptor is a G-protein coupled receptor that is widely expressed throughout the central and peripheral nervous system. The CB1 receptors, among other things, play an important role

[132] **Smith, T. H. Sim-Selley L. J. Selly, D. E.** 2010, British Journal of Pharmacology, Vol. 160, pp. 454-466.

in the central and peripheral regulation of food intake, fat accumulation and lipid and glucose metabolism.[133]

Different cannabinoid receptor ligands have been studied: agonist (ligand that binds a receptor and activates the receptor to produce a biological response) and antagonist (ligand that blocks responses rather than provoking a biological response itself upon binding to a receptor).

The first specific cannabinoid antagonist was Rimonabant reported in Figure 6.1. This drug reduces food intake and produces weight loss in animals. However, clinical data revealed serious side effects, notably psychiatric disturbances, limiting the therapeutic usefulness of rimonabant.

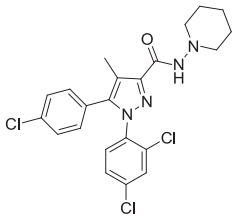

Figure 6.1. Structure of Rimonabant.

The aim of this part of the project is the synthesis of new CB1 receptor ligands with potential for clinical development, marked with PET-radionuclides (Positron Emission Tomography is a type of nuclear medicine imaging) to study where the CB1 receptors are predominately located and chelating with metals for synthesized intercalating agents.

[133] **Svizenska, I, Dubovy, P. Sulcova, A. 2008**, Pharmacology, Biochemistry and Behaviour, Vol. 90, pp. 501-511.

6.1 Synthesis and characterization of CB1 receptor ligands

The aim of the project has been the synthesis of new potential CB1 receptors for the endocannabinoid system[134]. The CB1 cannabinoid receptor is widely expressed throughout the central and peripheral nervous system. These receptors, among other things, play an important role in the central and peripheral regulation of food intake, fat accumulation and lipid and glucose metabolism.

The first specific cannabinoid antagonist was Rimonabant reported in Figure 6.2. This drug reduces food intake and produces weight loss in animals. However, clinical data revealed serious side effects, notably psychiatric disturbances, limiting the therapeutic usefulness of Rimonabant.

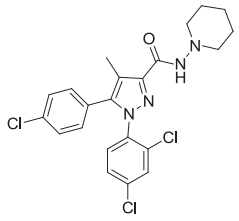

Figure 6.2. Chemical structure of Rimonabant.

The aim of this part of the thesis is the synthesis of new CB1 receptor ligands with potential for clinical development, marked with PET-radionuclides. Positron Emission Tomography is a type of nuclear

[134] **Lange, J. H. M. Kruse, C. G**. 2005, DDT, Vol. 10, 10, pp. 693

medicine imaging used to study where the CB1 receptors are predominately located.

Two different compounds have been synthesized with a design based on Ribonabant and a new molecule reported on Figure 6.3 with an improved biological activity.

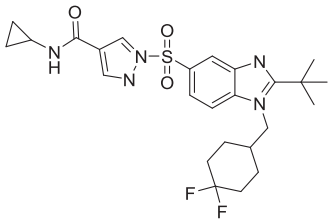

Figure 6.3. US Patent (US2011/0086853A1)

The approach used for the synthesis of these two molecules is reported in Scheme 6.1.

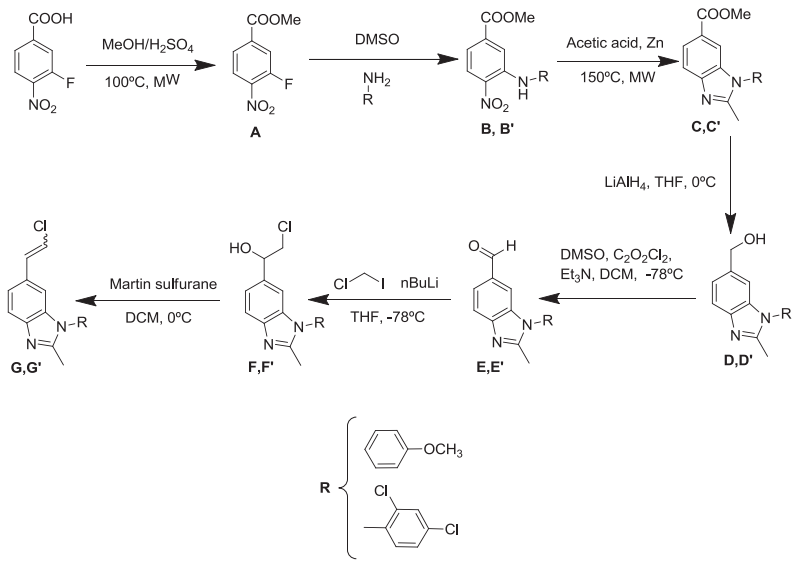

Scheme 6.1. Synthesis of two novel CB1 receptor candidates.

In particular, 3-Fluoro-4-nitrobenzoic acid was reacted with sulfuric acid in methanol to obtain the ester compound **A**. The reaction was stirred for 15 minutes by microwave irradiation (80°C), after that, another sulfuric amount was added to the mixture and stirred again by microwave in the same conditions. The product **A** was obtained in a good yield. Subsequently, to a solution of product **A** in DMSO was added the NH_2-R reagent for the nucleophilic aromatic substitution. The reaction was stirred for 90 minutes under nitrogen atmosphere at 80°C, affording the product **B** and **B'** which were purified by flash chromatography. For the synthesis of imidazoles **C** and **C'**, the products **B** and **B'** were reacted with Zn and acetic acid. The mixtures were stirred for 15 min in a microwave at 150°C, and the pure products were obtained after separation by flash chromatography. To a solution of **C** and **C'** in dry THF at 0°C under nitrogen atmosphere was added $LiAlH_4$ for the reduction of the ester group to alcohol. The reaction mixtures were stirred for 2-2.5 hours and products **D** and **D'** were obtained after purification in high yields. Solutions of **D** and **D'** in dry dichloromethane were added to mixture of dichloromethane, DMSO, oxalyl chloride and triethylamine at -78°C to obtain the aldehyde products **E** and **E'**. For the addition of chlorine, products **E** and **E'** were reacted with chloroiodomethane in dry THF. The reaction mixtures were stirred for 3 hours affording compounds **F** and **F'**. The final products were obtained by the reaction between **E** and **E'** with the Martin Sulfurane reagent in dry dichloromethane. The reactions were stirred for 4 hours, and products **G** and **G'** were obtained after purification by flash chromatography and preparative TLC.

All the products therein reported have been characterized by ^{1}H NMR and mass spectroscopy.

The ^{1}H NMR spectrum **A** shows in the aromatic part the proton signals belonging to the aromatic ring and in the aliphatic part a singlet belonging to the ester group at 4.01 ppm. In the case of complex **B** and **B'** the ^{1}H NMR spectra contains moreover the signals of the aromatic protons of the R group and the NH-R protons at 9.41 and 8.38 ppm respectively. The signal of the three protons of the imidazole methyl group at 2.54 ppm and 2.57 ppm confirm the successful obtaining of products **C** and **C'**. Furthermore, the ^{1}H NMR spectra of the compounds **D** and **D'** show the presence of the signals of the methanol group at 3.18 ppm and 4.66 ppm the exact mass confirm the formation of **D** and **D'**. The proton signal at 9.92 ppm and 9.93 ppm confirm the transformation from the alcohol group to aldehyde, and hence the formation of products **E** and **E'**. The signal of the alcohol group at 4.87 ppm and the mass peak confirm the formation of **F** and **F'**. Finally, the absence of the alcohol proton signal and the presence of all proton signals corresponding to the products **G** and **G'** confirm the formation of the final derivatives.

For all compounds the mass spectroscopy analysis confirm the mass of the correspondent derivatives.

These compounds will be further analyzed and their biological properties will be tested in collaboration with the Institute of Medical Sciences at Aberdeen University.

6.2 General equipment and procedures

All commercially available chemicals were purchase from Aldrich Chemical Co. and were used without further purification. 1H-NMR and 13C-NMR spectra were recorded on a Varina VNMRS-400 spectrometer and calibrated using residual undeuterated solvent as internal reference. Analyses (MS) were performed using Agilent 1200 HPLC system coupled to Agilent G6120 single quadrupole detector equipped with an electrospray ionization (ESI) source in direct infusion modality. ESI MS spectra were recorded in positive mode, unless otherwise noted.

6.2.1 General procedure for the preparation of compound A

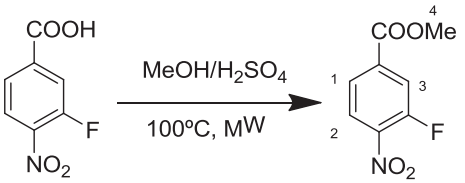

3-Fluoro-4-nitrobenzoic acid **A**

To a solution 3-Fluoro-4-nitrobenzoic acid (100mg, 0.54mmol) in MeOH (3mL) was added of catalytic amount of H_2SO_4 (0.1mL). The stirred reaction mixture was subsequently heated with microwave irradiation (80°C) for 15 minutes, after that, was added 0.1mL of H_2SO_4

and stirred again 15 minutes in the same conditions. After completion of the reaction, the reaction mixture was quenched with $NaHCO_3$, was extracted by dichloromethane and evaporated to give the 3-fluoro-4-nitrobenzoate (**A**), as a yellow solid (95% yield). ^{1}H-NMR (400MHz, $CDCl_3$) δ_H 8.13 (m, 1H, H_3), 8.00 (t, 1H, H_2), 7.97 (dd, 1H, H_1), 4.01 (s, 3H, H_4).

6.2.2 General procedure for the preparation of compound B

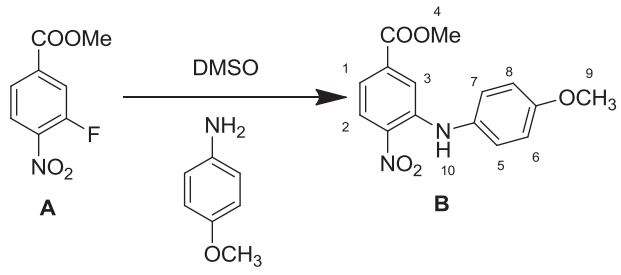

To a solution of **A** (20mg, 0.094 mmol) in DMSO (0.2mL), p-Anisidine (26mg, 0.211mmol) was added and the red mixture was stirred under N_2 for 90 minutes. After completion of the reaction, the reaction mixtures were extracted with ethyl acetate and evaporated to give the crude product. After purification by column chromatography (1:5 ethyl acetate/hexane) methyl 3-((4-methoxyphenyl)amino)-4-nitrobenzoate (**B**) was obtained as a red solid (80% yield). ^{1}H-NMR (400MHz, $CDCl_3$) δ_H 9.41 (s, 1H, H_{10}), 8.26 (d, 1H, *J*(H-H)= 8.9 Hz, H_2), 7.72 (s, 1H, H_1), 7.31, (dd, 1H, *J*(H-H)= 8.9, 1.7 Hz, H_3), 7.23 (d, 2H, *J*(H-

H)= 8.8 Hz, $H_{8,6}$), 7.00 (d, 2H, *J*(H-H)= 8.9 Hz, $H_{5,7}$), 3.89 (s, 3H, H_4), 3.88 (s, 3H, H_9). ESI MS m/z: 302.09; found: 303.1 $[M+H]^+$, 325.0 $[M+Na]^+$.

6.2.3 General procedure for the preparation of compound C

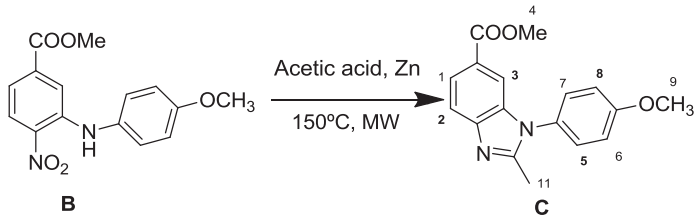

Compound **B** (20 mg, 0.063mmol) and Zn (62.12mg, 0.95mmol) were added to 1ml of acetic acid. The mixture was subsequently irradiated with stirring for 15 minutes (150°C) in a microware process vial. After that, 500μL of acetic acid was added ant the mixture was stirred 15 minutes at the same temperature. After completion of the reaction, the reaction mixture was quenching with $NaHCO_3$, was extracted by dichloromethane and evaporated to give the crude product. After purification by column chromatography (1:5 ethyl acetate/hexane) methyl 1-(4-methoxyphenyl)-2-methyl-1*H*-benzo[*d*]imidazole-6-carboxylate (**C**) was obtained as a purple solid (92% yield). ^{1}H-NMR (400MHz, $CDCl_3$) δ_H 7.87 (d, 1H, *J*(H-H)= 8.4 Hz, H_3), 7.71 (s, 1H, H_2), 7.63(d, 1H, *J*(H-H)= 8.4 Hz, H_1), 7.18(d, 2H, *J*(H-H)= 8.4 Hz, $H_{5,7}$), 6.99 (d, 2H, *J*(H-H)= 8.2 Hz, $H_{6,8}$), 3.94 (s, 3H, H_4), 3.91 (s, 3H, H_9), 2.54 (s, 3H, H_{11}). ESI MS m/z: 296.12; found: 297.1 $[M+H]^+$.

6.2.4 General procedure for the preparation of compound D

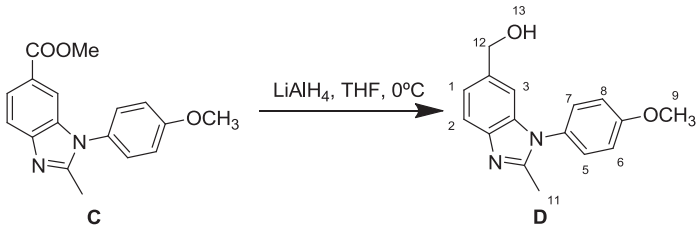

To a solution of **C** (18mg, 0.061mmol) in THF anhydrous (2.5mL) at 0°C and under N_2, was added $LiAlH_4$ (9mg, 0.134mmol). The reaction was stirred for 2.5 hours. After completion of the reaction, the reaction mixture was quenching with potassium sodium tartrate, was extracted by dichloromethane and evaporated to give the crude product. After purification by column chromatography (1:20 MeOH/CH_2Cl_2) (1-(4-methoxyphenyl)-2-methyl-1*H*-benzo[*d*]imidazole-6-yl)methanol (**D**) was obtained (70% yield). ^{1}H-NMR (400MHz, $CDCl_3$) δ_H 7.52 (d, 1H, *J*(H-H)= 8.2 Hz, H_1), 7.12 (m, 3H, $H_{2,3,5}$), 6.96 (m, 3H, $H_{6,7,8}$), 4.66 (s, 2H, H_{12}), 3.80 (s, 3H, H_9), 3.33 (s, 3H, H_{11}), 3.18 (s, 1H, H_{13}). ESI MS m/z: 268.12; found: 269.1 $[M+H]^+$.

6.2.5 General procedure for the preparation of compound E

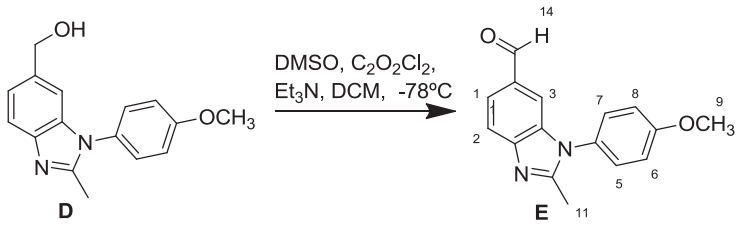

A mixture of dry CH_2Cl_2 (3mL) and dry DMSO (132μL, 1.86mmol) was stirred at -78°C under nitrogen. After 5 minutes, drop by drop was added of oxalyl chloride (63μL, 0.74 mmol). In another flask, a solution of compound **D** (100mg, 0.37mmol) in dry CH_2Cl_2 was stirred. After 15 minutes, the second solution was added drop by drop to the first solution. After 30 minutes, triethyl amine (617μL, 4.44mmol) was added drop by drop. The pink mixture was stirred for 2 hours. After quenching the solution with ammonium chloride, the residue was extracted by CH_2Cl_2. The organic layer was separated and dried in $MgSO_4$. The solvent was evaporated in *vacuo*, to give the product 1-(4-methoxyphenyl)-2-methyl-1*H*-benzo[*d*]imidazole-6-carbaldehyde (**E**) (86% yield). ^{1}H-NMR (400MHz, $CDCl_3$) δ_H 9.92 (s, 1H, H_{14}), 7.73 (s, 3H, $H_{1,2,3}$), 7.20 (d, 2H, *J*(H-H)= 8.8 Hz, $H_{5,7}$), 7.03 (d, 2H, *J*(H-H)= 8.8 Hz, $H_{6,8}$), 3.84 (s, 3H, H_9), 2.46 (s, 3H, H_{11}) . ESI MS m/z: 266.11; found: 267.7 $[M+H]^+$.

6.2.6 General procedure for the preparation of compound F

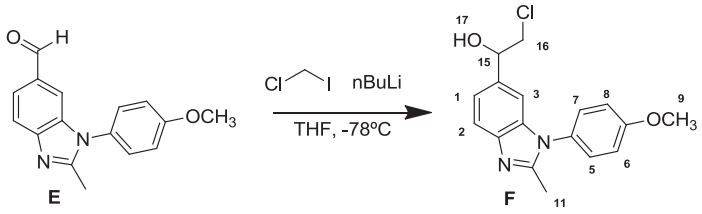

To a solution of **E** (23mg, 0.087mmol) in dry THF (2mL), under N_2 at -78°C, was added chloroiodomethane (10μL, 0.13mmol). After 5minutes BuLi (62μL, 0.10mmol) was added obtaining a yellow solution. After stirring for 3 hours, the reaction mixture was extracted by dichloromethane and evaporated to give the product 2-chloro-1-(1-(4-methoxyphenyl)-2-methyl-1*H*-benzo[*d*]imidazole-6-yl) ethanol (**F**) (85% yield). ^{1}H-NMR (400MHz, $CDCl_3$) δ_H 7.59 (d, 1H, *J*(H-H)= 8.3 Hz, H_1), 7.16 (m, 3H, $H_{2,3,5}$), 7.09 (s, 1H, H_7), 7.00 (m, 2H, $H_{6,8}$), 4.89 (dd, 1H, *J*(H-H)= 8.8, 3.5 Hz, H_{17}), 4.87 (s, 1H, H_{15}), 3.83 (s, 3H, H_9), 3.62 (m, 2H, H_{16}), 2.38 (s, 3H, H_{11}). ESI MS m/z: 316.10; found: 317.1 $[M+H]^+$.

6.2.7 General procedure for the preparation of compound G

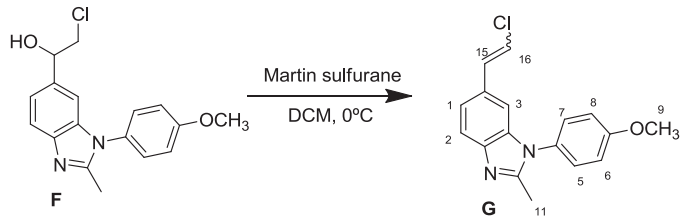

To a solution of **F** (22mg, 0.074mmol) in dry CH_2Cl_2 (2mL) under N_2 at 0°C, was added the Martin Sulfurane (59.72mg, 0.088). The reaction was stirred for 4 hours. After completion of the reaction, the reaction mixture was extracted by dichloromethane furnished the crude product, which was purified by column chromatography (silica gel, 1:20 MeOH/ CH_2Cl_2) to provide a crude product with starting material. The product 6-(2-chlorovinyl)-1-(4-methoxyphenyl)-2-methyl-1*H*-benzo[*d*]imidazole (**G**) was obtained after preparative TLC (20% yield). ^{1}H-NMR (400MHz, $CDCl_3$) δ_H 7.59 (d, 1H, *J*(H-H)= 8.52 Hz, H_1), 7.14 (m, 1H, H_3), 7.01 (m, 3H, $H_{2,5,7}$), 6.91 (s, 2H, $H_{6,8}$), 6.79 (d, 1H, *J*(H-H)= 13.6 Hz, H_{15}), 6.49 (d, 1H, *J*(H-H)= 13.6 Hz, H_{16}), 3.84 (s,3H, H_9), 2.40 (s, 3H, H_{11}). ESI MS m/z: 298.09; found: 299.1 $[M+H]^+$.

6.2.8 General procedure for the preparation of compound B'

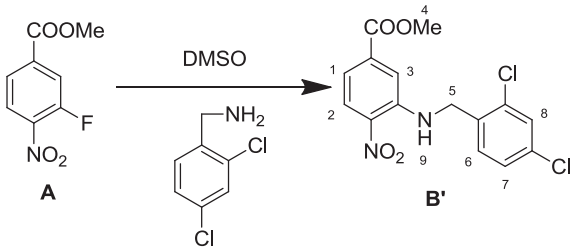

To a solution of **A** (20mg, 0.094mmol) in DMSO (0.2mL), 2,4-dichlorobenzylamine(33mg, 0.188mmol) was added and the red mixture was stirred under N_2 for 90 minutes al 80°C. After completion of the reaction, the reaction mixture was extracted by Ethyl acetate and evaporated furnished the crude product, which was purified by column chromatography (silica gel, 1:10 ethyl acetate/hexane) to provide the methyl 3-((2,4-dichlorobenzyl)amino)-4-nitrobenzoate (**B'**) as an orange solid (92% yield). ^{1}H-NMR (400MHz, $CDCl_3$) δ_H 8.38 (s, 1H, H_9), 8.27 (d, 1H, *J*(H-H)= 8.9 Hz, H_2), 7.49 (dd, 2H, *J*(H-H)= 11.9, 1.8 Hz, $H_{1,8}$), 7.28 (m, 3H, $H_{3,6,7}$), 4.68 (d, 2H, *J*(H-H)= 6.0 Hz, H_5), 3.94 (s, 3H, H_4).

6.2.9 General procedure for the preparation of compound C'

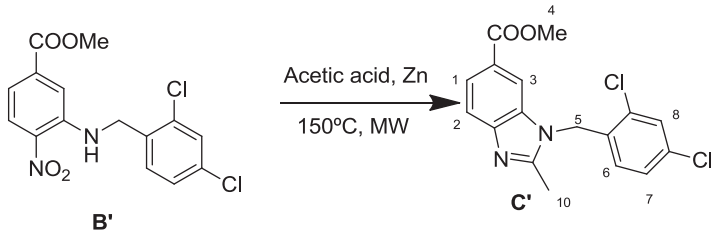

Compound **B'** (30 mg, 0.084mmol) and Zn (82.39mg, 1.26mmol) were added to 1ml of acetic acid. The mixture was subsequently irradiated with stirring for 15 minutes (150°C) in a microware process vial. After completion of the reaction, the reaction mixture was quenching with $NaHCO_3$, was extracted by dichloromethane and evaporated to give the crude product. After purification by column chromatography (1:10 ethyl acetate/hexane), methyl 1-(2,4-dichorobenzyl)-2-methyl-1*H*-benzo[*d*]imidazole-6-carboxylate (**C'**) was obtained as a yellow solid (85% yield). ^{1}H-NMR (400MHz, $CDCl_3$) δ_H 8 (dd, 1H, *J*(H-H)= 8.5, 1.5 Hz, H_2), 7.91 (s, 1H_3), 7.76(d, 1H, *J*(H-H)= 8.5 Hz, H_1), 7.50 (d, 1H, *J*(H-H)= 2.1 Hz, H_8), 7.09 (dd, 1H, *J*(H-H)= 8.4, 2.1 Hz, H_7), 6.33 (d, 1H, *J*(H-H)= 8.4 Hz, H_6), 5.40 (s, 2H, H_5), 3.91 (s, 3H, H_4), 2.57 (s, 3H, H_{10}). ESI MS m/z: 348.04; found: 349.0 $[M+H]^+$.

6.2.10 General procedure for the preparation of compound D'

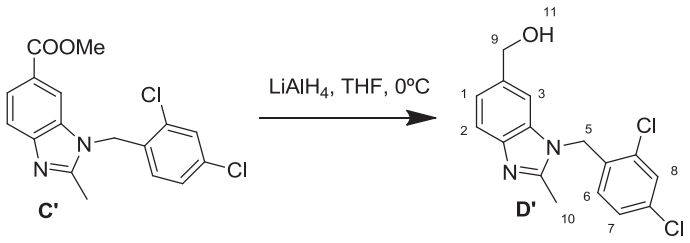

To a solution of **C'** (68mg, 0.19mmol) in dry THF (2.5mL) at 0°C and under N_2, was added $LiAlH_4$ (20mg, 0.42mmol). The reaction was stirred for 2 hours. After completion of the reaction, the reaction mixture was quenching with potassium sodium tartrate, was extracted by dichloromethane and evaporated to give the product (1-(2,4-dichlorobenzyl)-2-2methyl-1*H*-benzo[*d*]imidazole-6-yl)methanol (**D'**) (73% yield). ^{1}H-NMR (400MHz, $CDCl_3$) δ_H 7.52 (d, 1H, *J*(H-H)= 8.2 Hz, H_1), 7.12 (m, 2H, $H_{2,3}$), 6.96 (m, 3H, $H_{6,7,8}$), 5.40 (s, 2H, H_5), 4.66 (s, 2H, H_9), 3.18 (s, 1H, H_{11}), 2.57 (s, 3H, H_{10}). ESI MS m/z: 320.05; found: 321.0 $[M+H]^+$.

6.2.11 General procedure for the preparation of compound E'

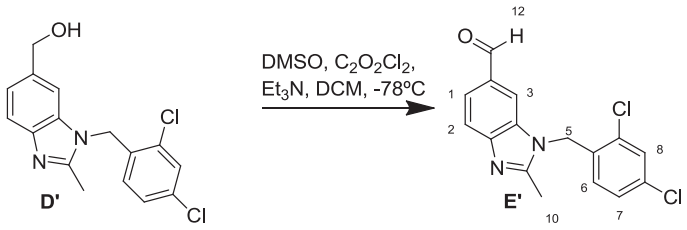

A mixture of dry CH_2Cl_2 (3mL) and dry DMSO (50μL, 0.7mmol) was stirred at -78°C under nitrogen. After 5 minutes, drop by drop was added of oxalyl chloride (24μL, 0.28 mmol). In another flask, a solution of compound **D'** (45mg, 0.14mmol) in dry CH_2Cl_2 was stirred. After 15 minutes, the second solution was added drop by drop to the first solution. After 30 minutes, triethyl amine (230μL, 1.68mmol) was added drop by drop. The transparent mixture was stirred for 2 hours. After quenching the solution with ammonium chloride, the residue was extracted by CH_2Cl_2. The organic layer was separated and dried in $MgSO_4$. The solvent was evaporated in *vacuo*, to give the product 1-(2,4-dichlorobenzyl)-2-methyl-1*H*-benzo[*d*]imidazole-6-carbaldehyde (**E'**) (98% yield). ^{1}H-NMR (400MHz, $CDCl_3$) δ_H 9.93 (s, 1H, H_{12}), 7.74 (m, 2H, $H_{2,3}$), 7.65 (s, 1H, H_1), 7.41 (s, 1H, H_8), 7.01 (d, 1H, *J*(H-H)= 8.4 Hz, H_7), 6.28 (d, 1H, *J*(H-H)= 8.4 Hz, H_6), 5.35 (s, 2H, H_5), 2.52 (s, 3H, H_{10}). ESI MS m/z: 318.03; found: 319.1 $[M+H]^+$.

6.2.12 General procedure for the preparation of compound F'

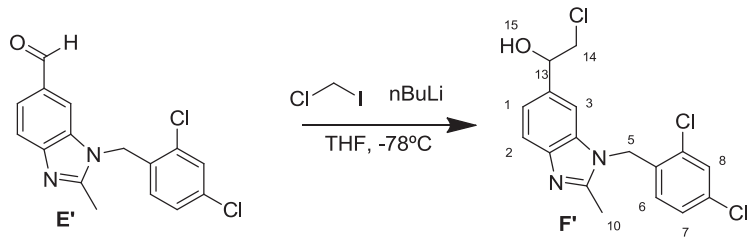

To a solution of **E'** (45mg, 0.14mmol) in 2mL of dry THF, under N_2 at -78°C, was added chloroiodomethane (15μL, 0.21mmol). After 5minutes BuLi (105μL, 0.168mmol) was added obtaining a yellow solution. After stirring for 3 hours, the reaction mixture was extracted by dichloromethane. The crude product was purified by column chromatography (silica gel, 1:20 MeOH/CH_2Cl_2) to give the crude product. After purification by column chromatography (1:20 MeOH/CH_2Cl_2), was obtained the 2-chloro-1-(-1-(2,4-dichlorobenzyl)-2-methyl-1*H*-benzo[*d*]imidazole-6-yl)ethanol (**F'**) (78% yield). ^{1}H-NMR (400MHz, $CDCl_3$) δ_H 7.56 (d, 1H, *J*(H-H)= 7.1 Hz, H_1), 7.38 (d, 1H, *J*(H-H)= 2 Hz, H_3), 7.19 (s, 1H, H_2), 7.13 (d, 1H, *J*(H-H)= 8.3 Hz, H_8), 6.95 (dd, 1H, *J*(H-H)= 8.30, 2 Hz, H_7), 6.23 (d, 1H, *J*(H-H)= 8.4 Hz, H_6), 5.23 (m, 2H, H_5), 4.91 (dd, 1H, *J*(H-H)= 8.4, 3.5 Hz, H_{15}), 4.87 (s, 1H, H_{13}), 3.64 (s, 3H, H_{10}), 2.42 (s, 1H, H_{14}). ESI MS m/z: 368.02; found: 369.0 $[M+H]^+$.

6.2.13 General procedure for the preparation of compound G'

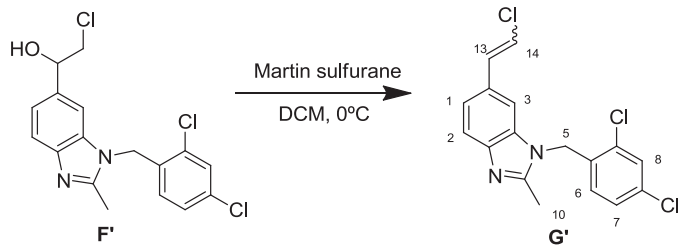

To a solution of **F'** (40mg, 0.11mmol) in dry CH_2Cl_2 (1mL) under N_2 at 0°C, was added the Martin Sulfurane (110.96mg, 0.165mmol). The reaction was stirred for 4 hours. After completion of the reaction, the reaction mixture was extracted by dichloromethane furnished the crude product, which was purified by column chromatography (silica gel, 1:1 Ethyl acetate/hexane) to provide a crude product with starting material. The product 2-chloro-1-(1-(2,4-dichlorobenzyl)-2-methyl-1*H*-benzo[*d*]imidazole-6-yl)ethanol (**G'**) was obtained after preparative TLC (1:30 MeOH/CH_2Cl_2 (25% yield). ^{1}H-NMR (400MHz, $CDCl_3$) δ_H 7.61 (d, 1H, *J*(H-H)= 8.3 Hz, H_1), 7.42 (d, 1H, *J*(H-H)= 2 Hz,H_2), 7.02 (dd, 1H, *J*(H-H)= 8.3, 2 Hz, H_3), 6.95 (s, 1H, H_8), 6.81 (d, 1H, *J*(H-H)= 13.6 Hz, H_7), 6.52 (d, 1H, *J*(H-H)= 13.6 Hz, H_6), 6.29 (d, 2H, *J*(H-H)= 8.4 Hz, $H_{13,14}$), 5.25 (s, 2H, H_5), 2.47 (s, 3H, H_{10}). ESI MS m/z: 350.01; found: 351.0 $[M+H]^+$.

Conclusions

New metal complexes have been synthesized with potential antitumor activity and structural characteristics able to make them intercalating agents and/or G-quadruplex binders. In this context, recently, a low cost Zn(II) complex, [(bpy-9)Zn(curc)Cl], **A**, has been synthetized showing promising cytotoxic activity against different human cancer cells. Nevertheless, a major drawback of this complex was its low water solubility (although it is soluble in dichloromethane, chloroform, ethanol, methanol, acetone and DMSO).

As presented in the introduction part of the present thesis, the current strategy for the design of anticancer metal-based drugs is centred on new metal complexes showing an alternative DNA binding mode based on non-covalent interactions. In particular, these non-classical antitumor metal agents, are new complexes that contains ligands with aromatic planar surface able to intercalate *via* π-π stacking interactions through two base pairs of DNA, or having functionalities able to interact through electrostatic or hydrogen bonding with DNA.

Therefore, several structural changes have been done starting from this model complex, in order to follow the influence of the structural variation around the metal ion on the solubility and biological activity of the resulting complexes and to investigate the structure-properties relationship in this class of derivatives. In particular, by varying the nature of the counterion, the modulation of

both the geometry and the electrostatic nature of the resulting Zn(II) complexes was performed.

It was observed that the ionic derivative **1** [(bpy-C9)ZnCurc][BF_4] resulted to have better solubility in water than complex **A**, probably due to the ionic character and the different coordination around the metal centre. On the other hand, complex **2** [$(bpy\text{-}C9)_2Zn_2(curc)_2SO_4$] maintains the same solubility as complex **A**, probably due to the neutral nature of this complex. Moreover, biological tests performed on complexes **1** and **2** showed better cytotoxic activity than complex **A**, in particular complex **1**. The higher biological activity of complexes **1** and **2** can be attributed to the water solubility of complex **1** and the dimeric molecular structure of complex **2**.

Furthermore, the change of the substituent groups on the N,N-chelating ligand, namely the bipyridine, was followed, introducing hydrophilic molecular substituents. Indeed, the introduction of hydrophilic OH groups, may not only increase the solubility properties of the resulting complexes, but also renders the obtained molecules suitable to form hydrogen bonds and hence, supramolecular assemblies, whose properties may differ substantially from the single molecular properties.

The model complex **B**, [(bpy-OH)Zn(curc)Cl], having already hydrophilic groups grafted on the bipyridinic ligand, showed low water solubility. In order to improve its physical properties, as well as its biological activity, structural changes concerning the variation of the O,O chelating ligand were performed. Therefore, the curcumin ligand has been replaced with tropolone ligand, and as a function of reaction

conditions and molar rates between the precursors, complexes with bpy-OH-to-tropolonate 1:1 and 1:2 stoichiometry ratio were obtained. Subsequently, the variation of the metal centre was pursued, and therefore, the analogues complexes containing Cu(II) metal centre and tropolone were obtained.

It was observed that the copper(II) complexes **8**, **13** with general formula [(bpy-OH)CuTropCl] and [(bpy-OH)CuTropSac], respectively, resulted to have highier solubility in water with respect to their Zn(II) analogues [(bpy-OH)ZnTropCl], **6** and [(bpy-OH)$_2$ZnTrop][Sac], **11**. In particular complex **8**, presents the highest water solubility, probably due to the its ionic character in water solutions related to the labile character of the chloride ligand. Therefore, once dissolved in water or methanol, the complex looses the chloride ligand converting into an ionic specie.

Due to the success in the highly improved water solubility of complex **8**, and considering its size, very similar to G-quadruplex structure, the binding properties of complex **8** with human telomeric DNA were investigated by isothermal titration calorimetry (ITC).. Unfortunately, preliminary results does not show any G-quadruplex binder behaviour of complex **8**.

As described before the Zn(II) tropolone-based metal complexes **6** and **7** [(bpy-OH)Zn(Trop)$_2$], suffer of scarce solubility in water. Due to the presence of molecular synthons such as the –CH$_2$OH groups on the bipyridine ligand, an organic molecule (saccharin) has been used in order to promote the formations of salts and co-crystals metal systems. Different methods, such as solution and liquid assisted

grinding, have been used for the synthesis of this salts/co-crystals. Although in both cases the formation of co-crystals has not been reached, new Zn(II) derivatives were obtained by hydrogen exchange between saccharine and the tropolonate coordinated ligand (acid/base reaction). This new complexes exhibit different solubility properties in particular complex **6** presents water solubility.

On the other hand, the same reactions have been conducted by using the Cu(II) complex **8**, in order to prove the validity of the reaction mechanism proposed for the complexes **6** and **7**. The attempt to obtain metal-based co-crystals has led to the formation of new copper derivatives, based on the same acid/base reactions. In this case, a neutral Cu(II) was obtained in which the saccharinate is coordinated to the metal centre.

Moreover, complexes with chromonic properties have been synthesized in order to be used as potential intercalating agents and/or G-quadruplex binders. These are the first examples of Ag(I) complexes showing the ability to organize into chromonic mesophases in water. The new ionic N,N-coordinated Ag(I) complexes have two 4,4'-dihydroxymethyl-2,2'-bipiyridine (bipy-OH) as chelated ligands, and, carboxylates with different alkyl chain length as counterions. The ability of these silver(I) complexes to organize into columnar structures is highlighted in the solid crystalline state, by means of single crystal X-ray analysis. Indeed, it was revealed a pre-chromonic organization in the crystalline state, with silver(I) cations stacking into columns reinforced by hydrogen bonding with the acetate counterions and water molecules. Due to the presence of molecules with an

unconventional shape for the generation of typical chromonic phases, a full characterization based on phase diagram analysis, completely resolved by POM and X-ray powder diffraction measurements, has been conducted. Moreover, cryo-TEM experiments have been carried out in order to confirm the appearance of nematic columnar phases. A "route" to drive the alignment of the liquid crystalline phases of these compounds has been developed, which is particularly important for future application in biophotonic devices. Finally, the presence of transient twisted periodical stripe structures has been observed, when an initial planar alignment is destroyed in favour of a homeotropic configuration of the molecules dictated by the confining surfaces.

In order to prove that the chromonic silver complex **14** [(bpy-OH)$_2$Ag][CH_3COO] can behave as a G-quadruplex binder *via* intercalation, its interaction with human telomeric DNA (TTAGGG)TT was investigated by isothermal titration calorimetry (ITC) and circular dichroism. However, this Ag(I) complex does not seem to interact with human telomeric DNA, and therefore does not stabilise the GQ structure probably due to the non-complete miscibility between complex **14** and the telomeric DNA.

Supporting information

Complex 5

```
_audit_creation_method           SHELXL-97
_chemical_name_systematic        ?
_chemical_name_common            ?
_chemical_formula_sum            'C24 H24 Cl2 N4 O4 Zn'
_chemical_melting_point          ?
_exptl_crystal_description       parallelepiped
_exptl_crystal_colour            pink
_diffrn_ambient_temperature      298(2)
_chemical_formula_weight         568.74
loop_
 _atom_type_symbol
 _atom_type_description
 _atom_type_scat_dispersion_real
 _atom_type_scat_dispersion_imag
 _atom_type_scat_source
'C'  'C'   0.0033   0.0016
 'International Tables Vol C Tables 4.2.6.8 and 6.1.1.4'
 'H'  'H'   0.0000   0.0000
 'International Tables Vol C Tables 4.2.6.8 and 6.1.1.4'
 'N'  'N'   0.0061   0.0033
```

```
 'International Tables Vol C Tables 4.2.6.8 and 6.1.1.4'
 'O'  'O'   0.0106   0.0060
 'International Tables Vol C Tables 4.2.6.8 and 6.1.1.4'
 'Cl'  'Cl'   0.1484   0.1585
 'International Tables Vol C Tables 4.2.6.8 and 6.1.1.4'
 'Zn'  'Zn'   0.2839   1.4301
 'International Tables Vol C Tables 4.2.6.8 and 6.1.1.4'
_symmetry_cell_setting           triclinic
_symmetry_space_group_name_H-M   ' P -1'
_chemical_absolute_configuration ?
loop_
 _symmetry_equiv_pos_as_xyz
 'x, y, z'
 '-x, -y, -z'
 _cell_length_a                   8.401(3)
_cell_length_b                   11.309(5)
_cell_length_c                   14.216(7)
_cell_angle_alpha                71.926(10)
_cell_angle_beta                 89.540(10)
_cell_angle_gamma                73.616(9)
_cell_volume                     1227.2(9)
_cell_formula_units_Z            2
_cell_measurement_temperature    293(2)
_cell_measurement_reflns_used    ?
```

```
_cell_measurement_theta_min       ?

_cell_measurement_theta_max       ?

_exptl_crystal_description        ?

_exptl_crystal_colour             ?

_exptl_crystal_size_max           0.70

_exptl_crystal_size_mid           0.60

_exptl_crystal_size_min           0.50

_exptl_crystal_density_meas       ?

_exptl_crystal_density_diffrn     1.539

_exptl_crystal_density_method     'not measured'

_exptl_crystal_F_000              584

_exptl_absorpt_coefficient_mu     1.257

_exptl_absorpt_correction_type    ?

_exptl_absorpt_correction_T_min   0.4731

_exptl_absorpt_correction_T_max   0.5721

_exptl_absorpt_process_details    ?

_exptl_special_details

;

 ?

;

_diffrn_ambient_temperature       293(2)

_diffrn_radiation_wavelength      0.71073

_diffrn_radiation_type            MoK\a

_diffrn_radiation_source          'fine-focus sealed tube'
```

```
_diffrn_radiation_monochromator   graphite

_diffrn_measurement_device_type   ?

_diffrn_measurement_method        ?

_diffrn_detector_area_resol_mean  ?

_diffrn_standards_number          ?

_diffrn_standards_interval_count  ?

_diffrn_standards_interval_time   ?

_diffrn_standards_decay_%         ?

_diffrn_reflns_number             20282

_diffrn_reflns_av_R_equivalents   0.0451

_diffrn_reflns_av_sigmaI/netI     0.0453

_diffrn_reflns_limit_h_min        -9

_diffrn_reflns_limit_h_max        10

_diffrn_reflns_limit_k_min        -11

_diffrn_reflns_limit_k_max        13

_diffrn_reflns_limit_l_min        -17

_diffrn_reflns_limit_l_max        17

_diffrn_reflns_theta_min          1.98

_diffrn_reflns_theta_max          25.68

_reflns_number_total              4377

_reflns_number_gt                 3236

_reflns_threshold_expression      >2sigma(I)

 _computing_data_collection        ?

_computing_cell_refinement        ?
```

```
_computing_data_reduction         ?

_computing_structure_solution     'SHELXS-97 (Sheldrick, 1990)'

_computing_structure_refinement   'SHELXL-97 (Sheldrick, 1997)'

_computing_molecular_graphics     ?

_computing_publication_material   ?

_refine_special_details

;

 Refinement of F^2^ against ALL reflections.  The weighted R-
factor wR and

 goodness of fit S are based on F^2^, conventional R-factors R are
based

 on F, with F set to zero for negative F^2^. The threshold
expression of

 F^2^ > 2sigma(F^2^) is used only for calculating R-factors(gt)
etc. and is

 not relevant to the choice of reflections for refinement.  R-
factors based

 on F^2^ are statistically about twice as large as those based on
F, and R-

 factors based on ALL data will be even larger.

;

 _refine_ls_structure_factor_coef  Fsqd

_refine_ls_matrix_type            full

_refine_ls_weighting_scheme       calc

_refine_ls_weighting_details

 'calc w=1/[\s^2^(Fo^2^)+(0.0586P)^2^+1.3125P] where
P=(Fo^2^+2Fc^2^)/3'
```

```
_atom_sites_solution_primary      direct
_atom_sites_solution_secondary    difmap
_atom_sites_solution_hydrogens    geom
_refine_ls_hydrogen_treatment     mixed
_refine_ls_extinction_method      none
_refine_ls_extinction_coef        ?
_refine_ls_number_reflns          4377
_refine_ls_number_parameters      316
_refine_ls_number_restraints      0
_refine_ls_R_factor_all           0.0708
_refine_ls_R_factor_gt            0.0466
_refine_ls_wR_factor_ref          0.1249
_refine_ls_wR_factor_gt           0.1107
_refine_ls_goodness_of_fit_ref    1.030
_refine_ls_restrained_S_all       1.030
_refine_ls_shift/su_max           0.000
_refine_ls_shift/su_mean          0.000
 loop_
 _atom_site_label
 _atom_site_type_symbol
 _atom_site_fract_x
 _atom_site_fract_y
 _atom_site_fract_z
 _atom_site_U_iso_or_equiv
```

```
 _atom_site_adp_type

 _atom_site_occupancy

 _atom_site_symmetry_multiplicity

 _atom_site_calc_flag

 _atom_site_refinement_flags

 _atom_site_disorder_assembly

 _atom_site_disorder_group

Zn Zn 0.69401(6) 0.82547(4) 0.75349(3) 0.03507(16) Uani 1 1 d . .
.

Cl2 Cl 0.43050(14) 0.83191(14) 0.78991(9) 0.0616(4) Uani 1 1 d . .
.

Cl3 Cl 0.30266(16) 0.65391(13) 0.20972(10) 0.0675(4) Uani 1 1 d .
. .

N1 N 0.7530(4) 0.9765(3) 0.6408(2) 0.0358(8) Uani 1 1 d . . .

N2 N 0.6739(4) 0.7737(3) 0.6230(2) 0.0330(7) Uani 1 1 d . . .

N3 N 0.7625(4) 0.8802(3) 0.8760(2) 0.0351(7) Uani 1 1 d . . .

N4 N 0.9027(4) 0.6693(3) 0.8249(2) 0.0320(7) Uani 1 1 d . . .

O1 O 0.8867(5) 1.3721(3) 0.4178(3) 0.0710(10) Uani 1 1 d . . .

H1A H 0.8081 1.4389 0.4023 0.107 Uiso 1 1 calc R . .

O2 O 0.5975(4) 0.5856(3) 0.3568(2) 0.0594(9) Uani 1 1 d . . .

H2A H 0.6852 0.5266 0.3746 0.089 Uiso 1 1 calc R . .

O3 O 0.9435(5) 0.8059(4) 1.2286(2) 0.0700(10) Uani 1 1 d . . .

H3A H 0.9711 0.8174 1.2795 0.105 Uiso 1 1 calc R . .

O4 O 1.4212(4) 0.2902(3) 0.9241(3) 0.0610(9) Uani 1 1 d . . .

H4A H 1.5126 0.2421 0.9509 0.092 Uiso 1 1 calc R . .
```

C1 C 0.7962(6) 1.0762(4) 0.6535(3) 0.0461(11) Uani 1 1 d . . .

H1C H 0.8064 1.0795 0.7177 0.055 Uiso 1 1 calc R . .

C2 C 0.8261(6) 1.1739(4) 0.5764(3) 0.0442(10) Uani 1 1 d . . .

H2C H 0.8552 1.2415 0.5888 0.053 Uiso 1 1 calc R . .

C3 C 0.8127(5) 1.1711(4) 0.4807(3) 0.0353(9) Uani 1 1 d . . .

C4 C 0.7713(5) 1.0674(4) 0.4670(3) 0.0343(9) Uani 1 1 d . . .

H4C H 0.7626 1.0621 0.4034 0.041 Uiso 1 1 calc R . .

C5 C 0.7426(5) 0.9713(4) 0.5473(3) 0.0311(8) Uani 1 1 d . . .

C6 C 0.6980(5) 0.8574(4) 0.5374(3) 0.0309(8) Uani 1 1 d . . .

C7 C 0.6833(5) 0.8368(4) 0.4473(3) 0.0351(9) Uani 1 1 d . . .

H7A H 0.7012 0.8960 0.3892 0.042 Uiso 1 1 calc R . .

C8 C 0.6421(5) 0.7282(4) 0.4436(3) 0.0366(9) Uani 1 1 d . . .

C9 C 0.6157(5) 0.6431(4) 0.5318(3) 0.0411(10) Uani 1 1 d . . .

H9A H 0.5875 0.5691 0.5323 0.049 Uiso 1 1 calc R . .

C10 C 0.6318(5) 0.6696(4) 0.6192(3) 0.0402(10) Uani 1 1 d . . .

H10A H 0.6126 0.6124 0.6780 0.048 Uiso 1 1 calc R . .

C11 C 0.8421(6) 1.2757(4) 0.3929(3) 0.0457(11) Uani 1 1 d . . .

H11A H 0.9296 1.2358 0.3577 0.055 Uiso 1 1 calc R . .

H11B H 0.7414 1.3156 0.3480 0.055 Uiso 1 1 calc R . .

C12 C 0.6272(7) 0.7047(5) 0.3468(3) 0.0530(12) Uani 1 1 d . . .

H12A H 0.5368 0.7747 0.3041 0.064 Uiso 1 1 calc R . .

H12B H 0.7291 0.7067 0.3146 0.064 Uiso 1 1 calc R . .

C13 C 0.6749(5) 0.9793(4) 0.9057(3) 0.0403(10) Uani 1 1 d . . .

H13A H 0.5805 1.0381 0.8661 0.048 Uiso 1 1 calc R . .

```
C14 C 0.7182(5) 0.9983(4) 0.9924(3) 0.0385(9) Uani 1 1 d . . .

H14A H 0.6551 1.0691 1.0098 0.046 Uiso 1 1 calc R . .

C15 C 0.8564(5) 0.9106(4) 1.0527(3) 0.0360(9) Uani 1 1 d . . .

C16 C 0.9477(5) 0.8082(4) 1.0218(3) 0.0337(9) Uani 1 1 d . . .

H16A H 1.0426 0.7485 1.0604 0.040 Uiso 1 1 calc R . .

C17 C 0.8985(5) 0.7946(4) 0.9342(3) 0.0308(8) Uani 1 1 d . . .

C18 C 0.9863(5) 0.6839(3) 0.8999(3) 0.0295(8) Uani 1 1 d . . .

C19 C 1.1382(5) 0.5983(4) 0.9423(3) 0.0361(9) Uani 1 1 d . . .

H19A H 1.1938 0.6115 0.9927 0.043 Uiso 1 1 calc R . .

C20 C 1.2098(5) 0.4921(4) 0.9106(3) 0.0357(9) Uani 1 1 d . . .

C21 C 1.1222(5) 0.4754(4) 0.8369(3) 0.0381(9) Uani 1 1 d . . .

H21A H 1.1641 0.4043 0.8148 0.046 Uiso 1 1 calc R . .

C22 C 0.9709(5) 0.5658(4) 0.7962(3) 0.0368(9) Uani 1 1 d . . .

H22A H 0.9133 0.5538 0.7460 0.044 Uiso 1 1 calc R . .

C23 C 0.9079(6) 0.9234(5) 1.1496(3) 0.0515(12) Uani 1 1 d . . .

H23A H 1.0057 0.9538 1.1416 0.062 Uiso 1 1 calc R . .

H23B H 0.8191 0.9883 1.1657 0.062 Uiso 1 1 calc R . .

C24 C 1.3776(5) 0.3997(4) 0.9565(3) 0.0499(11) Uani 1 1 d . . .

H24A H 1.4613 0.4452 0.9397 0.060 Uiso 1 1 calc R . .

H24B H 1.3764 0.3713 1.0282 0.060 Uiso 1 1 calc R . .

 loop_

 _atom_site_aniso_label

 _atom_site_aniso_U_11

 _atom_site_aniso_U_22
```

```
 _atom_site_aniso_U_33

 _atom_site_aniso_U_23

 _atom_site_aniso_U_13

 _atom_site_aniso_U_12

Zn 0.0386(3) 0.0353(3) 0.0270(2) -0.00777(19) -0.00346(18) -
0.0064(2)

Cl2 0.0408(7) 0.0944(10) 0.0500(7) -0.0316(7) 0.0038(5) -0.0114(6)

Cl3 0.0571(8) 0.0649(8) 0.0697(8) -0.0085(7) -0.0062(6) -0.0157(6)

N1 0.044(2) 0.0319(18) 0.0315(17) -0.0110(14) -0.0062(14) -
0.0097(15)

N2 0.0383(19) 0.0319(18) 0.0264(16) -0.0050(14) -0.0016(14) -
0.0116(15)

N3 0.0367(19) 0.0335(18) 0.0295(16) -0.0076(14) -0.0004(14) -
0.0044(15)

N4 0.0384(19) 0.0300(17) 0.0275(16) -0.0113(14) 0.0022(13) -
0.0074(14)

O1 0.100(3) 0.052(2) 0.070(2) -0.0126(18) 0.002(2) -0.042(2)

O2 0.086(2) 0.0382(18) 0.055(2) -0.0176(15) -0.0088(18) -
0.0164(17)

O3 0.089(3) 0.095(3) 0.0334(17) -0.0172(18) 0.0022(17) -0.041(2)

O4 0.049(2) 0.0377(18) 0.087(3) -0.0217(18) -0.0036(17) 0.0041(15)

C1 0.062(3) 0.043(3) 0.036(2) -0.014(2) -0.006(2) -0.020(2)

C2 0.060(3) 0.036(2) 0.041(2) -0.0118(19) -0.002(2) -0.021(2)

C3 0.033(2) 0.030(2) 0.037(2) -0.0065(17) -0.0004(17) -0.0041(17)

C4 0.039(2) 0.031(2) 0.0291(19) -0.0080(17) -0.0022(16) -
0.0058(18)
```

C5 0.030(2) 0.031(2) 0.0310(19) -0.0114(17) -0.0040(16) -
0.0064(16)

C6 0.032(2) 0.031(2) 0.0289(19) -0.0092(16) 0.0026(16) -0.0075(17)

C7 0.044(2) 0.033(2) 0.0279(19) -0.0072(17) 0.0023(17) -0.0123(18)

C8 0.037(2) 0.038(2) 0.035(2) -0.0143(18) 0.0030(17) -0.0093(18)

C9 0.049(3) 0.037(2) 0.042(2) -0.0138(19) 0.0006(19) -0.017(2)

C10 0.055(3) 0.035(2) 0.032(2) -0.0053(18) 0.0003(19) -0.020(2)

C11 0.049(3) 0.035(2) 0.050(3) -0.007(2) 0.007(2) -0.014(2)

C12 0.078(3) 0.049(3) 0.044(3) -0.024(2) 0.009(2) -0.028(3)

C13 0.040(2) 0.033(2) 0.039(2) -0.0093(18) -0.0012(18) 0.0010(18)

C14 0.038(2) 0.034(2) 0.041(2) -0.0163(19) 0.0064(18) -0.0030(18)

C15 0.039(2) 0.038(2) 0.037(2) -0.0172(18) 0.0081(18) -0.0143(19)

C16 0.032(2) 0.034(2) 0.032(2) -0.0109(17) -0.0018(16) -0.0051(17)

C17 0.029(2) 0.030(2) 0.0315(19) -0.0093(16) 0.0011(16) -
0.0060(16)

C18 0.035(2) 0.0264(19) 0.0259(18) -0.0075(15) 0.0018(16) -
0.0086(16)

C19 0.035(2) 0.039(2) 0.035(2) -0.0154(18) -0.0014(17) -0.0075(18)

C20 0.035(2) 0.034(2) 0.035(2) -0.0095(17) 0.0059(17) -0.0076(18)

C21 0.044(2) 0.036(2) 0.035(2) -0.0164(18) 0.0071(18) -0.0073(19)

C22 0.045(2) 0.037(2) 0.0287(19) -0.0144(18) 0.0002(17) -
0.0088(19)

C23 0.057(3) 0.055(3) 0.043(3) -0.026(2) -0.001(2) -0.006(2)

C24 0.043(3) 0.049(3) 0.054(3) -0.024(2) -0.004(2) 0.001(2)

_geom_special_details

;

All esds (except the esd in the dihedral angle between two l.s. planes)

are estimated using the full covariance matrix. The cell esds are taken

into account individually in the estimation of esds in distances, angles

and torsion angles; correlations between esds in cell parameters are only

used when they are defined by crystal symmetry. An approximate (isotropic)

treatment of cell esds is used for estimating esds involving l.s. planes.

;

loop_

_geom_bond_atom_site_label_1

_geom_bond_atom_site_label_2

_geom_bond_distance

_geom_bond_site_symmetry_2

_geom_bond_publ_flag

Zn N4 2.095(3) . ?

Zn N1 2.120(3) . ?

Zn N2 2.133(3) . ?

Zn N3 2.152(3) . ?

Zn Cl2 2.2558(15) . ?

N1 C1 1.340(5) . ?

N1 C5 1.353(5) . ?

N2 C10 1.338(5) . ?

N2 C6 1.344(5) . ?

N3 C13 1.341(5) . ?

N3 C17 1.350(5) . ?

N4 C22 1.333(5) . ?

N4 C18 1.359(5) . ?

O1 C11 1.389(5) . ?

O2 C12 1.403(5) . ?

O3 C23 1.405(6) . ?

O4 C24 1.406(5) . ?

C1 C2 1.373(6) . ?

C2 C3 1.378(5) . ?

C3 C4 1.380(5) . ?

C3 C11 1.504(5) . ?

C4 C5 1.384(5) . ?

C5 C6 1.485(5) . ?

C6 C7 1.384(5) . ?

C7 C8 1.383(5) . ?

C8 C9 1.384(6) . ?

C8 C12 1.493(5) . ?

C9 C10 1.381(5) . ?

C13 C14 1.383(5) . ?

C14 C15 1.380(6) . ?

```
C15 C16 1.389(5) . ?

C15 C23 1.508(5) . ?

C16 C17 1.382(5) . ?

C17 C18 1.483(5) . ?

C18 C19 1.372(5) . ?

C19 C20 1.390(5) . ?

C20 C21 1.374(5) . ?

C20 C24 1.505(6) . ?

C21 C22 1.381(5) . ?

 loop_

 _geom_angle_atom_site_label_1

 _geom_angle_atom_site_label_2

 _geom_angle_atom_site_label_3

 _geom_angle

 _geom_angle_site_symmetry_1

 _geom_angle_site_symmetry_3

 _geom_angle_publ_flag

N4 Zn N1 113.59(13) . . ?

N4 Zn N2 97.02(12) . . ?

N1 Zn N2 76.86(12) . . ?

N4 Zn N3 77.56(12) . . ?

N1 Zn N3 95.89(12) . . ?

N2 Zn N3 168.53(12) . . ?

N4 Zn Cl2 123.61(10) . . ?
```

```
N1 Zn Cl2 122.78(10) . . ?

N2 Zn Cl2 94.42(9) . . ?

N3 Zn Cl2 97.00(9) . . ?

C1 N1 C5 117.7(3) . . ?

C1 N1 Zn 126.3(3) . . ?

C5 N1 Zn 116.0(2) . . ?

C10 N2 C6 118.2(3) . . ?

C10 N2 Zn 125.5(3) . . ?

C6 N2 Zn 116.2(2) . . ?

C13 N3 C17 118.2(3) . . ?

C13 N3 Zn 127.0(3) . . ?

C17 N3 Zn 114.3(2) . . ?

C22 N4 C18 117.5(3) . . ?

C22 N4 Zn 126.1(3) . . ?

C18 N4 Zn 115.9(2) . . ?

N1 C1 C2 123.3(4) . . ?

C1 C2 C3 119.5(4) . . ?

C2 C3 C4 117.6(4) . . ?

C2 C3 C11 122.2(4) . . ?

C4 C3 C11 120.2(4) . . ?

C3 C4 C5 120.5(4) . . ?

N1 C5 C4 121.3(3) . . ?

N1 C5 C6 115.6(3) . . ?

C4 C5 C6 123.0(3) . . ?
```

```
N2 C6 C7 121.7(3) . . ?

N2 C6 C5 115.2(3) . . ?

C7 C6 C5 123.1(3) . . ?

C8 C7 C6 120.0(4) . . ?

C7 C8 C9 118.0(4) . . ?

C7 C8 C12 120.4(4) . . ?

C9 C8 C12 121.6(4) . . ?

C10 C9 C8 119.0(4) . . ?

N2 C10 C9 123.0(4) . . ?

O1 C11 C3 113.9(4) . . ?

O2 C12 C8 113.2(4) . . ?

N3 C13 C14 123.1(4) . . ?

C15 C14 C13 119.0(4) . . ?

C14 C15 C16 117.9(4) . . ?

C14 C15 C23 121.8(4) . . ?

C16 C15 C23 120.3(4) . . ?

C17 C16 C15 120.4(4) . . ?

N3 C17 C16 121.3(3) . . ?

N3 C17 C18 115.9(3) . . ?

C16 C17 C18 122.8(3) . . ?

N4 C18 C19 121.4(3) . . ?

N4 C18 C17 115.2(3) . . ?

C19 C18 C17 123.4(3) . . ?

C18 C19 C20 120.6(4) . . ?
```

```
C21 C20 C19 117.7(4) . . ?

C21 C20 C24 122.0(4) . . ?

C19 C20 C24 120.3(4) . . ?

C20 C21 C22 119.0(4) . . ?

N4 C22 C21 123.7(4) . . ?

O3 C23 C15 112.9(4) . . ?

O4 C24 C20 112.4(4) . . ?

 _diffrn_measured_fraction_theta_max    0.939

_diffrn_reflns_theta_full              25.68

_diffrn_measured_fraction_theta_full   0.939

_refine_diff_density_max    0.529

_refine_diff_density_min   -0.480

_refine_diff_density_rms    0.076
```

Complex VII

```
_audit_creation_method           SHELXL-97

_chemical_name_systematic        ?

_chemical_name_common            ?

_chemical_formula_sum           'C12 H14 Cl2 Cu N2 O3'


_chemical_melting_point          ?
```

```
_exptl_crystal_description       parallelepiped
_exptl_crystal_colour            blue green

_diffrn_ambient_temperature      298(2)
_chemical_formula_weight         368.69

loop_
 _atom_type_symbol
 _atom_type_description
 _atom_type_scat_dispersion_real
 _atom_type_scat_dispersion_imag
 _atom_type_scat_source
 'C'  'C'   0.0033   0.0016
 'International Tables Vol C Tables 4.2.6.8 and 6.1.1.4'
 'H'  'H'   0.0000   0.0000
 'International Tables Vol C Tables 4.2.6.8 and 6.1.1.4'
 'N'  'N'   0.0061   0.0033
 'International Tables Vol C Tables 4.2.6.8 and 6.1.1.4'
 'O'  'O'   0.0106   0.0060
 'International Tables Vol C Tables 4.2.6.8 and 6.1.1.4'
 'Cl'  'Cl'   0.1484   0.1585
 'International Tables Vol C Tables 4.2.6.8 and 6.1.1.4'
 'Cu'  'Cu'   0.3201   1.2651
 'International Tables Vol C Tables 4.2.6.8 and 6.1.1.4'
```

```
_symmetry_cell_setting           monoclinic
_symmetry_space_group_name_H-M   ' P 2/n'
_chemical_absolute_configuration ?

loop_
_symmetry_equiv_pos_as_xyz
 'x, y, z'
 '-x+1/2, y, -z+1/2'
 '-x, -y, -z'
 'x-1/2, -y, z-1/2'

_cell_length_a                   6.9309(11)
_cell_length_b                   9.6019(15)
_cell_length_c                   11.0089(18)
_cell_angle_alpha                90.00
_cell_angle_beta                 93.855(9)
_cell_angle_gamma                90.00
_cell_volume                     731.0(2)
_cell_formula_units_Z            2
_cell_measurement_temperature    293(2)
_cell_measurement_reflns_used    ?
_cell_measurement_theta_min      ?
_cell_measurement_theta_max      ?
```

```
_exptl_crystal_description        ?
_exptl_crystal_colour             green
_exptl_crystal_size_max           ?
_exptl_crystal_size_mid           ?
_exptl_crystal_size_min           ?
_exptl_crystal_density_meas       ?
_exptl_crystal_density_diffrn     1.675
_exptl_crystal_density_method     'not measured'
_exptl_crystal_F_000              374
_exptl_absorpt_coefficient_mu     1.866
_exptl_absorpt_correction_type    ?
_exptl_absorpt_correction_T_min   ?
_exptl_absorpt_correction_T_max   ?
_exptl_absorpt_process_details    ?

_exptl_special_details
;
 ?
;

_diffrn_ambient_temperature       298(2)
_diffrn_radiation_wavelength      0.71073
_diffrn_radiation_type            MoK\a
```

```
_diffrn_radiation_source          'fine-focus sealed tube'
_diffrn_radiation_monochromator   graphite
_diffrn_measurement_device_type   ?
_diffrn_measurement_method        ?
_diffrn_detector_area_resol_mean  ?
_diffrn_standards_number          ?
_diffrn_standards_interval_count  ?
_diffrn_standards_interval_time   ?
_diffrn_standards_decay_%         ?
_diffrn_reflns_number             15801
_diffrn_reflns_av_R_equivalents   0.0309
_diffrn_reflns_av_sigmaI/netI     0.0183
_diffrn_reflns_limit_h_min        -9
_diffrn_reflns_limit_h_max        9
_diffrn_reflns_limit_k_min        -13
_diffrn_reflns_limit_k_max        13
_diffrn_reflns_limit_l_min        -15
_diffrn_reflns_limit_l_max        15
_diffrn_reflns_theta_min          2.12
_diffrn_reflns_theta_max          29.57
_reflns_number_total              2066
_reflns_number_gt                 1802
_reflns_threshold_expression      >2sigma(I)
```

```
_computing_data_collection        ?

_computing_cell_refinement        ?

_computing_data_reduction         ?

_computing_structure_solution     'SHELXS-97 (Sheldrick, 1990)'

_computing_structure_refinement   'SHELXL-97 (Sheldrick, 1997)'

_computing_molecular_graphics     ?

_computing_publication_material   ?


_refine_special_details

;

 Refinement of F^2^ against ALL reflections.  The weighted R-
factor wR and

 goodness of fit S are based on F^2^, conventional R-factors R are
based

 on F, with F set to zero for negative F^2^. The threshold
expression of

 F^2^ > 2sigma(F^2^) is used only for calculating R-factors(gt)
etc. and is

 not relevant to the choice of reflections for refinement.  R-
factors based

 on F^2^ are statistically about twice as large as those based on
F, and R-

 factors based on ALL data will be even larger.

;


_refine_ls_structure_factor_coef  Fsqd
```

```
_refine_ls_matrix_type           full
_refine_ls_weighting_scheme      calc
_refine_ls_weighting_details
 'calc w=1/[\s^2^(Fo^2^)+(0.0429P)^2^+0.4247P] where
P=(Fo^2^+2Fc^2^)/3'
_atom_sites_solution_primary     direct
_atom_sites_solution_secondary   difmap
_atom_sites_solution_hydrogens   geom
_refine_ls_hydrogen_treatment    mixed
_refine_ls_extinction_method     none
_refine_ls_extinction_coef       ?
_refine_ls_number_reflns         2066
_refine_ls_number_parameters     102
_refine_ls_number_restraints     3
_refine_ls_R_factor_all          0.0347
_refine_ls_R_factor_gt           0.0279
_refine_ls_wR_factor_ref         0.0797
_refine_ls_wR_factor_gt          0.0744
_refine_ls_goodness_of_fit_ref   1.041
_refine_ls_restrained_S_all      1.045
_refine_ls_shift/su_max          0.000
_refine_ls_shift/su_mean         0.000

loop_
```

```
 _atom_site_label

 _atom_site_type_symbol

 _atom_site_fract_x

 _atom_site_fract_y

 _atom_site_fract_z

 _atom_site_U_iso_or_equiv

 _atom_site_adp_type

 _atom_site_occupancy

 _atom_site_symmetry_multiplicity

 _atom_site_calc_flag

 _atom_site_refinement_flags

 _atom_site_disorder_assembly

 _atom_site_disorder_group

Cu Cu 0.2500 0.26802(3) 0.2500 0.02528(10) Uani 1 2 d S . .

Cl1 Cl 0.48009(7) 0.43538(5) 0.28869(5) 0.03891(14) Uani 1 1 d . .
.

O1 O -0.3703(2) -0.23106(15) -0.02718(13) 0.0392(3) Uani 1 1 d . .
.

H1H H -0.4685 -0.2765 -0.0180 0.047 Uiso 1 1 calc R . .

O2 O -0.6831(3) -0.38771(19) 0.02609(19) 0.0516(4) Uani 1 1 d D .
.

H1W H -0.680(4) -0.437(3) 0.0855(19) 0.050 Uiso 1 1 d D . .

H2W H -0.749(4) -0.428(3) -0.028(2) 0.050 Uiso 1 1 d D . .

N1 N 0.07344(19) 0.10694(14) 0.19885(12) 0.0212(3) Uani 1 1 d . .
.

C1 C -0.1028(2) 0.11618(18) 0.13995(15) 0.0253(3) Uani 1 1 d . . .
```

H1 H -0.1578 0.2039 0.1278 0.030 Uiso 1 1 calc R . .

C2 C -0.2061(2) 0.00037(19) 0.09655(15) 0.0254(3) Uani 1 1 d . . .

H2 H -0.3265 0.0111 0.0551 0.030 Uiso 1 1 calc R . .

C3 C -0.1276(2) -0.13187(18) 0.11562(14) 0.0227(3) Uani 1 1 d . . .

C4 C 0.0541(2) -0.14179(17) 0.17945(15) 0.0237(3) Uani 1 1 d . . .

H4 H 0.1094 -0.2286 0.1957 0.028 Uiso 1 1 calc R . .

C5 C 0.1512(2) -0.02153(17) 0.21833(13) 0.0203(3) Uani 1 1 d . . .

C12 C -0.2291(3) -0.26210(19) 0.06851(17) 0.0299(4) Uani 1 1 d . . .

H12A H -0.1347 -0.3262 0.0390 0.036 Uiso 1 1 calc R . .

H12B H -0.2909 -0.3072 0.1345 0.036 Uiso 1 1 calc R . .

loop_

 _atom_site_aniso_label

 _atom_site_aniso_U_11

 _atom_site_aniso_U_22

 _atom_site_aniso_U_33

 _atom_site_aniso_U_23

 _atom_site_aniso_U_13

 _atom_site_aniso_U_12

Cu 0.02356(16) 0.01843(15) 0.03282(17) 0.000 -0.00590(11) 0.000

Cl1 0.0345(2) 0.0261(2) 0.0545(3) 0.00090(19) -0.0094(2) -0.00794(17)

O1 0.0346(7) 0.0444(8) 0.0359(7) 0.0085(6) -0.0165(6) -0.0156(6)

O2 0.0447(9) 0.0467(10) 0.0627(11) 0.0161(8) -0.0014(8) -0.0095(8)

N1 0.0208(6) 0.0212(6) 0.0211(6) 0.0008(5) -0.0027(5) 0.0008(5)

C1 0.0219(7) 0.0250(8) 0.0285(8) 0.0036(6) -0.0033(6) 0.0018(6)

C2 0.0196(7) 0.0302(8) 0.0255(8) 0.0023(6) -0.0044(6) -0.0010(6)

C3 0.0211(7) 0.0270(8) 0.0198(7) 0.0001(6) -0.0013(5) -0.0034(6)

C4 0.0240(7) 0.0217(7) 0.0246(7) 0.0004(6) -0.0050(6) -0.0008(6)

C5 0.0197(7) 0.0222(7) 0.0186(7) 0.0005(5) -0.0016(5) -0.0001(6)

C12 0.0294(8) 0.0295(9) 0.0293(8) 0.0011(7) -0.0091(7) -0.0071(7)

_geom_special_details

;

All esds (except the esd in the dihedral angle between two l.s. planes)

are estimated using the full covariance matrix. The cell esds are taken

into account individually in the estimation of esds in distances, angles

and torsion angles; correlations between esds in cell parameters are only

used when they are defined by crystal symmetry. An approximate (isotropic)

treatment of cell esds is used for estimating esds involving l.s. planes.

;

loop_

```
 _geom_bond_atom_site_label_1

 _geom_bond_atom_site_label_2

 _geom_bond_distance

 _geom_bond_site_symmetry_2

 _geom_bond_publ_flag

Cu N1 2.0283(14) . ?

Cu N1 2.0283(14) 2 ?

Cu Cl1 2.2838(5) . ?

Cu Cl1 2.2838(5) 2 ?

O1 C12 1.421(2) . ?

O2 O2 0.0000 1 ?

N1 C1 1.347(2) . ?

N1 C5 1.357(2) . ?

C1 C2 1.390(2) . ?

C2 C3 1.392(2) . ?

C3 C4 1.403(2) . ?

C3 C12 1.510(2) . ?

C4 C5 1.389(2) . ?

C5 C5 1.495(3) 2 ?


loop_

 _geom_angle_atom_site_label_1

 _geom_angle_atom_site_label_2

 _geom_angle_atom_site_label_3
```

```
 _geom_angle

 _geom_angle_site_symmetry_1

 _geom_angle_site_symmetry_3

 _geom_angle_publ_flag

N1 Cu N1 80.62(8) . 2 ?

N1 Cu Cl1 171.50(4) . . ?

N1 Cu Cl1 94.82(4) 2 . ?

N1 Cu Cl1 94.82(4) . 2 ?

N1 Cu Cl1 171.50(4) 2 2 ?

Cl1 Cu Cl1 90.56(3) . 2 ?

C1 N1 C5 118.26(14) . . ?

C1 N1 Cu 126.45(11) . . ?

C5 N1 Cu 115.06(10) . . ?

N1 C1 C2 122.83(16) . . ?

C1 C2 C3 119.42(15) . . ?

C2 C3 C4 117.77(15) . . ?

C2 C3 C12 122.38(15) . . ?

C4 C3 C12 119.84(15) . . ?

C5 C4 C3 119.82(15) . . ?

N1 C5 C4 121.87(14) . . ?

N1 C5 C5 114.53(8) . 2 ?

C4 C5 C5 123.59(9) . 2 ?

O1 C12 C3 111.29(15) . . ?
```

```
loop_
 _geom_torsion_atom_site_label_1
 _geom_torsion_atom_site_label_2
 _geom_torsion_atom_site_label_3
 _geom_torsion_atom_site_label_4
 _geom_torsion
 _geom_torsion_site_symmetry_1
 _geom_torsion_site_symmetry_2
 _geom_torsion_site_symmetry_3
 _geom_torsion_site_symmetry_4
 _geom_torsion_publ_flag
N1 Cu N1 C1 -175.75(17) 2 . . . ?
Cl1 Cu N1 C1 -117.7(3) . . . . ?
Cl1 Cu N1 C1 11.48(14) 2 . . . ?
N1 Cu N1 C5 -1.45(8) 2 . . . ?
Cl1 Cu N1 C5 56.6(3) . . . . ?
Cl1 Cu N1 C5 -174.22(11) 2 . . . ?
C5 N1 C1 C2 -1.3(2) . . . . ?
Cu N1 C1 C2 172.88(12) . . . . ?
N1 C1 C2 C3 1.1(3) . . . . ?
C1 C2 C3 C4 0.4(2) . . . . ?
C1 C2 C3 C12 -178.49(16) . . . . ?
C2 C3 C4 C5 -1.7(2) . . . . ?
C12 C3 C4 C5 177.29(15) . . . . ?
```

```
C1 N1 C5 C4 0.0(2) . . . . ?

Cu N1 C5 C4 -174.84(12) . . . . ?

C1 N1 C5 C5 178.63(16) . . . 2 ?

Cu N1 C5 C5 3.8(2) . . . 2 ?

C3 C4 C5 N1 1.5(2) . . . . ?

C3 C4 C5 C5 -177.04(17) . . . 2 ?

C2 C3 C12 O1 19.8(2) . . . . ?

C4 C3 C12 O1 -159.14(16) . . . . ?


loop_

 _geom_hbond_atom_site_label_D

 _geom_hbond_atom_site_label_H

 _geom_hbond_atom_site_label_A

 _geom_hbond_distance_DH

 _geom_hbond_distance_HA

 _geom_hbond_distance_DA

 _geom_hbond_angle_DHA

 _geom_hbond_site_symmetry_A

O1 H1H O2  0.82 1.92 2.734(2) 172.0 1


_diffrn_measured_fraction_theta_max    1.000

_diffrn_reflns_theta_full              29.57

_diffrn_measured_fraction_theta_full   1.000

_refine_diff_density_max    0.444
```

```
_refine_diff_density_min   -0.483

_refine_diff_density_rms    0.092
```

Complex 8

```
_audit_creation_method           SHELXL-97

_chemical_name_systematic        ?

_chemical_name_common            ?

_chemical_formula_sum           'C19 H19 Cl Cu N2 O5'

_chemical_melting_point          ?

_exptl_crystal_description       parallelepiped

_exptl_crystal_colour            blue

_diffrn_ambient_temperature      298(2)

_chemical_formula_weight         454.35

loop_

 _atom_type_symbol

 _atom_type_description

 _atom_type_scat_dispersion_real

 _atom_type_scat_dispersion_imag

 _atom_type_scat_source

 'C'  'C'   0.0033   0.0016

 'International Tables Vol C Tables 4.2.6.8 and 6.1.1.4'

 'H'  'H'   0.0000   0.0000
```

```
 'International Tables Vol C Tables 4.2.6.8 and 6.1.1.4'
 'N'  'N'   0.0061   0.0033
 'International Tables Vol C Tables 4.2.6.8 and 6.1.1.4'
 'O'  'O'   0.0106   0.0060
 'International Tables Vol C Tables 4.2.6.8 and 6.1.1.4'
 'Cl'  'Cl'   0.1484   0.1585
 'International Tables Vol C Tables 4.2.6.8 and 6.1.1.4'
 'Cu'  'Cu'   0.3201   1.2651
 'International Tables Vol C Tables 4.2.6.8 and 6.1.1.4'
_symmetry_cell_setting           triclinic
_symmetry_space_group_name_H-M   ' P -1'
_chemical_absolute_configuration ?
loop_
 _symmetry_equiv_pos_as_xyz
 'x, y, z'
 '-x, -y, -z'
 _cell_length_a                    9.109(2)
_cell_length_b                    10.048(3)
_cell_length_c                    11.646(3)
_cell_angle_alpha                 70.788(12)
_cell_angle_beta                  75.475(13)
_cell_angle_gamma                 75.667(13)
_cell_volume                      958.4(4)
_cell_formula_units_Z             2
```

```
_cell_measurement_temperature     293(2)

_cell_measurement_reflns_used     ?

_cell_measurement_theta_min       ?

_cell_measurement_theta_max       ?

 _exptl_crystal_description        ?

_exptl_crystal_colour             ?

_exptl_crystal_size_max           ?

_exptl_crystal_size_mid           ?

_exptl_crystal_size_min           ?

_exptl_crystal_density_meas       ?

_exptl_crystal_density_diffrn     1.574

_exptl_crystal_density_method     'not measured'

_exptl_crystal_F_000              466

_exptl_absorpt_coefficient_mu     1.313

_exptl_absorpt_correction_type    ?

_exptl_absorpt_correction_T_min   ?

_exptl_absorpt_correction_T_max   ?

_exptl_absorpt_process_details    ?

 _exptl_special_details

;

 ?

;

 _diffrn_ambient_temperature       293(2)

_diffrn_radiation_wavelength      0.71073
```

```
_diffrn_radiation_type           MoK\a
_diffrn_radiation_source         'fine-focus sealed tube'
_diffrn_radiation_monochromator  graphite
_diffrn_measurement_device_type  ?
_diffrn_measurement_method       ?
_diffrn_detector_area_resol_mean ?
_diffrn_standards_number         ?
_diffrn_standards_interval_count ?
_diffrn_standards_interval_time  ?
_diffrn_standards_decay_%        ?
_diffrn_reflns_number            15255
_diffrn_reflns_av_R_equivalents  0.0379
_diffrn_reflns_av_sigmaI/netI    0.0409
_diffrn_reflns_limit_h_min       -11
_diffrn_reflns_limit_h_max       11
_diffrn_reflns_limit_k_min       -12
_diffrn_reflns_limit_k_max       12
_diffrn_reflns_limit_l_min       -14
_diffrn_reflns_limit_l_max       14
_diffrn_reflns_theta_min         1.88
_diffrn_reflns_theta_max         26.37
_reflns_number_total             3860
_reflns_number_gt                2975
_reflns_threshold_expression     >2sigma(I)
```

```
 _computing_data_collection        ?

_computing_cell_refinement        ?

_computing_data_reduction         ?

_computing_structure_solution     'SHELXS-97 (Sheldrick, 1990)'

_computing_structure_refinement   'SHELXL-97 (Sheldrick, 1997)'

_computing_molecular_graphics     ?

_computing_publication_material   ?

 _refine_special_details

;

 Refinement of F^2^ against ALL reflections.  The weighted R-
factor wR and

 goodness of fit S are based on F^2^, conventional R-factors R are
based

 on F, with F set to zero for negative F^2^. The threshold
expression of

 F^2^ > 2sigma(F^2^) is used only for calculating R-factors(gt)
etc. and is

 not relevant to the choice of reflections for refinement.  R-
factors based

 on F^2^ are statistically about twice as large as those based on
F, and R-

 factors based on ALL data will be even larger.

;

 _refine_ls_structure_factor_coef  Fsqd

_refine_ls_matrix_type            full

_refine_ls_weighting_scheme       calc
```

```
_refine_ls_weighting_details

 'calc w=1/[\s^2^(Fo^2^)+(0.0145P)^2^+2.2034P] where
P=(Fo^2^+2Fc^2^)/3'

_atom_sites_solution_primary      direct

_atom_sites_solution_secondary    difmap

_atom_sites_solution_hydrogens    geom

_refine_ls_hydrogen_treatment     mixed

_refine_ls_extinction_method      none

_refine_ls_extinction_coef        ?

_refine_ls_number_reflns          3860

_refine_ls_number_parameters      270

_refine_ls_number_restraints      3

_refine_ls_R_factor_all           0.0658

_refine_ls_R_factor_gt            0.0444

_refine_ls_wR_factor_ref          0.1042

_refine_ls_wR_factor_gt           0.0954

_refine_ls_goodness_of_fit_ref    1.105

_refine_ls_restrained_S_all       1.105

_refine_ls_shift/su_max           0.001

_refine_ls_shift/su_mean          0.000

 loop_

 _atom_site_label

 _atom_site_type_symbol

 _atom_site_fract_x
```

```
 _atom_site_fract_y

 _atom_site_fract_z

 _atom_site_U_iso_or_equiv

 _atom_site_adp_type

 _atom_site_occupancy

 _atom_site_symmetry_multiplicity

 _atom_site_calc_flag

 _atom_site_refinement_flags

 _atom_site_disorder_assembly

 _atom_site_disorder_group

Cu Cu 0.57759(5) 0.82150(5) 0.68830(4) 0.03462(15) Uani 1 1 d . .
.

Cl Cl 0.73145(12) 0.78029(11) 0.87467(9) 0.0437(3) Uani 1 1 d . .
.

O1 O 0.7444(3) 0.8618(3) 0.5491(2) 0.0416(7) Uani 1 1 d . . .

O2 O 0.5182(3) 1.0266(3) 0.6436(2) 0.0382(6) Uani 1 1 d . . .

O3 O 0.7978(4) 0.0881(3) 0.7895(4) 0.0752(11) Uani 1 1 d . . .

H3A H 0.8015 0.0011 0.8115 0.113 Uiso 1 1 calc R . .

O4 O -0.1317(3) 0.7743(3) 1.0947(3) 0.0532(8) Uani 1 1 d . . .

H4A H -0.1639 0.7680 1.1683 0.080 Uiso 1 1 calc R . .

O5 O -0.1831(6) 0.6865(5) 1.3673(4) 0.0922(14) Uani 1 1 d D . .

H1W H -0.202(5) 0.754(4) 1.405(3) 0.050 Uiso 1 1 d D . .

H2W H -0.231(5) 0.706(5) 1.306(3) 0.050 Uiso 1 1 d D . .

N1 N 0.6148(3) 0.6106(3) 0.7226(3) 0.0321(7) Uani 1 1 d . . .

N2 N 0.3846(3) 0.7860(3) 0.8069(3) 0.0326(7) Uani 1 1 d . . .
```

C1 C 0.7369(4) 0.5281(4) 0.6739(4) 0.0380(9) Uani 1 1 d . . .

H1 H 0.8134 0.5720 0.6148 0.044(11) Uiso 1 1 calc R . .

C2 C 0.7547(4) 0.3815(4) 0.7069(4) 0.0376(9) Uani 1 1 d . . .

H2 H 0.8413 0.3278 0.6706 0.050(12) Uiso 1 1 calc R . .

C3 C 0.6421(4) 0.3145(4) 0.7951(4) 0.0348(9) Uani 1 1 d . . .

C4 C 0.5151(4) 0.3995(4) 0.8467(3) 0.0344(8) Uani 1 1 d . . .

H4 H 0.4375 0.3576 0.9060 0.047(12) Uiso 1 1 calc R . .

C5 C 0.5045(4) 0.5460(4) 0.8096(3) 0.0296(8) Uani 1 1 d . . .

C6 C 0.3736(4) 0.6466(4) 0.8591(3) 0.0311(8) Uani 1 1 d . . .

C7 C 0.2489(4) 0.6046(4) 0.9487(3) 0.0333(8) Uani 1 1 d . . .

H7 H 0.2452 0.5078 0.9851 0.040(11) Uiso 1 1 calc R . .

C8 C 0.1290(4) 0.7077(4) 0.9840(3) 0.0351(9) Uani 1 1 d . . .

C9 C 0.1401(5) 0.8496(4) 0.9280(4) 0.0440(10) Uani 1 1 d . . .

H9 H 0.0607 0.9212 0.9481 0.038(11) Uiso 1 1 calc R . .

C10 C 0.2697(4) 0.8852(4) 0.8416(4) 0.0407(9) Uani 1 1 d . . .

H10 H 0.2773 0.9814 0.8064 0.049(12) Uiso 1 1 calc R . .

C11 C -0.0073(4) 0.6617(5) 1.0820(4) 0.0466(11) Uani 1 1 d . . .

H11B H -0.0428 0.5901 1.0620 0.056 Uiso 1 1 calc R . .

H11A H 0.0264 0.6170 1.1609 0.056 Uiso 1 1 calc R . .

C12 C 0.6514(5) 0.1554(4) 0.8362(4) 0.0454(10) Uani 1 1 d . . .

H12B H 0.6318 0.1216 0.9259 0.054 Uiso 1 1 calc R . .

H12A H 0.5734 0.1312 0.8069 0.054 Uiso 1 1 calc R . .

C13 C 0.7488(4) 0.9981(4) 0.5048(3) 0.0349(9) Uani 1 1 d . . .

C14 C 0.8731(5) 1.0426(5) 0.4129(4) 0.0444(10) Uani 1 1 d . . .

H14 H 0.9428 0.9696 0.3856 0.048(13) Uiso 1 1 calc R . .

C15 C 0.9089(5) 1.1779(5) 0.3562(4) 0.0522(12) Uani 1 1 d . . .

H15 H 1.0020 1.1810 0.3004 0.060(14) Uiso 1 1 calc R . .

C16 C 0.8280(6) 1.3090(5) 0.3697(4) 0.0559(13) Uani 1 1 d . . .

H16 H 0.8745 1.3879 0.3244 0.059(13) Uiso 1 1 calc R . .

C17 C 0.6863(6) 1.3363(5) 0.4425(4) 0.0521(12) Uani 1 1 d . . .

H17 H 0.6469 1.4324 0.4367 0.050(13) Uiso 1 1 calc R . .

C18 C 0.5940(5) 1.2412(4) 0.5234(4) 0.0437(10) Uani 1 1 d . . .

H18 H 0.4997 1.2840 0.5608 0.047(12) Uiso 1 1 calc R . .

C19 C 0.6188(4) 1.0916(4) 0.5580(3) 0.0340(8) Uani 1 1 d . . .

loop_

_atom_site_aniso_label

_atom_site_aniso_U_11

_atom_site_aniso_U_22

_atom_site_aniso_U_33

_atom_site_aniso_U_23

_atom_site_aniso_U_13

_atom_site_aniso_U_12

Cu 0.0355(3) 0.0292(3) 0.0356(3) -0.0057(2) -0.00128(19) -0.00952(19)

Cl 0.0479(6) 0.0407(6) 0.0416(6) -0.0017(5) -0.0121(4) -0.0160(4)

O1 0.0410(15) 0.0346(15) 0.0408(16) -0.0062(13) 0.0013(12) -0.0070(12)

O2 0.0390(15) 0.0322(14) 0.0361(15) -0.0043(12) 0.0018(12) -0.0096(11)

O3 0.058(2) 0.0343(18) 0.114(3) -0.0184(19) 0.005(2) -0.0008(15)

O4 0.0410(16) 0.075(2) 0.0412(17) -0.0268(16) 0.0039(13) -0.0041(15)

O5 0.134(4) 0.074(3) 0.053(3) -0.026(2) 0.000(2) 0.003(3)

N1 0.0334(16) 0.0298(17) 0.0308(17) -0.0048(14) -0.0049(13) -0.0079(13)

N2 0.0343(17) 0.0283(16) 0.0347(18) -0.0079(14) -0.0045(13) -0.0080(13)

C1 0.034(2) 0.041(2) 0.038(2) -0.0125(18) -0.0007(17) -0.0088(17)

C2 0.041(2) 0.036(2) 0.038(2) -0.0179(18) -0.0050(17) -0.0023(17)

C3 0.043(2) 0.030(2) 0.035(2) -0.0120(17) -0.0109(17) -0.0057(16)

C4 0.039(2) 0.032(2) 0.032(2) -0.0063(17) -0.0054(16) -0.0114(16)

C5 0.0340(19) 0.031(2) 0.0250(19) -0.0078(16) -0.0070(15) -0.0072(15)

C6 0.0323(19) 0.031(2) 0.031(2) -0.0068(16) -0.0085(15) -0.0069(15)

C7 0.037(2) 0.035(2) 0.028(2) -0.0051(17) -0.0066(16) -0.0106(16)

C8 0.035(2) 0.041(2) 0.033(2) -0.0136(18) -0.0076(16) -0.0074(17)

C9 0.041(2) 0.041(2) 0.048(3) -0.018(2) -0.0012(19) -0.0030(18)

C10 0.043(2) 0.033(2) 0.046(2) -0.0144(19) -0.0033(18) -0.0069(17)

C11 0.038(2) 0.060(3) 0.037(2) -0.012(2) -0.0002(18) -0.009(2)

C12 0.053(3) 0.034(2) 0.049(3) -0.014(2) -0.006(2) -0.0070(19)

C13 0.038(2) 0.044(2) 0.024(2) -0.0049(17) -0.0090(15) -0.0111(17)

C14 0.038(2) 0.056(3) 0.036(2) -0.009(2) -0.0026(18) -0.013(2)

C15 0.044(2) 0.073(3) 0.034(2) 0.002(2) -0.0032(19) -0.028(2)

C16 0.064(3) 0.056(3) 0.046(3) 0.007(2) -0.012(2) -0.036(3)

C17 0.074(3) 0.037(3) 0.046(3) 0.000(2) -0.018(2) -0.021(2)

C18 0.051(3) 0.035(2) 0.042(2) -0.0044(19) -0.009(2) -0.0113(19)

C19 0.041(2) 0.038(2) 0.0240(19) -0.0054(16) -0.0082(16) -
0.0111(17)

_geom_special_details

;

All esds (except the esd in the dihedral angle between two l.s.
planes)

are estimated using the full covariance matrix. The cell esds
are taken

into account individually in the estimation of esds in distances,
angles

and torsion angles; correlations between esds in cell parameters
are only

used when they are defined by crystal symmetry. An approximate
(isotropic)

treatment of cell esds is used for estimating esds involving l.s.
planes.

;

loop_

_geom_bond_atom_site_label_1

_geom_bond_atom_site_label_2

_geom_bond_distance

_geom_bond_site_symmetry_2

_geom_bond_publ_flag

Cu O2 1.922(3) . ?

Cu O1 1.933(3) . ?

```
Cu N2 1.974(3) . ?

Cu N1 1.980(3) . ?

Cu Cl 2.7375(13) . ?

O1 C13 1.302(4) . ?

O2 C19 1.292(4) . ?

O3 C12 1.401(5) . ?

O4 C11 1.406(5) . ?

O5 O5 0.000(14) 1 ?

N1 C1 1.336(5) . ?

N1 C5 1.355(4) . ?

N2 C10 1.337(5) . ?

N2 C6 1.349(4) . ?

C1 C2 1.373(5) . ?

C2 C3 1.385(5) . ?

C3 C4 1.389(5) . ?

C3 C12 1.498(5) . ?

C4 C5 1.377(5) . ?

C5 C6 1.489(5) . ?

C6 C7 1.382(5) . ?

C7 C8 1.389(5) . ?

C8 C9 1.376(5) . ?

C8 C11 1.511(5) . ?

C9 C10 1.382(5) . ?

C13 C14 1.398(5) . ?
```

```
C13 C19 1.460(5) . ?

C14 C15 1.383(6) . ?

C15 C16 1.378(7) . ?

C16 C17 1.374(6) . ?

C17 C18 1.384(6) . ?

C18 C19 1.397(5) . ?

 loop_

 _geom_angle_atom_site_label_1

 _geom_angle_atom_site_label_2

 _geom_angle_atom_site_label_3

 _geom_angle

 _geom_angle_site_symmetry_1

 _geom_angle_site_symmetry_3

 _geom_angle_publ_flag

O2 Cu O1 83.34(11) . . ?

O2 Cu N2 94.73(12) . . ?

O1 Cu N2 169.39(13) . . ?

O2 Cu N1 171.77(12) . . ?

O1 Cu N1 98.37(12) . . ?

N2 Cu N1 82.11(12) . . ?

O2 Cu Cl 99.92(9) . . ?

O1 Cu Cl 98.75(9) . . ?

N2 Cu Cl 91.86(10) . . ?

N1 Cu Cl 87.81(9) . . ?
```

```
C13 O1 Cu 112.4(2) . . ?

C19 O2 Cu 113.2(2) . . ?

C1 N1 C5 118.3(3) . . ?

C1 N1 Cu 127.3(3) . . ?

C5 N1 Cu 114.3(2) . . ?

C10 N2 C6 118.6(3) . . ?

C10 N2 Cu 126.4(3) . . ?

C6 N2 Cu 115.0(2) . . ?

N1 C1 C2 123.0(4) . . ?

C1 C2 C3 119.2(4) . . ?

C2 C3 C4 118.2(3) . . ?

C2 C3 C12 122.9(3) . . ?

C4 C3 C12 119.0(3) . . ?

C5 C4 C3 119.7(3) . . ?

N1 C5 C4 121.6(3) . . ?

N1 C5 C6 114.4(3) . . ?

C4 C5 C6 124.0(3) . . ?

N2 C6 C7 121.7(3) . . ?

N2 C6 C5 114.0(3) . . ?

C7 C6 C5 124.4(3) . . ?

C6 C7 C8 119.7(4) . . ?

C9 C8 C7 118.0(4) . . ?

C9 C8 C11 122.4(4) . . ?

C7 C8 C11 119.7(4) . . ?
```

```
C8 C9 C10 119.8(4) . . ?

N2 C10 C9 122.2(4) . . ?

O4 C11 C8 114.0(4) . . ?

O3 C12 C3 110.0(3) . . ?

O1 C13 C14 119.0(4) . . ?

O1 C13 C19 115.1(3) . . ?

C14 C13 C19 125.9(4) . . ?

C15 C14 C13 130.3(4) . . ?

C16 C15 C14 129.9(4) . . ?

C17 C16 C15 127.3(4) . . ?

C16 C17 C18 129.3(5) . . ?

C17 C18 C19 130.7(4) . . ?

O2 C19 C18 118.6(4) . . ?

O2 C19 C13 115.2(3) . . ?

C18 C19 C13 126.2(4) . . ?

 loop_

 _geom_torsion_atom_site_label_1

 _geom_torsion_atom_site_label_2

 _geom_torsion_atom_site_label_3

 _geom_torsion_atom_site_label_4

 _geom_torsion

 _geom_torsion_site_symmetry_1

 _geom_torsion_site_symmetry_2

 _geom_torsion_site_symmetry_3
```

```
 _geom_torsion_site_symmetry_4

 _geom_torsion_publ_flag

O2 Cu O1 C13 8.0(3) . . . . ?

N2 Cu O1 C13 88.0(7) . . . . ?

N1 Cu O1 C13 179.8(3) . . . . ?

Cl Cu O1 C13 -91.1(2) . . . . ?

O1 Cu O2 C19 -7.3(3) . . . . ?

N2 Cu O2 C19 -176.9(3) . . . . ?

N1 Cu O2 C19 -109.8(8) . . . . ?

Cl Cu O2 C19 90.4(2) . . . . ?

O2 Cu N1 C1 111.4(8) . . . . ?

O1 Cu N1 C1 10.0(3) . . . . ?

N2 Cu N1 C1 179.3(3) . . . . ?

Cl Cu N1 C1 -88.5(3) . . . . ?

O2 Cu N1 C5 -71.5(9) . . . . ?

O1 Cu N1 C5 -172.9(2) . . . . ?

N2 Cu N1 C5 -3.6(3) . . . . ?

Cl Cu N1 C5 88.6(2) . . . . ?

O2 Cu N2 C10 -5.2(3) . . . . ?

O1 Cu N2 C10 -84.3(8) . . . . ?

N1 Cu N2 C10 -177.6(3) . . . . ?

Cl Cu N2 C10 94.9(3) . . . . ?

O2 Cu N2 C6 176.9(3) . . . . ?

O1 Cu N2 C6 97.9(7) . . . . ?
```

```
N1 Cu N2 C6 4.6(3) . . . . ?

Cl Cu N2 C6 -83.0(3) . . . . ?

C5 N1 C1 C2 0.7(6) . . . . ?

Cu N1 C1 C2 177.7(3) . . . . ?

N1 C1 C2 C3 -0.3(6) . . . . ?

C1 C2 C3 C4 -0.1(6) . . . . ?

C1 C2 C3 C12 179.6(4) . . . . ?

C2 C3 C4 C5 -0.1(6) . . . . ?

C12 C3 C4 C5 -179.8(4) . . . . ?

C1 N1 C5 C4 -0.8(5) . . . . ?

Cu N1 C5 C4 -178.2(3) . . . . ?

C1 N1 C5 C6 179.5(3) . . . . ?

Cu N1 C5 C6 2.2(4) . . . . ?

C3 C4 C5 N1 0.6(6) . . . . ?

C3 C4 C5 C6 -179.9(3) . . . . ?

C10 N2 C6 C7 -1.4(6) . . . . ?

Cu N2 C6 C7 176.6(3) . . . . ?

C10 N2 C6 C5 177.4(3) . . . . ?

Cu N2 C6 C5 -4.6(4) . . . . ?

N1 C5 C6 N2 1.6(5) . . . . ?

C4 C5 C6 N2 -178.0(3) . . . . ?

N1 C5 C6 C7 -179.7(3) . . . . ?

C4 C5 C6 C7 0.7(6) . . . . ?

N2 C6 C7 C8 1.9(6) . . . . ?
```

```
C5 C6 C7 C8 -176.8(3) . . . . ?

C6 C7 C8 C9 -0.4(6) . . . . ?

C6 C7 C8 C11 -180.0(4) . . . . ?

C7 C8 C9 C10 -1.5(6) . . . . ?

C11 C8 C9 C10 178.0(4) . . . . ?

C6 N2 C10 C9 -0.6(6) . . . . ?

Cu N2 C10 C9 -178.4(3) . . . . ?

C8 C9 C10 N2 2.1(7) . . . . ?

C9 C8 C11 O4 10.6(6) . . . . ?

C7 C8 C11 O4 -169.8(3) . . . . ?

C2 C3 C12 O3 10.1(6) . . . . ?

C4 C3 C12 O3 -170.3(4) . . . . ?

Cu O1 C13 C14 172.9(3) . . . . ?

Cu O1 C13 C19 -7.2(4) . . . . ?

O1 C13 C14 C15 -176.1(4) . . . . ?

C19 C13 C14 C15 4.0(7) . . . . ?

C13 C14 C15 C16 -3.7(8) . . . . ?

C14 C15 C16 C17 -2.0(8) . . . . ?

C15 C16 C17 C18 3.3(8) . . . . ?

C16 C17 C18 C19 2.6(8) . . . . ?

Cu O2 C19 C18 -175.7(3) . . . . ?

Cu O2 C19 C13 5.4(4) . . . . ?

C17 C18 C19 O2 174.7(4) . . . . ?

C17 C18 C19 C13 -6.5(7) . . . . ?
```

```
O1 C13 C19 O2 1.2(5) . . . . ?

C14 C13 C19 O2 -178.9(4) . . . . ?

O1 C13 C19 C18 -177.6(4) . . . . ?

C14 C13 C19 C18 2.3(6) . . . . ?

 loop_

 _geom_hbond_atom_site_label_D

 _geom_hbond_atom_site_label_H

 _geom_hbond_atom_site_label_A

 _geom_hbond_distance_DH

 _geom_hbond_distance_HA

 _geom_hbond_distance_DA

 _geom_hbond_angle_DHA

 _geom_hbond_site_symmetry_A

O4 H4A O5  0.82 2.17 2.948(5) 159.6 1


_diffrn_measured_fraction_theta_max    0.984

_diffrn_reflns_theta_full              26.37

_diffrn_measured_fraction_theta_full   0.984

_refine_diff_density_max    0.528

_refine_diff_density_min   -0.443

_refine_diff_density_rms    0.079
```

Complex 13

```
udit_creation_method           SHELXL-97

_chemical_name_systematic        ?

_chemical_name_common            ?

_chemical_formula_sum           'C26 H21 Cu N3 O7 S'

_chemical_melting_point          ?

_exptl_crystal_description       parallelepiped

_exptl_crystal_colour            blue

_diffrn_ambient_temperature      298(2)

_chemical_formula_weight         583.06

loop_

 _atom_type_symbol

 _atom_type_description

 _atom_type_scat_dispersion_real

 _atom_type_scat_dispersion_imag

 _atom_type_scat_source

 'C'  'C'   0.0033   0.0016

 'International Tables Vol C Tables 4.2.6.8 and 6.1.1.4'

 'H'  'H'   0.0000   0.0000

 'International Tables Vol C Tables 4.2.6.8 and 6.1.1.4'

 'N'  'N'   0.0061   0.0033
```

```
 'International Tables Vol C Tables 4.2.6.8 and 6.1.1.4'
 'O'  'O'   0.0106   0.0060
 'International Tables Vol C Tables 4.2.6.8 and 6.1.1.4'
 'S'  'S'   0.1246   0.1234
 'International Tables Vol C Tables 4.2.6.8 and 6.1.1.4'
 'Cu'  'Cu'   0.3201   1.2651
 'International Tables Vol C Tables 4.2.6.8 and 6.1.1.4'
_symmetry_cell_setting           triclinic
_symmetry_space_group_name_H-M   ' P -1'
_chemical_absolute_configuration ?
loop_
 _symmetry_equiv_pos_as_xyz
 'x, y, z'
 '-x, -y, -z'
 _cell_length_a                   10.555(5)
_cell_length_b                   10.670(4)
_cell_length_c                   11.522(5)
_cell_angle_alpha                87.02(3)
_cell_angle_beta                 88.25(3)
_cell_angle_gamma                68.34(3)
_cell_volume                     1204.3(10)
_cell_formula_units_Z            2
_cell_measurement_temperature    293(2)
_cell_measurement_reflns_used    ?
```

```
_cell_measurement_theta_min       ?

_cell_measurement_theta_max       ?

 _exptl_crystal_description        ?

_exptl_crystal_colour             ?

_exptl_crystal_size_max           ?

_exptl_crystal_size_mid           ?

_exptl_crystal_size_min           ?

_exptl_crystal_density_meas       ?

_exptl_crystal_density_diffrn     1.608

_exptl_crystal_density_method     'not measured'

_exptl_crystal_F_000              598

_exptl_absorpt_coefficient_mu     1.048

_exptl_absorpt_correction_type    ?

_exptl_absorpt_correction_T_min   ?

_exptl_absorpt_correction_T_max   ?

_exptl_absorpt_process_details    ?

 _exptl_special_details

;

 ?

;

_diffrn_ambient_temperature       293(2)

_diffrn_radiation_wavelength      0.71073

_diffrn_radiation_type            MoK\a

_diffrn_radiation_source          'fine-focus sealed tube'
```

```
_diffrn_radiation_monochromator   graphite

_diffrn_measurement_device_type   ?

_diffrn_measurement_method        ?

_diffrn_detector_area_resol_mean  ?

_diffrn_standards_number          ?

_diffrn_standards_interval_count  ?

_diffrn_standards_interval_time   ?

_diffrn_standards_decay_%         ?

_diffrn_reflns_number             16495

_diffrn_reflns_av_R_equivalents   0.0486

_diffrn_reflns_av_sigmaI/netI     0.0501

_diffrn_reflns_limit_h_min        -12

_diffrn_reflns_limit_h_max        12

_diffrn_reflns_limit_k_min        -12

_diffrn_reflns_limit_k_max        12

_diffrn_reflns_limit_l_min        -13

_diffrn_reflns_limit_l_max        13

_diffrn_reflns_theta_min          2.06

_diffrn_reflns_theta_max          25.35

_reflns_number_total              4353

_reflns_number_gt                 3244

_reflns_threshold_expression      >2sigma(I)

 _computing_data_collection        ?

_computing_cell_refinement        ?
```

```
_computing_data_reduction         ?

_computing_structure_solution     'SHELXS-97 (Sheldrick, 1990)'

_computing_structure_refinement   'SHELXL-97 (Sheldrick, 1997)'

_computing_molecular_graphics     ?

_computing_publication_material   ?

 _refine_special_details

;

 Refinement of F^2^ against ALL reflections.  The weighted R-
factor wR and

 goodness of fit S are based on F^2^, conventional R-factors R are
based

 on F, with F set to zero for negative F^2^. The threshold
expression of

 F^2^ > 2sigma(F^2^) is used only for calculating R-factors(gt)
etc. and is

 not relevant to the choice of reflections for refinement.  R-
factors based

 on F^2^ are statistically about twice as large as those based on
F, and R-

 factors based on ALL data will be even larger.

;

 _refine_ls_structure_factor_coef  Fsqd

_refine_ls_matrix_type            full

_refine_ls_weighting_scheme       calc

_refine_ls_weighting_details

 'calc w=1/[\s^2^(Fo^2^)+(0.0473P)^2^+0.2222P] where
P=(Fo^2^+2Fc^2^)/3'
```

```
_atom_sites_solution_primary      direct
_atom_sites_solution_secondary    difmap
_atom_sites_solution_hydrogens    geom
_refine_ls_hydrogen_treatment     mixed
_refine_ls_extinction_method      none
_refine_ls_extinction_coef        ?
_refine_ls_number_reflns          4353
_refine_ls_number_parameters      343
_refine_ls_number_restraints      0
_refine_ls_R_factor_all           0.0609
_refine_ls_R_factor_gt            0.0365
_refine_ls_wR_factor_ref          0.0957
_refine_ls_wR_factor_gt           0.0855
_refine_ls_goodness_of_fit_ref    1.043
_refine_ls_restrained_S_all       1.043
_refine_ls_shift/su_max           0.001
_refine_ls_shift/su_mean          0.000
loop_
 _atom_site_label
 _atom_site_type_symbol
 _atom_site_fract_x
 _atom_site_fract_y
 _atom_site_fract_z
 _atom_site_U_iso_or_equiv
```

```
 _atom_site_adp_type

 _atom_site_occupancy

 _atom_site_symmetry_multiplicity

 _atom_site_calc_flag

 _atom_site_refinement_flags

 _atom_site_disorder_assembly

 _atom_site_disorder_group

Cu Cu 0.87933(3) 0.67258(3) 0.52239(3) 0.03175(13) Uani 1 1 d . .
.

N1 N 1.0342(2) 0.7335(2) 0.53183(19) 0.0268(5) Uani 1 1 d . . .

N2 N 0.8417(2) 0.7919(2) 0.3790(2) 0.0278(5) Uani 1 1 d . . .

N3 N 0.8707(2) 0.8655(2) 0.8112(2) 0.0368(6) Uani 1 1 d . . .

S1 S 0.71842(7) 0.89133(7) 0.76928(6) 0.02988(19) Uani 1 1 d . . .

O1 O 0.93483(19) 0.53734(18) 0.64918(18) 0.0373(5) Uani 1 1 d . .
.

O2 O 0.7255(2) 0.61632(18) 0.51351(17) 0.0358(5) Uani 1 1 d . . .

O3 O 0.6257(2) 1.02757(18) 0.7874(2) 0.0459(6) Uani 1 1 d . . .

O4 O 0.7197(2) 0.85006(19) 0.65062(17) 0.0385(5) Uani 1 1 d . . .

O5 O 0.7648(2) 1.19605(19) 0.10908(18) 0.0407(5) Uani 1 1 d . . .

H5A H 0.8302 1.2176 0.0920 0.061 Uiso 1 1 calc R . .

O6 O 1.4454(2) 0.8376(2) 0.61683(19) 0.0501(6) Uani 1 1 d . . .

H6A H 1.5184 0.8476 0.6065 0.075 Uiso 1 1 calc R . .

O7 O 1.0219(2) 0.7286(2) 0.9472(2) 0.0572(7) Uani 1 1 d . . .

C1 C 1.1286(3) 0.6966(3) 0.6152(2) 0.0314(7) Uani 1 1 d . . .

H1A H 1.1201 0.6401 0.6768 0.038 Uiso 1 1 calc R . .
```

C2 C 1.2381(3) 0.7388(3) 0.6138(3) 0.0310(7) Uani 1 1 d . . .

H2A H 1.3012 0.7113 0.6735 0.037 Uiso 1 1 calc R . .

C3 C 1.2528(3) 0.8231(2) 0.5218(2) 0.0261(6) Uani 1 1 d . . .

C4 C 1.1515(3) 0.8644(2) 0.4361(2) 0.0272(6) Uani 1 1 d . . .

H4A H 1.1567 0.9225 0.3746 0.033 Uiso 1 1 calc R . .

C5 C 1.0446(3) 0.8190(2) 0.4430(2) 0.0245(6) Uani 1 1 d . . .

C6 C 0.9320(3) 0.8552(2) 0.3562(2) 0.0248(6) Uani 1 1 d . . .

C7 C 0.9179(3) 0.9426(3) 0.2598(2) 0.0281(6) Uani 1 1 d . . .

H7A H 0.9789 0.9864 0.2469 0.034 Uiso 1 1 calc R . .

C8 C 0.8115(3) 0.9649(3) 0.1818(3) 0.0291(6) Uani 1 1 d . . .

C9 C 0.7214(3) 0.8985(3) 0.2063(3) 0.0350(7) Uani 1 1 d . . .

H9A H 0.6495 0.9108 0.1566 0.042 Uiso 1 1 calc R . .

C10 C 0.7394(3) 0.8143(3) 0.3048(3) 0.0354(7) Uani 1 1 d . . .

H10A H 0.6780 0.7715 0.3202 0.042 Uiso 1 1 calc R . .

C11 C 1.3731(3) 0.8674(3) 0.5124(3) 0.0368(7) Uani 1 1 d . . .

H11A H 1.4331 0.8216 0.4497 0.044 Uiso 1 1 calc R . .

H11B H 1.3414 0.9637 0.4942 0.044 Uiso 1 1 calc R . .

C12 C 0.7934(3) 1.0616(3) 0.0768(3) 0.0371(7) Uani 1 1 d . . .

H12A H 0.8758 1.0321 0.0294 0.045 Uiso 1 1 calc R . .

H12B H 0.7192 1.0594 0.0302 0.045 Uiso 1 1 calc R . .

C13 C 0.8391(3) 0.4907(2) 0.6786(2) 0.0276(6) Uani 1 1 d . . .

C14 C 0.8581(3) 0.4013(3) 0.7760(3) 0.0348(7) Uani 1 1 d . . .

H14A H 0.9374 0.3858 0.8169 0.042 Uiso 1 1 calc R . .

C15 C 0.7770(4) 0.3315(3) 0.8217(3) 0.0419(8) Uani 1 1 d . . .

```
H15A H 0.8131 0.2737 0.8857 0.050 Uiso 1 1 calc R . .
C16 C 0.6514(4) 0.3352(3) 0.7863(3) 0.0455(9) Uani 1 1 d . . .
H16A H 0.6164 0.2768 0.8262 0.055 Uiso 1 1 calc R . .
C17 C 0.5722(3) 0.4168(3) 0.6975(3) 0.0426(8) Uani 1 1 d . . .
H17A H 0.4871 0.4112 0.6895 0.051 Uiso 1 1 calc R . .
C18 C 0.6018(3) 0.5062(3) 0.6185(3) 0.0348(7) Uani 1 1 d . . .
H18A H 0.5313 0.5538 0.5682 0.042 Uiso 1 1 calc R . .
C19 C 0.7203(3) 0.5366(3) 0.6020(2) 0.0278(6) Uani 1 1 d . . .
C20 C 0.6838(3) 0.7733(3) 0.8676(2) 0.0269(6) Uani 1 1 d . . .
C21 C 0.5689(3) 0.7405(3) 0.8811(3) 0.0352(7) Uani 1 1 d . . .
H21A H 0.4922 0.7824 0.8356 0.042 Uiso 1 1 calc R . .
C22 C 0.5743(3) 0.6413(3) 0.9666(3) 0.0408(8) Uani 1 1 d . . .
H22A H 0.4990 0.6168 0.9791 0.049 Uiso 1 1 calc R . .
C23 C 0.6900(4) 0.5784(3) 1.0335(3) 0.0452(8) Uani 1 1 d . . .
H23A H 0.6908 0.5119 1.0893 0.054 Uiso 1 1 calc R . .
C24 C 0.8050(3) 0.6130(3) 1.0184(3) 0.0410(8) Uani 1 1 d . . .
H24A H 0.8823 0.5706 1.0632 0.049 Uiso 1 1 calc R . .
C25 C 0.8003(3) 0.7132(3) 0.9340(2) 0.0299(7) Uani 1 1 d . . .
C26 C 0.9093(3) 0.7693(3) 0.8981(3) 0.0360(7) Uani 1 1 d . . .
 loop_
 _atom_site_aniso_label
 _atom_site_aniso_U_11
 _atom_site_aniso_U_22
 _atom_site_aniso_U_33
```

_atom_site_aniso_U_23

_atom_site_aniso_U_13

_atom_site_aniso_U_12

Cu 0.0285(2) 0.0337(2) 0.0368(2) 0.00837(16) -0.00408(16) -0.01691(17)

N1 0.0255(13) 0.0302(12) 0.0252(13) 0.0003(10) 0.0014(11) -0.0111(11)

N2 0.0238(13) 0.0300(12) 0.0317(14) 0.0009(10) -0.0007(11) -0.0126(11)

N3 0.0307(14) 0.0422(14) 0.0458(17) 0.0049(12) -0.0057(12) -0.0233(12)

S1 0.0293(4) 0.0289(4) 0.0346(4) 0.0022(3) -0.0010(3) -0.0148(3)

O1 0.0291(11) 0.0384(11) 0.0472(14) 0.0129(10) -0.0083(10) -0.0169(10)

O2 0.0383(12) 0.0386(11) 0.0369(13) 0.0101(9) -0.0069(10) -0.0227(10)

O3 0.0445(13) 0.0296(11) 0.0603(16) -0.0019(10) 0.0014(12) -0.0098(10)

O4 0.0418(13) 0.0440(12) 0.0304(12) 0.0010(9) -0.0013(10) -0.0167(11)

O5 0.0372(12) 0.0388(11) 0.0454(14) 0.0097(10) 0.0004(10) -0.0149(10)

O6 0.0399(13) 0.0767(16) 0.0443(14) 0.0060(12) -0.0132(11) -0.0341(13)

O7 0.0392(14) 0.0690(16) 0.0731(18) 0.0193(13) -0.0223(13) -0.0326(13)

C1 0.0329(17) 0.0359(15) 0.0249(16) 0.0047(13) 0.0007(14) -0.0130(14)

C2 0.0262(16) 0.0347(15) 0.0302(17) -0.0005(13) -0.0043(13) -0.0089(13)

C3 0.0262(15) 0.0248(13) 0.0275(16) -0.0054(12) 0.0004(13) -
0.0092(12)

C4 0.0287(16) 0.0265(13) 0.0283(16) 0.0032(12) -0.0028(13) -
0.0129(13)

C5 0.0216(14) 0.0203(13) 0.0295(16) -0.0036(11) 0.0027(13) -
0.0051(12)

C6 0.0206(14) 0.0229(13) 0.0303(16) -0.0027(12) 0.0017(13) -
0.0073(12)

C7 0.0238(15) 0.0291(14) 0.0336(17) -0.0008(12) -0.0011(13) -
0.0123(13)

C8 0.0252(15) 0.0289(14) 0.0296(17) -0.0041(12) 0.0033(13) -
0.0056(13)

C9 0.0284(16) 0.0395(16) 0.0389(19) -0.0002(14) -0.0099(14) -
0.0141(14)

C10 0.0290(17) 0.0422(17) 0.0422(19) -0.0003(14) -0.0004(15) -
0.0219(15)

C11 0.0317(17) 0.0411(17) 0.0410(19) 0.0072(14) -0.0092(15) -
0.0180(15)

C12 0.0323(17) 0.0451(18) 0.0348(19) 0.0038(14) -0.0031(14) -
0.0157(15)

C13 0.0293(16) 0.0240(13) 0.0298(16) -0.0057(12) 0.0044(13) -
0.0099(13)

C14 0.0410(18) 0.0353(15) 0.0282(17) -0.0018(13) 0.0006(14) -
0.0141(15)

C15 0.062(2) 0.0384(16) 0.0253(18) 0.0006(14) 0.0086(16) -
0.0197(17)

C16 0.061(2) 0.0428(18) 0.041(2) -0.0023(16) 0.0167(18) -
0.0307(18)

C17 0.043(2) 0.0476(18) 0.048(2) -0.0093(16) 0.0087(17) -
0.0287(17)

C18 0.0336(17) 0.0367(16) 0.0391(19) -0.0023(14) -0.0032(14) -0.0184(14)

C19 0.0314(16) 0.0251(13) 0.0280(16) -0.0034(12) 0.0006(13) -0.0114(13)

C20 0.0285(15) 0.0277(13) 0.0283(16) -0.0036(12) 0.0041(13) -0.0147(13)

C21 0.0281(16) 0.0393(16) 0.0403(19) -0.0018(14) 0.0004(14) -0.0148(14)

C22 0.0410(19) 0.0434(17) 0.046(2) -0.0008(15) 0.0095(16) -0.0264(16)

C23 0.055(2) 0.0424(18) 0.043(2) 0.0072(15) 0.0081(18) -0.0249(17)

C24 0.045(2) 0.0397(17) 0.039(2) 0.0053(14) -0.0063(16) -0.0169(16)

C25 0.0309(16) 0.0328(15) 0.0303(17) -0.0031(13) 0.0004(14) -0.0166(14)

C26 0.0302(17) 0.0396(16) 0.0423(19) 0.0006(14) -0.0053(15) -0.0176(15)

_geom_special_details

;

All esds (except the esd in the dihedral angle between two l.s. planes)

are estimated using the full covariance matrix. The cell esds are taken

into account individually in the estimation of esds in distances, angles

and torsion angles; correlations between esds in cell parameters are only

used when they are defined by crystal symmetry. An approximate (isotropic)

```
 treatment of cell esds is used for estimating esds involving l.s.
planes.

;

loop_

 _geom_bond_atom_site_label_1

 _geom_bond_atom_site_label_2

 _geom_bond_distance

 _geom_bond_site_symmetry_2

 _geom_bond_publ_flag

Cu O2 1.935(2) . ?

Cu O1 1.941(2) . ?

Cu N1 1.977(2) . ?

Cu N2 1.989(2) . ?

N1 C1 1.342(4) . ?

N1 C5 1.365(3) . ?

N2 C10 1.341(4) . ?

N2 C6 1.370(3) . ?

N3 C26 1.354(4) . ?

N3 S1 1.612(3) . ?

S1 O3 1.444(2) . ?

S1 O4 1.456(2) . ?

S1 C20 1.780(3) . ?

O1 C13 1.310(3) . ?

O2 C19 1.306(3) . ?
```

```
O5 C12 1.421(3) . ?

O6 C11 1.403(4) . ?

O7 C26 1.247(4) . ?

C1 C2 1.386(4) . ?

C2 C3 1.397(4) . ?

C3 C4 1.408(4) . ?

C3 C11 1.509(4) . ?

C4 C5 1.382(4) . ?

C5 C6 1.502(4) . ?

C6 C7 1.388(4) . ?

C7 C8 1.402(4) . ?

C8 C9 1.395(4) . ?

C8 C12 1.518(4) . ?

C9 C10 1.383(4) . ?

C13 C14 1.404(4) . ?

C13 C19 1.470(4) . ?

C14 C15 1.403(4) . ?

C15 C16 1.385(5) . ?

C16 C17 1.388(5) . ?

C17 C18 1.396(4) . ?

C18 C19 1.408(4) . ?

C20 C21 1.382(4) . ?

C20 C25 1.391(4) . ?

C21 C22 1.394(4) . ?
```

```
C22 C23 1.391(5) . ?

C23 C24 1.397(4) . ?

C24 C25 1.395(4) . ?

C25 C26 1.519(4) . ?

 loop_

 _geom_angle_atom_site_label_1

 _geom_angle_atom_site_label_2

 _geom_angle_atom_site_label_3

 _geom_angle

 _geom_angle_site_symmetry_1

 _geom_angle_site_symmetry_3

 _geom_angle_publ_flag

O2 Cu O1 84.06(8) . . ?

O2 Cu N1 178.94(8) . . ?

O1 Cu N1 96.52(9) . . ?

O2 Cu N2 97.41(9) . . ?

O1 Cu N2 171.95(9) . . ?

N1 Cu N2 82.13(10) . . ?

C1 N1 C5 118.6(2) . . ?

C1 N1 Cu 126.00(18) . . ?

C5 N1 Cu 115.40(19) . . ?

C10 N2 C6 118.5(2) . . ?

C10 N2 Cu 126.67(19) . . ?

C6 N2 Cu 114.84(18) . . ?
```

C26 N3 S1 111.12(19) . . ?

O3 S1 O4 113.56(13) . . ?

O3 S1 N3 112.26(13) . . ?

O4 S1 N3 110.91(13) . . ?

O3 S1 C20 111.48(13) . . ?

O4 S1 C20 109.52(12) . . ?

N3 S1 C20 98.06(13) . . ?

C13 O1 Cu 111.93(18) . . ?

C19 O2 Cu 111.83(18) . . ?

N1 C1 C2 123.0(2) . . ?

C1 C2 C3 119.3(3) . . ?

C2 C3 C4 117.5(2) . . ?

C2 C3 C11 121.9(3) . . ?

C4 C3 C11 120.6(2) . . ?

C5 C4 C3 120.2(2) . . ?

N1 C5 C4 121.4(3) . . ?

N1 C5 C6 113.8(2) . . ?

C4 C5 C6 124.8(2) . . ?

N2 C6 C7 121.3(2) . . ?

N2 C6 C5 113.8(2) . . ?

C7 C6 C5 124.9(2) . . ?

C6 C7 C8 120.0(2) . . ?

C9 C8 C7 117.7(3) . . ?

C9 C8 C12 121.5(3) . . ?

C7 C8 C12 120.7(2) . . ?

C10 C9 C8 119.6(3) . . ?

N2 C10 C9 122.8(3) . . ?

O6 C11 C3 110.7(2) . . ?

O5 C12 C8 112.0(2) . . ?

O1 C13 C14 119.1(3) . . ?

O1 C13 C19 115.1(2) . . ?

C14 C13 C19 125.8(3) . . ?

C15 C14 C13 130.6(3) . . ?

C16 C15 C14 130.0(3) . . ?

C15 C16 C17 126.8(3) . . ?

C16 C17 C18 129.4(3) . . ?

C17 C18 C19 131.0(3) . . ?

O2 C19 C18 118.3(3) . . ?

O2 C19 C13 115.8(2) . . ?

C18 C19 C13 125.8(3) . . ?

C21 C20 C25 123.5(3) . . ?

C21 C20 S1 130.4(2) . . ?

C25 C20 S1 106.06(19) . . ?

C20 C21 C22 116.4(3) . . ?

C23 C22 C21 121.4(3) . . ?

C22 C23 C24 121.3(3) . . ?

C25 C24 C23 117.9(3) . . ?

C20 C25 C24 119.5(3) . . ?

```
C20 C25 C26 111.2(2) . . ?

C24 C25 C26 129.3(3) . . ?

O7 C26 N3 125.1(3) . . ?

O7 C26 C25 121.3(3) . . ?

N3 C26 C25 113.6(2) . . ?

 _diffrn_measured_fraction_theta_max    0.987

_diffrn_reflns_theta_full              25.35

_diffrn_measured_fraction_theta_full   0.987

_refine_diff_density_max    0.288

_refine_diff_density_min   -0.515

_refine_diff_density_rms    0.073
```

Complex 13a

```
udit_creation_method           SHELXL-97

_chemical_name_systematic        ?

_chemical_name_common            ?

_chemical_formula_sum           'C27 H22 Cu N3 O7 S'

_chemical_melting_point          ?

_exptl_crystal_description       parallelepiped

_exptl_crystal_colour            green

_diffrn_ambient_temperature      298(2)

_chemical_formula_weight         596.08
```

```
loop_
 _atom_type_symbol
 _atom_type_description
 _atom_type_scat_dispersion_real
 _atom_type_scat_dispersion_imag
 _atom_type_scat_source
 'C'  'C'   0.0033   0.0016
 'International Tables Vol C Tables 4.2.6.8 and 6.1.1.4'
 'H'  'H'   0.0000   0.0000
 'International Tables Vol C Tables 4.2.6.8 and 6.1.1.4'
 'N'  'N'   0.0061   0.0033
 'International Tables Vol C Tables 4.2.6.8 and 6.1.1.4'
 'O'  'O'   0.0106   0.0060
 'International Tables Vol C Tables 4.2.6.8 and 6.1.1.4'
 'S'  'S'   0.1246   0.1234
 'International Tables Vol C Tables 4.2.6.8 and 6.1.1.4'
 'Cu'  'Cu'   0.3201   1.2651
 'International Tables Vol C Tables 4.2.6.8 and 6.1.1.4'
_symmetry_cell_setting           triclinic
_symmetry_space_group_name_H-M   ' P -1'
_chemical_absolute_configuration ?
loop_
 _symmetry_equiv_pos_as_xyz
 'x, y, z'
```

```
'-x, -y, -z'
_cell_length_a                    10.48(3)
_cell_length_b                    10.96(3)
_cell_length_c                    11.11(3)
_cell_angle_alpha                 86.33(9)
_cell_angle_beta                  87.40(7)
_cell_angle_gamma                 81.78(7)
_cell_volume                      1260(6)
_cell_formula_units_Z             2
_cell_measurement_temperature     293(2)
_cell_measurement_reflns_used     ?
_cell_measurement_theta_min       ?
_cell_measurement_theta_max       ?
_exptl_crystal_description        ?
_exptl_crystal_colour             ?
_exptl_crystal_size_max           ?
_exptl_crystal_size_mid           ?
_exptl_crystal_size_min           ?
_exptl_crystal_density_meas       ?
_exptl_crystal_density_diffrn     1.571
_exptl_crystal_density_method     'not measured'
_exptl_crystal_F_000              612
_exptl_absorpt_coefficient_mu     1.004
_exptl_absorpt_correction_type    ?
```

```
_exptl_absorpt_correction_T_min   ?
_exptl_absorpt_correction_T_max   ?
_exptl_absorpt_process_details    ?
 _exptl_special_details
;
 ?
;
 _diffrn_ambient_temperature       293(2)
_diffrn_radiation_wavelength      0.71073
_diffrn_radiation_type            MoK\a
_diffrn_radiation_source          'fine-focus sealed tube'
_diffrn_radiation_monochromator   graphite
_diffrn_measurement_device_type   ?
_diffrn_measurement_method        ?
_diffrn_detector_area_resol_mean  ?
_diffrn_standards_number          ?
_diffrn_standards_interval_count  ?
_diffrn_standards_interval_time   ?
_diffrn_standards_decay_%         ?
_diffrn_reflns_number             22203
_diffrn_reflns_av_R_equivalents   0.0328
_diffrn_reflns_av_sigmaI/netI     0.0315
_diffrn_reflns_limit_h_min        -13
_diffrn_reflns_limit_h_max        13
```

```
_diffrn_reflns_limit_k_min        -12

_diffrn_reflns_limit_k_max        13

_diffrn_reflns_limit_l_min        -13

_diffrn_reflns_limit_l_max        13

_diffrn_reflns_theta_min          2.52

_diffrn_reflns_theta_max          26.59

_reflns_number_total              5216

_reflns_number_gt                 4082

_reflns_threshold_expression      >2sigma(I)

 _computing_data_collection        ?

_computing_cell_refinement        ?

_computing_data_reduction         ?

_computing_structure_solution     'SHELXS-97 (Sheldrick, 1990)'

_computing_structure_refinement   'SHELXL-97 (Sheldrick, 1997)'

_computing_molecular_graphics     ?

_computing_publication_material   ?

 _refine_special_details

;

 Refinement of F^2^ against ALL reflections.  The weighted R-
factor wR and

 goodness of fit S are based on F^2^, conventional R-factors R are
based

 on F, with F set to zero for negative F^2^. The threshold
expression of

 F^2^ > 2sigma(F^2^) is used only for calculating R-factors(gt)
etc. and is
```

```
 not relevant to the choice of reflections for refinement.  R-
factors based

 on F^2^ are statistically about twice as large as those based on
F, and R-

 factors based on ALL data will be even larger.

;

 _refine_ls_structure_factor_coef  Fsqd

_refine_ls_matrix_type            full

_refine_ls_weighting_scheme       calc

_refine_ls_weighting_details

 'calc w=1/[\s^2^(Fo^2^)+(0.0760P)^2^+0.9884P] where
P=(Fo^2^+2Fc^2^)/3'

_atom_sites_solution_primary      direct

_atom_sites_solution_secondary    difmap

_atom_sites_solution_hydrogens    geom

_refine_ls_hydrogen_treatment     mixed

_refine_ls_extinction_method      none

_refine_ls_extinction_coef        ?

_refine_ls_number_reflns          5216

_refine_ls_number_parameters      358

_refine_ls_number_restraints      3

_refine_ls_R_factor_all           0.0629

_refine_ls_R_factor_gt            0.0447

_refine_ls_wR_factor_ref          0.1364

_refine_ls_wR_factor_gt           0.1206
```

```
_refine_ls_goodness_of_fit_ref    1.034

_refine_ls_restrained_S_all       1.038

_refine_ls_shift/su_max           0.257

_refine_ls_shift/su_mean          0.006

 loop_

 _atom_site_label

 _atom_site_type_symbol

 _atom_site_fract_x

 _atom_site_fract_y

 _atom_site_fract_z

 _atom_site_U_iso_or_equiv

 _atom_site_adp_type

 _atom_site_occupancy

 _atom_site_symmetry_multiplicity

 _atom_site_calc_flag

 _atom_site_refinement_flags

 _atom_site_disorder_assembly

 _atom_site_disorder_group

Cu Cu 0.62631(4) 0.99218(3) 0.61558(3) 0.03594(14) Uani 1 1 d . .
.

S1 S 0.76884(9) 0.22486(8) 0.77137(8) 0.0459(2) Uani 1 1 d . . .

O1 O 0.5832(2) 1.1306(2) 0.50122(19) 0.0390(5) Uani 1 1 d . . .

O2 O 0.7729(2) 0.9539(2) 0.5079(2) 0.0439(5) Uani 1 1 d . . .

O3 O 0.7697(3) 0.0994(2) 0.7391(2) 0.0564(7) Uani 1 1 d . . .
```

O4 O 0.8623(3) 0.2365(3) 0.8611(3) 0.0717(8) Uani 1 1 d . . .

O5 O 0.7164(3) 0.5740(3) 1.1052(3) 0.0752(8) Uani 1 1 d . . .

H5A H 0.6523 0.5635 1.1475 0.113 Uiso 1 1 calc R . .

O6 O 0.0889(3) 1.1865(3) 0.9843(3) 0.0752(9) Uani 1 1 d . . .

H6A H 0.0267 1.1814 0.9436 0.113 Uiso 1 1 calc R . .

O7 O 0.4815(3) 0.4516(3) 0.7435(3) 0.0745(9) Uani 1 1 d . . .

O8 O 0.9627(4) 0.5633(4) 0.1960(4) 0.1104(14) Uani 1 1 d D . .

H1W H 0.994(3) 0.566(4) 0.108(2) 0.050 Uiso 1 1 d D . .

H2W H 0.866(2) 0.572(3) 0.184(3) 0.050 Uiso 1 1 d D . .

N1 N 0.4796(2) 1.0308(2) 0.7292(2) 0.0310(5) Uani 1 1 d . . .

N2 N 0.6575(2) 0.8420(2) 0.7256(2) 0.0337(5) Uani 1 1 d . . .

N3 N 0.6278(3) 0.2881(3) 0.8107(3) 0.0517(7) Uani 1 1 d . . .

C1 C 0.3906(3) 1.1311(3) 0.7215(3) 0.0391(7) Uani 1 1 d . . .

H1B H 0.3977 1.1901 0.6585 0.047 Uiso 1 1 calc R . .

C2 C 0.2889(3) 1.1497(3) 0.8038(3) 0.0407(7) Uani 1 1 d . . .

H2B H 0.2284 1.2203 0.7961 0.049 Uiso 1 1 calc R . .

C3 C 0.2767(3) 1.0623(3) 0.8990(3) 0.0389(7) Uani 1 1 d . . .

C4 C 0.3709(3) 0.9583(3) 0.9079(3) 0.0373(7) Uani 1 1 d . . .

H4A H 0.3666 0.8989 0.9712 0.045 Uiso 1 1 calc R . .

C5 C 0.4701(3) 0.9447(3) 0.8219(3) 0.0321(6) Uani 1 1 d . . .

C6 C 0.5736(3) 0.8370(3) 0.8209(3) 0.0321(6) Uani 1 1 d . . .

C7 C 0.5862(3) 0.7384(3) 0.9072(3) 0.0381(7) Uani 1 1 d . . .

H7A H 0.5270 0.7370 0.9721 0.046 Uiso 1 1 calc R . .

C8 C 0.6865(3) 0.6424(3) 0.8963(3) 0.0411(7) Uani 1 1 d . . .

C9 C 0.7722(3) 0.6487(3) 0.7973(3) 0.0438(8) Uani 1 1 d . . .

H9A H 0.8409 0.5861 0.7868 0.053 Uiso 1 1 calc R . .

C10 C 0.7543(3) 0.7489(3) 0.7148(3) 0.0427(7) Uani 1 1 d . . .

H10A H 0.8120 0.7518 0.6488 0.051 Uiso 1 1 calc R . .

C11 C 0.1666(3) 1.0743(4) 0.9916(3) 0.0552(9) Uani 1 1 d . . .

H11A H 0.1142 1.0096 0.9819 0.066 Uiso 1 1 calc R . .

H11B H 0.2016 1.0613 1.0715 0.066 Uiso 1 1 calc R . .

C12 C 0.7031(4) 0.5347(3) 0.9906(3) 0.0561(10) Uani 1 1 d . . .

H12A H 0.6287 0.4912 0.9913 0.067 Uiso 1 1 calc R . .

H12B H 0.7787 0.4775 0.9688 0.067 Uiso 1 1 calc R . .

C13 C 0.6764(3) 1.1441(3) 0.4218(3) 0.0317(6) Uani 1 1 d . . .

C14 C 0.6637(3) 1.2466(3) 0.3399(3) 0.0389(7) Uani 1 1 d . . .

H14A H 0.5868 1.2999 0.3485 0.047 Uiso 1 1 calc R . .

C15 C 0.7470(4) 1.2825(3) 0.2473(3) 0.0481(8) Uani 1 1 d . . .

H15A H 0.7167 1.3545 0.2024 0.058 Uiso 1 1 calc R . .

C16 C 0.8685(4) 1.2258(3) 0.2127(3) 0.0545(9) Uani 1 1 d . . .

H16A H 0.9096 1.2647 0.1482 0.065 Uiso 1 1 calc R . .

C17 C 0.9356(4) 1.1187(3) 0.2624(3) 0.0500(9) Uani 1 1 d . . .

H17A H 1.0177 1.0967 0.2282 0.060 Uiso 1 1 calc R . .

C18 C 0.8999(3) 1.0382(3) 0.3559(3) 0.0437(8) Uani 1 1 d . . .

H18A H 0.9613 0.9701 0.3735 0.052 Uiso 1 1 calc R . .

C19 C 0.7858(3) 1.0435(3) 0.4278(3) 0.0352(6) Uani 1 1 d . . .

C20 C 0.7924(3) 0.3237(3) 0.6416(3) 0.0424(7) Uani 1 1 d . . .

C21 C 0.8954(4) 0.3260(4) 0.5598(4) 0.0558(9) Uani 1 1 d . . .

H21A H 0.9694 0.2684 0.5664 0.067 Uiso 1 1 calc R . .

C22 C 0.8838(4) 0.4178(4) 0.4672(4) 0.0610(11) Uani 1 1 d . . .

H22A H 0.9516 0.4215 0.4107 0.073 Uiso 1 1 calc R . .

C23 C 0.7741(5) 0.5038(4) 0.4568(4) 0.0624(11) Uani 1 1 d . . .

H23A H 0.7692 0.5642 0.3938 0.075 Uiso 1 1 calc R . .

C24 C 0.6714(4) 0.5007(3) 0.5397(3) 0.0545(9) Uani 1 1 d . . .

H24A H 0.5974 0.5583 0.5331 0.065 Uiso 1 1 calc R . .

C25 C 0.6818(3) 0.4088(3) 0.6333(3) 0.0437(8) Uani 1 1 d . . .

C26 C 0.5867(4) 0.3853(3) 0.7338(3) 0.0493(8) Uani 1 1 d . . .

loop_

_atom_site_aniso_label

_atom_site_aniso_U_11

_atom_site_aniso_U_22

_atom_site_aniso_U_33

_atom_site_aniso_U_23

_atom_site_aniso_U_13

_atom_site_aniso_U_12

Cu 0.0365(2) 0.0386(2) 0.0291(2) 0.00562(15) 0.00936(15)
0.00034(15)

S1 0.0476(5) 0.0474(5) 0.0433(5) 0.0030(4) -0.0105(4) -0.0085(4)

O1 0.0345(11) 0.0456(12) 0.0326(11) 0.0073(9) 0.0104(9) 0.0017(9)

O2 0.0470(13) 0.0415(12) 0.0373(12) 0.0081(9) 0.0141(10)
0.0044(10)

O3 0.0607(16) 0.0428(13) 0.0657(17) 0.0027(11) -0.0107(13) -
0.0069(11)

O4 0.075(2) 0.0765(19) 0.0668(19) 0.0044(15) -0.0365(16) -
0.0141(15)

O5 0.076(2) 0.078(2) 0.068(2) 0.0140(15) -0.0066(16) -0.0098(16)

O6 0.0526(17) 0.089(2) 0.078(2) -0.0070(17) 0.0142(15) 0.0068(15)

O7 0.0603(18) 0.083(2) 0.0689(19) 0.0070(15) 0.0181(15) 0.0179(16)

O8 0.073(2) 0.114(3) 0.137(4) 0.034(3) -0.014(3) -0.007(2)

N1 0.0321(13) 0.0313(12) 0.0290(12) 0.0004(10) 0.0047(10) -
0.0053(10)

N2 0.0320(13) 0.0358(13) 0.0319(13) 0.0008(10) 0.0068(10) -
0.0030(10)

N3 0.0560(18) 0.0568(18) 0.0406(16) 0.0026(13) 0.0049(14) -
0.0064(14)

C1 0.0409(17) 0.0364(16) 0.0387(17) 0.0047(13) 0.0025(13) -
0.0056(13)

C2 0.0342(16) 0.0421(17) 0.0439(18) -0.0027(14) 0.0039(13) -
0.0009(13)

C3 0.0302(15) 0.0516(18) 0.0349(16) -0.0062(13) 0.0036(12) -
0.0058(13)

C4 0.0356(16) 0.0434(17) 0.0319(15) 0.0030(13) 0.0060(12) -
0.0067(13)

C5 0.0310(15) 0.0379(15) 0.0278(14) -0.0038(12) 0.0012(11) -
0.0060(12)

C6 0.0305(15) 0.0386(16) 0.0273(14) -0.0013(12) 0.0019(11) -
0.0063(12)

C7 0.0409(17) 0.0411(17) 0.0316(16) 0.0009(13) 0.0051(13) -
0.0065(13)

C8 0.0492(19) 0.0365(16) 0.0363(17) 0.0015(13) -0.0010(14) -
0.0038(14)

C9 0.0439(18) 0.0385(17) 0.0453(19) 0.0010(14) 0.0034(15)
0.0040(14)

C10 0.0400(17) 0.0461(18) 0.0392(17) -0.0003(14) 0.0089(14) -0.0012(14)

C11 0.0378(19) 0.074(3) 0.049(2) -0.0016(18) 0.0116(16) 0.0029(17)

C12 0.078(3) 0.0424(19) 0.043(2) 0.0032(15) 0.0034(18) 0.0031(18)

C13 0.0312(15) 0.0372(15) 0.0264(14) -0.0018(11) 0.0021(11) -0.0049(12)

C14 0.0416(17) 0.0358(16) 0.0385(17) -0.0017(13) 0.0045(13) -0.0051(13)

C15 0.062(2) 0.0358(17) 0.0451(19) 0.0102(14) 0.0084(16) -0.0100(15)

C16 0.066(2) 0.053(2) 0.043(2) 0.0070(16) 0.0227(17) -0.0180(18)

C17 0.046(2) 0.056(2) 0.047(2) -0.0062(16) 0.0198(16) -0.0112(16)

C18 0.0406(18) 0.0457(18) 0.0413(18) 0.0002(14) 0.0122(14) 0.0007(14)

C19 0.0394(17) 0.0346(15) 0.0305(15) -0.0008(12) 0.0058(12) -0.0040(12)

C20 0.0432(18) 0.0434(18) 0.0429(18) -0.0023(14) -0.0041(14) -0.0130(14)

C21 0.043(2) 0.062(2) 0.065(2) -0.0092(19) 0.0045(18) -0.0146(17)

C22 0.060(2) 0.072(3) 0.057(2) -0.005(2) 0.0127(19) -0.032(2)

C23 0.081(3) 0.061(2) 0.049(2) 0.0067(18) 0.003(2) -0.028(2)

C24 0.061(2) 0.048(2) 0.053(2) 0.0034(16) -0.0043(18) -0.0062(17)

C25 0.0471(19) 0.0439(18) 0.0407(18) -0.0053(14) -0.0013(15) -0.0069(15)

C26 0.052(2) 0.053(2) 0.0413(19) -0.0050(15) 0.0036(16) -0.0024(17)

_geom_special_details

```
;

 All esds (except the esd in the dihedral angle between two l.s.
planes)

 are estimated using the full covariance matrix.  The cell esds
are taken

 into account individually in the estimation of esds in distances,
angles

 and torsion angles; correlations between esds in cell parameters
are only

 used when they are defined by crystal symmetry.  An approximate
(isotropic)

 treatment of cell esds is used for estimating esds involving l.s.
planes.

;

 loop_

 _geom_bond_atom_site_label_1

 _geom_bond_atom_site_label_2

 _geom_bond_distance

 _geom_bond_site_symmetry_2

 _geom_bond_publ_flag

Cu O2 1.919(4) . ?

Cu O1 1.931(5) . ?

Cu N1 1.960(5) . ?

Cu N2 1.984(5) . ?

S1 O3 1.442(5) . ?

S1 O4 1.453(4) . ?
```

```
S1 N3 1.595(5) . ?

S1 C20 1.776(5) . ?

O1 C13 1.304(4) . ?

O2 C19 1.300(5) . ?

O5 C12 1.389(6) . ?

O6 C11 1.375(6) . ?

O7 C26 1.235(5) . ?

N1 C1 1.338(5) . ?

N1 C5 1.362(5) . ?

N2 C10 1.339(5) . ?

N2 C6 1.348(5) . ?

N3 C26 1.354(6) . ?

C1 C2 1.373(5) . ?

C2 C3 1.395(6) . ?

C3 C4 1.399(5) . ?

C3 C11 1.507(5) . ?

C4 C5 1.379(5) . ?

C5 C6 1.485(5) . ?

C6 C7 1.394(5) . ?

C7 C8 1.385(5) . ?

C8 C9 1.393(6) . ?

C8 C12 1.523(6) . ?

C9 C10 1.381(6) . ?

C13 C14 1.395(5) . ?
```

```
C13 C19 1.474(5) . ?

C14 C15 1.392(5) . ?

C15 C16 1.385(6) . ?

C16 C17 1.376(6) . ?

C17 C18 1.393(6) . ?

C18 C19 1.403(5) . ?

C20 C21 1.381(6) . ?

C20 C25 1.384(6) . ?

C21 C22 1.389(7) . ?

C22 C23 1.383(7) . ?

C23 C24 1.388(6) . ?

C24 C25 1.397(6) . ?

C25 C26 1.498(6) . ?

loop_

 _geom_angle_atom_site_label_1

 _geom_angle_atom_site_label_2

 _geom_angle_atom_site_label_3

 _geom_angle

 _geom_angle_site_symmetry_1

 _geom_angle_site_symmetry_3

 _geom_angle_publ_flag

O2 Cu O1 83.77(18) . . ?

O2 Cu N1 178.45(10) . . ?

O1 Cu N1 97.22(19) . . ?
```

```
O2 Cu N2 97.37(18) . . ?

O1 Cu N2 174.31(10) . . ?

N1 Cu N2 81.76(18) . . ?

O3 S1 O4 113.14(19) . . ?

O3 S1 N3 112.0(2) . . ?

O4 S1 N3 111.6(3) . . ?

O3 S1 C20 111.1(3) . . ?

O4 S1 C20 110.3(2) . . ?

N3 S1 C20 97.7(2) . . ?

C13 O1 Cu 112.6(2) . . ?

C19 O2 Cu 112.3(2) . . ?

C1 N1 C5 119.2(3) . . ?

C1 N1 Cu 125.8(2) . . ?

C5 N1 Cu 115.0(2) . . ?

C10 N2 C6 118.4(3) . . ?

C10 N2 Cu 126.1(3) . . ?

C6 N2 Cu 115.5(2) . . ?

C26 N3 S1 111.1(3) . . ?

N1 C1 C2 122.1(3) . . ?

C1 C2 C3 119.8(3) . . ?

C2 C3 C4 118.1(3) . . ?

C2 C3 C11 123.1(3) . . ?

C4 C3 C11 118.7(3) . . ?

C5 C4 C3 119.2(3) . . ?
```

```
N1 C5 C4 121.6(3) . . ?

N1 C5 C6 114.5(3) . . ?

C4 C5 C6 123.9(3) . . ?

N2 C6 C7 121.6(3) . . ?

N2 C6 C5 113.2(3) . . ?

C7 C6 C5 125.2(3) . . ?

C8 C7 C6 120.1(3) . . ?

C7 C8 C9 117.7(3) . . ?

C7 C8 C12 120.9(3) . . ?

C9 C8 C12 121.4(3) . . ?

C10 C9 C8 119.4(3) . . ?

N2 C10 C9 122.9(3) . . ?

O6 C11 C3 114.1(3) . . ?

O5 C12 C8 111.8(4) . . ?

O1 C13 C14 119.1(3) . . ?

O1 C13 C19 114.3(3) . . ?

C14 C13 C19 126.6(3) . . ?

C13 C14 C15 130.7(3) . . ?

C16 C15 C14 129.0(4) . . ?

C17 C16 C15 127.6(3) . . ?

C16 C17 C18 130.1(4) . . ?

C17 C18 C19 130.2(3) . . ?

O2 C19 C18 118.9(3) . . ?

O2 C19 C13 115.5(3) . . ?
```

```
C18 C19 C13 125.6(3) . . ?

C21 C20 C25 122.1(4) . . ?

C21 C20 S1 131.5(3) . . ?

C25 C20 S1 106.4(3) . . ?

C20 C21 C22 117.2(4) . . ?

C23 C22 C21 121.8(4) . . ?

C22 C23 C24 120.5(4) . . ?

C23 C24 C25 118.4(4) . . ?

C20 C25 C24 120.1(4) . . ?

C20 C25 C26 110.8(3) . . ?

C24 C25 C26 129.1(4) . . ?

O7 C26 N3 124.7(4) . . ?

O7 C26 C25 121.2(4) . . ?

N3 C26 C25 114.1(3) . . ?

 _diffrn_measured_fraction_theta_max    0.989

_diffrn_reflns_theta_full              26.59

_diffrn_measured_fraction_theta_full   0.989

_refine_diff_density_max    1.038

_refine_diff_density_min   -0.526

_refine_diff_density_rms    0.074
```

Dalton Transactions

RSC Publishing

PAPER

View Article Online
View Journal | View Issue

Cite this: *Dalton Trans.*, 2013, **42**, 9679

Improving the bioactivity of Zn(II)-curcumin based complexes†

Daniela Pucci,*[a] Alessandra Crispini,[a] Bárbara Sanz Mendiguchía,[a] Sante Pirillo,[a] Mauro Ghedini,[a] Sabrina Morelli[b] and Loredana De Bartolo[b]

Received 25th February 2013,
Accepted 15th April 2013

DOI: 10.1039/c3dt50513h

www.rsc.org/dalton

New Zn(II)-curcumin based heteroleptic complexes (**1–5**) have been synthesized and fully characterized, with the aim to improve the bioactivity of the precursor derivative [(bpy-9)Zn(curc)Cl] (**A**), a potentially intercalating antitumor agent recently reported. Some structural changes have been made starting from the reference complex **A**, in order to introduce new functionalities, such as electrostatic and/or covalent interactions. In particular, keeping the same N,N chelating ligand, namely bpy-9, two completely different Zn(II) species have been obtained: a tetracoordinated Zn(II) cation with tetrafluoroborate as counterion (**1**) and a dimeric neutral complex in which the sulfate anion acts as a bridging group through two Zn(II) centres (**2**). Moreover, by changing the N,N chelating unit, [(L^n)Zn(curc)Cl] complexes (**3–5**), in which the Zn(II) ion shows the same pentacoordination seen in the precursor complex **A**, have been obtained. The antitumour activity of all new Zn(II) complexes was tested *in vitro* against the human neuroblastoma cell line SH-SY5Y in a biohybrid membrane system and the results indicate that all species exhibit strong cytotoxic activity. In particular the ionic tetrafluoroborate Zn(II) complex, **1**, and the neutral phenanthroline based Zn(II) derivative, **4**, show the strongest growth inhibition, being even more effective than the model complex **A**. Both complexes have a dose-dependent anti-proliferative effect on cells as demonstrated by the decrease of viability and the increase of Annexin V and PI-positive cells with the increase of their concentration. Cells treated with complexes **1** and **4** undergo apoptosis that involves the activation of JNK, caspase 3 and MMP changes. Finally, complex **1** is more effective in the induction of caspase-3 activation demonstrating its ability to trigger the execution-phase of cell apoptosis.

Introduction

Over the last decade medicinal chemistry has been the scene of a massive investigation into cytotoxicity and genotoxicity of new metal-based antitumor complexes able to overcome cisplatin resistance and toxicity. A rational drug design has focused on a number of transition metal complexes other than platinum which could offer unique properties such as variable redox states, photophysical properties, the possibility of tailoring substrate specificity and ability of targeting DNA through non covalent modes of action.[1–7]

In this context, due to the physiological roles of zinc in cells and organs, a large interest is growing in the use of Zn(II) coordination complexes with low toxicity and low side effects in medicinal therapeutic applications,[8] for treating diabetes mellitus[9] or cancer.[10–17]

In this context we have recently proposed low cost Zn(II) complexes with promising cytotoxic activity against different human cancer cells, focusing on pentacoordinated Zn(II) complexes whose coordination sphere is filled by a potentially intercalating N,N ligand and one or two O,O chelating bioactive ligands.[12,16] Substantial results have been obtained for this class of compounds in the case of the curcumin (curc, 1,7-bis-(4-hydroxy-3-methoxyphenyl)-1,6-heptadiene-3,5-dione) derivative of the 4,4′-dinonyl-2,2′-bipyridine, complex **A** shown in Fig. 1.[16] The disadvantages of curcumin (relatively poor bioavailability, easily oxidised and photodegraded) responsible

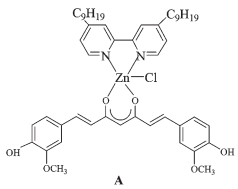

A

Fig. 1 Structure of the model complex [(bpy-9)Zn(curc)Cl] (**A**).

[a]*Centro di Eccellenza CEMIF.CAL-LASCAMM, CR-INSTM Unità della Calabria, Dipartimento di Chimica e Tecnologie Chimiche, Università della Calabria, Via P. Bucci Cubo 14C, Italy. E-mail: d.pucci@unical.it; Fax: +39 0984 492066*
[b]*Institute on Membrane Technology, National Research Council of Italy, ITM-CNR, c/o University of Calabria, Via P. Bucci, cubo 17/C, 87030 Rende (CS), Italy*
†Electronic supplementary information (ESI) available: UV spectra and confocal images of Zn(II) complexes. See DOI: 10.1039/c3dt50513h

for its limited use as a therapeutic agent[18–20] is overcome after coordination to the Zn(II) ion, leading to a highly stable species of increased biological activity with respect to the commercial curc precursor.

Moreover, the intrinsic fluorescence of these curcumin-based Zn(II) compounds enabled a detailed investigation of their interaction with DNA through a new optical method, suggesting a partial inter-base intercalation.[16]

Being convinced that these photoactive complexes may be used also as theragnostic agents,[21] we are reporting here an extension of this work with the aim to explore the role played by each single structural unit of the model molecule A on the cytotoxic activity. Therefore, keeping the Zn(II)-curcumin fragment, we have alternatively changed the nature of the complementary chloride ligand or of the main nitrogen ligand. Therefore, we have investigated the cytotoxic effects of the newly synthesized Zn(II) curcumin-based complexes **1–5** (Fig. 2) on human neuroblastoma cell line SH-SY5Y, in a biohybrid membrane system, able to support cell adhesion, proliferation and differentiation.[22–24] In particular, a polycaprolactone membrane system was used as an *in vitro* platform for creating a permissive environment for the cell growth. This membrane system, due to its selective physico-chemical, morphological and permeability properties, ensures a highly controlled microenvironment at the molecular level for cell culture being thus a valuable tool for *in vitro* testing.[24] In an attempt to explore how these Zn(II) complexes can induce apoptosis and necrosis in SH-SY5Y cells, the cellular viability and apoptosis have been analyzed at various concentrations, through activation of N-terminal c-Jun protein kinase (JNK), caspase-3, changes in mitochondrial membrane potential (MMP) and expression of Annexin V and propidium iodide.

Results and discussion

Synthesis and characterization

The first structural change around the general framework of **A** concerned the variation of the complementary ligand filling the coordination sphere of the Zn(II) centre. This change has been made by using alternately two zinc salts in the reaction with curcumin and the nitrogen ligand, containing anions of different coordinating ability, in order to modulate both the geometry and the electrostatic nature of the resulting Zn(II) complexes. In particular, a slight excess of zinc tetrafluoroborate or zinc sulfate reacts with the main bpy-9 ligand at room temperature, giving rise, in good yields, to the corresponding Zn(II) precursors **I** and **II**. The strong band centered at 1058 cm^{-1} observed in the IR spectrum of **I** is compatible with a structure in which the tetrafluoroborate acts as counterion while the presence of three bands, centered at 1024, 1090 and 1144 cm^{-1} and the neutral character, established by conductivity measurements performed in CH_2Cl_2 solution, led us to assume that in **II** the sulfate group acts as a μ_2-bridging ligand, connecting two Zn(II) ions to form a dimer, as already observed in the case of the 2,2′-bipyridine analogous.[25]

The final Zn(II) complexes **1–2** were then obtained in good yield (80–90%) through reaction of **I** and **II** with one equivalent of purified curc[26] in the presence of triethylamine, in dichloromethane, at room temperature (Scheme 1). In the IR spectra, the carbon–oxygen band typical of the free curc is shifted from 1625 cm^{-1} to 1606 cm^{-1} (**1**) and 1589 cm^{-1} (**2**), and the broad band due to the H-bonded enol proton in the region of 2600–3800 cm^{-1} is completely absent, confirming that the coordination of curc to the Zn(II) ion took place. In the ^{1}H-NMR spectra of **1–2**, the lack of the intramolecular hydrogen bonded enolic proton of the curc, validates the Zn(II) coordination to the curc ligand and the intensities of the signals are in agreement with a 1 : 1 : 1 metal-to-N,N ligand-to-curc stoichiometry. Depending on the coordinating ability of the ancillary ligand, the ionic or neutral character of the precursors **I–II** are preserved in the corresponding Zn(II) curcumin derivatives. Moreover, TGA analysis indicates a monomeric structure with the Zn(II) ion in a tetracoordinated environment.

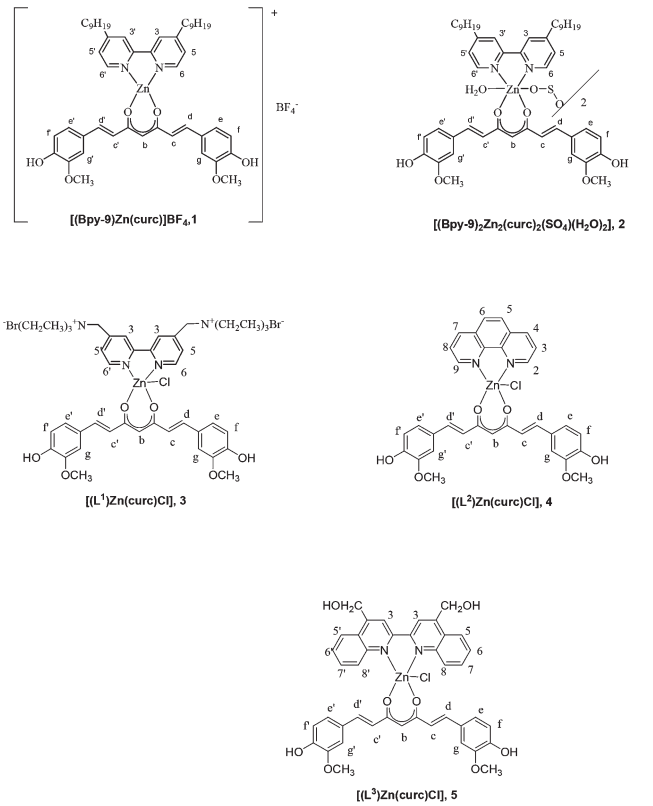

Fig. 2 Molecular formula of complexes **1–5**.

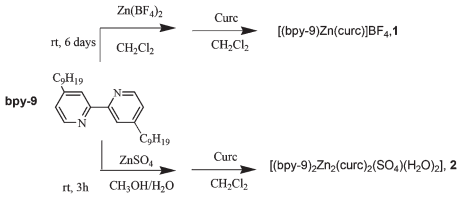

Scheme 1 Synthesis of complexes **1** and **2**.

On the contrary, the neutral character found in dichloromethane solution for **2** and the characteristic bands of the sulfate anion at 1284, 1121 and 1032 cm^{-1} in the IR spectrum suggest that the sulfate is coordinated in a bridging fashion between two Zn(II) ions. TGA analysis of **2** revealed a desolvation process of two molecules of water (experimental mass loss = 2%) in a broad range of temperature around 100 °C, corresponding to a large transition peak in the DSC (23.17 kJ mol^{-1}). This is consistent with the presence of one solvent molecule coordinated to each Zn(II) centre thus achieving an overall six-coordination (Fig. 2).

The photophysical behavior of **1–2** has been investigated by UV/VIS spectroscopy in ethanol solution where they exhibit strong absorption bands in the range 293–430 nm. In order to test their stability in solution, absorption measurements have also been conducted over time and in physiological pH conditions. In contrast with the consistent degradation observed for the free curc ligand,[20] the Zn(II) complexes **1** and **2** show a good stability because both the shape and the absorption maximum positions remain unchanged after 24, 48 and 96 h (see ESI†). Moreover, **1–2** preserve the luminescence characteristic of the curcumin molecule, being emissive in ethanol (549 and 553 nm, respectively ESI†) with photoluminescence quantum yields higher (Φ = 0.076 **1**; 0.073 **2**) than that of free curc (Φ = 0.033).[20]

Very interestingly, the ionic character of **1** allows a drastic improvement of the solubility properties with respect to both the neutral compounds **2** and **A**.

The second synthetic approach used in this work has been based on the change of the main N,N chelating ligand in the molecular structure of the model compound **A**. Thus three different nitrogen ligands with an increasing number of aromatic rings have been used in coordination with the Zn(II) ion (Fig. 3). In the case of 4,4′-bis(triethylaminobromide)-2,2′-bipyridine ($\mathbf{L^1}$)[27] electrostatic interactions through the nature of the terminal groups on the chelating ligand have been introduced. Alternatively, to enhance the intercalating attitude of the N,N moiety, an increase of aromaticity and rigidity of the nitrogen ligand has been introduced with the use of 1,10-phenanthroline $\mathbf{L^2}$ or 4,4′-bis(hydroxymethyl)-2,2′-biquinoline[28] $\mathbf{L^3}$.

Three new curcumin based Zn(II) complexes, **3–5**, were prepared starting from the dichloro precursors **III–V** in turn synthesised from the appropriate N,N chelating ligand (Scheme 2). The structures of all complexes have been assigned on the basis of elemental analysis, IR and ^{1}H NMR spectroscopy. Conductivity measurements indicate the neutral nature of all

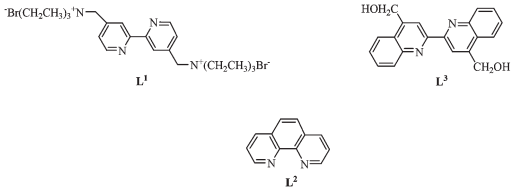

Fig. 3 Drawing of the ligands used in this work.

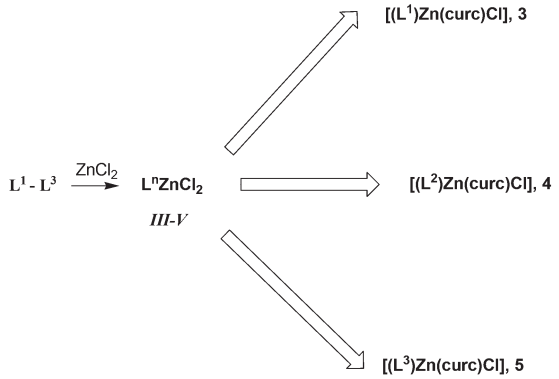

Scheme 2

Zn(II) compounds, also in solution, leading to assuming a penta-coordination of the Zn(II) ion, with two chelating units, the N,N and the O,O-curcumin ligands, and an apical chloride ion, with a molecular structure similar to that of the analogous bipyridine reference complex **A**.[16]

The UV-vis spectra of complexes **3–5**, recorded in DMSO solution, are very similar among them and to that of the reference complex **A**. They all exhibit strong absorption in the UV-vis region, with absorption maxima in the range 408–450 nm and they are all found to be emissive, in DMSO solution, with fluorescence maxima between 534 and 545 nm and photoluminescence quantum yields of about 7%, similar to complexes **1** and **2**.

Even in the case of complexes **3–5**, the absorption measurements are also conducted under physiological pH conditions over time, proving the good stability of these systems after 24 and 48 h. However, in terms of solubility they behave in the same way as the model analogous to **A**.

Biological evaluation

The biological activity of the all new Zn(II) complexes **1–5** has been evaluated by investigating the viability of human neuroblastoma cell line SH-SY5Y, incubated with various concentrations of the compounds. On the basis of the confocal images of cells treated with the Zn(II) curcumin based complexes, which are fluorescent, the complexes were uptaken by cells and principally localised into the nucleus of cells at the nucleoli level (see ESI†).

Even if the free ligands do not exhibit toxic effects,[16] all complexes show a dose-dependent effect on the viability of cells incubated for 24 and 48 h, as evidenced in Fig. 4. The percentage of metabolically active cells decreases with the increase of administered Zn(II) complex concentration.

However, a significant decrease of cell viability has been detected already at low concentrations, especially in the presence of complexes **1** and **4**. Both compounds show a relevant cytotoxicity with an IC50 of 7.9 and 8.8 μM after 24 h, respectively while complexes **A**, **2**, **3** and **5** exhibit 50% of toxicity at higher concentrations, but always in the range of 10–30 μM

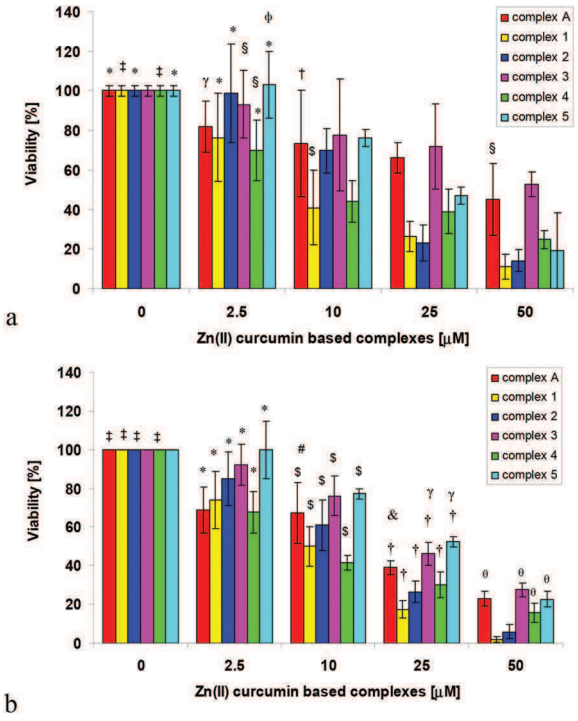

Fig. 4 Changes in the cell viability of SHSY5Y cells after 24 h (a) and 48 h (b) of treatment with various concentrations of Zn(II) complexes **A**, **1**, **2**, **3**, **4** and **5**. The results are expressed as a percentage of control and as average ± standard deviation. Data statistically significant according to ANOVA followed Bonferroni *t*-test. **p* < 0.05 *vs.* 10, 25 and 50 μM of the same compound; ‡*p* < 0.05 *vs.* all concentrations of the same compound; $*p* < 0.05 *vs.* 25 and 50 μM of the same complex; †*p* < 0.05 *vs.* 50 μM of the same complex; §*p* < 0.05 *vs.* complexes **1**, **2**, at the same concentration; γ*p* < 0.05 *vs.* complexes **1**, **2** and **4** at the same concentration; ϕ*p* < 0.05 *vs.* complex **2** at the same concentration; #*p* < 0.05 *vs.* complex **4** at the same concentration; &*p* < 0.05 *vs.* complex **1** at the same concentration; θ*p* < 0.01 *vs.* complexes **1** and **2** at the same concentration.

Table 1 IC50 values of Zn(II) curcumin based complexes calculated on average values of % inhibition at various molecule concentrations

Complexes	IC50 μM (24 h)	IC50 μM (48 h)
A	24.36	11.79
1	7.90	7.55
2	14.66	11.28
3	30.08	19.31
4	8.75	6.84
5	18.85	20.33

concentrations (Table 1). The activity of complexes **1** and **4** at low concentrations is also remarkable after 48 h of treatment.

On the basis of these results, complexes **1** and **4** seem to be the most interesting candidates for anti-proliferative treatment. For this purpose we decided to investigate the cells progressing according to their Annexin V and propidium iodide staining pattern, in order to evaluate whether the cell response is due to apoptotic or necrotic mechanisms. Early apoptotic cells bind Annexin V but are not sensitive to intracellular staining with propidium iodide. This process is followed by changes in cell morphology and ultimate cell death.

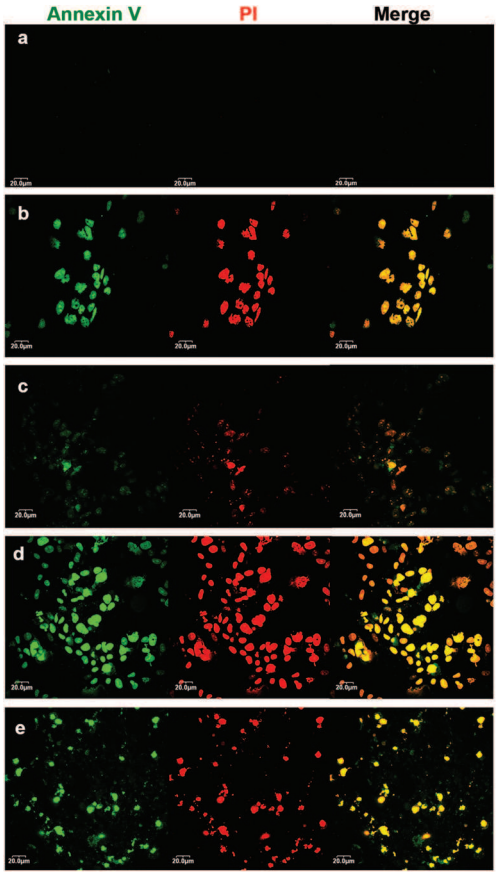

Fig. 5 LSCM images of SHSY5Y cells stained with Annexin V-FITC and PI after 24 h of culturing under: normal conditions (a); treatment with Zn(II) complex **1** at 8 μM (b) and 25 μM (d); treatment with Zn(II) complex **4** at 8 μM (c) and 25 μM (e).

As cells progress through apoptosis, the integrity of the plasma membrane is lost, allowing PI to penetrate and label the cells with a strong yellow–red fluorescence (Fig. 5b–e). The induced apoptosis effect of Zn(II) complexes **1** and **4**, at two different concentrations, on human neuroblastoma cells were evaluated in order to determine if cells are viable, apoptotic, or necrotic through differences in plasma membrane integrity and permeability. Cells treated with complexes **1** and **4** expressed both PI and bind Annexin V, as we can see from Fig. 5. The percentage of Annexin V and PI- positive cells markedly increased when cells were treated with high concentration of the Zn(II) complexes (Fig. 5d and e). A peak of fluorescence intensity for Annexin V and propidium iodide was detected after treatment with complexes **1** and **4** at concentration of 25 μM, and in particular with complex **1**, as result of the apoptosis induction (Fig. 5d).

Quantitative analysis of fluorescence intensity confirmed the effective increase of Annexin V and PI-positive cells after the treatment with Zn(II) complexes, at concentration of 25 μM especially when complex **1** was administered (Fig. 6).

In order to understand the molecular mechanism underlying the apoptotic effect, we investigated the activation of JNK, caspase 3 and changes in MMP.

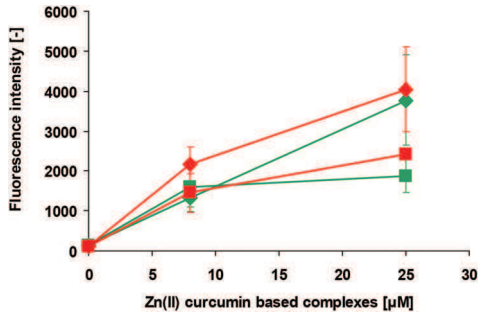

Fig. 6 Fluorescence intensity of Annexin V (green) and PI (red) of complexes **1** (rhomb) and **4** (square) (f).

Activation of the JNK pathway is essential for apoptosis. Complexes **1** and **4** stimulated the activation of JNK that occurs through phosphorylation. The phosphorylated JNK (p-JNK) is localised in the perinuclear region and into the nucleus of cells as demonstrated by LSCM images (Fig. 7a and b). This localisation is the result of its migration from cytoplasm and subsequent translocation occurred after activation. High percentage of p-JNK positive cells (88–92%) are found in cells treated with complexes **1** and **4** at a concentration of 25 μM (Fig. 7e). JNK signaling is involved in the extrinsic apoptotic pathway initiated by death receptors as well as the intrinsic pathway initiated by mitochondrial events.[29] JNK plays an essential role through its ability to interact and modulate the activities of diverse pro- and anti-apoptotic proteins in response to both the extrinsic and intrinsic apoptotic stimuli. In order to evaluate if the apoptosis is induced by Zn(II) complexes *via* a mitochondria-dependent apoptotic pathway, we investigated the effect of **1** and **4** at different concentrations on mitochondrial membrane potential changes.

In the normal cells, JC-1 exists as a monomer in the cytosol (green) and also accumulates as aggregates (red) in the mitochondria induced by higher mitochondrial membrane potential (Fig. 8) whereas, in apoptotic cells, JC-1 exists in monomeric form and stains the cytosol green. The fluorescent intensity ratio value of JC-1 in SHSY5Y cells decreased with the addition of both Zn(II) complexes **1** and **4** in a dose dependent manner, indicating significant loss of membrane potential.

To further investigate the underlying signaling mechanisms of Zn(II) complexes-induced apoptosis, we monitored the expression of caspase-3, which is activated during apoptosis of multiple cell types triggered by various stimuli. As expected a strong activation of caspase-3 was relieved after treatment with complexes **1** and **4** at a concentration of 25 μM (Fig. 7c and d). As shown in Fig. 7e, complex **1** induced a nearly six fold increase of percentage of caspase-3 positive cells when compared with the control, demonstrating its ability to trigger the execution-phase of cell apoptosis. The cysteine protease, which is proteolytically activated by cleavage of pro-caspase-3 by caspase-8, cleaves several intracellular proteins. This process is a very rapid process and occurs almost simultaneously with a depolarization of the mitochondrial membrane potential,

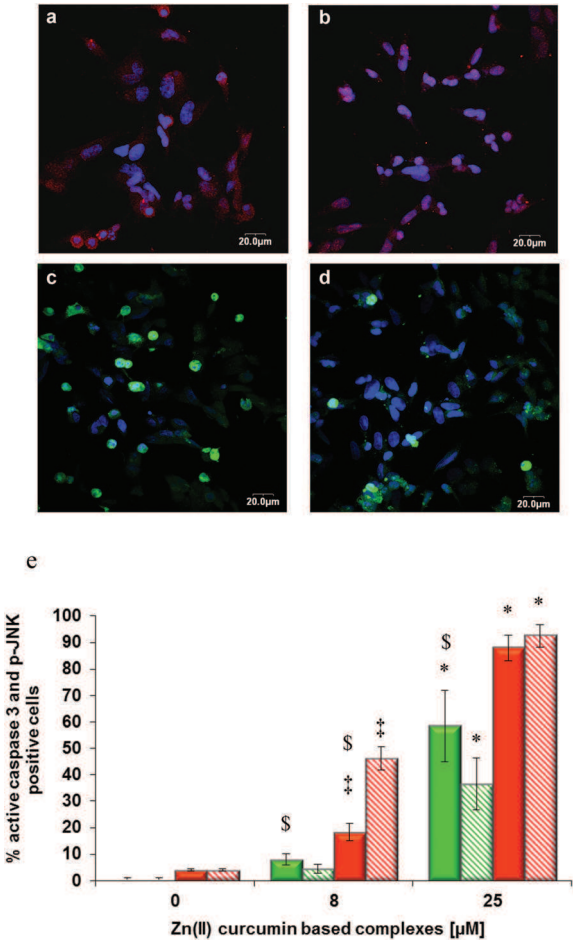

Fig. 7 Merged LSCM images confirmed (a–b) p-JNK (red) and active caspase-3 (green) (c–d) expressing cells after treatment with Zn(II) complex **1** (a–c) and **4** (b–d). (e) Percentage of positive cells expressing active caspase 3 (green bars) and p-JNK (red bars) after treatment of complex **1** (full bar) and 4 (dashed bar). Data statistically significant according to ANOVA followed Bonferroni *t*-test. *$p < 0.05$ *vs.* control and 8 μM of the same compound; ‡$p < 0.05$ *vs.* control; \$$p < 0.002$ *vs.* complex **4** at the same concentration.

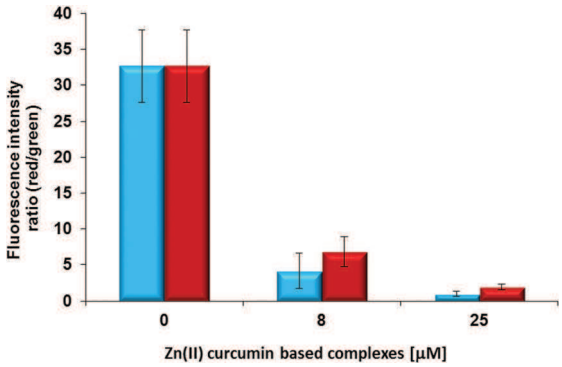

Fig. 8 Mitochondrial membrane potential (MMP) in cells treated with different concentrations of complexes **1** (azure bar) and **4** (red bar) measured with potential-sensing fluorescence probe JC-1. The fluorescence intensity of both mitochondrial JC-1 monomers (λ_{ex} 514 nm, λ_{em} 529 nm) and aggregates (λ_{ex} 585 nm, λ_{em} 590 nm) was measured and the MMP was calculated as the fluorescence ratio of red to green. Data statistically significant according to ANOVA followed Bonferroni *t*-test. *$p < 0.05$ *vs.* control; ‡$p < 0.05$ *vs.* complex **4** at the same concentration.

which is rapidly followed by changes in cell morphology and ultimate cell death.

The obtained results indicate that complexes **1** and **4** are upstream activators of JNK, which possibly controls downstream events, such as loss of mitochondrial membrane potential and caspase-3, to trigger apoptotic processes in the treated cells.

Conclusions

The synthesis and characterization of five new heteroleptic Zn(II) curcumin based complexes have been achieved.

Structural changes have been made starting from the reference complex [(bpy-9)Zn(curc)Cl], **A**, in order to introduce new functionalities, such as electrostatic and/or covalent interactions. In particular, keeping the same N,N chelating ligand, namely bpy-9, two completely different Zn(II) species have been obtained by changing the chloride ligand with tetrafluoroborate and sulfate anions. In the first case, the ionic derivative $[(bpy\text{-}9)Zn(curc)]BF_4$, **1**, has been obtained, while with the use of the sulfate ion acting as a bridging group through two Zn(II) centre, a dimeric neutral derivative $[(Bpy\text{-}9)_2Zn_2(curc)_2(SO_4)(H_2O)_2]$, **2**, has been isolated. Moreover, by changing the N,N chelating unit, $[(L^n)Zn(curc)Cl]$, complexes (**3–5**), in which the Zn(II) ion shows the same pentacoordination seen in the precursor complex **A**, have been synthesized with the intention to introduce both electrostatic interactions at the periphery level of the neutral molecule and enhance the possible intercalating attitude of the N,N moiety, through an increase of the aromaticity and rigidity of the nitrogen ligand. All new Zn(II) derivatives have been fully characterized both in the solid and solution state, showing great stability in aqueous medium even in physiological conditions and, in the case of the ionic derivative **1** better solubility in hydrophilic solvents, with respect to the new neutral derivatives as well as the reference complex **A**.

In order to investigate the possible effects obtained by the structural changes performed around the Zn(II)-curcumin fragment, the biological activity of all new complexes **1–5** has been evaluated by investigating the viability of human neuroblastoma cell line SH-SY5Y cultured in a biohybrid membrane system, able to support cell adhesion, proliferation and differentiation, incubated with various concentrations of the Zn(II) compounds.

All the new derivatives exhibit significant cytotoxic activity, showing IC50 values of micromolar order, in most cases superior with respect to the reference compound [(bpy-9)Zn(curc)Cl], A, already reported. Interestingly, two complexes, $[(bpy\text{-}9)Zn(curc)]BF_4$ (**1**) and $[(L^2)Zn(curc)]$ (**4**) have higher cytotoxicity, probably caused by the ionic character inducing better solubility properties in the case of **1**, or by the broadening aromatic zone of **4**, which is the requisite for a drug to act as a good intercalator. On the basis of these results, in order to evaluate whether the cell response is due to apoptotic or necrotic mechanisms, in the case of complexes **1** and **4**, the cells progressing according to their Annexin V and propidium iodide staining pattern have been investigated. Since a peak of fluorescence intensity for Annexin V and propidium iodide was detected after treatment with complexes **1** and **4** at concentrations of 25 μM, and in particular with complex **1** we can conclude that this is an evidence of the apoptosis induction. Additionally, the investigation of apoptotic markers indicates that complexes **1** and **4** induce cell apoptosis through a molecular mechanism involving the activation of JNK, caspase-3 and changes in MMP.

Concluding, the substitution of single building blocks around the Zn(II) curcumin fragment results in a concrete strategy in order to obtain more performing and even more promising emissive species to be used as highly active theragnostic agents.

Experimental section

Materials and measurements

All commercially available starting materials were used as received without further purification while the curcumin ligand was used after separation into individual components by silica gel chromatography.[26] ^1H NMR spectra were acquired on a Bruker Avance DRX-300 spectrometer in $CDCl_3$ solution, with TMS as internal standard. Infrared spectra were recorded with a Spectrum One FT-IR Perkin-Elmer spectrometer. Elemental analyses were performed with a Perkin-Elmer 2400 microanalyzer by the Microanalytical Laboratory at University of Calabria. Conductivity measurements were performed in dichloromethane and acetone, with an InoLab Cond Level 1-720 conductometer equipped with a LR 325/001 immersion cell. Spectrofluorimetric grade solvents were used for the photophysical investigations in solution, at room temperature. A Perkin Elmer Lambda 900 spectrophotometer was employed to obtain the absorption spectra. Steady-state emission spectra were recorded on a HORIBA Jobin-Yvon Fluorolog-3 FL3-211 spectrometer equipped with a 450 W xenon arc lamp, double-grating excitation and single-grating emission monochromators (2.1 nm mm^{-1} dispersion; 1200 grooves per mm), and a Hamamatsu R928 photomultiplier tube. Emission and excitation spectra were corrected for source intensity (lamp and grating) and emission spectral response (detector and grating) by standard correction curves. Emission quantum yields were determined using the standard $Ru(bpy)_3Cl_2$.

Synthesis

$[(bpy\text{-}9)Zn(curc)](BF_4)$, 1. 4,4′-Dinonyl-2,2′-bipyridine (0.50 g, 1.22 mmol) was dissolved in dichloromethane (20 ml) and then $Zn(BF_4)_2$ (0.435 g, 1.83 mmol) was added. The reaction mixture was stirred for 6 days, was filtered on Celite and the solvent evaporated *in vacuo.* 332 mg (0.54 mmol) of this intermediate product, **I**, recrystallized by CH_3Cl/Et_2O was then dissolved in CH_2Cl_2 (10 ml) and added to a red solution obtained by dissolving 200 mg (0.54 mmol) of curcumin and triethylamine (54.64 mg, 0.54 mmol) in CH_2Cl_2 (10 ml), under

nitrogen. The resulting orange solution was stirred under nitrogen for 3 days at room temperature. The solvent was evaporated *in vacuo* and then the product was recrystallized from petroleum ether to give a red solid in a 91% yield. Mp 103 °C. IR (ν_{max}/cm^{-1}): 3426 (–OH curc), 2925, 2853 (C–H aliphatic), 1626 (C═C), 1606 (C═O), 1587 (C═N), 1514 (C–C–C chelated ring) 1058–1015 (B–F). ^{1}H-NMR (300 MHz, $CDCl_3$): δ_H, 8.05 (s, 2H, $H_{6,6'}$), 7.89 (d, 2H, J = 5.3 Hz, $H_{3,3'}$), 7.59 (d, 2H, J = 15.6 Hz, $H_{c,c'}$), 7.47 (d, 2H, J = 4.6 Hz, $H_{5,5'}$), 7.11 (d, 2H, J = 6.58 Hz, $H_{e,e'}$), 7.05 (d, 2H, $H_{g,g'}$), 6.92 (d, 2H, J = 8.23 Hz, $H_{f,f'}$), 6.47 (d, 2H, J = 7.7 Hz, $H_{d,d'}$), 5.80 (s, 2H, $H_{b,b'}$), 3.92 (s, 6H, OCH_3), 2.78 (t, 4H, J = 8.0 Hz, $CH_2(CH_2)_7CH_3$), 1.67 (m, 4H, CH_2CH_3), 1.33 (m, 24H, $(CH_2)_6CH_3$), 0.86 (t, 6H, J = 6.6 Hz, CH_3). Anal. Calc. for $C_{49}H_{63}O_6N_2ZnBF_4$: C, 63.40; H, 6.82; N, 3.01%. Found: C, 62.95; H, 7.02; N, 2.98%. UV-vis (EtOH) λ_{max} (ε, M^{-1} cm^{-1}): 293 nm, 304 nm, 429 nm; λ_{em} = 549 nm.

[(bpy-9)$_2$Zn$_2$(curc)$_2$(SO$_4$)(H$_2$O)$_2$], 2. A solution of 4,4′-dinonyl-2,2′-bipyridine (500 mg, 1.22 mmol) in MeOH (20 ml) was added to a solution of $ZnSO_4{\cdot}7H_2O$ (544 mg, 1.83 mmol) in water (5 ml). After stirring for 3 h, the white solid formed, **II**, was filtered and washed in Et_2O to give the pure product in a 77% yield. Mp 158 °C. IR (ν_{max}/cm^{-1}): 3346 (OH), 2926, 2853 (CH), 1618 (C═C), 1561 (C═N), 1144, 1090, 1024 (S═O). ^{1}H NMR (300 MHz, $CDCl_3$): δ_H, 8.88 (d, 2H, J = 5.3 Hz, $H_{6,6'}$), 8.45 (s, 2H, $H_{3,3'}$), 7.60 (d, 2H, J = 5.3 Hz, $H_{5,5'}$), 4.92 (m, 4H, $CH_2(CH_2)_7CH_3$), 1.77 (m, 4H, CH_2CH_3), 1.38 (m, 24H, $(CH_2)_6CH_2CH_3$), 0.88 (t, 6H, J = 6.6 Hz, CH_3). 200 mg (0.54 mmol) of curcumin were dissolved in dichloromethane (10 ml) and to the resulting orange solution was added triethylamine (54.64 mg, 0.54 mmol), under nitrogen. Once the solution color changed to red a dichloromethane solution (10 ml) of precursor **II** (332 mg, 0.54 mmol) was added and the reaction mixture was stirred under nitrogen for 5 days, at room temperature. The solvent was evaporated *in vacuo* and the product crystallized from petroleum ether to give a deep orange waxy solid in a 84% yield. Mp 108 °C. IR (ν_{max}/cm^{-1}): 3391 (–OH curc), 2924, 2852 (C–H aliphatic), 1622 (C═C), 1589 (C═O), 1561 (C═N), 1511 (C–C–C chelate ring) 1159–1123 (S═O). ^{1}H NMR (300 MHz, $CDCl_3$): δ_H, 9.37 (d, 2H, J = 5.1 Hz, $H_{6,6'}$), 7.84 (s, 2H, $H_{3,3'}$), 7.56 (d, 2H, J = 15.78 Hz, $H_{d,d'}$), 7.00 (d, 4H, J = 11.39 Hz, $H_{e,e',g,g'}$), 6. 45 (d, 2H, J = 15.8 Hz, $H_{c,c'}$), 5.77 (s, 1H, H_b), 3.91 (s, 6H, OCH_3), 2.68 (t, 4H, J = 7.6 Hz, $CH_2(CH_2)_7CH_3$), 1.64 (m, 4H, CH_2CH_3), 1.26 (m, 24H, $(CH_2)_6CH_3$), 0.86 (t, 6H, J = 6.6 Hz, CH_3). Anal. Calc. for $C_{98}H_{126}N_4O_{16}Zn_2(SO_4)$: C, 65.04; H, 6.97; N, 3.01%. Found: C, 65.69; H, 7.76; N, 3.89%. UV-vis (EtOH) λ_{max} (ε, M^{-1} cm^{-1}): 293 nm, 304 nm, 430 nm; λ_{em} = 553 nm.

[(L^1)Zn(curc)(Cl)], 3. 1.5 equiv. of $ZnCl_2$ (63 mg, 0.46 mmol) was added to a solution of L^1 (150 mg, 0.31 mmol) in water (20 ml). After stirring for 48 h (r.t.) the suspension was filtered and the white solid, **III**, was washed with ethanol (77% yield). M.p. 265 °C. IR (ν_{max}/cm^{-1}): 2978 (C–H aliphatic), 1618 (C═C), 1563 (C═N), 3065 (C–H aromatic). ^{1}H-NMR (300 MHz, D_2O): δ_H, 8.99 (br s, 2H, $H_{6,6'}$), 8.65 (s, 2H, $H_{3,3'}$), 8.0 (d, 2H, $H_{5,5'}$, J(H,H) = 4.46 Hz), 4.76 (s, 4H, CH_2N), 3.22 (m, 12H, CH_2CH_3), 1.41 (t, 18H, J(H,H) = 7.06 Hz, CH_3). Anal. Calc. for $C_{24}H_{40}N_4Br_2ZnCl_2$: C, 42.33; H, 5.92; N, 8.26%. Found: C, 42.17; H, 5.74; N, 8.05%. UV/Vis (H_2O): λ_{max} (ε, M^{-1} cm^{-1}): 237 (11 676), 288 nm (14 838); λ_{em}: 335 nm.

An orange solution curc (16 mg, 0.043 mmol) in MeOH (3 ml) was added to triethylamine (4.2 mg, 0.043 mmol) under nitrogen at room temperature. After ten minutes the resulting red solution was added to a solution of **III** (30 mg, 0.043 mmol) in water (1 ml). The resulting yellow–orange suspension was stirred under nitrogen (24 hours, r.t.) and after filtration, the dark orange solid was washed with water and MeOH (62% yield). M.p. 275 °C. IR (ν_{max}/cm^{-1}): 3400 (OH), 1617 (C═O), 1590 (C═N), 1510 (C–C–C– chelate ring). ^{1}H NMR (300 MHz, DMSO-d_6): δ_H, 9.47 (br s, 1H, H_6), 8.85 (s, 2H, $H_{5,5'}$), 8.56 (s, 2H, $H_{3,3'}$), 7.62 (s, 1H, $H_{6'}$), 7.40 (d, 2H, $H_{d,d'}$, J(H,H) = 15.6 Hz), 7.24 (s, 2H, $H_{g,g'}$), 7.06 (s, 2H, $H_{e,e'}$), 6.77 (d, 2H, $H_{f,f'}$, J(H,H) = 7.8 Hz), 6.65 (br s, 2H, $H_{c,c'}$), 5.60 (br s, 1H. H_b), 4.63 (s, 4H, –CH_2N), 3.80 (s, 6H, –OCH_3), 3.23 (m, 12H, CH_2CH_3), 1.33 (m, 18H, –CH_3). Anal. Calc. for $C_{45}H_{59}N_4O_6ZnClBr_2$: C, 53.31; H, 5.86; N, 5.55. Found: C, 53.03; H, 5.65; N, 5.38%. UV/Vis (DMSO): λ_{max} (ε, M^{-1} cm^{-1}): 293 (9727); 342 nm (6478), 382 nm (6897), 406 nm (22 774), 430 nm (35 344), 452 nm (32 139); λ_{em}: 534 nm.

[(L^2)Zn(curc)(Cl)], 4. 1.5 equiv. of $ZnCl_2$ (567 mg, 4.16 mmol) was added to a solution of L^2 (500 mg, 2.77 mmol) in $CHCl_3$ (50 ml). After stirring for 24 h (r.t.) the white suspension was filtered and the solid **IV** was washed with $CHCl_3$ (90% yield). M.p. > 300 °C. IR (ν_{max}/cm^{-1}): 3048 (C–H aliphatic), 1622 (C═C), 1582 (C═N), ^{1}H NMR (300 MHz, DMSO-d_6): δ_H, 8.86 (4H, d, J(H,H) = 7.33 $H_{4,7}$, $H_{2,9}$), 8.26 (2H, s, $H_{5,6}$), 8.01 (2H, m, $H_{3,8}$). Anal. Calc. for $C_{12}H_8N_2ZnCl_2$: C, 45.54; H, 2.55; N, 8.55%. Found C, 45.12; H, 2.51; N, 8.32%. UV/Vis (DMSO): λ_{max} (ε, M^{-1} cm^{-1}): 294 nm (8889), 314 nm (1866), 326 nm (1471); λ_{em}: 396 nm. An orange solution of curcumin (173 mg, 0.47 mmol) in MeOH (5 ml) was added to triethylamine (47.6 mg, 0.47 mmol) under nitrogen at room temperature, giving rise to a red solution which was added to a solution of **IV** (150 mg, 0.47 mmol) in DMSO (2 ml). The resulting orange suspension was stirred under nitrogen (24 hours, r.t.) and after filtration, the orange solid was washed with MeOH (54% yield). M.p. 240 °C. IR (ν_{max}/cm^{-1}): 3400 (OH), 1625 (C═O), 1589 (C═N), 1513 (C–C–C chelated ring). ^{1}H NMR (300 MHz, DMSO-d_6): δ_H, 9.49 (2H, s, $H_{2,9}$), 8.89 (2H, d, J(H,H) = 7.67 Hz, $H_{4,7}$), 8.27 (2H, s, $H_{5,6}$), 8.14 (2H, s, $H_{3,8}$), 7.50 (2H, s, $H_{d,d'}$), 7.27 (2H, s, $H_{g,g'}$), 7.10 (2H, s, $H_{e,e'}$), 6.78 (2H, d, J(H,H) = 8.11 Hz, $H_{f,f'}$), 6.69 (2H, d, J(H,H) = 15.34 Hz, $H_{c,c'}$), 5.72 (1H, s, H_b), 3.82 (6H, s, OCH_3). Anal. Calc. for $C_{33}H_{27}N_2O_6ZnCl$: C, 61.12; H, 4.19; N, 4.33%. Found C, 61.04; H, 4.15; N, 4.18%. UV/Vis (DMSO): λ_{max} (ε, M^{-1} cm^{-1}): 295 nm (5201), 406 nm (12 925), 432 nm (20 336), 453 nm (18 440); λ_{em}: 545 nm.

[(L^3)Zn(curc)(Cl)], 5. 1.5 equiv. of $ZnCl_2$ (384 mg, 2.82 mmol) was added to a solution of L^3 (700 mg, 1.88 mmol) in acetone (140 ml). After stirring for 24 h (r.t.) the suspension was filtered and the yellow solid was washed with acetone (82% yield). M.p. > 300 °C. IR (ν_{max}/cm^{-1}): 3517 (OH), 3121–3079 (CH aliphatic), 2907 (CH_2), 1614 (C═C). ^{1}H NMR (300 MHz, DMSO-d_6): δ_H, 8.90 (2H, s, $H_{3,3'}$), 8.20 (2H, d,

J(H,H) = 8.07 Hz, $H_{8,8'}$), 8.05 (2H, d, J(H,H) = 7.7 Hz, $H_{5,5'}$), 7.82 (2H, t, J(H,H) = 14.67 Hz, $H_{7,7'}$), 7.67 (2H, t, J(H,H) = 7.34 Hz, $H_{6,6'}$), 5.75 (2H, s, –OH), 5.15 (4H, d, J(H,H) = 4.77 Hz, $-CH_2$). Anal. Calc. for $C_{20}H_{16}N_2O_2ZnCl_2$: C, 53.07; H, 3.56; N, 6.21. Found: C, 53.20; H, 3.30; N, 6.10%. An orange solution of curcumin (100 mg, 0.27 mmol) in MeOH (20 ml) was added to triethylamine (27.4 mg, 0.27 mmol) under nitrogen at room temperature to obtain a red solution which was added to a solution of **V** (122 mg, 0.27 mmol) in DMSO (3 ml). The resulting red suspension was stirred under nitrogen (24 h, r.t.) and after filtration, the red solid was washed with MeOH and water (54% yield). M.p. > 300 °C. IR (ν_{max}/cm^{-1}): 3400 (OH curc), 1619 (C═O), 1590 (C═N), 1510 (C–C–C chelated ring). ^{1}H NMR (300 MHz, DMSO-d$_6$): δ_H, 8.48 (s, 2H, $H_{3,3'}$), 7.82 (d, 2H, $H_{8,8'}$, J(H,H) = 20.54 Hz), 7.71 (d, 2H, $H_{5,5'}$, J(H–H) = 24.95 Hz), 7.48 (t, 2H, $H_{7,7'}$, J(H,H) = 38.51 Hz), 7.28 (t, 2H, $H_{6,6'}$, J(H,H) = 20.72 Hz), 7.20 (br s, 2H, $H_{d,d'}$), 6.95 (br s, 2H, $H_{g,g'}$), 6.81 (br s, 2H, $H_{e,e'}$), 6.61 (br s, 2H, $H_{f,f'}$),6.32 (br s, 2H, $H_{c,c'}$), 5.33 (t, 1H, H_b, J(H,H) = 5.51 Hz), 4.71 (d, 4H, CH_2, J(H,H) = 5.13 Hz), 3.37 (s, 6H, OCH_3). Anal. Calc. for $C_{41}H_{35}N_2O_8ZnCl$: C, 62.76; H, 4.49; N, 3.58%. Found C, 62.45; H, 4.34; N, 3.28%. UV/Vis (DMSO): λ_{max} (ε, M^{-1} cm^{-1}): 313 (17 213), 340 nm (16 372), 430 nm (32 528), 450 nm (29 854); λ_{em}: 540 nm.

Cell culture and treatments

The human neuroblastoma cell line SH-SY5Y (ICLC-IST, Genova, Italy) was cultured in a polycaprolactone (PCL) membrane system in flat configuration, which was prepared by an inverse phase technique, as previously described.[24] Cells were cultured routinely in a 1 : 1 mixture of Ham's F12 (Invitrogen, Milan, Italy) and Minimum Essential Eagle's medium (EMEM) supplemented with 10% (v/v) heat-inactivated FBS (Lonza), 2 mM glutamine, 100 μg ml^{-1} penicillin–streptomycin. Cells were maintained in a 5% CO_2 humidified incubator at 37 °C in 75 cm^2 flasks (PBI international, Milan, Italy). For cell culture experiments, SH-SY5Y were detached by means of Trypsin/EDTA solution (Sigma, Milan, Italy), re-suspended in Ham's F12-EMEM and seeded at a concentration of 2.6 × 10^4 cells cm^{-2} in PCL membrane systems. After 24 h the culture medium was replaced with fresh Ham's F12-EMEM containing various concentration (0–50 μM) of Zn(II) complexes **1–5**.

Cell viability

The cell viability was measured by using the quantitative colorimetric MTT assay, showing the mitochondrial activity of living cells. Cells were incubated at 37 °C under 5% CO_2 humidified air incubator for 72 h. After the first day of culture, the SH-SY5Y cells were treated with various concentrations (0–50 μM) of Zn(II) complexes **1–5**. After treatment the medium was removed and 400 μl of medium, containing 40 μl of MTT solution (5 mg ml^{-1} in PBS), were added to each well and the cells were incubated at 37 °C. After 2 h of incubation at 37 °C, the reaction was stopped by adding 400 μl of lysis buffer (10% SDS, 0,6% acetic acid in DMSO, pH 4.7). The quantity of formazan product was directly proportional to the number of metabolically active living cells. The optical density of each well was spectrophotometrically measured at 570 nm. Results were expressed as the percentage of the control without treatment.

Apoptosis detection

The apoptosis of cells was investigated by Annexin V-Apoptosis detection kit (Santa Cruz Biotechnology) and by investigating the expression of Caspase-3 by using Laser Scanning Confocal Microscope (LSCM). Normal viable cells in culture are negative for Annexin V-FITC and negative for PI. Cells that are induced to undergo apoptosis are positive for Annexin V FITC and negative for PI. Both cells in the later stages of apoptosis and necrotic cells are positive for Annexin V-FITC and PI. Controls and samples treated with the Zn(II) complexes **1–5**, SH-SY5Y cells were rinsed and washed once with 500 μl of 1 × Assay Buffer per well. Following 100 μl of Assay Buffer was added to each well, containing 1 μg of Annexin V-FITC and 10 μl of propidium iodide. After the incubation of cells for 15 min at room temperature in the dark, the fluorescence intensity of Annexin V-FITC and of propidium iodide was evaluated with LSCM. Data were analyzed and expressed as a percentage of the control without H_2O_2 and didymin. For the analysis of active N-terminal c-Jun protein kinase (p-JNK) and caspase-3 expression the SH-SY5Y cells were rinsed with PBS, fixed for 15 min with paraformaldehyde (4%), permeabilized for 10 min with 0.25% Triton X-100 and subsequently blocked for 30 min with 1% BSA at room temperature. p-JNK expression was detected using anti-mouse monoclonal p-JNK antibody (1 : 250; Santa Cruz Biotechnology, CA) over night at 4 °C and anti mouse IgG Cy3-conjugated (1 : 400; Jackson Immunoresearch) for 60 min at room temperature. Caspase-3 expression was detected using rabbit anti-caspase-3 antibody (1 : 250; BD, Milan Italy) over night at 4 °C and goat anti rabbit IgG FITC-conjugated (1 : 100; Invitrogen) for 60 min at room temperature. Nucleic acids were counterstained with DAPI[30] (200 ng ml^{-1}; Sigma, Milan Italy). Images were taken by using LSCM. Mitochondrial membrane potential (MMP) in SH-SY5Y cells was measured using a fluorescent probe, JC-1 (5,5′,6,6′-tetrachloro-1,1′,3,3′-tetraethylbenzimidazolyl-carbocyanine iodide).[31] SH-SY5Y cells were treated with different concentrations of Zn(II) complexes **1** and **4** as above and then incubated with JC-1 staining solution (5 μg ml^{-1}) for 20 min at 37 °C. The fluorescence intensity of both mitochondrial JC-1 monomers (λ_{ex} 514 nm, λ_{em} 529 nm) and aggregates (λ_{ex} 585 nm, λ_{em} 590 nm) were detected by using LSCM. The MMP of SH-SY5Y cells, for each treatment, was calculated as the fluorescence ratio of red to green.

Statistical analysis

The statistical significance of the experimental results was calculated using ANOVA test followed by Bonferroni t-test ($p < 0.05$).

Acknowledgements

Financial support received from the Ministero dell'Istruzione, dell'Università e della Ricerca (MIUR) through the Centro di Eccellenza CEMIF.CAL (CLAB01TYEF) and (PRIN2010-2011 N. 2010LKE4CC) "Building with DNA bricks: A combined experimental, numerical and theoretical study" is gratefully acknowledged. The authors acknowledge also King Abdulaziz City for Science and Technology (KACST), Kingdom of Saudi Arabia for funding the project "Membrane systems in regenerative medicine, tissue engineering and biotechnology" (KACST-ITM 03).

References

1 I. Otto and R. Gust, *Arch. Pharm.*, 2007, **340**, 117.
2 M. J. Hannon, *Pure Appl. Chem.*, 2007, **79**(12), 2243.
3 M. A. Jakupec, M. Galanski, V. B. Arion, C. G. Hartinger and B. K. Keppler, *Dalton Trans.*, 2008, 183.
4 C. A. Bruijnincx and P. J. Sadler, *Curr. Opin. Chem. Biol.*, 2008, **12**, 197.
5 S. H. van Rijt and P. J. Sadler, *Drug Discovery Today*, 2009, **14**, 1089.
6 J. Reedijk, *Eur. J. Inorg. Chem.*, 2009, 1283.
7 G. Sava, A. Bergamo and P. J. Dyson, *Dalton Trans.*, 2011, **40**, 9069.
8 J. A. Drewry and P. T. Gunning, *Coord. Chem. Rev.*, 2011, **255**, 459.
9 Y. Yoshikawa and H. Yasui, *Curr. Top. Med. Chem.*, 2012, **12**, 210.
10 Q. Jiang, J. Zhu, Y. Zhang, N. Xiao and Z. Guo, *BioMetals*, 2008, **22**, 297.
11 J. Tan, B. Whang and L. Zhu, *Bioorg. Med. Chem.*, 2009, **17**, 614.
12 P. F. Liguori, A. Valentini, M. Palma, A. Bellusci, S. Bernardini, M. Ghedini, M. L. Panno, C. Pettinari, F. Marchetti, A. Crispini and D. Pucci, *Dalton Trans.*, 2010, **39**, 4205.
13 C.-Y. Gao, X. Qiao, Z.-Y. Ma, Z-G. Wang, J. Lu, J.-L. Tian, J.-Y. Xub and S.-P. Yan, *Dalton Trans.*, 2012, **41**, 12220.
14 M. Terenzi, G. Fanelli, G. Ambrosi, S. Amatori, V. Fusi, L. Giorgi, V. Turco Liveri and G. Barone, *Dalton Trans.*, 2012, **41**, 4389.
15 S. Anbu, R. Ravishankaran, A. A. Karandeb and M. Kandaswamy, *Dalton Trans.*, 2012, **41**, 12970.
16 D. Pucci, T. Bellini, A. Crispini, I. D'Agnano, P. F. Liguori, P. Garcia-Orduña, S. Pirillo, A. Valentini and G. Zanchetta, *Med. Chem. Commun.*, 2012, **3**, 462.
17 Y. Nakamura, Y. Taruno, M. Sugimoto, Y. Kitamura, H. L. Seng, S. M. Kong, C. H. Nge and M. Chikira, *Dalton Trans.*, 2013, **42**, 3337.
18 P. Anand, A. B. Kunnumakkara, R. A. Newman and B. B. Aggarwal, *Mol. Pharmaceutics*, 2007, **4**, 807.
19 E. Burgos-Moro, J. M. Calderon-Montano, J. Salvador, A. Robles and M. Lopez-Lazaro, *Int. J. Cancer*, 2010, **126**, 1771.
20 K. Indira Priyadarsini, *J. Photochem. Photobiol., C*, 2009, **10**, 81.
21 D. Majumdar, X.-Hong Peng and D. M. Shin, *Curr. Top. Med. Chem.*, 2010, **10**, 1211.
22 L. De Bartolo, M. Rende, S. Morelli, G. Giusi, S. Salerno, A. Piscioneri, A. Gordano, A. Di Vito, M. Canonaco and E. Drioli, *J. Membr. Sci.*, 2008, **325**, 139.
23 S. Morelli, S. Salerno, A. Piscioneri, B.J. Papenburg, A. Di Vito, G. Giusi, M. Canonaco, D. Stamatialis, E. Drioli and L. De Bartolo, *Biomaterials*, 2010, **31**, 7000.
24 S. Morelli, A. Piscioneri, A. Messina, S. Salerno, M. B. Al-Fageeh, E. Drioli and L. De Bartolo, *J. Tissue Eng. Regen. Med.*, 2012, DOI: 10.1002/term.1618.
25 A. Manohar, K. Ramalingam, G. Bocelli, A. Cantoni and J. Serb, *Chem. Soc.*, 2010, **75**(8), 1085.
26 D. Pucci, R. Bloise, A. Bellusci, S. Bernardini, M. Ghedini, S. Pirillo and A. Valentini, *J. Inorg. Biochem.*, 2007, **101**, 1013.
27 W.-Y. Wu, S.-N. Chen and F.-Y. Tsai, *Tetrahedron Lett.*, 2006, **47**, 9267.
28 D. Pucci, A. Crispini, M. Ghedini, E. I. Szerb and M. La Deda, *Dalton Trans.*, 2011, **40**, 4614.
29 S. Elmore, *Toxicol. Pathol.*, 2007, **35**, 495–516.
30 S. Salerno, C. Campana, S. Morelli, E. Drioli and L. De Bartolo, *Biomaterials*, 2011, **32**, 8848.
31 K. Chen, Q. Zhang, J. Wang, F. Liu, M. Mi, H. Xu, F. Chen and K. Zeng, *Brain Res.*, 2009, **1279**, 131–138.

Dalton Transactions

RSC Publishing

PAPER

View Article Online
View Journal | View Issue

Cite this: *Dalton Trans.*, 2013, **42**, 6768

Non-classical anticancer agents: on the way to water soluble zinc(II) heteroleptic complexes†

Barbara Sanz Mendiguchia,[a] Daniela Pucci,*[a] Teresa F. Mastropietro,[a] Mauro Ghedini[a] and Alessandra Crispini*[b]

Received 6th February 2013,
Accepted 18th February 2013

DOI: 10.1039/c3dt50367d

www.rsc.org/dalton

Two new heteroleptic Zn(II) complexes of the 4,4′-bis(hydroxymethyl)-2,2′-bipyridine have been synthesized by using different stoichiometric ratios of tropolone. In an attempt to induce the formation of metal complex co-crystals, liquid assisted solid state reaction followed by solvent crystallization has been conducted by using the new Zn(II) tropolonate derivatives **1** and **2** with saccharin. The novel Zn(II) species obtained exhibits different structures and properties with respect to their precursors, due to a hydrogen exchange between saccharin and the tropolonate coordinated ligand.

New metal-based therapeutics are continuously proposed as effective alternatives to antitumor agents currently used in chemotherapy, with the intention to overcome toxicity and drug-resistance phenomena typical of platinum-based anticancer drugs.[1] In the field of non-classical anticancer agents, Zn(II) derivatives have proved to be potential anticancer agents with low *in vivo* toxicity and perhaps new modes of action and cellular targets with respect to the classical metallodrugs.[2] However, the limited solubility of neutral metal-based drugs, which often imply low bioavailability, together with toxic side effects and resistance, represent major limitations on their effective use.[3] Traditional strategies to affect the solubility of drugs have been mainly based on the transformation of the active pharmaceutical ingredient (API) into the corresponding salts by using pharmaceutically acceptable salt formers.[4] Recently, taking advantage of supramolecular synthesis, the formation of pharmaceutical "multicomponent molecular crystals" (co-crystals) is becoming a new frontier in the improvement of properties such as dissolution rate, solubility, thermal and hydration stability or compressibility.[5] The formation of a co-crystal implies an API and one or more pharmaceutically acceptable molecules (coformers), assembled by means of complementary types of interactions, including hydrogen bonds, π-stacking and van der Waals forces. Saccharin has been used in the past as both a salt former (an acid) in conjunction with APIs bearing ionizable groups and as a coformer in the formation of co-crystals containing APIs of sufficiently low basicity.[6]

Although the formation of inorganic co-crystals is considered unfavourable since the two components show different geometries and therefore do not possess similar lattice packing forces, some examples have been reported up to now.[7] This approach could be in principle used in the generation of co-crystal metal-based drugs, when inorganic complexes are co-crystallized with pharmaceutically acceptable molecules.

Our recent works have focused on the synthesis of new biologically active neutral complexes containing two different chelating organic frameworks tethered to the Zn(II) ion: an aromatic *N*,*N* ligand (disubstituted-2,2′-bipyridines) and biologically active *O*,*O* ligands (tropoloids, 1-phenyl-3-methyl-4-*R*-5-pyrazolones, curcumin), both able to induce synergistic effects in the resulting derivatives.[2c,8] All of these complexes suffer scarce solubility in water, therefore some of these systems can be used as probes in the formation of inorganic co-crystals/salts. In this paper we report the use of two Zn(II) derivatives of the general formula [(bpy-OH)Zn(Trop)Cl] (**1**) and [(bpy-OH)Zn(Trop)$_2$] (**2**), in reaction with an organic molecule (saccharin) in order to promote the formation of salts and/or co-crystals metal systems. Although in both cases the formation of co-crystals has not been reached neither by solid state reaction nor by solution methods, new Zn(II) derivatives **1a** and **2a** have been isolated due to a hydrogen exchange between saccharin and the tropolonate coordinated ligand. The structural changes induced by this ligand exchange around the Zn(II) coordination sphere are responsible for the enhancement of the stability and solubility of the new adducts with respect to the precursors, possibly keeping similar biological activities.

[a]*Centro di Eccellenza CEMIF.CAL, LASCAMM CR-INSTM and Laboratorio Regionale Licryl, CNR-INFM, Dipartimento di Chimica, Università della Calabria, 87030 Arcavacata di Rende (CS), Italy. E-mail: d.pucci@unical.it*

[b]*Centro di Eccellenza CEMIF.CAL, LASCAMM CR-INSTM, Dipartimento di Chimica, Dipartimento di Scienze Farmaceutiche, Università della Calabria, Italy. E-mail: a.crispini@unical.it*

†Electronic supplementary information (ESI) available: Water-solubility and hygroscopicity results; PXRD patterns of **2** and **2a**. CCDC 901447–901448; 922725–922726. For ESI and crystallographic data in CIF or other electronic format see DOI: 10.1039/c3dt50367d

Experimental section

Materials and methods

All commercially available starting materials were used as received without further purification. The 4,4′-bis(hydroxymethyl)-2,2′-bipyridine (bpy-OH) has been synthesized by slightly modifying a procedure previously described.[9]

Physical techniques

^{1}H NMR spectra were acquired on a Bruker Avance DRX-300 spectrometer in $(CD_3)CO$ and CD_3OD solutions, with TMS as an internal standard. Infrared spectra were recorded with a Perkin-Elmer Spectrum One FT-IR spectrometer (KBr pellets). Elemental analyses were performed with a Perkin-Elmer 2400 microanalyzer by the Microanalytical Laboratory at University of Calabria. Thermogravimetry (TGA) measurements were performed on a Perkin-ElmerTGA6 Thermogravimetric Analyser, and differential scanning calorimetry (DSC) measurements on a Perkin-Elmer Pyris1 Differential Scanning Calorimeter. The TGA traces were obtained on heating the samples at 10 °C min^{-1} from 25 to 350 °C for TGA, respectively from 25 to 250 °C for DSC experiments.

Spectrofluorimetric grade acetone (Acros Organics) was used for the photophysical investigations in solution. Steady-state emission spectra were recorded on a Horiba Jobin Yvon Fluorolog 3 spectrofluorimeter, equipped with a Hamamatsu R-928 photomultiplier tube.

Emission quantum yields of the sample in solution were determined using the optically dilute method on deaerated solutions whose absorbance at excitation wavelengths was <0.1; $Ru(bpy)_3Cl_2$ (bpy = 2,2′-bipyridine) in H_2O was used as a standard (Φ = 0.028).[10] The experimental uncertainty on the emission quantum yields is 10%.

Preparation of the complexes

[(bpy-OH)ZnCl$_2$]. To a solution of [(bpy-OH)] (0.3 g, 1.38 mmol) in hot acetone (50 ml) was added $ZnCl_2$ (0.28 g, 2.07 mmol). After stirring for 1 day the obtained solid was filtered and washed in hot acetone (95% yield). Mp > 350 °C. IR (KBr) ν/cm^{-1}: 3484 (OH), 3077 (C–H), 1618 (C═C), 1560 (C═N). ^{1}H NMR: (300 MHz, DMSO): δ_H 9.36 (2H, s, $H_{3,3'}$), 9.28 (2H, s, $H_{1,1'}$), 8.37 (2H, s, $H_{2,2'}$), 6.51 (2H, s, OH), 5.51 (4H, d, J(H,H) = 5.42 Hz, CH_2). Anal. Calc. for $C_{12}H_{12}O_2N_2ZnCl_2$: C, 40.88; H, 3.43; N, 7.95. Found: C, 40.67; H, 3.36; N, 7.88. UV-vis (DMSO) λ_{abs} (ε, mol^{-1} dm^3 cm^{-1}): 286 (4085). λ_{em}: 351 nm.

[(Bpy-OH)Zn(Trop)Cl], 1. A solution of [(bpy-OH)Zn(Cl)$_2$] (0.3 g, 0.851 mmol) in hot water (9 ml) was added dropwise to a solution of potassium tropolonate (0.136 g, 0.851 mmol) in MeOH (75 ml) in an ice bath. The resulting yellow solution was stirred under nitrogen for 5 days and then the solvent was evaporated *in vacuo.* The product was recrystallized by EtOH to give a yellow solid (0.21 g, 54% yield). Mp 232 °C. Conductivity in EtOH: 15.4 cm^2 Ω^{-1} mol^{-1}. IR (KBr)ν/cm^{-1}: 3280 (OH), 2882–2833 (C–H), 1614, 1591 (C═O). ^{1}H NMR: (300 MHz, CD_3OD): δ_H 8.76 (2H, m, $H_{3,3'}$), 8.53 (2H, s, $H_{1,1'}$), 7.71 (2H, s, $H_{2,2'}$), 7.44 (4H, m, $H_{a,b,d,e}$), 6.98 (1H, t, H_c). Anal. Calc. for $C_{19}H_{17}ClN_2O_4Zn$: C, 52.08; H, 3.91; N, 6.39. Found: C, 51.87; H, 3.83; N, 6.20. UV-vis (MeOH) λ_{abs} (ε, mol^{-1} dm^3 cm^{-1}): 302 (3467); 351 (4319); 368 (16 818). λ_{em}: 421 nm.

[(bpy-OH)$_2$Zn(Trop)][Sac], 1a

Solid state reaction. [(Bpy-OH)Zn(Trop)Cl] (0.05 g, 0.109 mmol), saccharin (0.04 g, 0.218 mmol) and water (40 μl) have been grinded in a ball mill for 8 h. From slow evaporation of a water solution of the obtained powder, suitable crystals of **1a** have been obtained.

Data of crystals of **1a**: Mp 240 °C. IR (KBr) ν/cm^{-1}: 3365 (OH), 2924 (C–H), 1667 (C═O). ^{1}H NMR: (300 MHz, D_2O): δ_H 8.27 (4H, s, $H_{3,3'}$), 8.15 (4H, s, $H_{1,1'}$), 7.71–7.60 (4H, m, H_{sacc}), 7.41 (6H, m, $H_{2,2',a,e}$), 7.22 (2H, d, $H_{b,d}$), 6.98 (1H, t, H_c). UV-vis (water): λ_{abs} (ε, mol^{-1} dm^3 cm^{-1}): 292 (23 379); 304 (20 237); 319 (8912); 382 (4590). λ_{em}: 413 nm.

Solution reaction. [(Bpy-OH)Zn(Trop)Cl] (0.07 g, 0.153 mmol) was added to a water solution of saccharin (0.06 g, 0.307 mmol). The resulting mixture was refluxed for 24 hours; then the temperature was decreased to room temperature and the yellow precipitate formed was filtered out. Data of powder of **1a**: Mp 240 °C. IR (KBr) ν/cm^{-1}: 3365 (OH), 2923 (C–H), 1667 (C═O). ^{1}H NMR: (300 MHz, D_2O): δ_H 8.27 (4H, s, $H_{3,3'}$), 8.15 (4H, s, $H_{1,1'}$), 7.71–7.60 (4H, m, H_{sacc}), 7.41 (6H, m, $H_{2,2',a,e}$), 7.22 (2H, d, $H_{b,d}$), 6.98 (1H, t, H_c). UV-vis (water) λ_{abs} (ε, mol^{-1} dm^3 cm^{-1}): 292 (35 294); 304 (31 249); 322 (16 852); 382 (9272). λ_{em}: 412 nm. Anal. Calc. for $C_{38}H_{33}N_5O_9ZnS$: C, 57.35; H, 4.12; N, 8.75. Found: C, 57.07; H, 4.03; N, 8.62.

[(bpy-OH)Zn(Trop)$_2$], 2. A solution of potassium tropolonate (0.227 g, 1.42 mmol) in hot MeOH (8 ml) was added to a solution of [(bpy-OH)ZnCl$_2$] (0.25 g, 0.709 mmol) in hot water (15 ml). The resulting yellow solution was stirred under nitrogen (19 h, r.t.). The yellow solid obtained was filtered and washed with water (0.341 g, 92% yield). Mp 290 °C. IR (KBr) ν/cm^{-1}: 3306 (OH), 2832 (C–H), 1618, 1593 (C═O). ^{1}H NMR: (300 MHz, MeOD) δ_H 8.61 (2H, s, $H_{3,3'}$), 8.46 (2H, s, $H_{1,1'}$), 7.56 (2H, d, J(H–H) = 5.35 Hz, $H_{2,2'}$), 7.38 (4H, m, $H_{b,d,b',d'}$), 6.89 (4H, d, J(H–H) = 11 Hz, $H_{a,e,a',e'}$), 6.89 (2H, d, J(H–H) = 9.35 Hz, $H_{c,c'}$), 4.81 (4H, s, CH_2). Anal. Calc. for $C_{26}H_{22}O_6N_2Zn$: C, 59.65; H, 4.21; N, 5.35. Found: C, 59.48; H, 4.10; N, 5.12. UV-vis (DMSO) λ_{abs} (ε, mol^{-1} dm^3 cm^{-1}): 283 (16 855); 295 (11 757); 329 (29 497); 337 (33 551); 374 (16 385); 383 (18 927); 393 (17 325). λ_{em}: 422 nm.

[(bpy-OH)Zn(Trop)(Sac)], 2a

Solid state reaction. [(bpy-OH)Zn(Trop)$_2$] (0.05 g, 0.14 mmol), saccharin (0.05 g, 0.28 mmol) and EtOH (20 μl) have been grinded in the ball mill for 4 h. From slow evaporation of an ethanolic solution of the obtained powder, suitable crystals of **2a** have been obtained.

X-ray powder diffraction

All the powder X-ray diffraction patterns of the new complexes as well as the reaction product after grinding in the synthesis of **1a** and **2a** were obtained using a Bruker AXS General Area Detector Diffraction System (D8 Discover with GADDS) with Cu-Kα radiation (λ = 1.54056 Å). Measurements were performed by placing samples in Lindemann capillary tubes with

an inner diameter of 0.05 mm. The highly sensitive area detector was placed at a distance of 20 cm from the sample (2θ detector placed at 14°).

X-ray crystallographic analysis

Single crystal XRD data of **1–1a** and **2–2a** were collected at room temperature with a Bruker-Nonius X8APEXII CCD area detector system equipped with a graphite monochromator with radiation Mo Kα (λ = 0.71073 Å). These data were processed through the SAINT[11] reduction and SADABS[12] absorption software. The structures were solved by direct methods through the *SHELXTL-NT*[13] structure determination package and refined by full-matrix least-squares based on F^2. Generally, all non-hydrogen atoms were refined anisotropically and hydrogen atoms were included as idealized riding atoms. The unit cell parameters are listed in Table 1 together with a summary of the structure refinement data. The final geometrical calculations and the graphical manipulations were performed using the XP utility of the SHELXTL system program.

Results and discussion

Synthesis and characterization of the precursor complexes 1 and 2

Two new Zn(II) complexes of general formula [(bpy-OH)Zn(Trop)Cl] (**1**) and [(bpy-OH)Zn(Trop)$_2$] (**2**) have been synthesized, as summarized in Scheme 1, starting from the 4,4′-bis(hydroxymethyl)-2,2′-bipyridine (bpy-OH) obtained by slightly modifying a three steps reaction previously reported.[9] The dichloro derivative [(bpy-OH)ZnCl$_2$] was used as a precursor in the reaction with the potassium tropolonate to give rise to the desired mono or diketonate derivatives **1–2** in good yield (Scheme 1).

The characterization of the new complexes relies on elemental analysis, IR and ^{1}H NMR spectroscopies which are in agreement with the proposed structures (see the Experimental section). Both complexes have been structurally characterised through single crystal X-ray analysis (Fig. 1).

In complex **1**, the Zn(II) ion is in a five-coordinate distorted square pyramidal geometry. The basal plane is formed by the two chelating ligands, bipy-OH and Trop respectively, while the chloride ion is located on the apex of the pyramid. Differently, in complex **2** the central metal ion is six-coordinated by four oxygen atoms of two bidentate tropolonates and two nitrogen atoms of the bipyridine ligand. The "bite" angles as well as the Zn–O bond distances of the two chelated tropolonate ligands are comparable with those found recently in a similar bis-tropolonate Zn(II) derivative.[2c]

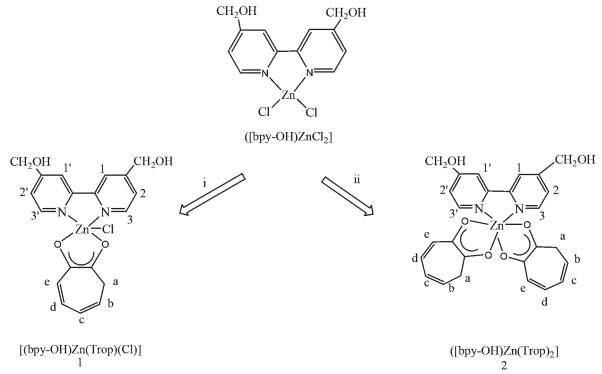

Scheme 1 Synthesis of complexes **1** and **2**.

Table 1 Details of data collection and structure refinements for complexes **1–1a** and **2–2a**

	1	**1a**	**2**	**2a**
Formula	$C_{19}H_{19}ClN_2O_5Zn$	$C_{38}H_{37}N_5O_{11}SZn$	$C_{26}H_{23}N_2O_7Zn$	$C_{26}H_{23}N_3O_8SZn$
M_r	456.18	837.11	540.83	602.93
Crystal size [mm]	0.20 × 0.15 × 0.10	0.10 × 0.08 × 0.02	0.06 × 0.04 × 0.02	0.14 × 0.10 × 0.05
Crystal system	Monoclinic	Triclinic	Tetragonal	Triclinic
Space group	$P2_1/c$	$P\bar{1}$	$I\bar{4}3d$	$P\bar{1}$
a [Å]	10.467(2)	11.709(3)	28.256(5)	9.3725(15)
b [Å]	9.202(2)	12.543(3)	28.256(5)	9.8002(15)
c [Å]	19.691(5)	15.172(3)	6.2531(13)	15.568(2)
α [°]	90	106.757(9)	90	78.243(7)
β [°]	90.412(7)	97.995(9)	90	76.235(7)
γ [°]	90	110.642(9)	90	73.493(7)
V [Å^3]	1896.6(8)	1923.3(7)	4992.5(16)	1317.3(4)
Z	4	2	8	2
ρ cald [g cm^{-3}]	1.598	1.446	1.442	1.520
μ [mm^{-1}]	1.470	0.760	1.032	1.066
θ range [°]	2.44–30.46	1.86–26.72	2.28–25.04	2.31–26.08
Data collected	45 512	71 295	52 578	31 835
Unique data, R_{int}	5711, 0.0379	8050, 0.0237	2490, 0.0713	5180, 0.0391
Obs. data [$I > 2\sigma(I)$]	4484	7452	1984	4180
No. of parameters	259	532	167	358
R_1 [obs. data]	0.0297	0.0301	0.0446	0.0427
wR_2 [all data]	0.0885	0.0858	0.1173	0.1249
GOF	0.983	1.055	1.080	1.043

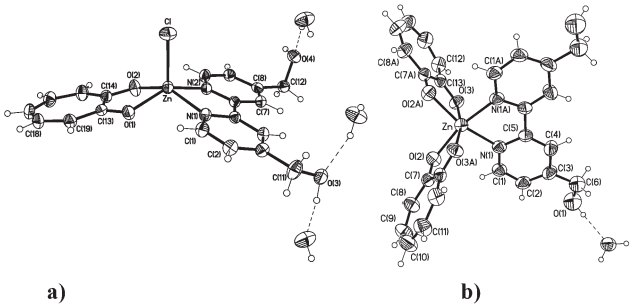

a) b)

Fig. 1 Molecular structures of complexes **1** (a) and **2** (b) with the atomic numbering scheme (ellipsoids at the 40% level).

Reaction of 1 and 2 with saccharin

The presence of water molecules in both crystalline solids has confirmed that the choice of the hydroxyl substituents on the bipyridine ligand in these complexes helps in the formation of solvate species through co-crystallization *via* hydrogen bonds. Neither of the two complexes are water soluble.

Encouraged by this result, complexes **1** and **2** have been used in the reaction with saccharin in an attempt to induce the formation of metal complex co-crystals. Knowing that the formation of co-crystals of pharmaceutical molecules is often achieved by mechano-chemical grinding and, in particular, by liquid-assisted grinding,[14] solid state reactions using a ball mill mixing the two complexes **1** and **2** with a twofold molar amount of saccharin with the addition of drops of solvent have been performed. The reaction products have been characterized by X-ray diffraction powder and the corresponding patterns compared with those calculated on the basis of the single crystal structures.

In particular, grinding complex **1** with saccharin in the presence of traces of water yields a crystalline powder reaction product the crystallization of which, in water, has allowed the formation of pale yellow single crystals in high yield (namely **1a**). The comparison between the powder diffraction pattern of the crystalline powder as obtained after the grinding and the one recorded from the crystals isolated from solution crystallization in water reveals some important points (Fig. 2).

First of all, the final product isolated from the solution as single crystals shows a very different diffractogram when compared to that calculated on the basis of the single crystal structure of **1**.

However, the powder obtained mechanochemically contains only a small amount of the final product isolated from solution, while a large portion of the unreacted complex **1** is still present, as shown by the presence of the same diffraction peaks.

The single crystal analysis performed on the yellow crystals of **1a** has revealed the formation of an ionic hydrate derivative of the general formula $[(bpy\text{-}OH)_2Zn(Trop)]Sac\cdot 2H_2O$ (**1a**). The Zn(II) ion of the complex cation is in an octahedral geometry, coordinated to two bipyridine and one tropolonate chelated ligands (Fig. 3a).

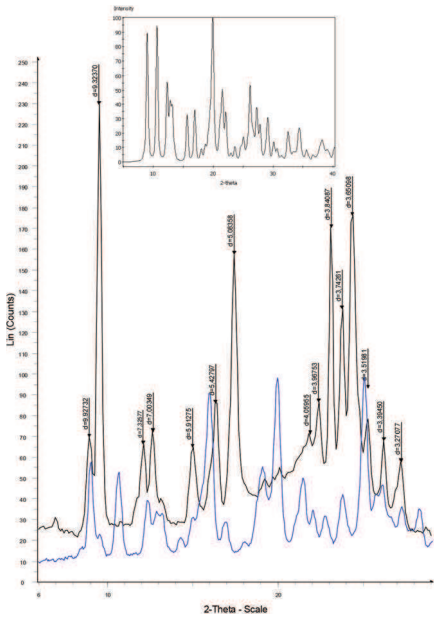

Fig. 2 Comparison between (black) the X-ray powder diffractogram measured on single crystals of **1a** and (blue) that measured on the crystalline powder obtained by grinding. In the inset the powder pattern of **1** calculated from single crystal analysis.

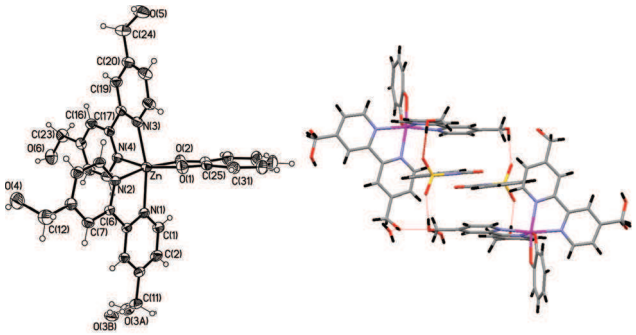

a) b)

Fig. 3 Molecular structure of **1a** showing the complex cation with the atomic numbering scheme (ellipsoids at the 40% level) (a) and (b) its hydrogen bonding network with both the saccharinate anion and water molecules.

The saccharinate (Sac), transformed by using saccharin, behaves as the counter ion but also establishes strong S═O–H–O hydrogen bonds with the complex cation. The co-crystallized water molecules strongly interact with the hydroxyl groups of another bipyridine ligand.

Due to the evidence that conversion of complex **1** into the new ionic derivative **1a** is complete after the crystallization process in water and in order to check the reproducibility of this synthesis, the reaction between **1** and saccharin was conducted also in water. In this case, complex **1a** has been isolated as a yellow powder in high yield as a unique product. The powder pattern is found perfectly superimposable with both diffraction patterns measured and calculated on single crystals of **1a** (Fig. 4).

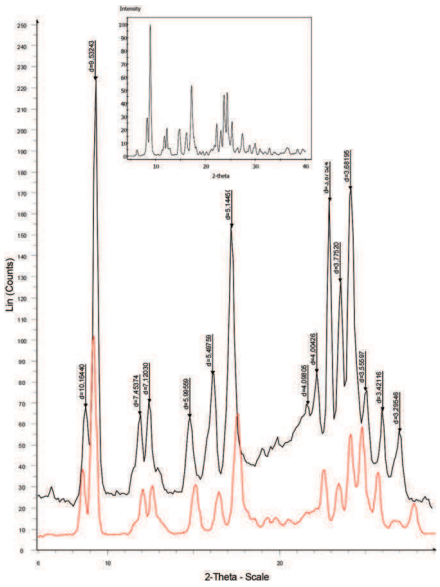

Fig. 4 Comparison between (black) the X-ray powder diffractogram measured on single crystals of **1a** and (red) that measured on the yellow powder obtained by the solution synthesis procedure. In the inset the powder pattern of **1a** calculated from single crystal analysis.

The inclusion of water molecules into the solid state crystalline structure of **1a** has a fundamental role in the formation of the new ionic species. Indeed, both the powder and the single crystals of **1a** are found to be highly stable with time and no water loss is observed with time exposure in air, as confirmed by performing repetitive powder X-ray diffraction measurements. Moreover, performing hygroscopicity experiments at 85% RH of salt **1a**, no significant water absorption has been observed, proving its stability in the solid state and the lack of hydrogen bond sites still available for the interactions with water molecules (ESI†).

In water solution, **1a** has been characterized by both ^{1}H NMR and UV-vis spectroscopies, proving its noticeable stability (see the Experimental section). In particular, due to its increased water solubility compared to complex **1**, absorption measurements are conducted in water solution over time (Fig. 5) and both the shape and absorption maxima positions remain unchanged after 24 and 72 h. Moreover, from preliminary water-solubility studies conducted by ICP-MS on both **1** and **1a** complexes, a distinct increased water solubility of **1a** has been proved, being nearly three times higher (ESI†).[15]

The drastic rearrangement of the coordination sphere around the Zn(II) ion in **1a** has been tentatively explained on the basis of an effective acid–base reaction between saccharine and the tropolonate ligand carried by the complex precursor **1**, proving the ability of saccharin to behave as a salt former even in the presence of a metal coordinated potential base like tropolonate. Although the reactions performed both in the solid state and in solution were conducted in excess of saccharine, knowing the exact structure of the so formed complex **1a**, the real stoichiometry ratio between complex **1** and saccharine should be indicated as 2 : 1 (Scheme 2).

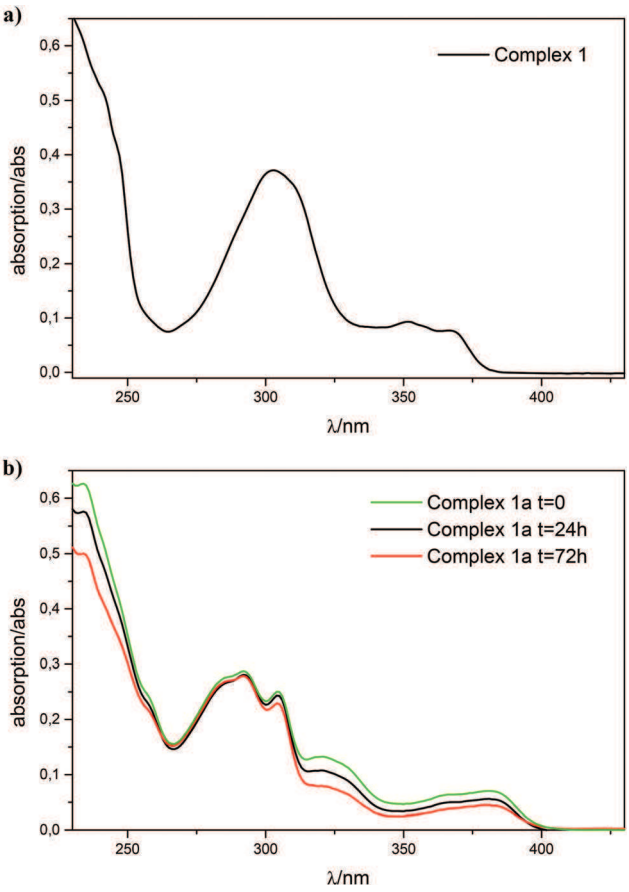

Fig. 5 Absorption spectra at room temperature of (a) **1** in methanol solution and (b) **1a** in water solution.

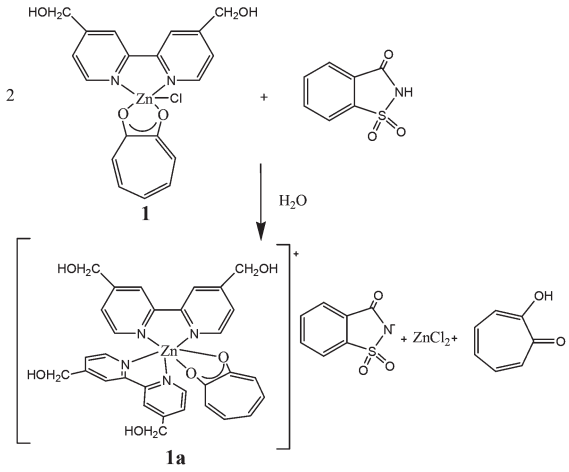

Scheme 2 Proposed effective reaction in the formation of **1a** salt.

The proposed synthetic reaction has been confirmed by the reaction between complex **2** and saccharine. This reaction was conducted by grinding the two powders with drops of methanol and the reaction product was analyzed by X-ray diffraction (ESI†). Although its diffractogram does not show any new reflections when compared to those of the raw reactants,

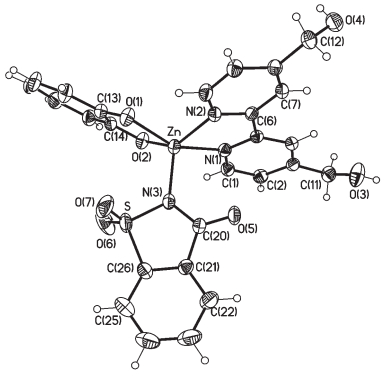

Fig. 6 Molecular structures of complex **2a** with the atomic numbering scheme (ellipsoids at the 30% level).

single crystals of a new species (namely **2a**) have been isolated in small amounts after slow evaporation of a methanol solution of the reaction product. The single crystal analysis has revealed the formation of the hydrate complex [(bpy-OH)Zn-(Trop)(Sac)]·H_2O (**2a**), in which one chelated tropolonate has been replaced by the saccharinate ion (Fig. 6).

The overall geometry around the Zn(II) ion is very similar to that of complex **1**, with the saccharinate ligand coordinated through the nitrogen atom on the apex of the pyramid. In this case, due to the hexa-coordination of the starting complex **2**, the proton transfer between saccharin and one coordinated tropolonate leaves the Zn(II) ion, now bis-chelated by one bipyridine and the remaining tropolonate, ready for the coordination to the so formed saccharinate ion. Eventually, this process is not particularly favourable, and very low yield of the new species **2a** is only reached by a long crystallization process in a methanol solution of the crystalline reaction product.

Conclusions

In summary, in an attempt to induce the formation of metal complex co-crystals, liquid assisted solid state reaction followed by solvent crystallization has been conducted by using the new Zn(II) tropolonate derivatives **1** and **2** with saccharin. The reaction gets complete after crystallization in water or methanol solution yielding two new Zn(II) derivatives **1a** and **2a**. In the case of **1a**, the same product has been obtained in high yield through a classical solution synthesis routine. The single crystal X-ray characterization of **1a** and **2a** has demonstrated that the expected formation of co-crystals has not been reached, clearly proving how difficult and complicated by the somehow unexpected reactivity of the inorganic moiety is the achievement of metal-based co-crystals. The effective reaction, induced by an acid–base proton transfer between saccharin and one coordinated tropolonate, leads to the formation of the two new species, **1a** and **2a**, *via* ligand exchange. In particular, in the case of the reaction between derivative **1** and saccharin, the inorganic saccharinate salt [(bpy-$OH)_2$Zn(Trop)]Sac·$2H_2O$ (**1a**) formed shows improved solubility, being water soluble, when compared to derivative **1**. Moreover, being aware that the transformation of complex **1** in the salt **1a** is accompanied by a rearrangement of the coordination sphere around the Zn(II) ion, and, therefore, this process is not a simple transformation of a possible API (complex **1**) into the corresponding salt, the new species can in principle keep or enhance similar biological activities with respect to its precursor. In this direction, further studies are under way.

Acknowledgements

Financial support received from the Ministero dell'Istruzione, dell'Università e della Ricerca (MIUR) through the Centro di Eccellenza CEMIF.CAL (CLAB01TYEF) and the Italian PRIN funding 2008F3734A003 is gratefully acknowledged. The authors thank Dr Emilia Furia for water-solubility studies.

Notes and references

1 (*a*) P. C. A. Bruijnincx and P. J. Sadler, *Curr. Opin. Chem. Biol.*, 2008, **12**, 197; (*b*) G. Sava, A. Bergamo and P. J. Dyson, *Dalton Trans.*, 2011, **40**, 9069; (*c*) J. A. Drewrya and P. T. Gunninga, *Coord. Chem. Rev.*, 2011, **255**, 459.

2 (*a*) J. Tan, B. Wang and L. Zhu, *Bioorg. Med. Chem.*, 2009, **17**, 614; (*b*) Q. Jiang, J. Zhu, Y. Zhang, N. Xiao and Z. Guo, *Biometals*, 2009, **22**, 297; (*c*) P. F. Liguori, A. Valentini, M. Palma, A. Bellusci, S. Bernardini, M. Ghedini, M. L. Panno, C. Pettinari, F. Marchetti, A. Crispini and D. Pucci, *Dalton Trans.*, 2010, **39**, 4205.

3 (*a*) M. A. Jacupek, M. Galanski, V. B. Arion, C. G. Hartinger and B. K. Keppler, *Dalton Trans.*, 2008, 183; (*b*) T. W. Hambley, *Dalton Trans.*, 2007, 4929; Z. Ma and B. Moulton, *Cryst. Growth Des.*, 2007, **7**, 2196.

4 C. L. Cooke and R. J. Davey, *Cryst. Growth Des.*, 2008, **8**, 3483.

5 S. Aitipamula, R. Banerjee, A. K. Bansal, K. Biradha, M. L. Cheney, A. R. Choudhury, G. R. Desiraju, A. G. Dikundwar, R. Dubey, N. Duggirala, P. P. Ghogale, S. Ghosh, P. K. Goswami, N. R. Goud, R. R. K. R. Jetti, P. Karpinski, P. Kaushik, D. Kumar, V. Kumar, B. Moulton, A. Mukherjee, A. S. Myerson, V. Puri, A. Ramanan, C. A. Reddy, N. Rodriguez-Hornedo, R. D. Rogers, T. N. Guru Row, P. Sanphui, N. Shan, G. Shete, A. Singh, C. C. Sun, J. A. Swift, R. Thaimattam, T. S. Thakur, R. K. Thaper, S. P. Thomas, S. Tothadi, V. R. Vangala, N. Variankaval, P. Vishweshwar, D. R. Weyna and M. J. Zaworotko, *Cryst. Growth Des.*, 2012, **12**, 2147 and references therein.

6 R. Banerjee, P. M. Bhatt, N. V. Ravindra and G. R. Desiraju, *Cryst. Growth Des.*, 2005, **5**, 2299.

7 (*a*) P. Mukherjee, M. G. B. Drew, C. J. Gomez-Garcia and A. Ghosh, *Inorg. Chem.*, 2009, **48**, 4817; (*b*) K. Li, Y. Liu, C. Yan, L. Fu, S.-C. Wei, H.-P. Wang, M. Pan and C.-Y. Su, *CrystEngComm*, 2012, **14**, 3868; (*c*) S. Sasmal, S. Hazra, S. Sarkar and S. Mohanta, *J. Coord. Chem.*, 2010, **63**, 1666.

8 D. Pucci, T. Bellini, A. Crispini, I. D'Agnano, P. F. Liguori, P. Garcia-Orduña, S. Pirillo, A. Valentini and G. Zanchetta, *Med. Chem. Commun.*, 2012, **3**, 462.
9 G. Will, G. Boschloo, S. Nagara Rao and D. Fitzmaurice, *J. Phys. Chem. B*, 1999, **103**, 8069.
10 K. Nakamaru, *Bull. Soc. Chem. Jpn.*, 1982, **5**, 2697.
11 *SAINT, Version 6.45 Copyright©*, Bruker Analytical X-ray Systems Inc., 2003.
12 G. M. Sheldrick, *SADABS. Version 2.10*, Bruker AXS Inc., Madison, USA, 2003.
13 *SHELXTL-NT, Version 5.1 Copyright©*, Bruker Analytical X-ray Systems Inc., 1999.
14 S. L. James, C. J. Adams, C. Bolm, D. Braga, P. Coltier, T. Friscic, F. Grepioni, K. D. M. Harris, G. Hyett, W. Jones, A. Krebs, J. Mack, L. Maini, A. G. Orpen, I. P. Parkin, S. H. Shearouse, J. W. Steed and D. C. Waddell, *Chem. Soc. Rev.*, 2012, **41**, 413 and references therein.
15 E. Furia, A. Naccarato, G. Sindona, G. Stabile and A. Tagarelli, *J. Agric. Food Chem.*, 2011, **15**, 59.

Journal of Materials Chemistry C

PAPER

Cite this: J. Mater. Chem. C, 2014, 2, 8780

Unconventionally shaped chromonic liquid crystals formed by novel silver(I) complexes†‡

Daniela Pucci,*[a] Barbara Sanz Mendiguchia,[a] Caterina Maria Tone,[b] Elisabeta Ildyko Szerb,[a] Federica Ciuchi,[c] Min Gao,[d] Mauro Ghedini[a] and Alessandra Crispini*[a]

Received 5th August 2014
Accepted 28th August 2014

DOI: 10.1039/c4tc01736f

www.rsc.org/MaterialsC

The synthesis of the first chiral Ag(I) bis chelated bipyridine ionic complexes showing chromonic liquid crystalline behaviour in water is reported. Single crystal X-ray analysis revealed a pre-chromonic organization in the crystalline state, with silver(I) cations stacking into columns reinforced by hydrogen bonding with the acetate counterions and water molecules. Due to the presence of molecules with an unconventional shape for the generation of typical chromonic phases, a full characterization based on phase diagram analysis, completely resolved by POM, DSC and X-ray powder diffraction measurements, has been conducted. Moreover, cryo-TEM experiments have been carried out in order to confirm the appearance of nematic columnar phases. A "route" to drive the alignment of the liquid crystalline phases of these compounds has been developed, which is particularly important for future application in biophotonic devices. Finally, the presence of transient twisted periodical stripe structures has been observed, when an initial planar alignment is destroyed in favour of a homeotropic configuration of the molecules dictated by the confining surfaces.

Introduction

Chromonics are a very interesting class of lyotropic liquid crystals (LLCs), which have become, over the last few years, an important research topic in several domains, like optical materials and devices in high technology, molecular electronics and biological sensing.[1–3] Although the behaviour of these dynamic 'soft' phases is not completely understood yet, Lydon, Attwood and co-workers showed the main differences between the chromonic molecules and the conventional amphiphilic lyotropic liquid crystals.[1,4] The main structural features of the compounds forming this class of LLCs are the lack of amphiphilic nature and the presence of a planar, aromatic π-delocalised core (with a disk-like shape), with solubilising groups (*e.g.* CO_2^-, SO_3^-) in the periphery of the molecules. In a polar solvent, molecules tend to aggregate into stacks due to weak intermolecular interactions, mainly van der Waals between the aromatic cores (π–π stacking), hydrophobic and electrostatic interactions. At all concentrations, there is some degree of aggregation and as the concentration increases, the distribution of the aggregate size shifts to higher and higher numbers of molecules. Therefore, instead of exhibiting a critical micellar concentration, these systems show isodesmic aggregation.[5] If the concentration is high enough to form large and interacting rod-like aggregates, liquid crystalline phases are formed. The stability of these phases depends on both temperature and concentration, and the nematic phase, with just orientational order, together with the columnar phase, with hexagonal packing, have been observed.[1,2] The majority of lyotropic chromonic liquid crystals (LCLCs) reported to date are based on organic systems featuring the properties highlighted above. All these features, together with their ability to organize themselves into columns forming ordered phases and their possibility to align between surfaces, make LCLCs ideal candidates for a new branch of application in photonic devices or biosensing.[6]

Lately, some metal complexes have been shown to form LCLC phases.[7] Metal complexes have a broad range of oxidation states and coordination geometries offering new opportunities for the design of original LCLC mesophases, rendering them

[a]Centro di Eccellenza CEMIF.CAL, LASCAMM CR-INSTM and Laboratorio Regionale Licryl, CNR-INFM, Dipartimento di Chimica e Tecnologie Chimiche, Università della Calabria, 87030 Arcavacata di Rende, CS, Italy. E-mail: a.crispini@unical.it

[b]Physics Department, University of Calabria, Via P. Bucci 33B, 87036 Arcavacata di Rende, CS, Italy. E-mail: caterina.tone@fis.unical.it

[c]IPCF-CNR UOS Cosenza, c/o Physics Department, University of Calabria, Via P. Bucci, 33B, 87036 Arcavacata di Rende, CS, Italy. E-mail: federica.ciuchi@cnr.it

[d]Liquid Crystal Insitute and Chemical Physics Interdisciplinary Program, Kent State University, Kent, OH 44242, USA. E-mail: mgao@kent.edu

† Dedicated to the late Prof. Daniela Pucci.

‡ Electronic supplementary information (ESI) available: Phase diagram tables of **1** and **2**; TGA traces of **1**, **2**, and **3** complexes; solid state PXRD pattern of **1**; low angle PXRD pattern of complex **2** in its nematic phase; POM images of the nematic phase of complexes **1** and **2** aligned between Cytop treated glasses; simplified sketch of an LC director inside stripes. CCDC 1017854 for **1**. For ESI and crystallographic data in CIF or other electronic format. See DOI: 10.1039/c4tc01736f

advantageous over their organic counterparts.[8,9] Indeed, metal complexes may offer different functionalities, modulated by the type of coordinated ligand, as well as intriguing spectroscopic, catalytic and redox properties.

The chemistry of Ag(I) complexes is in general extremely versatile in building supramolecular 'soft' ionic systems by coordination with oligopyridines and varying counterions. Indeed, D. Pucci *et al.* reported previously the synthesis of several thermotropic Ag(I) complexes, built up using differently functionalized *N*,*N*-donor ligands and counterions, that exhibited lamellar or columnar 'soft' organizations with different symmetries.[10] Herein, we report the synthesis and characterization of new carboxylate ionic *N*,*N*-coordinated Ag(I) complexes, in which the length of the counterions has been varied (complexes **1–3** in Fig. 1). Moreover, the choice of hydroxyl substituents on the bipyridine ligand is related to their potential ability to help in the formation of solvate species and then to form networks of intermolecular interactions *via* hydrogen bonds.[11]

The ability of these silver(I) complexes to organize into columnar structures is highlighted in the solid crystalline state, by means of single crystal X-ray analysis performed on complex **1**.

These complexes spontaneously self-assemble in water into LCLC phases, characterized by their phase diagram completely resolved by polarized optical microscopy (POM) and X-ray powder diffraction techniques. Cryo-TEM experiments have also been carried out in order to directly reveal the chromonic nature at a suitable water concentration.[12] Furthermore, the LCLC phases have been aligned between two polymer covered glasses, following a method already reported in the literature[6i] and showing transient twisted periodical stripe structures, a sign of elastic anisotropy.

Results and discussion

Synthesis and characterization

For the synthesis of the Ag(I) complexes **1–3**, the ligand 4,4′-bis(hydroxymethyl)-2,2′-bipyridine (bpy-OH) was previously prepared according to a method reported in the literature.[13] The ligand was further reacted with half equivalent of AgX, X = CH_3COO, C_2H_5COO and $C_5H_{11}COO$ respectively, for 4–6 h in EtOH, under a nitrogen atmosphere in a vessel protected from light. The final complexes were obtained in relatively high yields as yellowish solids, after recrystallization from EtOH–hexane. The complexes were dried for several days under high pressure vacuum.

These complexes were fully characterized and their proposed structures were confirmed by IR, ^{1}H NMR and elemental analysis. Indeed, the IR spectra of all complexes show the corresponding asymmetric and symmetric stretching vibration frequencies for the carboxylate counterions at around 1560 cm^{-1} (ν_{as} (COO^-)) and at 1390 cm^{-1} (ν_{asy}(COO^-)), respectively.[14] Furthermore, the IR spectra show a large band at approx. 3400 cm^{-1}, regardless of several attempts to dry the powders, and therefore reasonably attributable to the 2,2′-bipyridine and $-CH_2OH$ substituents. The presence of solvent was revealed by TGA analysis. The thermograms show loss of weight corresponding to one water molecule for all compounds (see ESI, Fig. S1–S3‡).

The ^{1}H NMR spectra of the complexes recorded in MeOD solutions show the signals corresponding to the protons of the carboxylate counterions and the protons of the coordinated ligand, the integration being indicative of the 2 : 1 stoichiometry ratio.

The ionic nature was confirmed by conductivity measurements performed in MeOH solution (see the Experimental section). Indeed, the conductivity values obtained for these complexes are characteristic of univalent electrolytes.[15]

The molecular structure of **1** has been obtained by single crystal X-ray analysis performed on suitable crystals grown by very slow evaporation of a methanol solution. The ionic nature of complex **1** is finally confirmed, with the metal cation containing the Ag(I) ion in a tetra-coordination geometry bis-chelated by two bipyridine ligands (Fig. 2a). The asymmetric unit is then completed by the presence of the acetate anion and two water molecules, one of which is probably crystallized over the long crystallization process. Bond distances and angles around the silver ion are in good agreement with those already reported for similar complexes.[16]

Both coordinated bipyridine ligands deviate from planarity, showing the internal torsion angles N–C–C–N of 9.4(5) and 4.4(5)°, respectively. Generally, symmetric bis-chelate pseudo tetrahedral complexes themselves are not chiral. Nevertheless complex **1** crystallizes in the chiral orthorhombic *P*2(1)2(1)2(1)

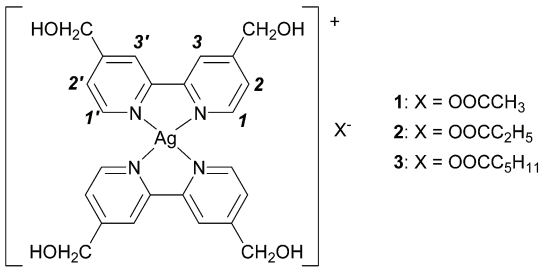

Fig. 1 Chemical structures of the silver(I) complexes **1**, **2** and **3**.

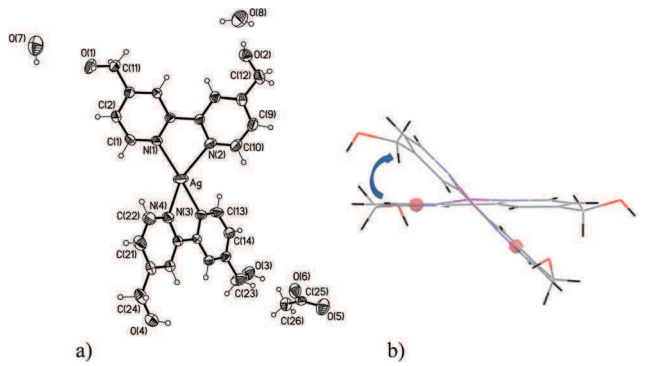

Fig. 2 Perspective view of ionic complex **1** with an atomic numbering scheme (ellipsoids at the 50% level) (a) and the crystallographic independent complex cation in *Λ* configuration (b).

space group. The symmetry within each bipyridine is broken by means of the different mutual orientations of the $-CH_2OH$ substituents (torsion angles around the C_{arom}–C bond of: C(2)–C(3)–C(11)–O(1) 35.0(6)°, C(9)–C(8)–C(12)–O(2) 163.0(4)°, C(14)–C(15)–C(23)–O(3) 16.6(7)°, C(21)–C(20)–C(24)–O(4) 175.5(4)°), generating chirality around the metal centre. The relative orientation of the two ligands creates a helicity around the metal ion, and the absolute configuration has been properly resolved. Labelling the aromatic ring bearing the $-CH_2OH$ group with the same orientation in the two bipyridine ligands allows identification of the single crystallographic independent complex cation in *Λ* configuration (Fig. 2b).[17]

The analysis of the intermolecular interactions existing within the asymmetric unit and in the 3D crystal packing of **1** is of particular interest for understanding the relationships between the structure and LCLC properties of this class of complexes. The presence of water molecules both in the powder and in the crystalline solid state of **1** has confirmed the usefulness of the properly functionalized 2,2′-bipyridine with hydroxyl groups as well as the use of acetate anions in the formation of water aggregates species. The presence of water molecules and the acetate anion interacting *via* hydrogen bonds with the hydroxyl groups at the periphery of the metal containing cation generates the formation of cation dimeric repeating units despite the potential electrostatic repulsion (Fig. 3).

Within the dimeric unit, cations interact through aromatic π–π stacking interactions with a distance of about 3.6 Å (defined as the distance between the centroid of one aromatic ring and the mean plane passing through the above aromatic coplanar ring) and the silver ions of the closest cations are forced at a distance of 3.951(2) Å. The dimeric unit, regularly repeating along the *a* axis, gives rise to metal containing columns. A tight hydrogen bonding network is formed in the 3D space and the columns of metal cations are segregated between layers of acetate ions and water molecules by means of the O···H hydrogen bond type (Fig. 4a).

The repetition of columns viewed down the *a* axis (in the *bc* plane) shows clearly that columns are organized in a close-packed hexagonal structure with an average intermolecular distance of about 17 Å (Fig. 4b).

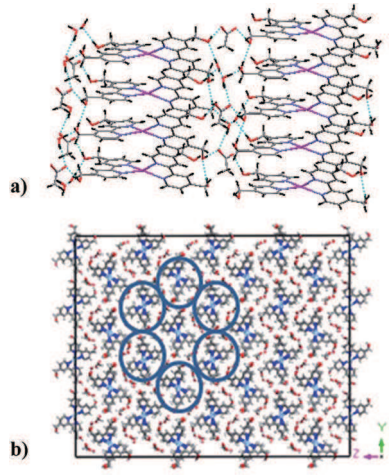

Fig. 4 Solid state organization of complex **1** showing the formation of metal containing cation columns running along the *a* axis, held together by means of hydrogen bonds formed with acetate anions and water molecules (a) and the repetition of columns in the *bc* plane forming a 2D hexagonal structure (b).

Phase diagram in water solutions

The phase diagram of complexes **1** and **2** were completely determined by POM and the relative type of mesophase confirmed by X-ray diffraction analysis. The phase diagram of complex **3** was not investigated since the nematic phase appears at a concentration above 50 wt%. The decrease of the complex hydrophilicity is related to the increase of the carboxylate counterion chain lengths.

Water solutions of complex **1** exhibit LC phases from 15 wt% to 60 wt% of concentration. In Fig. 5, the phase diagram of complex **1** is reported with some POM pictures of the textures observed inside the cell.

At room temperature, from 15 wt% to nearly 50 wt% of concentration, complex **1** presents a nematic (N) region as proved by typical textures observed on POM. This phase directly melts into the isotropic phase by increasing temperature. At higher concentration complex **1** organizes into a hexagonal phase at room temperature. While at 50 wt% the hexagonal phase transforms into the N phase by increasing temperature before isotropization, at 60 wt% the nematic phase is suppressed, and the hexagonal phase is stable until isotropization

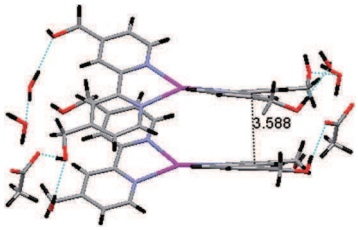

Fig. 3 View of the repeating unit of metal containing cations of complex **1** within columns showing the shortest π–π stacking distance and external hydrogen bonds.

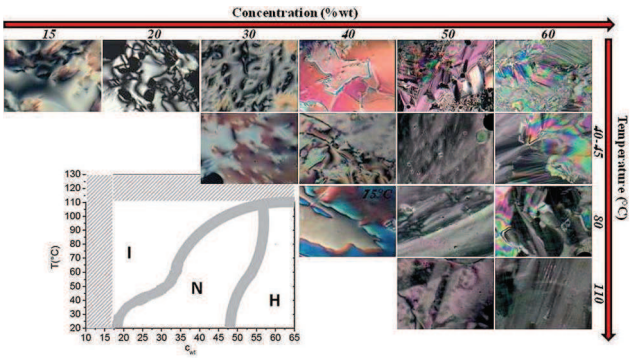

Fig. 5 Phase diagram of complex **1** and POM pictures of the texture observed at different temperatures and concentrations, confirming the presence of LC phases.

at 120 °C (Table S1 in the ESI‡). In the case of complex **2** the phase diagram shows the existence of only the nematic phase at all tested concentrations (see Fig. 6 and Table S2 ESI‡). Over 60 wt% complex **2** does not completely dissolve in water solution.

The presence of nematic and hexagonal phases at different weight concentrations together with the non-amphiphilic nature of these new metal based complexes and their ability to dissolve in water forming ordered aggregates confirm their chromonic nature.

X-ray powder diffraction analysis

In addition to phase diagrams and POM characterization, X-ray powder diffraction measurements (PXRD) were carried out, at room temperature, on both 20 wt% and 60 wt% LCLC non-aligned phases of complex **1** and on 20 wt% in the case of complex **2**.

In the case of complex **1**, the nematic diffuse peak in the PXRD pattern is centered at $2\theta = 2.5°$, corresponding to a d value of 35.3 Å (Fig. 7).

A moderately sharp reflection in the high-angle region of the PXRD pattern is centered at 3.48 Å corresponding to the average stacking repeat distance within columns. The intensity of this high-angle reflection, sharper than the usually broad stacking repeat peak encountered in the discotic nematic phase, points towards the existence of a truly N chromonic phase.

By changing concentration, moving to 60 wt%, the low angle reflection moves to $2\theta = 4.88°$, which corresponds to a much lower d value of 18.1 Å (Fig. 8).

This observed d value reduction with the complex concentration in the water solution is consistent with a decrease of the average column distance due to the diminished amount of "sea water" in-between chromonic molecules and concomitant increase of columnar organization order.[1a] The presence of two other reflections in the small angle region, together with the first one in the ratio $1 : \sqrt{3} : \sqrt{4}$, are characteristic of a 2D lattice of a hexagonal columnar phase, corresponding to the indexation $(hk) = (10)$, (11) and (20), with a cell parameter $a = 20.8$ Å. This value is similar to the intermolecular distance found in the close-packed hexagonal structure of the crystal phase (of about 17 Å) indicating that the hexagonal arrangement in the mesophase is obtained from the crystalline solid state through decorrelation between columns with maintenance of the intra column interactions. Indeed, the major feature of the presence of a chromonic M phase in the PXRD pattern of **1** is a sharp high-angle reflection corresponding to the stacking repeat distance of 3.51 Å. This value is found to be slightly larger than the stacking repeat distance of 3.40 Å, usually reported for organic chromonic molecules. This increase is fundamentally due to the stacking within columns of non-planar molecules, aggregated through aromatic interactions between facing bipyridine fragments and is consistent with the aromatic π–π stacking distance of about 3.6 Å found in the crystalline solid state.

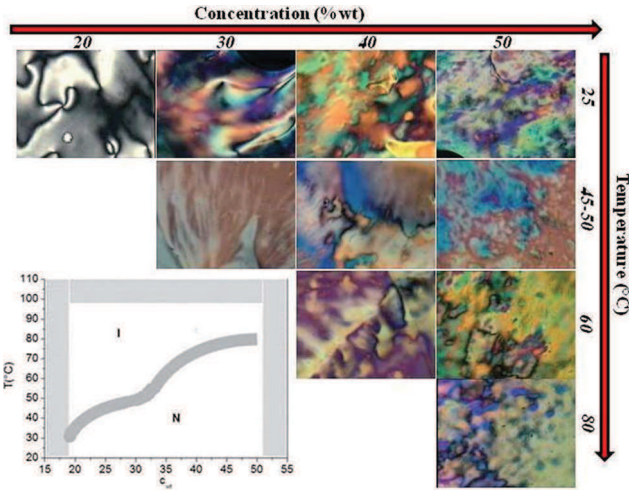

Fig. 6 Phase diagram of complex **2** and POM pictures of the texture observed at different temperatures and concentrations, confirming the presence of LC phases.

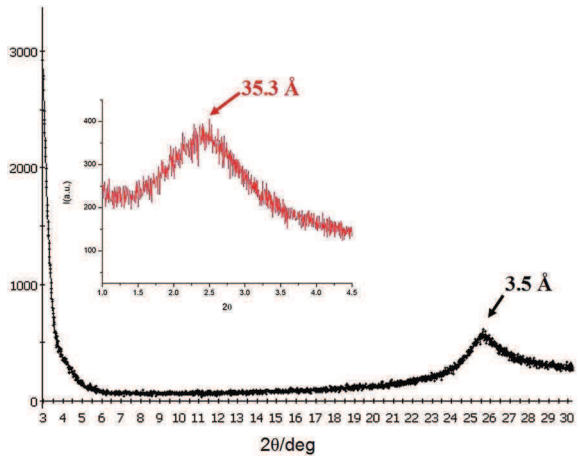

Fig. 7 Complex **1** X-ray diffraction pattern (low angle region in the inset) acquired at room temperature in the nematic phase at 20 wt% concentration.

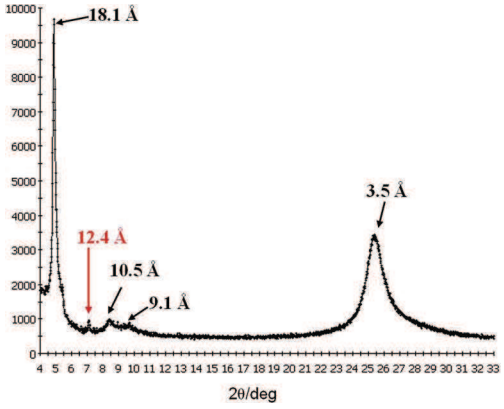

Fig. 8 Complex **1** X-ray diffraction pattern acquired at room temperature in the hexagonal phase at 60 wt% concentration.

Furthermore, the peak centred at 12.4 Å is due to some polymorphic crystalline microdomains that remain underneath the LCLC phase, as confirmed by the comparison of the liquid crystalline pattern with the PXRD pattern of the crystalline powder of complex **1** (see S4 in the ESI‡).[18]

At room temperature, the PXRD pattern of complex **2** at 20 wt% in water shows at low angle a nematic peak at $2\theta = 2.3°$, corresponding to a d value of 38.4 Å (see Fig. S5 in the ESI‡). This increase of the nematic d-spacing when compared with the one of complex **1** recorded under the same conditions should be related to the increase of the molecular length, *i.e.* the increase of the carboxylate counterion chain length.

Cryo-TEM analysis

Cryo-TEM analysis carried out on complex **1** solution in its nematic phase (20 wt%) directly demonstrates the assembly of the molecules into columnar aggregates and the nematic arrangement of the aggregates. Fig. 9a and b show typical side-view (corresponding to a planar orientation of the columns with the electron beam perpendicular to the LC film) and top-view (a homeotropic orientation) of the aggregates, respectively. The aggregates are represented by the dark stripes (Fig. 9a) and dots (Fig. 9b).[11] The length of the aggregates mostly varies between 10 nm and 60 nm, measured from the side-views by assuming a planar orientation. Fig. 9a also reveals that the elongated aggregates are oriented along roughly the same direction which is also the long axis of the aggregates.

The top-views of the aggregates enable the direct observation of the distribution pattern of the aggregates in the plane perpendicular to the aggregate axis. The aggregates can arrange themselves into approximate hexagons and roughly straight lines (Fig. 9b and its inset) in local regions. However, it is quite clear that the overall distribution is random and no long-range order is formed.

The distances measured between the adjacent aggregates from the top views normally fall within the range of 3–4 nm with an average of 3.4 nm, which is in excellent agreement with the XRD results (35.3 Å). The ones measured from the side views are slightly smaller due the projection effect and have an average of ~3 nm. The fast Fourier transform (FFT) pattern in Fig. 9a shows two major diffused bright spots which are also elongated perpendicular to the aggregate axis. This indicates a rather largely varying distance between the aggregates and a slightly changing aggregate orientation. The above results clearly confirm that the 20 wt% complex **1** solution has a nematic structure. It should be mentioned that currently it is still challenging for us to carry out cryo-TEM observation on highly viscous LCLCs (*e.g.*, 60 wt% complex **1**), as discussed in ref. 12.

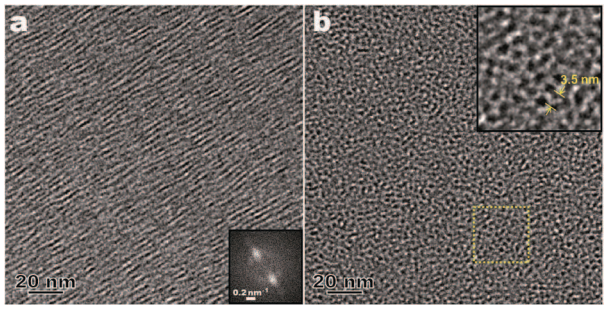

Fig. 9 Cryo-TEM images of complex **1** aggregates in its nematic phase at 20 wt%: side view (a) and top view (b). The inset of (a) is the corresponding FFT pattern. The inset of (b) is a magnified image of the marked area (30 nm × 30 nm) with a dashed square.

Alignment

The alignment of LCLC phases was carried out by confining complexes **1** and **2** between two properly treated surfaces. As reported in a previous study, it is possible to align chromonic liquid crystal phases by means of polymeric substrates characterized by different surface energies.[6i] A high surface energy (polymethyl-methacrylate – PMMA) and a low surface energy (Cytop) material were used in this work (see the Experimental section for details).

Just after filling, the nematic phase of complex **1** (20 wt%) confined between PMMA treated glasses shows textures characterized by the coexistence of degenerate planar alignment and homeotropic anchoring. With time, the degenerate planar anchoring (Fig. 10a–c) evolves into an ordered structure, characterized by stripes, disappearing after about 60–70 minutes in favor of stable homeotropic anchoring (confirmed by Maltese cross in conoscopy). The hexagonal phase, instead, shows immediately the homeotropic anchoring (Fig. 10d).

Recently, J. Jeong *et al.* reported the presence of transient stripes in the sunset yellow nematic LCLC phase when confined between parylene coated glasses.[19] The transient stripes reported are, on average, aligned parallel to the direction of the initial flow, inducing a planar alignment. The authors' model was further confirmed by compensator and POM measurements. Even if a different polymer was used in our case, the stripes observed are transient too, and disappear in favor of the homeotropic configuration after about one and a half hours. It is possible to re-induce stripe formation by heating up the cell

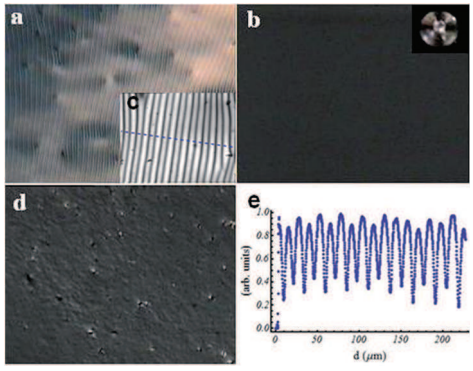

Fig. 10 POM images of the nematic phase (a–c) and the hexagonal phase (d) of complex **1** confined between PMMA treated glasses. (a, b and d) are acquired using a 5× objective, while (c) using a 20× objective. (e) Line profile highlighting the periodicity of the stripes observed in (c). The mean pitch measured is 25 μm, with a modulation in the middle at about 13 μm.

to 60 °C and slowly cooling down the system, until the homeotropic alignment is reached again. In order to evaluate the stripe periodicity, the images were analyzed using a home-made program written in Mathematica, obtaining a periodicity of about 25 μm, with a modulation in the middle at about 13 μm.

The stripes were investigated by crossing and uncrossing a polarizer and an analyzer, and inserting in the optical path a tilting compensator (5λ) confirming the twisting nature of the periodicity observed (Fig. 11).[19]

A detailed analysis is reported in Fig. 11; all images reported were acquired in the same region using a 20× objective. The direction of the analyzer and the polarizer is reported in the pictures. The stripes are not clearly visible when the polarizer and the analyzer are parallel or when only one polarizing plate is present. The sketch of the model proposed by J. Jeong *et al.*[19] and reported for clarity in Fig. S6 in the ESI,‡ may be taken into consideration.

These stripes appear as a balance of confining surface energy, self assembly properties and LCLC elastic constant anisotropy: the twist constant is at least one order of magnitude less than the splay and bent ones; the cell thickness plays as well an important role in stripe dimensions. The tilting compensator rotated in both directions compensates alternatively the stripes doubling their spacing and confirming their twisted nature. The same experiments were done using LC solutions of complex **2** at 20 wt% and no stripes were observed (data not reported).

A different scenario is observed for the "low surface energy material" used as an alignment layer. Indeed, when complex **1** (*i.e.* 20 wt%) is confined between Cytop treated glasses, an initial perfect planar alignment is observed that rapidly disappears in favor of well ordered stripes that cover the whole cell. After 3 hours, the molecules reorient in the whole cell, reaching a homeotropic alignment. The stripe pitch is in this case about 14 μm. If an external stress is applied to the cell, the planar alignment could be reproduced and follows the same evolution in time as described above (Fig. S7 in the ESI‡). A similar behavior but with an initial quasi-perfect planar alignment with some characteristic defects (Schlieren texture) is observed for complex **2** but in this case, the periodicity of the stripes is doubled (25 μm) (Fig. S8 in the ESI‡).

From the optical observation reported here, a discotic-like behaviour for the compounds may be suggested. A planar alignment of the LC phases, for both complexes, was achieved temporarily only with highly hydrophobic surfaces even if the final configuration is always the homeotropic one. It seems that highly hydrophobic substrates are able to disrupt in some way the aggregates forming the LC phases, allowing an initial planar (complex **1**) and quasi planar (complex **2**) alignment, that is lost in favor of a more stable homeotropic configuration. This means that in the competition between the alignment imposed by the substrates and the forces that bond the aggregates together, the π–π stacking between the disks wins the anchoring energy.

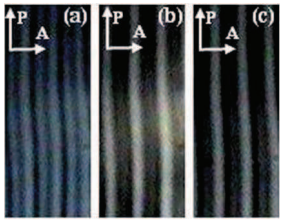

Fig. 11 Optical microscopy images of the stripe textures under crossed polarizers. White arrows represent the directions of the input polarizer (P) and the analyzer (a). In (b) and (c) the tilting compensator is inserted in the optical path.

Table 1 Details of data collection and structure refinements for complex **1**

1	
Formula	$C_{26}H_{31}AgN_4O_8$
M_r	635.42
Crystal size [mm]	0.32 × 0.18 × 0.12
Crystal system	Orthorhombic
Space group	$P2_12_12_1$
a [Å]	7.7993(4)
b [Å]	16.4226(8)
c [Å]	20.2988(11)
α [°]	90
β [°]	90
γ [°]	90
V [Å^3]	2600.0(2)
Z	4
ρ cald [g cm^{-3}]	1.623
μ [cm^{-1}]	0.833
θ range [°]	1.59–24.94
Data collected	48 505
Unique data, R_{int}	4542, 0.0360
Obs. data [$I > 2\sigma(I)$]	4100
No. Parameters	364
Flack parameter	0.00(3)
R_1 [Obs. data]	0.0335
wR_2 [all data]	0.0996
GOF	1.106

Conclusions

The synthesis and characterization of the ionic Ag(I) complexes **1**, **2** and **3**, having aliphatic carboxylate counterions with different chain lengths, are reported. The single crystal X-ray structure analysis of complex **1** has confirmed its ionic nature as well as the great affinity to aggregate in water. The presence of co-crystallized water molecules and the acetate anion interacting *via* hydrogen bonds with the hydroxyl groups at the periphery of the metal containing cation generates the formation of cation dimeric repeating units despite the potential electrostatic repulsion. In the 3D space, cations organize themselves into columns along the *a* axis and the metal containing columns are imbibed between layers of strongly interacting water molecules and acetate anions.

The cations stack into columns held together by π–π interactions helped by hydrogen bonding with the acetate counterions and water molecules. The repetition of columns in the *bc*

plane shows clearly their organization in a close-packed hexagonal structure with an average intermolecular distance of about 17 Å.

Even if the structural features of these new Ag(I) complexes do not fit the characteristic class of molecules forming LCLC phases, complexes **1** and **2** spontaneously self-assemble into nematic and hexagonal chromonic phases in water.

The suppression of the hexagonal phase in complexes **2** and **3** and also the appearance of the nematic organization at higher concentration with respect to complex **1** (particularly in the case of complex **3**) are clearly related to the counterion. With the increase of the counterion chain length, its facility to be involved in hydrogen bonding with water molecules should be inhibited, probably blocking the formation of the cation dimeric repeating units and favoring their electrostatic repulsions.

Therefore, the characterization of the LCLC formed phases has been performed on complexes **1** and **2** in water solution at different concentrations.

The phase diagram of complexes **1** and **2**, completely resolved by POM, has firstly indicated the formation of nematic and hexagonal phases in the case of complex **1** at 20 wt% and 60 wt% of concentration, while only nematic aggregation is observed in the case of complex **2**. PXRD measurements performed at the various concentrations have confirmed the formation of chromonic phases by dispersion of complexes **1** and **2** in water. Both nematic and hexagonal phases in the case of complex **1** have shown a reflection centered at about 3.5 Å in the wide angle region of the PXRD pattern, whose intensity and sharpness point towards the existence of truly N and M chromonic phases. The same feature has been confirmed in the case of complex **2** in the only observed N phase. Moreover, the hexagonal cell parameter of 20.8 Å calculated in the M mesophase in the case of **1** is in agreement with the intermolecular distance found in its close-packed hexagonal organization in the crystalline solid state (of about 17 Å), indicating that the mesophase is most probably arising from the crystalline phase through decorrelation between columns with maintenance of the intra-column interactions.

The direct cryo-TEM observation of the 20 wt% solution of complex **1** has revealed the top- and side-views of the elongated column, and confirms the self-assembly of the molecules into columnar aggregates. The aggregates are normally 10–60 nm long and are preferentially oriented along their long axis. The distribution of the aggregates is rather random and has no long-range order in the plane perpendicular to the aggregate axis, consistent with a nematic nature. In addition, the distance between the aggregate axis measured from the cryo-TEM results matches closely the XRD results. Based on the cryo-TEM and XRD results, it is reasonable to assume a hexagonal lattice for higher concentration solutions, though a direct cryo-TEM observation is still not available.

In addition, the LCLC phases of both complexes were aligned between two polymer covered glasses showing transient twisted periodical stripe structures that are a sign of elastic anisotropy, proving their potential for applications in optical devices or biosensing.

In conclusion, the synthesis and characterization of unconventional Ag(I) chromonic complexes have been reported. Most probably these complexes assemble in water forming LCLC phases due to the presence of suitable building blocks, such as the right anions and *N*,*N*-coordinated ligand substituents, as well as the metal ion. A route for future synthesis of metal based chromonic compounds has been highlighted, as well as the opening to a new branch of applications in biocompatible devices.

Experimental

Materials and measurements

All commercially available starting materials were used as received without further purification.

Instrumentation

The ^{1}H NMR spectra were recorded on a BrukerAvance AC-300 spectrometer in MeOD solution, using tetramethylsilane (TMS) as an internal standard. Elemental analyses (CHN) were performed with a Perkin Elmer 2400 microanalyzer by the Microanalytical Laboratory at the University of Calabria. Infrared spectra (KBr) were recorded on a Spectrum One FT-IR Perkin Elmer spectrometer. A Perkin-Elmer Lambda 900 spectrophotometer was used to record the absorption spectra of complexes in water solutions. An AInoLab Cond Level 1-720 conductometer equipped with a LR 325/001 immersion cell was used to take conductivity measurements. The thermal stability was measured on a Perkin-Elmer Thermogravimetric Analyser Pyris 6 TGA. Bright field, polarized optical microscopy (POM) images and conoscopy images were collected using a microscope (Zeiss) with a 5×, 20× objective or a 100× objective, respectively. The calibration of the microscope hot stage was performed by checking the transition temperatures of the E7 liquid crystal. The samples were rotated on a circular stage located between a polarizer and an analyzer. Most images were taken with a colour CCD camera under polychromatic illumination.

X-ray crystallography

X-ray data for **1** were collected at room temperature on a Bruker-Nonius X8 Apex CCD area detector equipped with a graphite monochromator and Mo Kα radiation (λ = 0.71073 Å). Data were processed through the SAINT[20] reduction and SADABS[21] absorption software. The structures were solved by standard Patterson methods through the SHELXTL-NT[22] structure determination package and refined by full-matrix least-squares based on F^2. In general, all non-hydrogen atoms were refined anisotropically and hydrogen atoms were included as idealized atoms riding on the respective carbon atoms with C–H bond lengths appropriate to the carbon atom hybridization. Hydrogen atoms of the co-crystallized water molecules have been included in calculated positions and restrained bond distances and angles have been used.

Details of data and structure refinements are given in Table 1.‡

Powder X-ray diffraction

The powder X-ray diffraction patterns of complex **1** in its hexagonal phase and nematic phase in the wide angle region as well as in the solid state were obtained at room temperature by using a Bruker D2 PHASER Diffraction System equipped with a 1D high speed solid state LinxEye detector and Cu-Kα radiation (λ = 1.54056 Å). Measurements were performed by placing samples on a zero background sample holder with protection for solvent evaporation along the measurements.

The X-ray patterns of complexes **1** and **2** in their nematic phase at low angle were obtained at room temperature using a D8 Discover, Bruker-AXS with Cu-Kα radiation (λ = 1.5418 Å). The LC solutions were hosted in a glass capillary (Mark tubes, Hilgenberg, 80 mm length, outside diameter 0.8 mm or 1 mm and wall thickness 0.1 mm) placed in a home-made sample holder.

Cryo-TEM measurements

The cryo-TEM observation was carried out using a FEI Tecnai F20 microscope (200 KV) equipped with an anti-contaminator, a low-dose operation mode, and a Gatan UltraScan 4000 CCD camera. To prepare cryo-TEM specimens, we employ a FEI Vitrobot (environmental chamber set to 22 °C) to plunge-freeze liquid crystal thin films supported by holey carbon coated grids. Liquid ethane was used as the cryogen in the rapid cooling process to ensure the preservation of the native structure. The vitrified LC specimens were then mounted on a Gatan 626-DH cryo-holder and transferred into the TEM. During the whole specimen transfer and TEM observation process, the TEM specimen was kept at temperatures below −170 °C. The TEM images shown here were all taken from the electron-transparent areas suspended in the holes of the supporting carbon films.

Synthesis of complexes 1–3

[(Bpy-OH)$_2$Ag][CH$_3$COO]·H$_2$O, 1. To a solution of 2 eq. of bpy-OH (100 mg, 0.46 mmol) in EtOH was added 1 eq. of AgOOCCH$_3$ (30 mg, 0.23 mmol). The solution was stirred for 4 hours under nitrogen and darkness. The solution was filtered, washed with EtOH, concentrated under reduced pressure and recrystallized from *n*-hexane (203 mg, 72% yield). Mp 182 °C. IR ν_{max}/cm^{-1}: 3369 (OH), 2920–2818 (CH), 1602 (C–C), 1560(ν_{asy} C═O), 1407 (ν_{sym} C═O). ^{1}H NMR (300 MHz, MeOD): δ_H 8.58 (d, 4H, J(H–H) = 5.07 Hz, H$_{1,1'}$), 8.39 (s, 4H, H$_{3,3'}$), 7.58 (d, 4H, J(H–H) = 4.66 Hz, H$_{2,2'}$), 4.91 (s, 8H, CH$_2$), 1.89 (s, 3H, CH$_3$). Anal. calc. for C$_{26}$H$_{29}$AgN$_4$O$_7$ (671.40 g mol^{-1}): C, 50.58; H, 4.73; N, 9.07. Found: C, 50.41; H, 4.57; N, 9.14%. UV-vis (H$_2$O) λ_{max} (ε, M^{-1} cm^{-1}): 235 nm (61 699), 281 nm (72 087). Λ_{MeOH} = 82.72 Ω^{-1} cm^2 mol^{-1}.

[(Bpy-OH)$_2$Ag][CH$_3$CH$_2$COO]·H$_2$O, 2. To a solution of 2 eq. of bpy-OH (100 mg, 0.46 mmol) in EtOH was added 1 eq. of AgOOCCH$_2$CH$_3$ (41.6 mg, 0.23 mmol). The solution was stirred for 4 hours under nitrogen and darkness. The solution was filtered, washed with EtOH, concentrated under reduced pressure and recrystallized from *n*-hexane. (176 mg, 63% yield). Mp 171 °C (dec.). IR ν_{max}/cm^{-1}: 3370 (OH), 2884–2833 (CH), 1603 (C–C), 1562 (ν_{asy} C═O), 1407 (ν_{sym} C═O). ^{1}H NMR (300 MHz, MeOD): δ_H 8.58 (d, 4H, J(H–H) = 5.1 Hz, H$_{1,1'}$), 8.38 (s, 4H, H$_{3,3'}$), 7.58 (d, 4H, J(H–H) = 4.6 Hz, H$_{2,2'}$), 4.83 (s, 8H, CH$_2$), 2.15 (q, 2H, J(H–H) = 22.86, H$_a$), 1.08 (s, 3H, CH$_3$). Anal. calc. for C$_{27}$H$_{31}$AgN$_4$O$_7$ (631.43 g mol^{-1}): C, 51.36; H, 4.95; N, 8.87. Found: C, 51.26; H, 5.14; N, 8.86%. UV-vis (H$_2$O) λ_{max} (ε, M^{-1} cm^{-1}): 234 nm (13 608), 282 nm (14 822). Λ_{MeOH} = 87.83 Ω^{-1} cm^2 mol^{-1}.

[(Bpy-OH)$_2$Ag][CH$_3$CH$_2$CH$_2$CH$_2$CH$_2$COO]·H$_2$O, 3. To a solution of 2 eq. of Bpy-OH (100 mg, 0.46 mmol) in EtOH was added 1 eq. of AgOOCCH$_2$CH$_2$CH$_2$CH$_2$CH$_3$ (51 mg, 0.23 mmol). The solution was stirred for 6 hours under nitrogen and darkness. The solution was filtered, washed with EtOH, concentrated under reduced pressure and recrystallized from *n*-hexane. (108 mg, 71% yield). Mp 139 °C (dec.). IR (ν_{max}/cm^{-1}: 3369 (OH), 1604 (C–C), 1564 (ν_{asy} C═O), 1408 (ν_{sym} C═O). ^{1}H NMR (300 MHz, MeOD): δ_H 8.57 (d, 4H, J(H–H) = 5.25 Hz, H$_{1,1'}$), 8.38 (s, 4H, H$_{3,3'}$), 7.57 (d, 4H, J(H–H) = 6.53 Hz, H$_{2,2'}$), 4.82 (s, 8H, CH$_2$), 2.13 (t, 2H, J(H–H) = 7.8, H$_a$), 1.58 (q), 2H, J(H–H) = 7.52, H$_b$), 1.31 (m, 4H, H$_{c,d}$),0.88 (t, 3H, J(H–H) = 6.91, CH$_3$). Anal. calc. for C$_{30}$H$_{37}$AgN$_4$O$_7$ (673.51 g mol^{-1}): C, 53.50; H, 5.54; N, 8.32. Found: C, 53.38; H, 5.51; N, 8.45%. UV-vis (H$_2$O) λ_{max} (ε, M^{-1} cm^{-1}): 235 nm (16 008), 283 nm (19 439). Λ_{MeOH} = 59.49 Ω^{-1} cm^2 mol^{-1}.

Mesophase and cell preparation

Liquid crystal solutions of both compounds were prepared by dissolving an amount of complexes **1** and **2** in pure distilled water (Millipore, 18 MΩ cm) in a range of concentrations between 15 wt% and 60 wt%. Glass slides used for the preparation of the cells were obtained from Pearl, China. They were cleaned in a NaOH bath, sonicated for 15 minutes and rinsed several times with Millipore water before drying them under a heat flow. For the phase diagram studies, we used bare glasses for the preparation of the cells, while for the alignment studies, the glasses were pre-treated by covering them with polymeric films, in order to obtain planar or homeotropic alignment of the LCLC solutions. Polymethyl-methacrylate (PMMA) was purchased from Sigma Aldrich, while Cytop, a highly transparent fluoropolymer, has been obtained from Asahi Glass. Polymeric thin films were prepared by a spin coating technique, at 3000 rpm, using a spin coater from Calctec (Italy), followed by an appropriate thermal treatment. PMMA treated glasses, after cooling down, were rubbed using a custom built machine, with a rotating velvet cloth.

Cells were assembled using two glasses with the same surface treatment and 12 μm mylar stripes as spacers, hence they were filled with the LC solution in the isotropic phase and sealed by epoxy glue, in order to avoid water evaporation. After filling, each cell was slowly cooled down and observed by polarized optical microscopy (POM). Each cell has been subjected to a temperature cycle in order to test the sealing. We focused our attention on complexes **1** and **2**, because complex **3** presents the nematic phase only at very high concentrations (50 wt%).

Acknowledgements

Financial support from the Ministero dell'Istruzione, dell'Università e della Ricerca (MIUR) through the Centro di Eccellenza CEMIF.CAL (CLAB01TYEF), from the Italian PRIN founding no. 2006038447 and from the European Community's Seventh Framework Program (FP7 2007–2013), through MATERIA project (PONa3_00370) is gratefully acknowledged. The TEM results were taken at the TEM Lab of the Liquid Crystal Institute (LCI) at Kent State University, supported by the Ohio Research Scholars Program Research Cluster on Surfaces in Advanced Materials. M.G. thanks the LCI Characterization Facility for the support of his TEM study. E.I.S. further acknowledges the European Union and Regione Calabria (Fondo Sociale Europeo, POR Calabria FSE 2007–2013) for partial funding.

Notes and references

1 (*a*) J. Lydon, in *Handbook of Liquid Crystals*, ed. D. Demus, J. Goodby, G. W. Gray, H.-W. Spiess and V. Vill, Wiley-VCH, Weinheim, 1998, vol. 2B, p. 98; (*b*) J. Jydon, *Curr. Opin. Colloid Interface Sci.*, 2004, **8**, 480–490; (*c*) J. Lydon, *J. Mater. Chem.*, 2010, **20**, 10071–10099; (*d*) J. Lydon, *Liq. Cryst.*, 2011, **38**, 1663–1681.

2 S. Tam-Chang and L. Huang, *Chem. Commun.*, 2008, 1957–1967.

3 (*a*) S. V. Shiyanovskii, O. D. Lavrentovich, T. Scneider, T. Ishikawa, I. I. Smalyukh, C. J. Woolverton, G. D. Niehaus and K. J. Doane, *Mol. Cryst. Liq. Cryst.*, 2005, **434**, 259/[587]–270/[598]; (*b*) S. L. Helfinstine, O. D. Lavrentovich and C. J. Woolverton, *Lett. Appl. Microbiol.*, 2006, **43**, 27–32; (*c*) V. G. Nazarenko, O. P. Boiko, M. I. Anisimov, A. K. Kadaschuk, Y. A. Nastishin, A. B. Golovin and O. D. Lavrentovich, *Appl. Phys. Lett.*, 2010, **97**, 263305.

4 T. K. Attwood, J. E. Lydon, C. Hall and G. J. T. Tiddy, *Liq. Cryst.*, 1990, **7**, 657–668.

5 (*a*) P. K. Maiti, Y. Lansac, M. A. Glaser and N. A. Clark, *Liq. Cryst.*, 2002, **29**, 619–626; (*b*) M. R. Tomasik and P. J. Collins, *J. Phys. Chem. B*, 2008, **112**, 9883–9889; (*c*) P. J. Collings, A. J. Dickinson and E. C. Smith, *Liq. Cryst.*, 2010, **37**, 701–710.

6 (*a*) I. K. Iverson and S. Tam-Chang, *J. Am. Chem. Soc.*, 1999, **121**, 5801–5802; (*b*) D. Matsunaga, T. Tamaki, H. Akiyama and K. Ichimura, *Adv. Mater.*, 2002, **14**, 1477; (*c*) I. K. Iverson, S. M. Casey, W. Seo and S. Tam-Chang, *Langmuir*, 2002, **18**, 3510–3516; (*d*) T. Fujiwara and K. Ichimura, *J. Mater. Chem.*, 2002, **12**, 3387–3391; (*e*) Y. A. Nastishin, H. Liu, T. Scheneider, V. Nazaremko, R. Vasyuta, S. V. Shiyanovskii and O. D. Lavrentovich, *Phys. Rev. E: Stat., Nonlinear, Soft Matter Phys.*, 2005, **72**, 041711; (*f*) O. D. Lavrentovich*et al.*, *US Pat.*, 7, 294, 370, 13 November 2007; (*g*) V. G. Nazarenko, O. P. Boiko, H. S. Park, O. M. Brodyn, M. M. Omelchenko, L. Tortora, Y. A. Nastishin and O. D. Lavrentovich, *Phys. Rev. Lett.*, 2010, **105**, 017801; (*h*) K. A. Simon, E. A. Burton, F. Cheng, N. Varghese, E. R. Falcone, L. Wu and Y. Luk, *Chem. Mater.*, 2010, **22**, 2434–2441; (*i*) C. M. Tone, M. P. De Santo, M. G. Buonomenna, G. Golemme and F. Ciuchi, *Soft Matter*, 2012, **8**, 8478–8482.

7 (*a*) W. Lu, Y. Chen, V. A. L. Roy, S. S.-Y. Chui and C. Che, *Angew. Chem., Int. Ed.*, 2009, **48**, 7621–7625; (*b*) J. E. Halls, R. W. Bourne, K. J. Wright, L. I. Partington, M. G. Tamba, Y. Z. T. Ramakrishnappa, G. H. Mehl, S. M. Kelly and J. D. Wadhawan, *Electrochem. Commun.*, 2012, **19**, 50–54; (*c*) Y. J. Yadav, B. Heinrich, G. de Luca, A. Talarico, T. F. Mastropietro, M. Ghedini, B. Donnio and E. I. Szerb, *Adv. Optical Mater.*, 2013, **1**, 844–854; (*d*) X.-S. Xiao, W. Lu and C.-M. Che, *Chem. Sci.*, 2014, **5**, 2482–2488.

8 B. Donnio, *Curr. Opin. Colloid Interface Sci.*, 2002, **7**, 371–394.

9 (*a*) *Metallomesogens, Synthesis, Properties and Applications*, ed. J. L. Serrano, VCH, Weinheim, Germany, 1996; (*b*) B. Donnio and D. W. Bruce, in *Liquid Crystals II, Structure and Bonding*, Springer, Berlin Heidelberg, 1999, vol. 95, pp. 193–247; (*c*) B. Donnio, D. Guillon, R. Deschenaux and D. W. Bruce, in *Comprehensive Coordination Chemistry II*, ed. J. A. McCleverty and T. J. Meyer, Elsevier, Oxford, UK, 2003, pp. 357–627.

10 (*a*) D. Pucci, G. Barberio, A. Bellusci, A. Crispini, M. La Deda, M. Ghedini and E. I. Szerb, *Eur. J. Inorg. Chem.*, 2005, 2457–2463; (*b*) D. Pucci, G. Barberio, A. Bellusci, A. Crispini, M. Ghedini and E. I. Szerb, *Mol. Cryst. Liq. Cryst.*, 2005, **441**, 251–260; (*c*) D. Pucci, G. Barberio, A. Bellusci, A. Crispini, B. Donnio, L. Giorgini, M. Ghedini and E. I. Szerb, *Chem.–Eur. J.*, 2006, **12**, 6738–6747; (*d*) A. Bellusci, M. Ghedini, L. Giorgini, F. Gozzo, E. I. Szerb, A. Crispini and D. Pucci, *Dalton Trans.*, 2009, 7381–7389; (*e*) D. Pucci, A. Crispini, M. Ghedini, E. I. Szerb and M. La Deda, *Dalton Trans.*, 2011, 4614–4622; (*f*) E. I. Szerb, D. Pucci, A. Crispini and M. La Deda, *Mol. Cryst. Liq. Cryst.*, 2013, **573**, 34–45.

11 B. S. Mendiguchia, D. Pucci, T. F. Mastropietro, M. Ghedini and A. Crispini, *Dalton Trans.*, 2013, 6768–6774.

12 M. Gao, Y.-K. Kim, C. Zhang, V. Borshch, S. Zhou, H.-S. Park, A. Jákli, O. D. Lavrentovich, M.-G. Tamba, A. Kohlmeier, G. H. Mehl, W. Weissflog, D. Studer, B. Zuber, H. Gnägi and F. Lin, *Microsc. Res. Tech.*, 2014, DOI: 10.1002/jemt.22397.

13 G. Will, G. Boschloo, S. Nagaraja Rao and D. Fitzmaurice, *J. Phys. Chem. B*, 1999, **103**, 8067–8079.

14 N. W. Alcock and V. M. Tracy, *J. Chem. Soc., Dalton Trans.*, 1976, 2243–2246.

15 W. J. Geary, *Coord. Chem. Rev.*, 1971, **7**, 81.

16 A. Bellusci, A. Crispini, D. Pucci, E. I. Szerb and M. Ghedini, *Cryst. Growth Des.*, 2008, **8**, 3114–3122.

17 U. Knof and A. von Zelewsky, *Angew. Chem., Int. Ed.*, 1999, **38**, 302–322.

18 L. Wu, J. Lal, K. A. Simon, E. A. Burton and Y.-Y. Luk, *J. Am. Chem. Soc.*, 2009, **131**, 7430–7443.

19 J. Jeong, G. Han, A. T. Charlie Johnson, P. J. Collings, T. C. Lubensky and A. G. Yodh, *Langmuir*, 2014, **30**, 2914.

20 *SAINT, version 6.45*, Bruker Analytical X-ray Systems Inc, 2003.

21 G. M. Sheldrick, *SADABS. Version 2.10*, Bruker AXS Inc., Madison, WI, USA, 2003.

22 *SHELXTL-NT, version 5.1*, Bruker Analytical X-ray Systems Inc, 1999.

Acknowledgements

During these three years, I received a constant support from my supervisors and my colleagues.

I would like to express my gratitude to Prof. Alessandra Crispini for guiding me with her knowledge and her experience.

I am grateful to Prof. Mauro Ghedini, Dr. Iolinda Aiello, Dr. Massimo La Deda and Dr. Nicolas Godbert for their valuable scientific support.

I would like to thank Prof. Matteo Zanda for allowing me to spend nine useful months in his group.

I would also like to thank Dr. Elisabeta I. Szerb, Dr. Anna Maria Talarico, Dr. Teresa Mastropietro, Dr. Paola Liguori, Dr. Sante Pirillo, Dr. Emilia Furia, Prof. Concetta Giancola, with whom I have profitably collaborated and my colleagues Dr. Yogesh Yadav, Dr. Luigi Rizzuti Dr. Loredana Ricciardi and Dr. Andreea Ionescu for all the goods moments spent together.